

AD-A078 781

CALIFORNIA UNIV DAVIS SIGNAL AND IMAGE PROCESSING LAB F/G 9/4  
APPLICATIONS OF STOCHASTIC MODELS FOR IMAGE DATA COMPRESSION.(U)  
SEP 79 S WANG , A K JAIN DAA629-78-G-0206

UNCLASSIFIED

ARO-16222.3-EL

NL

1 OF 3  
AD-A078781



REPORT DOCUMENTATION PAGE		READ INSTRUCTIONS BEFORE COMPLETING FORM
1. REPORT NUMBER 16222.3-EL	2. GOVT ACCESSION NO.	3. RECIPIENT'S CATALOG NUMBER
4. TITLE (and Subtitle) Applications of Stochastic Models for Image Data Compression	5. TYPE OF REPORT & PERIOD COVERED Technical	
7. AUTHOR(s) Sheng-Huey Wang Anil K. Jain	6. PERFORMING ORG. REPORT NUMBER	
PERFORMING ORGANIZATION NAME AND ADDRESS University of California Davis, California 95616	8. CONTRACT OR GRANT NUMBER(s) DAAG29 78 G 0206	
CONTROLLING OFFICE NAME AND ADDRESS U. S. Army Research Office P. O. Box 12211 Research Triangle Park, NC 27709	10. PROGRAM ELEMENT, PROJECT, TASK AREA & WORK UNIT NUMBERS	
12. REPORT DATE September 1979	13. NUMBER OF PAGES 237	
15. SECURITY CLASS. (of this report) Unclassified	15a. DECLASSIFICATION/DOWNGRADING SCHEDULE	
16. DISTRIBUTION STATEMENT (of this Report) Approved for public release; distribution unlimited.		
17. DISTRIBUTION STATEMENT (of the abstract entered in Block 20, if different from Report)		
18. SUPPLEMENTARY NOTES The view, opinions, and/or findings contained in this report are those of the author(s) and should not be construed as an official Department of the Army position, policy, or decision, unless so designated by other documentation.		
19. KEY WORDS (Continue on reverse side if necessary and identify by block number) data compression                      coding images mathematical models stochastic processes		
20. ABSTRACT (Continue on reverse side if necessary and identify by block number) Intraframe image data compression systems are analyzed in this thesis using stochastic modeling concepts. The formulations of stochastic image models are obtained from different classes of partial differential equations. Their application to the coding problem shows the connection between predictive, hybrid and transform coding schemes. The resulting coding schemes are evaluated in terms of tangible system terms such as signal to noise ratio, mean square error and rate distortion curve.		

ADA 078781

DDC FILE COPY

**LEVEL**

**DDC  
RECEIVED  
DEC 27 1979  
RECEIVED  
E**



ADA 078781

APPLICATIONS OF STOCHASTIC MODELS FOR IMAGE DATA COMPRESSION

Technical Report

by

Shenq-Huey Wang

Anil K. Jain

Signal & Image Processing Laboratory

Department of Electrical Engineering

University of California

Davis, California 95616

DDC FILE COPY

September, 1979

79-12 27 026

12

6

APPLICATIONS OF STOCHASTIC MODELS FOR IMAGE DATA COMPRESSION.

9

Technical Report

by

10

Shenq-Huey/Wang\*

Anil K./Jain

DDC  
REF ID: A66112  
DEC 28 1979  
E

Signal & Image Processing Laboratory

Department of Electrical Engineering

University of California

Davis, California 95616

15 DAAG29-78-G-0206

11

Sep 1979

12 256

18 ARD

19 16222.3-EL

This document has been approved  
for public release and sale; its  
distribution is unlimited.

\*The author was with the Signal & Image Processing Laboratory,  
Department of Electrical Engineering, University of California,  
Davis, California 95616. He is now with the Picker Corporation,  
Mayfield Village, Ohio 44143.

411 110

mt



The research work reported in this dissertation has been supported in part by the Naval Ocean Systems Center, San Diego, California, under contract N6600-1-78-C015MJE, and in part by the U.S. Army Research Office, Durham, North Carolina, under grant DAAG29-78-G0206.

Accession For	
NTIS GRA&I	<input checked="checked" type="checkbox"/>
DDC TAB	<input type="checkbox"/>
Unannounced	<input type="checkbox"/>
Justification	
By _____	
Distribution/	
Availability Codes	
Dist	Availand/or special
<i>A</i>	

## TABLE OF CONTENTS

	Page
ABSTRACT . . . . .	vii
ACKNOWLEDGMENTS . . . . .	ix
LIST OF FIGURES . . . . .	x
LIST OF TABLES . . . . .	xvi
CHAPTER ONE: INTRODUCTION	
1.1 The Problem . . . . .	1
1.2 Background Material . . . . .	3
1.2.1 Differential Pulse Code Modulation (DPCM) . . .	3
1.2.2 Transform Coding . . . . .	3
1.2.3 Hybrid (Transform/DPCM) Coding . . . . .	4
1.2.4 Contour Coding and Edge Extraction . . . . .	5
1.3 Organization . . . . .	5
CHAPTER TWO: DISCRETE GAUSSIAN RANDOM FIELDS AND STOCHASTIC IMAGE MODELS	
2.1 Introduction . . . . .	7
2.2 Causal, Semicausal and Noncausal Estimates . . . . .	7
2.2.1 Causal Estimate . . . . .	7
2.2.2 Semicausal Estimate . . . . .	8
2.2.3 Noncausal Estimate . . . . .	8
2.3 Stochastic Representations of Gaussian Random Field .	9
2.3.1 Minimum Variance Representation . . . . .	9
2.3.2 White Noise Driven Representation . . . . .	10
2.4 Spectral Density Function of the Gaussian Random Field Represented by Linear Models . . . . .	10
2.5 Image Representations . . . . .	12
2.5.1 Causal Representation . . . . .	12



2.5.2	Semicausal Representations . . . . .	13
2.5.3	Noncausal Representations . . . . .	16
2.6	Basis Restriction Data Compression Efficiency of Image Models . . . . .	19
2.6.1	Zonal Filter Design . . . . .	20
2.6.2	Experimental Results . . . . .	21
2.7	Summary and Conclusions . . . . .	22

### CHAPTER THREE: SEMICAUSAL MODELS AND HYBRID CODING

3.1	Introduction . . . . .	35
3.2	Semicausal Image Models and Hybrid Coding . . . . .	35
3.2.1	Hybrid Coding of Separable Covariance Image Fields . . . . .	36
3.2.2	Semicausal Representations as Two Source Models for Finite Random Fields . . . . .	38
3.2.3	Stochastic Decoupling of Semicausal Models by the Cosine Transform . . . . .	41
3.2.4	Stochastic Decoupling of Stationary Semicausal Fields . . . . .	44
3.3	Hybrid Coder Design for Semicausal Random Fields . . . . .	46
3.3.1	DPCM Equations . . . . .	46
3.3.2	Bit Allocation . . . . .	47
3.3.3	Integer Bit Allocation . . . . .	54
3.4	Adaptive Hybrid Coding . . . . .	55
3.4.1	Adaptive Variance Estimation . . . . .	55
3.4.2	Adaptive Classification . . . . .	58
3.5	Experimental Results . . . . .	60
3.5.1	Nonadaptive Hybrid Coding . . . . .	61
3.5.2	Adaptive Variance Estimation . . . . .	62
3.5.3	Adaptive Classification . . . . .	62

3.6	Extensions of Hybrid Coding . . . . .	66
3.6.1	Hybrid Encoded Image with Channel Error . . . .	66
3.6.2	Higher Order Predictor in DPCM Loop of Hybrid Coding . . . . .	67
3.6.3	Hybrid Coding of Noisy Image . . . . .	68
3.7	Summary of Results and Conclusions . . . . .	71

#### CHAPTER FOUR: NONCAUSAL MODELS AND TRANSFORM CODING

4.1	Introduction . . . . .	106
4.2	Image Transform . . . . .	107
4.3	Stochastic Decoupling of Noncausal Models by Sine Transform . . . . .	112
4.3.1	NC1 Model . . . . .	113
4.3.2	NC2 Model . . . . .	116
4.3.3	NC3 Model . . . . .	120
4.4	Stochastic Formulation of Noncausal Models by Cosine Transform . . . . .	122
4.5	Transform Coder Design for Noncausal Models via Cosine Transform . . . . .	125
4.6	Fast KL (Sine) Transform Data Compression . . . . .	128
4.7	Experimental Results . . . . .	129
4.8	Classification Transform Coding . . . . .	130

#### CHAPTER FIVE: IMAGE MODELS FOR FEATURE CODING

5.1	Introduction . . . . .	144
5.2	Feature Extraction via Image Models . . . . .	144
5.2.1	Image Modeling Operator . . . . .	145
5.2.2	Approximate Rational Function Operator . . . .	149
5.2.3	Edge Information Subtraction Procedure . . . .	149
5.2.4	Image Enhancement . . . . .	151

5.3	Transform Coding using Nonstationary Image Representation . . . . .	152
5.4	Experimental Results and Comparisons . . . . .	157
5.4.1	Feature Transform Coding . . . . .	158
5.4.2	Classification Feature Transform Coding . . . . .	159
5.4.3	Conclusions . . . . .	160
CHAPTER SIX: SUMMARY AND RECOMMENDATIONS FOR FUTURE RESEARCH . .		180
APPENDICES		
APPENDIX A: QUANTIZER CONSIDERATIONS		
A.1	Introduction . . . . .	183
A.2	Quantizer Structures . . . . .	183
A.2.1	Optimum Nonuniform Quantizer . . . . .	184
A.2.2	Optimum Uniform Quantizer . . . . .	185
A.2.3	Useful Approximation to the Optimum Nonuniform Quantizer . . . . .	187
A.3	Results and Comparisons . . . . .	189
A.4	Conclusions . . . . .	195
APPENDIX B: DERIVATION OF APPROXIMATE RATIONAL FUNCTION OPERATOR . . . . .		224
APPENDIX C: UNIQUE INVERSE SOLUTION OF FUNCTION $g_1'(x)$ . . .		229
LIST OF REFERENCES . . . . .		231
VITA . . . . .		237



## ABSTRACT

Intraframe image data compression systems are analyzed in this thesis using stochastic modeling concepts. The formulations of stochastic image models are obtained from different classes of partial differential equations. Their application to the coding problem shows the connection between predictive, hybrid and transform coding schemes. The resulting coding schemes are evaluated in terms of tangible system terms such as signal to noise ratio, mean square error and rate distortion curve.

Most of the existed intraframe coding schemes are either ad hoc or lack a complete mathematical basis. By paying attention to the boundary points of an image random field, it is shown that the remaining image random field can be fairly described by stochastic image models which in turn can be processed via well-defined fast transform algorithms (Sine and Cosine transforms are used here). The eigenvalues associated with these transform algorithms are important for coding application. To properly handle a nonstationary image random field, a new method based on representing an image as a composition of two sources, viz., stochastic and deterministic, is suggested. The stochastic part is dealt with by known statistical properties of stochastic image models and the deterministic part representing features such as edges, is obtained as the residual after the stochastic part is removed. Two simple adaptive schemes, i.e., Adaptive Variance Estimation and Adaptive Classification, are considered for updating the model parameters with the variations in image statistics. The computational complexity is increased only marginally, but the improvement in the reconstructed image quality is substantial.



Simulation studies are performed on three image data consisting of Girl, Earth and Chemical Plant images. The Results indicate that the proposed schemes can be practically implemented and will reproduce a good image at comparable signal to noise ratio. Hybrid coding of noisy image and sensitivity of human viewer to the sharp features are also partially addressed.

## ACKNOWLEDGMENTS

I wish to express my gratefulness and appreciation to my thesis advisor, Professor Anil K. Jain. I cannot thank him adequately for the guidance, encouragement and support which he has so generously given me during the course of this research.

I would like to thank Dr. Peter D. Scott and Dr. Demetrios G. Lainiotis for graciously agreeing to serve on my Ph.D. program committee, and Dr. Gary Ford of the University of California, Davis, for serving as the outside reader.

Valuable discussions and assistance provided by Mr. Jaswant R. Jain and Mr. Surendra Ranganath, both Ph.D. students under Professor Jain's supervision, are also greatly appreciated.

Finally, a special note of thanks goes to Ms. Nora Rogers for the difficult job of typing the manuscript and putting extra hours on weekends to meet my schedule.

# LIST OF FIGURES

Figure		Page
2.1	The Region S for Estimating (i,j) . . . . .	24
2.2	Basis Restriction Efficiency Implementation . . . . .	24
2.3	Causal Model (C1) Fourier Transform Domain Model Zonal Patterns for a 32 x 32 Image Block Size with Various Sample Reduction Ratios . . . . .	25
2.4	Semicausal Model (SC1) Fourier Transform Domain Model Zonal Patterns for a 32 x 32 Image Block Size with Various Sample Reduction Ratios . . . . .	26
2.5	Noncausal Model (NC1 or NC2-A or NC2-B) Fourier Transform Domain Model Zonal Patterns for a 32 x 32 Image Block Size with Various Sample Reduction Ratios . . . . .	27
2.6	Basis Restriction Mean Square Error versus Sample Reduction Ratio for the Fourier Transform Model Zonal Sampling of a 256 x 256 Girl Image with 16 x 16 Image Block Size . . . . .	28
2.7	Basis Restriction Mean Square Error versus Sample Reduction Ratio for the Fourier Transform Model Zonal Sampling of a 256 x 256 Earth Image with 16 x 16 Image Block Size . . . . .	28
*2.8	Fourier Transform Model Zonal Sampled Girl Image with 16 x 16 Image Block Size . . . . .	29
*2.9	Fourier Transform Model Zonal Sampled Earth Image with 16 x 16 Image Block Size . . . . .	30
3.1	Hybrid Coding System . . . . .	74
3.2	The i-th DPCM Channel . . . . .	74
3.3	Realization of Semicausal Model Decomposition . . . . .	75
3.4	Adaptive Variance Estimation Hybrid Coding Scheme . . . . .	76
3.5	Adaptive Classification Hybrid Coding Scheme . . . . .	76
3.6	Nonadaptive Hybrid Coding Scheme for Various Image Models of the Girl Image Encoded via 16 x 256 Image Strip, (a) Rate Distortion Curve (b) Signal to Noise Ratio versus Bit Rate .	77
3.7	Nonadaptive Hybrid Coding Scheme for Various Image Models of the Chemical Plant Image Encoded via 16 x 256 Image Strip, (a) Rate Distortion Curve (b) Signal to Noise Ratio versus Bit Rate . . . . .	77

\* These figures contain images



3.8	Comparison of Adaptive Variance Estimation Hybrid Coding Scheme for Various Image Models of the Girl Image Encoded via $16 \times 256$ Image Strip, (a) Rate Distortion Curve (b) Signal to Noise Ratio versus Bit Rate . . . . .	78
3.9	Comparison of Adaptive Variance Estimation Hybrid Coding Scheme for Various Image Models of the Chemical Plant Image Encoded via $16 \times 256$ Image Strip, (a) Rate Distortion Curve (b) Signal to Noise Ratio versus Bit Rate . . . . .	78
3.10	Classification Map of the Left Quarter Portion $16 \times 32$ Transformed Sub-columns of an Image with 16 DPCM Channels (a) Girl Image (b) Chemical Plant Image . . . . .	79
3.11	Comparison of Adaptive Classification Hybrid Coding Scheme for Various Image Models of the Girl Image Encoded via $16 \times 256$ Image Strip, (a) Rate Distortion Curve (b) Signal to Noise Ratio versus Bit Rate . . . . .	80
3.12	Comparison of Adaptive Classification Hybrid Coding Scheme for Various Image Models of the Chemical Plant Image Encoded via $16 \times 256$ Image Strip, (a) Rate Distortion Curve (b) Signal to Noise Ratio versus Bit Rate . . . . .	80
3.13	Bit Allocations for Adaptive Classification, $k = 4$ , Girl Image, (a) Actual Measurement Model (b) SC1 Model (c) SC2 Model . . . . .	81
3.14	Bit Allocations for Adaptive Classification, $k = 4$ , Chemical Plant Image, (a) Actual Measurement Model (b) SC1 Model (c) SC2 Model . . . . .	82
3.15	Histogram of Image Column Activities (Variances), Girl Image is Used . . . . .	83
3.16	Histogram of Image Column Activities (Variances), Chemical Plant Image is Used . . . . .	84
3.17	Hybrid Coding Results for Separable Covariance Model of the Girl Image Encoded via $16 \times 256$ Image Strip, (a) Rate Distortion Curve (b) Bit Rate versus Signal to Noise Ratio . . . . .	85
3.18	Hybrid Coding Results for SC1 Model of the Girl Image Encoded via $16 \times 256$ Image Strip, (a) Rate Distortion Curve (b) Bit Rate versus Signal to Noise Ratio . . . . .	85
3.19	Hybrid Coding Results for SC2 Model of the Girl Image Encoded via $16 \times 256$ Image Strip, (a) Rate Distortion Curve (b) Bit Rate versus Signal to Noise Ratio . . . . .	85
3.20	Hybrid Coding Results for SC1 Model of the Chemical Plant Image Encoded via $16 \times 256$ Image Strip, (a) Rate Distortion Curve (b) Bit Rate versus Signal to Noise Ratio . . . . .	86



3.21	Hybrid Coding Results for SC2 Model of the Chemical Plant Image Encoded via $16 \times 256$ Image Strip, (a) Rate Distortion Curve (b) Bit Rate versus Signal to Noise Ratio . . . . .	86
* 3.22	Hybrid Encoded Girl Image at 1 Bit/Pixel Approximately . . .	87
* 3.23	Hybrid Encoded Girl Image at 1.7 to 2 Bits/Pixel Approximately . . . . .	88
* 3.24	Hybrid Encoded Chemical Plant Image at 1 Bit/Pixel Approximately . . . . .	89
* 3.25	Hybrid Encoded Chemical Plant Image at 1.7 to 2 Bits/Pixel Approximately . . . . .	90
* 3.26	Actual Measurement Model Hybrid Encoded Image at 1 and 2 Bits/Pixel Approximately . . . . .	91
3.27	Model of a Binary Symmetric Channel . . . . .	92
3.28	Effect of Channel Errors . . . . .	92
* 3.29	Hybrid Encoded Girl Image with Channel Error $p_e = 0.0001$ at 1 Bit/Pixel Approximately . . . . .	93
* 3.30	Hybrid Encoded Girl Image with Channel Error $p_e = 0.001$ at 1 Bit/Pixel Approximately . . . . .	94
3.31	Higher Order Predictor and DPCM Channel . . . . .	95
3.32	Kalman Filter DPCM Loop for the $i$ -th Channel in Hybrid Coding . . . . .	95
* 3.33	Restored Images of the Kalman Filter DPCM Loop Scheme Implemented on a Noisy Girl Image ( $S/N = 5$ ) . . . . .	96
4.1	Conventional Image Transform Coding System . . . . .	133
4.2	Spatial Structures of Three Noncausal Image Representations .	133
4.3	Realization of Noncausal Model Decomposition . . . . .	134
4.4	Transform Coding via 2-Dimensional Noncausal Model (a) Cosine Transform (b) Fast KL (Sine) Transform . . . . .	135
4.5	Integer Bit Allocation for NC1 Model Cosine Transform Encoded Girl Image with Average Bit Rate = 1 Bit/Pixel . . .	136
4.6	Transform Coding Results of NC1 Model of the Girl Image with Block Size $64 \times 64$ (a) Rate Distortion Curve (b) Bit Rate vs. SNR. . . . .	137

4.7	Transform Coding Results of NC1 Model of the Chemical Plant Image with Image Block Size $64 \times 64$ , (a) Rate Distortion Curve (b) Bit Rate vs. SNR . . . . .	137
* 4.8	Cosine Transform Encoded Girl Image (a) 0.5 Bit/Pixel Standard (b) 1 Bit/Pixel, Standard (c) 2 Bits/Pixel, Standard (d) 0.5 Bit/Pixel, Classification (e) 1 Bit/Pixel, Classification (f) 2 Bits/Pixel, Classification . . .	138
* 4.9	Cosine Transform Encoded Chemical Plant Image (a) 0.5 Bits/Pixel, Standard (b) 1 Bit/Pixel, Standard (c) 2 Bits/Pixel, Standard (d) 0.5 Bit/Pixel, Classification (e) 1 Bit/Pixel, Classification (f) 2 Bits/Pixel, Classification . . .	139
4.10	Bit Allocation with Classification ( $k = 2$ , Girl Image and $64 \times 64$ Image Block Size) . . . . .	140
4.11	Classification Map and Image Block Measure Variances with Two Classes and Equal Probabilities ( $p_k = 0.5$ ) (a) Girl Image (b) Chemical Plant Image . . . . .	141
* 5.1	Edge Pictures with $t = 2\sigma$ , (a) Discrete Fourier Transform (b) Discrete Cosine Transform . . . . .	162
5.2	Realization of Stochastic Decomposition . . . . .	163
* 5.3I	Image Decomposition of the Girl Image with 3111 ( $t = 2\sigma$ ) Edge Points . . . . .	164
* 5.3II	Image Enhancement of the Girl Image with 3111 ( $t = 2\sigma$ ) Edge Points . . . . .	165
* 5.4I	Image Decomposition of the Chemical Plant with 3653 ( $t = 2\sigma$ ) Edge Points . . . . .	166
* 5.4II	Image Enhancement of the Chemical Plant with 3653 ( $t = 2\sigma$ ) Edge Points . . . . .	167
5.5	Transform Coding Based on Stochastic Segmentation . . . . .	168
5.6	Feature Transform Coding Results for the Girl Image versus Various Edge Quantizer's Bits with 5737 ( $t = 1.5\sigma$ ) Detected Edge Points . . . . .	169
5.7	Feature Transform Coding Results for the Girl Image versus Various Edge Quantizer's Bits with 3111 ( $t = 2\sigma$ ) Detected Edge Points . . . . .	169
5.8	Feature Transform Coding Results for the Girl Image versus Various Thresholds with 2 Bits Assigned to the Edge Point Quantizer . . . . .	170

5.9	Classification Feature Transform Coding Results for the Girl Image versus Various Thresholds with 2 Bits Assigned to the Edge Quantizer . . . . .	170
5.10	Feature Transform Coding Results for the Chemical Plant Image versus Various Edge Quantizer's Bits with 7079 ( $t = 1.5\sigma$ ) Detected Edge Points . . . . .	171
5.11	Feature Transform Coding Results for the Chemical Plant Image versus Various Edge Quantizer's Bits with 3653 ( $t = 2\sigma$ ) Detected Edge Points . . . . .	171
5.12	Feature Transform Coding Results for the Chemical Plant Image versus Various Thresholds with 2 Bits Assigned to the Edge Quantizer . . . . .	172
5.13	Classification Feature Transform Coding Results for the Chemical Plant Image versus Various Thresholds with 2 Bits Assigned to the Edge Quantizer . . . . .	172
* 5.14	Comparison of Standard Transform and Feature Transform Encoded Girl Images . . . . .	173
* 5.15	Comparison of Standard Transform and Feature Transform Encoded Chemical Plant Images . . . . .	174
* 5.16	Feature Transform Encoded Girl Image with $n_e = 2$ Bits and $t = 1.5\sigma$ (5737 Detected Edge Points) . . . . .	175
* 5.17	Feature Transform Encoded Chemical Plant Image with $n_e = 2$ Bits and $t = 1.5\sigma$ (7079 Detected Edge Points) . . . . .	176
A.1	Quantizer Characteristics . . . . .	196
A.2	Nonuniform Quantizer (Compandor) . . . . .	197
A.3	Analog Model for Nonlinear Quantization . . . . .	197
A.4	Flow Chart of Determining the 'Decision Levels' and 'Quantization Levels' for an Optimum Nonuniform Quantizer with a Given Probability Density Function, $p(x)$ . . . . .	198
A.5	Mean Square Error vs. Number of Quantizer Bits for Signal with Gaussian Density (Mean = 0, Variance = 1) . . . . .	199
A.6	Mean Square Error vs. Number of Quantizer Bits for Signal with Laplacian Density (Mean = 0, Variance = 1) . . . . .	199
A.7	Signal to Noise Ratio vs. Number of Quantizer Bits for Signal with Gaussian Density (Mean = 0, Variance = 1) . . . . .	200



A.8	Signal to Noise Ratio vs. Number of Quantizer Bits for Signal with Laplacian Density (Mean = 0, Variance = 1) . . .	200
A.9	Entropy vs. Number of Quantizer Bits for Signal with Gaussian Density (Mean = 0, Variance = 1) . . . . .	201
A.10	Entropy vs. Number of Quantizer Bits for Signal with Laplacian Density (Mean = 0, Variance = 1) . . . . .	201
A.11	Quantizer Output Levels and their Probability Distribution (N = 8) . . . . .	202
B.1	Construction Diagram of $R^{(1)}(z_1, z_2)$ . . . . .	225
B.2	Construction Diagram of $R^{(2)}(z_1, z_2)$ . . . . .	225
B.3	Construction Diagram of $R^{(3)}(z_1, z_2)$ . . . . .	226
B.4	Construction Diagram of $R^{(4)}(z_1, z_2)$ . . . . .	227
B.5	Construction Diagram of $R^{(5)}(z_1, z_2)$ . . . . .	228



# LIST OF TABLES

Table		Page
2.1	Summary of Some PDE Models and Their Discrete Approximates $D[u] = \epsilon$ Used for Image Modeling . . . . .	31
2.2	Actual Parameters Measured for Various Models of the $256 \times 256$ Image to Match the $16 \times 16$ Covariance Matrix of the Image . . . . .	32
2.3	Basis Restriction Mean Square Error of the Girl Image Represented by (a) Causal Image Model (C1) (b) Semicausal Image Model (SC1) (c) Noncausal Image Model (NC1 or NC2-A or NC2-B) . . . . .	33
2.4	Basis Restriction Mean Square Error of the Earth Image Represented by (a) Causal Image Model (C1) (b) Semicausal Image Model (SC1) (c) Noncausal Image Model (NC1 or NC2-A or NC2-B) . . . . .	34
3.1	Bit Allocation Patterns Based on Equation (3.3.2-25), Girl Image (a) SC1 Model (b) SC2 Model . . . . .	97
3.2	Bit Allocation Patterns Based on Equation (3.3.2-21), Girl Image (a) Separable Covariance Model (b) SC1 Model (c) SC2 Model . . . . .	98
3.3	Parameters of Image Models Used in Hybrid Coding . . . . .	99
3.4	Hybrid Coding Results of the Girl Image Encoded via $16 \times 256$ Image Strip (a) Separable Covariance Model (b) SC1 Model (c) SC2 Model (d) Actual Measurement Model . . . . .	100
3.5	Hybrid Coding Results of the Chemical Plant Image Encoded via $16 \times 256$ Image Strip (a) SC1 Model (b) SC2 Model (c) Actual Measurement Model . . . . .	101
3.6	Hybrid Coding Results with Communication Channel Errors, Girl Image Encoded via $16 \times 256$ Image Strip (a) Separable Covariance Model (b) SC1 Model (c) SC2 Model (d) Actual Measurement Model . . . . .	102
3.7	The Experimental Results of Higher Order Predictor Imple- mented on the Girl Image with 16 DPCM Channels . . . . .	103
3.8	Predictor Coefficients of Various Orders for Different Channels in Hybrid Coding . . . . .	103
3.9	Discrete Kalman Filter and DPCM Algorithms . . . . .	104

3.10	The Experimental Results of Kalman Filter Implemented on the Noisy Girl Image (a) S/N = 1 (b) S/N = 2 (c) S/N = 5 . . .	105
4.1	Summary of Important Formulas of Noncausal Represented Image Random Fields . . . . .	142
4.2	Girl Image, Cosine Transform Coding Results, NC1 Model with 64 × 64 Image Block . . . . .	143
4.3	Chemical Plant Image, Cosine Transform Coding Results, NC1 Model with 64 × 64 Image Block . . . . .	143
5.1	Thresholds and No. of Detected Edge Points Relation (a) Girl Image (b) Chemical Plant Image . . . . .	177
5.2	Feature Transform Coding Results for the Girl Image with 5737 ( $t = 1.5\sigma$ ) Detected Edge Points . . . . .	178
5.3	Feature Transform Coding Results for the Girl Image with 3111 ( $t = 2\sigma$ ) Detected Edge Points . . . . .	178
5.4	Feature Transform Coding Results for the Girl Image with 2 Bits Assigned to the Edge Quantizer . . . . .	178
5.5	Classification Transform Coding Results for the Girl Image with 2 Bits Assigned to the Edge Quantizer . . . . .	178
5.6	Feature Transform Coding Results for the Chemical Plant Image with 7079 ( $t = 1.5\sigma$ ) Detected Edge Points . . . . .	179
5.7	Feature Transform Coding Results for the Chemical Plant Image with 3653 ( $t = 2\sigma$ ) Detected Edge Points . . . . .	179
5.8	Feature Transform Coding Results for the Chemical Plant Image with 2 Bits Assigned to the Edge Quantizer . . . . .	179
5.9	Classification Feature Transform Coding Results for the Chemical Plant Image with 2 Bits Assigned to the Edge Quantizer . . . . .	179
A.1	Approximate Average Amount of CDC Cyber 173 Computer Time Required to Determine the Quantizer Structure with Gaussian Distributed Input Signal . . . . .	203
A.2	Approximate Average Amount of CDC Cyber 173 Computer Time Required to Determine the Quantizer Structure with Laplacian Distributed Input Signal . . . . .	203

A.3	Optimum Uniform Quantizers for Signal with Gaussian Density (Mean = 0, Variance = 1) . . . . .	204
A.4	Optimum Uniform Quantizers for Signal with Laplacian Density (Mean = 0, Variance = 1) . . . . .	204
A.5	Optimum Nonuniform Quantizers for Signal with Gaussian Density (Mean = 0, Variance = 1) . . . . .	205
A.6	Optimum Nonuniform Quantizers for Signal with Laplacian Density (Mean = 0, Variance = 1) . . . . .	207
A.7	Compandors for Signal with Gaussian Density (Mean = 0, Variance = 1) . . . . .	209
A.8	Compandors for Signal with Laplacian Density (Mean = 0, Variance = 1) . . . . .	211
A.9I	Analytic Models for Some Often Used Quantizer for Unity Variance Probability Density Functions . . . . .	213
A.9II	Formulas for $h(x)$ for Different Quantizers . . . . .	214
A.10	Optimum Nonuniform Quantizers with Quantization Levels $N = 2, \dots, 36$ for Signal with Gaussian Density (Mean = 0, Variance = 1) . . . . .	215
A.11	Optimum Nonuniform Quantizer with Quantization Levels $N = 2, \dots, 36$ for Signal with Laplacian Density (Mean = 0, Variance = 1) . . . . .	217
A.12	Optimum Uniform Quantizers with Quantization Levels $N = 2, \dots, 36$ for Signal with Gaussian Density (Mean = 0, Variance = 1) . . . . .	219
A.13	Optimum Uniform Quantizers with Quantization Levels $N = 2, \dots, 36$ for Signal with Laplacian Density (Mean = 0, Variance = 1) . . . . .	219
A.14	Compandors with Quantization Levels $N = 2, \dots, 36$ for Signal with Gaussian Density (Mean = 0, Variance = 1) . . . .	220
A.15	Compandors with Quantization Levels $N = 2, \dots, 36$ for Signal with Laplacian Density (Mean = 0, Variance = 1) . . . .	222



## CHAPTER ONE

### INTRODUCTION

#### 1.1 The Problem

Digital image processing has attracted attention and found applications in diverse fields such as transmission of satellite pictures, enhancement of biomedical images, radar, seismic signal communication and many others. Generally speaking, digital image processing deals with two-dimensional data which is first sampled in spatial coordinates and then quantized in brightness. For typical images (used here),  $256 \times 256$  image samples are taken and the brightness is quantized to  $2^8$  levels. This amounts to an equivalent data rate of  $256 \times 256 \times 8 = 5.24 \times 10^5$  bits per image. Based on the current telemetry channel capacity of the order of 16.2 kbits/second [ 10 ], it would take about 32 seconds to transmit  $5.24 \times 10^5$  bits. For many other data sources, such as satellite and biomedical image sources, the data rate are even higher. The large quantities of image data generated for real-time digital processing make it mandatory to consider data compression techniques. Data compression refers to representing an image by as small a number of bits as possible at an acceptable fidelity level.

Most image data are highly redundant, so that compression can be achieved by removing this redundancy before transmission over a communication channel. Data compression schemes for two- and three-dimensional images have been studied by many researchers. One particular class of methods is called statistical data compression where a class of images is characterized by a stochastic process which is described in terms of a mean and covariance function represented by a mathematical model.

Franks [ 12 ] has suggested a model for spectral density of two-dimensional video signals from which a separable covariance function can be developed. Nahi et al [ 48,49 ] and Habibi [ 20 ] and others have used this separable function model for processing images. This model, although mathematically convenient, is not very representative for many images. Jain [ 31 ] has proposed an approach where the image models are obtained by a finite difference approximation of second order partial differential equations (PDEs). This approach offers a rich mathematical basis for formulating and solving many important problems in image processing.

In this research, there are several objectives to be achieved. The primary objective is to further investigate the two-dimensional image models developed by Jain [ 31 ] for intraframe image data compression. The use of image models, i.e., *causal*, *semicausal* and *noncausal*, shows the connection between predictive, hybrid and transform coding schemes. From the choice of an appropriate image model, one would be able to determine an efficient algorithm for data compression. The second objective is to extend these modeling concepts to images which may be viewed as a composition of a stationary field and a deterministic field (e.g., edges which may vary with different images). Therefore, a coding technique can be designed to the sharp brightness changes and also to preserve the nice property of conventional transform coding. This technique is called feature transform coding.

## 1.2 Background Material

There are several important data compression techniques or concepts relevant to this research. They are briefly stated as follows:

### 1.2.1 Differential Pulse Code Modulation (DPCM)

The basic principle of a DPCM system is to quantize and encode the changes between successive samples, rather than the instantaneous sample values. It was first proposed by Cutler [ 9 ] in 1952 that a reduction in quantization noise for the same bit rate could be obtained by taking advantage of the redundancy or correlation between samples. Such correlation exists in practically all signals. It can be shown that the variance of the difference signals is considerably smaller than the variance of the original signals unless there is no correlation between successive samples. Harrison [ 23 ] showed the DPCM concept through the use of prediction theory. Later work published by O'Neal [ 50 ] showed a design procedure for DPCM and its application to television signals. His results gave some verification of modeling video signals by a first order Markov process. Other work related to the design of DPCM systems may be found in [10,45,68]. In our work we will use DPCM schemes in conjunction with transform coding and show their origin in some of the image models.

### 1.2.2 Transform Coding

An ideal transform coding system consists of a unitary, linear mapping of a block of correlated samples into a set of statistically independent coefficients. Data compression is then accomplished by



sorting and quantizing the transform coefficients according to their information capacity.

Andrews and Pratt [ 5 ] introduced the concept of transform coding of images via Fourier transform in 1968, which led to the investigation of utilizing various unitary transforms for image processing [1,3,4,21,26,55,70]. Among the candidates for transform coding, the Karhunen-Loeve transform provides minimum mean square error for any fixed rate. Common image transforms are discrete Fourier, Hadamard, Cosine, Sine, Slant, etc. (refer to Chapter 4).

In our work we will show that a particular class of image models, namely noncausal models, lead naturally to transform coding algorithms. It will be shown that the choice of transform and the coder design parameters are determined via the model parameters.

### 1.2.3 Hybrid (Transform/DPCM) Coding

Hybrid coding is a technique which combines the advantages of transform coding and DPCM coding, which was first proposed by Habibi [ 17 ] for two-dimensional images modeled by a separable covariance function. Subsequently, Roese et al [ 58 ] extended this technique for interframe coding of images. Recursive filtering of two- and three-dimensional images based on hybrid coding concept was proposed by Jain and Angel [ 33 ]. Other studies of hybrid coding schemes can be found in [ 18 ].

In our work, semicausal image models lead naturally to the hybrid coding algorithms and the adaptive and nonadaptive schemes of implementing those algorithms are presented in detail.

#### 1.2.4 Contour Coding and Edge Extraction

Since a significant amount of visual information in an image lies in the edges, it is reasonable to consider coding schemes where the edges are treated more adequately so that the processed image would appear acceptable to a human observer.

In 1958 Schreiber and Graham [15,62-65] introduced an edge coding technique called synthetic highs, in which a scanned video signal is segmented into its high and low frequency components and they are transmitted separately. The high frequency component essentially contains the edge information. At the receiver, the high frequency component is synthesized from the addresses of the image edges and combined with low frequency component to generate the original video signal. Yan and Sakrison [74] proposed a similar scheme where an image is represented by two sources, texture and edge. Image quality can be improved by simply preprocessing with an appropriate method before transmission and postprocessing with its inverse after reception.

Use of image models for segmenting high and low frequency components will be shown in this research where several simulation results are illustrated to show the effectiveness of the new process.

#### 1.3 Organization

Having outlined the background material and the importance of data compression, we can now describe the organization of the thesis. Chapter two provides a general discussion of image models and their properties. The efficiency of these models is measured by comparing their data compression ability in terms of basis restriction errors (for definition see Chapter two). Chapter three is devoted to the development of

Hybrid (Transform/DPCM) coding algorithms. It is shown that the semicausal class of models leads to such algorithms. Four different semicausal models have been considered. Adaptive schemes are designed by simply adapting the model parameters to cope with the changes in image statistics. The effect of a noisy transmission channel on the Hybrid coding system is also studied. It is shown that the semicausal image models may be used to develop a Hybrid coding system for compression of noisy images. In Chapter four, we show how the noncausal image models may be used to design transform coders. Adaptive and nonadaptive algorithms are considered. In Chapter five, we extend the algorithms of Chapter four to represent images as a composition of two sources. One of the sources is a stationary component and the other is a nonstationary or deterministic component. Examples of computer simulation of all the algorithms on image data are given and comparisons are made.

Finally, the Appendices contain the derivation and proofs that relate to various topics throughout the thesis. In particular, Appendix A provides useful tabulated data for various quantizers and serves as a good reference for engineers interested in designing quantizers for image processing applications.



## CHAPTER TWO

### DISCRETE GAUSSIAN RANDOM FIELDS AND STOCHASTIC IMAGE MODELS

#### 2.1 Introduction

In discussing image representations, we think of characterizing images as two-dimensional random fields. If  $D$  is a constant coefficient difference equation operator, we consider representations of the form

$$D[u_{ij}] = \epsilon_{ij} \quad (2.1-1)$$

where  $\{u_{ij}\}$  denotes the array of image pixels,  $\{\epsilon_{ij}\}$  is a two dimensional white noise process or a moving average field.

In this chapter, we consider causal, semicausal and noncausal representations which are of the form of (2.1-1). These representations, as we will see in Chapters 3, 4 and 5, will aid in developing useful algorithms for many image coding problems. Here we will study data compression efficiency of these models measured by the basis restriction error.

#### 2.2 Causal, Semicausal and Noncausal Estimates

Let  $\{u_{i,j}\}$  represent a zero mean, stationary two-dimensional discrete Gaussian random field whose covariance function is defined as

$$E u_{i,j} u_{i+k,j+l} = r(k,l) . \quad (2.2-1)$$

Let  $\bar{u}_{i,j}$  denote an estimate of the random variable  $u_{i,j}$ . We consider the following three types of estimates.

##### 2.2.1 Causal Estimate

Suppose the elements of the random field  $\{u_{i,j}\}$  are arranged in any

desired, one-dimensional, ordered sequence. Then  $\bar{u}_{i,j}$  is a causal estimate of  $u_{i,j}$  if it depends only on the elements that occur before the element  $u_{i,j}$ . A common example occurs when the image is scanned column by column and  $\bar{u}_{i,j}$  is a linear estimate based on all the elements scanned before arriving at  $(i,j)$ , i.e.,

$$\bar{u}_{i,j} = \sum_{m,n \in S} a(m,n) u_{i-m,j-n} \quad (2.2.1-1)$$

where  $S = \{m,n: n > 0, \forall m\} \cup \{m,n: n = 0, m > 0\}$ . Fig. 2.1(a) shows the set  $S$  for causal estimate at  $(i,j)$ .

### 2.2.2 Semicausal Estimate

If the estimate  $\bar{u}_{i,j}$  is causal in one of the coordinates and noncausal in the other, it is called a semicausal estimate. For example, a linear semicausal estimate which is causal in "j" and noncausal in "i" would be of the form

$$\bar{u}_{i,j} = \sum_{m,n \in S} a(m,n) u_{i-m,j-n} \quad (2.2.2-1)$$

where  $S = \{m,n: n > 0, \forall m\} \cup \{m,n: n = 0, \forall m \neq 0\}$  and is shown in Fig. 2.1(b).

### 2.2.3 Noncausal Estimate

The quantity  $\bar{u}_{i,j}$  is a linear noncausal estimate of  $u_{i,j}$  if it can be written as a linear function of possibly all the variables in the random field, except  $u_{i,j}$  itself. For example, a linear noncausal estimate would be of the type

$$\bar{u}_{i,j} = \sum_{m,n \in S} a(m,n) u_{i-m,j-n} \quad (2.2.3-1)$$

where  $S = \{m,n: \forall(m,n) \neq (i,j)\}$  and is shown in Fig. 2.1(c). Note that  $\bar{u}_{i,j}$  contains terms from all the four quadrants about the point  $(i,j)$ .

### 2.3 Stochastic Representations of Gaussian Random Field

Let  $\bar{u}_{i,j}$  be an arbitrary estimate of  $u_{i,j}$ , then a stochastic representation of the Gaussian random field  $\{u_{i,j}\}$  is defined as

$$u_{i,j} = \bar{u}_{i,j} + \epsilon_{i,j} \quad (2.3-1)$$

where  $\{\epsilon_{i,j}\}$  is another random field.

There are two types of representations which are of interest to be considered here. These are as follows:

- 1) Minimum variance representation.
- 2) White noise driven representation.

#### 2.3.1 Minimum Variance Representation

A minimum variance estimate is one which minimizes the mean square error

$$e_{i,j} = E(u_{i,j} - \bar{u}_{i,j})^2 \quad (2.3.1-1)$$

at each  $(i,j)$ . For Gaussian random field, the minimum variance estimate would be linear. The coefficients  $a(m,n)$  in (2.2.1-1), (2.2.2-1) or (2.2.3-1) could be determined from the covariance function  $r(k,l)$  and the orthogonality relation



$$E(u_{i,j} - \bar{u}_{i,j})u_{p,q} = E\left[u_{i,j} - \sum_{m,n \in S} a(m,n)u_{i-m,j-n}\right]u_{p,q} = \beta_{i,j}^2 \delta_{i,p} \delta_{j,q}$$

$$\text{for all } p, q \in \hat{S}. \quad \hat{S} = SU(i, j) \quad (2.3.1-2)$$

where  $S$  depends on whether  $\bar{u}_{i,j}$  is causal, semicausal or noncausal, and  $\beta_{i,j}^2$  is defined to be the minimized value of  $e_{i,j}$  of (2.3.1-1).

For minimum variance representation,  $\bar{u}_{i,j}$  is chosen to be a minimum variance estimate. This representation could be causal, semicausal or noncausal in its spatial structure.

### 2.3.2 White Noise Driven Representation

A white noise random field  $\{x_{i,j}\}$  is defined as one whose elements are mutually uncorrelated, i.e.,

$$Ex_{i,j}x_{k,l} = \beta_{i,j}^2 \delta_{i,k} \delta_{j,l}. \quad (2.3.2-1)$$

For white noise driven representation,  $\{e_{i,j}\}$  in (2.3-1) is chosen to be a white noise random field.

### 2.4 Spectral Density Functions of the Gaussian Random Field Represented by Linear Models

Consider the stationary Gaussian random field  $\{u_{i,j}\}$  defined on the infinite plane,  $-\infty < i, j < \infty$ . The two-dimensional z-transform\* of the covariance function, called the covariance generating function, is defined as

\* Two-dimensional z-transform is defined as

$$F(z_1, z_2) = \sum_{i=-\infty}^{\infty} \sum_{j=-\infty}^{\infty} f(i, j) z_1^{-i} z_2^{-j}.$$

$$S_u(z_1, z_2) = \sum_{k=-\infty}^{\infty} \sum_{\ell=-\infty}^{\infty} r(k, \ell) z_1^{-k} z_2^{-\ell} \quad (2.4-1)$$

Substituting  $e^{j\omega_1}$  and  $e^{j\omega_2}$  for  $z_1$  and  $z_2$ , respectively, we have

$$S_u(\omega_1, \omega_2) = S_u(z_1, z_2) \Big|_{z_1 = e^{j\omega_1}, z_2 = e^{j\omega_2}} \quad (2.4-2)$$

This becomes the spectral density function (SDF) of  $\{u_{i,j}\}$ . For simplicity, we refer to  $S_u(z_1, z_2)$  as the spectral density function of the Gaussian random field  $\{u_{i,j}\}$  at various places in the following chapters without further notification.

The discrete operator of (2.1-1) can be written as

$$D(z_1, z_2) = 1 - \sum_{m,n \in S} a(m,n) z_1^{-m} z_2^{-n} \quad (2.4-3)$$

If  $S_e(z_1, z_2)$  is the spectral density function of  $\{e_{i,j}\}$ , then the spectral density function of  $\{u_{i,j}\}$  is given by

$$S_u(z_1, z_2) = \frac{S_e(z_1, z_2)}{D(z_1, z_2) D(z_1^{-1}, z_2^{-1})} \quad (2.4-4)$$

The covariance function of  $\{u_{i,j}\}$  is obtained simply by the inverse Fourier transform of  $S_u(z_1, z_2)$

$$R(k, \ell) = \frac{1}{4\pi^2} \int_0^{2\pi} \int_0^{2\pi} S_u(\omega_1, \omega_2) \exp(j\omega_1 k + j\omega_2 \ell) d\omega_1 d\omega_2 \quad (2.4-5)$$

## 2.5 Image Representations

Now we consider different types of random field representations as candidates for image modeling.

### 2.5.1 Causal Representations

The general form of causal representations of an image field is given by

$$u_{i,j} = \bar{u}_{i,j} + \epsilon_{i,j} \quad (2.3-1)$$

where  $\bar{u}_{i,j}$  is the causal estimate of  $u_{i,j}$  defined in (2.2.1-1).

As an example, one causal representation is of the type

$$u_{i,j} = a_1 u_{i-1,j} + a_2 u_{i,j-1} + a_3 u_{i-1,j-1} + \epsilon_{i,j} \quad (2.5.1-1)$$

whose spatial structure is depicted in Table 2.1 and it is obvious that  $u_{i,j}$  is causally related with three points which occurred at the left upper quadrant. It has been shown that this equation and other similar causal representations can be obtained by discrete approximation of hyperbolic partial differential equations [34].

Using the spatial structure and measured covariances of a given image field, one may identify the coefficients  $a_1$ ,  $a_2$ ,  $a_3$  and the random field  $\{\epsilon_{i,j}\}$  via least square regression techniques. For the covariance function

$$r(k,\ell) = E u_{i,j} u_{i+k,j+\ell} = \rho_1^{|k|} \rho_2^{|\ell|} \quad (2.5.1-2)$$

where  $\rho_1$  and  $\rho_2$  are the vertical and horizontal correlations respectively.



The model of (2.5.1-1) is its exact realization when

$$a_1 = \rho_1, a_2 = \rho_2, a_3 = -\rho_1 \rho_2 \quad (2.5.1-3)$$

and  $\{\epsilon_{i,j}\}$  is a white noise field with zero mean and covariance function

$$E \epsilon_{i,j} \epsilon_{i+k,j+l} = \beta^2 \delta_{k,0} \delta_{l,0}, \quad \beta^2 = (1-\rho_1^2)(1-\rho_2^2). \quad (2.5.1-4)$$

The corresponding discrete operator and spectral density function of (2.5.1-1) subject to (2.5.1-3) are given as follows:

$$D(z_1, z_2) = (1-\rho_1 z_1^{-1})(1-\rho_2 z_2^{-1}) \quad (2.5.1-5a)$$

$$S_e(z_1, z_2) = \beta^2 = (1-\rho_1^2)(1-\rho_2^2) \quad (2.5.1-5b)$$

$$S_u(z_1, z_2) = \frac{\beta^2}{(1-\rho_1 z_1^{-1})(1-\rho_1 z_1^{-1})(1-\rho_2 z_2^{-1})(1-\rho_2 z_2^{-1})} \quad (2.5.1-5c)$$

In image processing literature, this model has been used for differential PCM and filtering of images [34].

## 2.5.2 Semicausal Representations

A semicausal representation is causal in one of the image coordinates (say,  $j$ ) and is noncausal in the other (say,  $i$ ). For example,

$$u_{i,j} = \alpha(u_{i-1,j} + u_{i+1,j}) + \gamma u_{i,j-1} + \epsilon_{i,j} \quad (2.5.2-1)$$

$$\text{where } |\alpha| < \frac{1}{2}, |\gamma| < 1 \text{ and } |2\alpha + \gamma| < 1. \quad (2.5.2-1a)$$

This is a semicausal representation of the Gaussian random field. Conditions of (2.5.2-1a) insure the stability of (2.5.2-1). The covariance function generated by this equation depends on the covariance

function chosen for the random field  $\{\epsilon_{i,j}\}$ . For example, when  $\{\epsilon_{i,j}\}$  is a white noise field, i.e.,

$$r_{\epsilon}(k,l) = E\epsilon_{i,j}\epsilon_{i+k,j+l} = \beta^2\delta_{k,0}\delta_{l,0}. \quad (2.5.2-2)$$

The spectral density function of  $\{u_{i,j}\}$  is then given by

$$S_u(z_1, z_2) = \frac{\beta^2}{(1-\alpha z_1 - \alpha z_1^{-1} - \gamma z_2)(1-\alpha z_1^{-1} - \alpha z_1 - \gamma z_2^{-1})}. \quad (2.5.2-3)$$

This white noise driven representation will be called the white noise driven SCl model.

As a generalization, consider the case when  $\{\epsilon_{i,j}\}$  has its covariance function given by

$$r_{\epsilon}(k,l) = E\epsilon_{i,j}\epsilon_{i+k,j+l} = \beta^2\delta_{l,0}(\delta_{k,0} - \alpha_1\delta_{k-1,0} - \alpha_1\delta_{k+1,0}). \quad (2.5.2-4)$$

The corresponding SDFs are given by

$$S_{\epsilon}(z_1, z_2) = \beta^2[1 - \alpha_1(z_1 + z_1^{-1})] \quad (2.5.2-5a)$$

$$S_u(z_1, z_2) = \frac{S_{\epsilon}(z_1, z_2)}{(1-\alpha z_1 - \alpha z_1^{-1} - \gamma z_2)(1-\alpha z_1^{-1} - \alpha z_1 - \gamma z_2^{-1})}. \quad (2.5.2-5b)$$

For  $\alpha_1 = 0$ , (2.5.2-3) results, we have white noise driven model.

For  $\alpha_1 = \alpha$ , the quantity [see (2.5.2-1)]

$$u_{i,j}^* = \alpha(u_{i-1,j} + u_{i+1,j}) + \gamma u_{i,j-1} \quad (2.5.2-6)$$

becomes the best linear mean square estimate of  $u_{i,j}$  given  $k, l$  belonging to

$$S = \{k, l: l < j, \forall k\} \cup \{k, l: l = j, \forall k \neq i\}.$$

This follows by observing that the orthogonality relation

$$Eu_{i,j}^* (u_{i,j} - u_{i,j}^*) = Eu_{i,j}^* \epsilon_{i,j} = 0, \forall i,j \quad (2.5.2-7)$$

is satisfied when  $\alpha_1 = \alpha$ .

Then (2.5.2-1) becomes a minimum variance SC1 representation, since  $E(u_{i,j} - u_{i,j}^*)^2$  is minimum over the set of lattice points of  $S$ . The spectral density function of the minimum variance semicausal representation is obtained by setting  $\alpha_1 = \alpha$  in (2.5.2-5).

It has been shown by Jain [ 28 ] that the separable covariance function [see (2.5.1-2)] has a semicausal minimum variance realization given by

$$u_{i,j} = \alpha_1(u_{i-1,j} + u_{i+1,j}) - \rho_2 \alpha_1(u_{i-1,j-1} + u_{i+1,j-1}) + \rho_2 u_{i,j-1} \epsilon_{i,j} \quad (2.5.2-8)$$

where  $\{\epsilon_{i,j}\}$  is chosen to have its covariance given as

$$r_\epsilon(k, \ell) = \frac{(1-\rho_1^2)(1-\rho_2^2)}{(1+\rho_1^2)} \delta_{\ell,0} (-\alpha_1 \delta_{k,-1} - \alpha_1 \delta_{k,1} + \delta_{k,0}) \quad (2.5.2-9)$$

and

$$\alpha_1 = \frac{\rho_1}{1+\rho_1^2}$$

with corresponding SDF

$$S_\epsilon(z_1, z_2) = \frac{(1-\rho_1^2)(1-\rho_2^2)}{(1+\rho_1^2)} (1-\alpha_1 z_1 - \alpha_1 z_1^{-1}) . \quad (2.5.2-10)$$

This will be called the minimum variance SC2 representation.

Interestingly, the spectral density function  $S_u(z_1, z_2)$  of this minimum variance SC2 representation and that of the white noise driven C1 representation are identical. For more general minimum variance semicausal models, see [ 34 ].



The semicausal representations will be shown to lead some useful hybrid algorithms for image coding. A hybrid algorithm is a recursive algorithm obtained after transforming each row (or column) of the image by a unitary transformation. Note that above mentioned semicausal representations can also be obtained by discrete difference approximation of parabolic partial differential equations [ 34 ].

### 2.5.3 Noncausal Representations

The noncausal representations are boundary value problems in each coordinate and have correspondence with the elliptic class of partial differential equations (PDEs) [ 34 ]. For example, the noncausal representation (NC1)

$$u_{i,j} = \alpha(u_{i-1,j} + u_{i+1,j} + u_{i,j-1} + u_{i,j+1}) + \epsilon_{i,j}, \quad |\alpha| < \frac{1}{4} \quad (2.5.3-1)$$

is a discrete approximation of a Poisson PDE.

In general,  $\{\epsilon_{i,j}\}$  may be chosen such that

$$r_{\epsilon}(k,l) = E\epsilon_{i,j}\epsilon_{i+k,j+l} = \beta^2[\delta_{k,0}\delta_{l,0} - \alpha_1(\delta_{k,-1} + \delta_{k,1})\delta_{l,0} - \alpha_1(\delta_{l,-1} + \delta_{l,1})\delta_{k,0}] , \quad |\alpha_1| < \frac{1}{4} \quad (2.5.3-2)$$

The spectral density functions for  $\{\epsilon_{i,j}\}$  and  $\{u_{i,j}\}$  are then obtained as

$$S_{\epsilon}(z_1, z_2) = \beta^2[1 - \alpha_1(z_1 + z_1^{-1} + z_2 + z_2^{-1})] \quad (2.5.3-3)$$

$$S_u(z_1, z_2) = \frac{S_{\epsilon}(z_1, z_2)}{[1 - \alpha(z_1 + z_1^{-1} + z_2 + z_2^{-1})]^2} . \quad (2.5.3-4)$$

There are three types of NCI models to be considered here.

- a.  $\alpha_1 = 0$ .  $\{e_{i,j}\}$  becomes a white noise process and (2.5.3-1) is a white noise driven NCI representation.
- b.  $\alpha_1 = \alpha$ , we get the minimum variance NCI representation. Note that in the spectral density function  $S_u$  a pole-zero cancellation occurs and the  $S_u$  becomes

$$S_u(z_1, z_2) = \frac{\beta^2}{[1 - \alpha(z_1 + z_1^{-1} + z_2 + z_2^{-1})]} \quad (2.5.3-5)$$

- c. For  $\alpha_1 \neq \alpha$ , (2.5.3-1) may be considered as a noncausal autoregressive moving average (ARMA) model, denotes a NCI ARMA model. According to Jain [ 34 ], model identification experiments have shown for several images (for example, Girl, Moon and Earth) that this model gives a better fit to the real data than the previous two models.

Another type of noncausal representation can be derived from a biharmonic PDE [ 34 ], and gives a 13-neighbor model

$$u_{i,j} = a(u_{i-1,j} + u_{i+1,j} + u_{i,j-1} + u_{i,j+1}) - a\alpha(u_{i-1,j-1} + u_{i-1,j+1} + u_{i+1,j-1} + u_{i+1,j+1}) - \frac{a\alpha}{2}(u_{i-2,j} + u_{i+2,j} + u_{i,j-2} + u_{i,j+2}) + \frac{\epsilon_{i,j}}{(1+4\alpha^2)} \quad (2.5.3-6)$$

$$\text{where } a = \frac{2\alpha}{(1+4\alpha^2)}.$$

If covariances of  $\{\epsilon_{i,j}\}$  are taken as

$$r_{\epsilon}(k, l) = E\epsilon_{i,j}\epsilon_{i+k,j+l} = \beta^2 \begin{cases} -a_1 & , \text{ if } l = \pm 1, k=0 \text{ or } l=0, k = \pm 1 \\ a_1\alpha_1 & , \text{ if } l = \pm 1, k = \pm 1 \\ \frac{a_1\alpha_1}{2} & , \text{ if } l = \pm 2, k=0 \text{ or } k = \pm 2, l=0 \\ 1 & , \text{ if } k=l=0 \\ 0 & , \text{ otherwise} \end{cases}$$

$$\text{where } |a_1| < \frac{2}{5}, \quad |\alpha_1| < \frac{1}{4}; \quad (2.5.3-7)$$

$$\text{then, for } a_1 = a, \quad \alpha_1 = \alpha$$

Eqn. (2.5.3-6) becomes a minimum variance NC2 representation. Spectral density functions for this mode are given by

$$S_{\epsilon}(z_1, z_2) = \beta^2 [1 - \alpha_1(z_1 + z_1^{-1} + z_2 + z_2^{-1})]^2 \quad (2.5.3-8)$$

$$S_u(z_1, z_2) = \frac{S_{\epsilon}(z_1, z_2)}{[1 - \alpha(z_1 + z_1^{-1} + z_2 + z_2^{-1})]^4} \quad (2.5.3-9)$$

The noncausal representations discussed above often realize nearly isotropic  $S_u(z_1, z_2)$ .

Not all noncausal models give near-isotropic random fields. For example, consider the noncausal model (NC3)

$$u_{i,j} = \alpha_1(u_{i-1,j} + u_{i+1,j}) + \alpha_2(u_{i,j-1} + u_{i,j+1}) - \alpha_1\alpha_2(u_{i+1,j+1} + u_{i+1,j-1} + u_{i-1,j+1} + u_{i-1,j-1}) + \epsilon_{i,j} \quad (2.5.3-10)$$

If the covariances of  $\{\epsilon_{i,j}\}$  are given by



$$r_{\epsilon}(k, l) = E\epsilon_{i,j}\epsilon_{i+k,j+l} = \beta^2 \begin{cases} 1, & \text{if } k=l=0 \\ -\alpha_1, & \text{if } k= \pm 1, l=0 \\ -\alpha_2, & \text{if } k=0, l= \pm 1 \\ \alpha_1\alpha_2, & \text{if } k= \pm 1, l= \pm 1 \\ 0, & \text{otherwise} \end{cases} \quad (2.5.3-11)$$

$$\text{where } \beta^2 = \frac{(1-\rho_1^2)(1-\rho_2^2)}{(1+\rho_1^2)(1+\rho_2^2)}, \quad \alpha_1 = \frac{\rho_1}{(1+\rho_1^2)}, \quad \alpha_2 = \frac{\rho_2}{(1+\rho_2^2)}.$$

SDFs of (2.5.3-10) are given by

$$S_{\epsilon}(z_1, z_2) = \frac{\beta^2}{[1 - \alpha_1(z_1 + z_1^{-1})][1 - \alpha_1(z_2 + z_2^{-1})]} \quad (2.5.3-12)$$

$$S_u(z_1, z_2) = \frac{(1-\rho_1^2)(1-\rho_2^2)}{(1-\rho_1 z_1)(1-\rho_1 z_1^{-1})(1-\rho_2 z_2)(1-\rho_2 z_2^{-1})}. \quad (2.5.3-13)$$

Notice that the form of  $S_u(z_1, z_2)$  is the same as the SDF of causal DPCM C1 model and semicausal SC2 model, so it generates the separable covariance model which is non-isotropic.

## 2.6 Basis Restriction Data Compression Efficiency of Image Models

The performance of the foregoing image models in image data compression can be analyzed by studying their basis restriction efficiency. The scheme is shown in Fig. 2.2. First, the original image  $\{u_{i,j}\}$  is transformed by a unitary matrix  $A$  (see Chapter 4, the definition of transformation). Next, a two-dimensional sample selection function  $\{w(i,j)\}$  (also called zonal filter), which at each  $(i,j)$  takes on the

value of zero or one, is applied to the transformed image  $\{v_{i,j}\}$ . Only those samples for which  $\{w(i,j)=1\}$  are stored, zeros placed at other locations. This zonal filtered image  $\{\hat{v}_{i,j}\}$  is inverse transformed by  $A^{-1}$  to give  $\{\hat{u}_{i,j}\}$ .

The basis restriction mean square error (B.R.M.S.E.) is defined as

$$\begin{aligned} \text{B.R.M.S.E.} &= \frac{\sum_i \sum_j E (u_{i,j} - \hat{u}_{i,j})^2}{\sum_i \sum_j u_{i,j}^2} \\ &= \frac{\sum_i \sum_j E (v_{i,j} - \hat{v}_{i,j})^2}{\sum_i \sum_j v_{i,j}^2} \\ &= \frac{\sum_i \sum_j E [v_{i,j} (1 - w(i,j))]^2}{\sum_i \sum_j v_{i,j}^2} \quad (2.6-1) \end{aligned}$$

where we have used the fact that  $A$  is a unitary transform. Associated with this error is the sample reduction ratio (S.R.R.)

$$\text{S.R.R.} = \frac{\text{Number of image samples}}{\text{Number of samples selected by zonal filter}} \quad (2.6-2)$$

This ratio is a measure of data compression.

#### 2.6.1 Zonal Filter Design

The zonal filter  $w(i,j)$  is designed as follows.

1. Let  $t_n$  be the number of samples to be selected for transmission for a given S.R.R. Clearly  $t_n = NM/\text{S.R.R.}$  for an  $M \times N$  image.
2. Find the variances  $\sigma_{m,n}^2$  of the transformed image samples  $v_{m,n}$ . If  $A$  is the DFT, and  $N$  is large, an estimate of  $\sigma_{m,n}^2$  is

$$\sigma_{m,n}^2 = \begin{cases} s_u\left(\frac{2\pi m}{M}, \frac{2\pi n}{N}\right) & , \quad 0 \leq |m| \leq \frac{M}{2}, 0 \leq |n| \leq \frac{N}{2} \\ \sigma_{M-m, N-n}^2 & , \quad \text{otherwise} \end{cases}$$

3. Arrange  $\sigma_{m,n}^2$  in a decreasing order. Then  $w(m,n) = 1$  for the first  $t_n$  addresses  $(m,n)$  and  $w(m,n) = 0$  otherwise.

Since  $w(m,n)$  depend on  $\sigma_{m,n}^2$  or the SDF, the zonal filter functions will be different for different image models.

### 2.6.2 Experimental Results

For easy reference, all the image representations (models) presented in Section 2.5 are summarized in Table 2.1. It is seen that various partial differential equation (PDE) operators are also listed. Table 2.2 shows model parameters used for three different images. These parameters were found by least square matching of the  $16 \times 16$  image covariances with the model covariances.

Simple basis restriction error experiments have been performed to compare the various image models for the Girl and Earth images. We have used the discrete Fourier transform to be the unitary transform operator. Since the image models differ in their SDFs, in the transform domain, the variances of the samples  $v_{1,j}$  will have different distributions. Figs. 2.3 - 2.5 show the zonal filters at various sample reduction ratios for causal, semicausal and noncausal models. Table 2.3 lists the results of basis restriction mean square error versus image block size for the Girl image. Table 2.5 lists the corresponding results for the Earth image. Figs. 2.6 - 2.7 show the plots of basis restriction errors versus



sample reduction ratios. In general, basis restriction error of the noncausal model is lower for most sample reduction ratios (indicating its superior fitting of the image data than the other two types of models. For very large sample reduction ratios, since few transform domain image pixels are transmitted, all the models select the same pixels (see Figs. 2.6 - 2.7)).

The above conclusion could also be drawn from Figs. 2.8 and 2.9, which show the Basis Restriction Data Compression of Girl and Earth images using a  $16 \times 16$  image block size. Clearly, noncausal models give the best results followed by semicausal models.

## 2.7 Summary and Conclusions

In summary, several image representations have been considered. They originate from finite difference approximations of certain PDEs. These models have been compared on the basis of their data compression efficiency based on a basis restriction error criterion.

The following conclusions are made.

1. The models C1, SC2 and NC3 all generate random fields whose covariance functions are the same as the separable model [see (2.5.1-2)].
2. For  $\alpha_1 = \alpha$ , the spectral density of NC2 is the same as that of NC1 for  $\alpha_1 = 0$ . However, NC2 is a minimum variance noncausal representation, whereas NC1 is a white noise driven model.
3. In a data compression application, the noncausal models give the best performance. A similar conclusion has been made in image filtering applications [34].

4. Figs. 2.3 - 2.5 could be interpreted as the spectral density function indicators. Different types of image models would achieve different shapes of spectral density functions. Figs. 2.3 - 2.5 show the contours of approximately equal spectrum values.
5. Higher order models may be needed to represent image SDFs more accurately. Identification of such models remains an open problem.

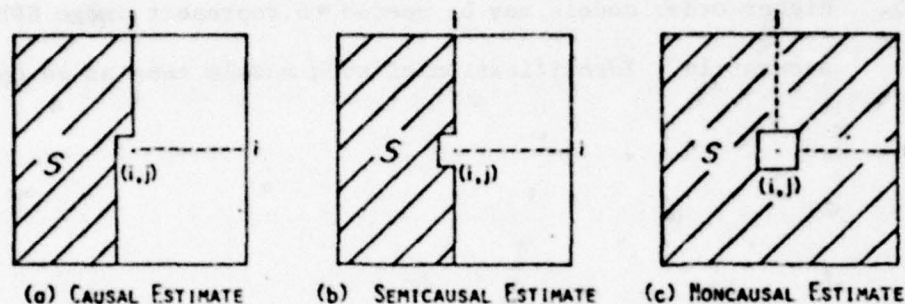


Figure 2.1 The Region  $S$  for Estimating  $(i, j)$

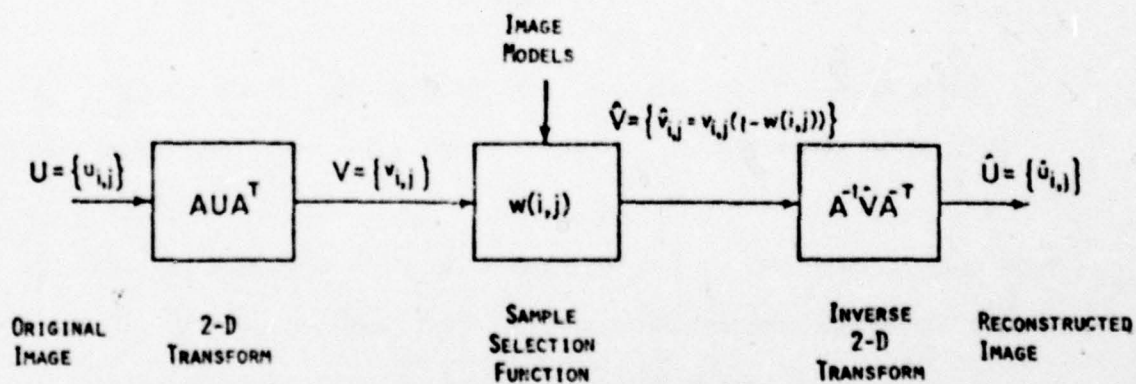


Figure 2.2 Basis Restriction Efficiency Implementation



(a) 2:1 Sample Reduction

(b) 4:1 Sample Reduction

(c) 8:1 Sample Reduction

(d) 16:1 Sample Reduction

25





### (a) 2:1 Sample Reduction

### (c) 8:1 Sample Reduction

(b) 4:1 Sample Reduction

(d) 16:1 Sample Reduction

27



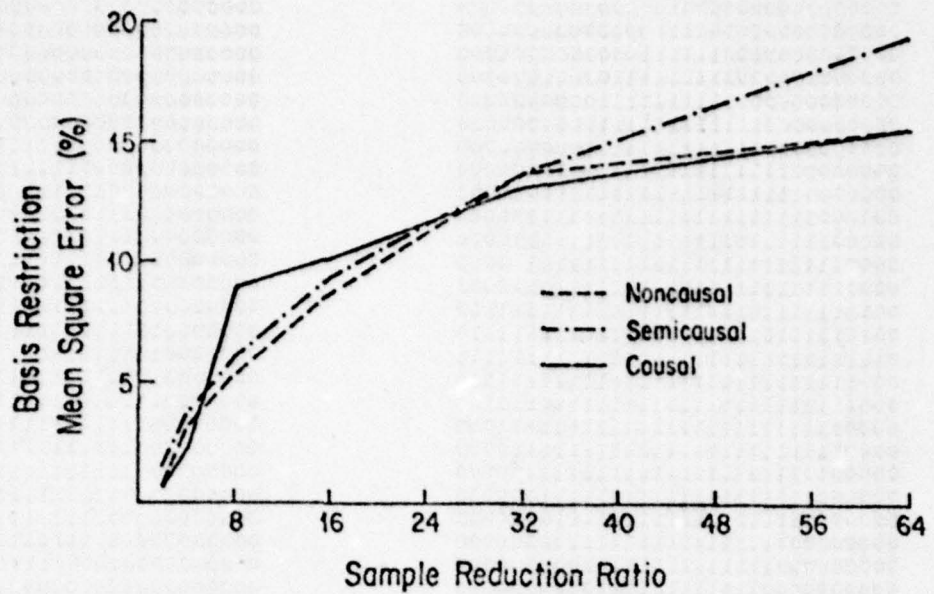


Figure 2.6 Basis Restriction Mean Square Error versus Sample Ratio for the Fourier Transform Model Zonal Sampling of a  $256 \times 256$  Girl Image with  $16 \times 16$  Image Block Size

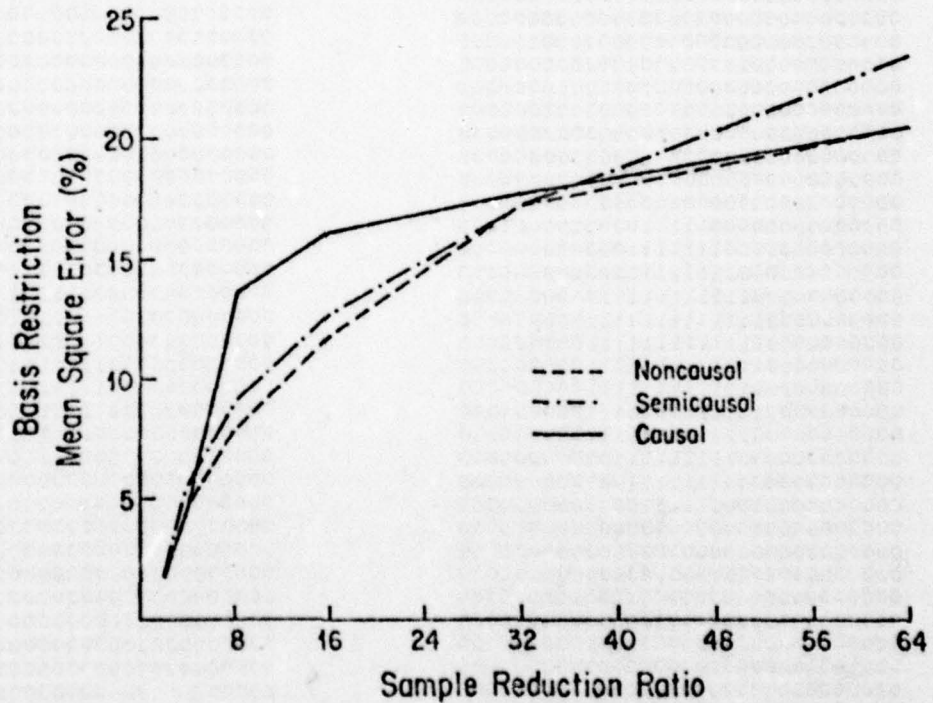


Figure 2.7 Basis Restriction Mean Square Error versus Sample Reduction Ratio for the Fourier Transform Model Zonal Sampling of a  $256 \times 256$  Earth Image with  $16 \times 16$  Image Block Size



(a) NC1, NC2-A, NC2-B,  
8:1 Sample Reduction



(d) NC1, NC2-A, NC2-B,  
16:1 Sample Reduction



(b) SC1,  
8:1 Sample Reduction



(e) SC1,  
16:1 Sample Reduction



(c) C1,  
8:1 Sample Reduction



(f) C1,  
16:1 Sample Reduction

Figure 2.8 Fourier Transform Model Zonal Sampled Girl Image with  
16 x 16 Image Block Size



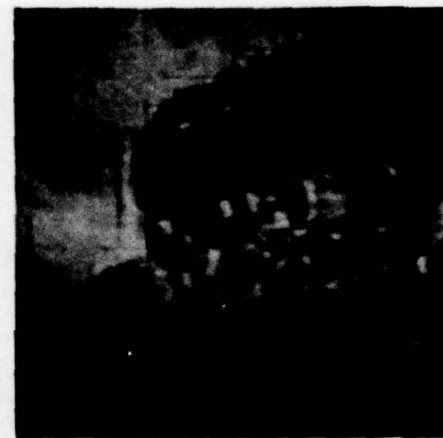
(a) NC1, NC2-A, NC2-B,  
8:1 Sample Reduction



(d) NC1, NC2-A, NC2-B,  
16:1 Sample Reduction



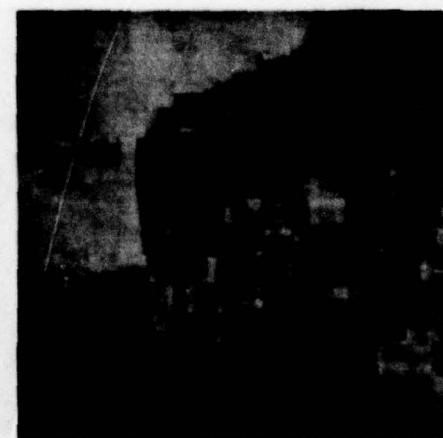
(b) SC1,  
8:1 Sample Reduction



(e) SC1,  
16:1 Sample Reduction



(c) C1,  
8:1 Sample Reduction



(f) C1,  
16:1 Sample Reduction

Figure 2.9 Fourier Transform Model Zonal Sampled Earth Image with



Table 2.1 Summary of Some PDF Models and Their Discrete Approximates  $D[u] = \epsilon$  Used for Image Modeling




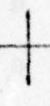


Model	PDF Operator	Discrete Operator $D(z_1, z_2)$	Spectral Density of $\epsilon$ $S_\epsilon(z_1, z_2)$	Spectral Density of $u$ $S_u(z_1, z_2)$	Spatial Structure	Comments
Causal C1	$\frac{\partial^2}{\partial x \partial y} + a_1 \frac{\partial}{\partial x} + a_2 \frac{\partial}{\partial y} + a_3$	$(1 - pz_1^{-1})(1 - pz_2^{-1})$	$(1 - \sigma^2)^2 = \beta^2$	$\frac{(1 - \sigma^2)^2}{(1 - \sigma z_1^{-1})(1 - \sigma z_2^{-1})}$		Hyperbolic wave equation Covariance $R(k, l) = \sigma^2  k  +  l $
Semicausal SC1	$\frac{\partial}{\partial y} + a_1 \frac{\partial^2}{\partial x^2} + a_1$	$1 - \sigma z_1^{-1} - \sigma z_1^{-1} \gamma_2^{-1}$	$\beta^2$	$\frac{\beta^2}{(1 - \sigma z_1^{-1} - \gamma_2^{-1})(1 - \sigma z_1^{-1} - \sigma z_1^{-1} \gamma_2^{-1})}$		Parabolic diffusion equation White noise driven model
Semicausal SC2	$(\frac{\partial^2}{\partial x^2} + a_1)(\frac{\partial}{\partial y} + a_2)$	$1 - \sigma(1 - pz_2^{-1})(z_1^{-1} - \sigma z_1^{-1}) - \sigma z_2^{-1}$	$\beta^2 [1 - \sigma(z_1^{-1} + z_2^{-1})]$	Same as C1		$\sigma = \frac{\epsilon}{1 + \beta^2} \cdot \beta^2 = \frac{(1 - \sigma^2)^2}{(1 + \sigma^2)}$ Minimum variance model
Noncausal NC1	$\frac{\partial^2}{\partial x^2} + \frac{\partial^2}{\partial y^2} + a_1$	$1 - \sigma(z_1^{-1} + z_2^{-1} + z_1 z_2^{-1})$	$\beta^2 [1 - \sigma(z_1^{-1} + z_2^{-1} + z_1 z_2^{-1})]$	$\frac{\beta^2 [1 - \sigma(z_1^{-1} + z_2^{-1} + z_1 z_2^{-1})]}{[1 - \sigma(z_1^{-1} + z_2^{-1} + z_1 z_2^{-1})]^2}$		Elliptic potential equation Minimum variance model when $\sigma_1 = \sigma$
Noncausal NC2	$(\frac{\partial^2}{\partial x^2} + \frac{\partial}{\partial y})^2 + a_1$	$[1 - \sigma(z_1^{-1} + z_2^{-1} + z_1 z_2^{-1})]^2$	$\beta^2 [1 - \sigma(z_1^{-1} + z_2^{-1} + z_1 z_2^{-1})]^2$	$\frac{\beta^2 [1 - \sigma(z_1^{-1} + z_2^{-1} + z_1 z_2^{-1})]^2}{[1 - \sigma(z_1^{-1} + z_2^{-1} + z_1 z_2^{-1})]^4}$		Elliptic biharmonic equation Minimum variance model when $\sigma_1 = \sigma$ NC2-A when $\sigma_1 = \sigma$ NC2-B when $\sigma_1 = 0$
Noncausal XC3	$(\frac{\partial^2}{\partial x^2} + a_1)(\frac{\partial^2}{\partial y^2} + a_2)$	$[1 - \sigma(z_1^{-1} + z_2^{-1})][1 - \sigma(z_2^{-1} + z_1^{-1})]$	$\beta^2 [1 - \sigma(z_1^{-1} + z_2^{-1})][1 - \sigma(z_2^{-1} + z_1^{-1})]$	Same as C1		$\beta^2 = \frac{(1 - \sigma^2)^2}{(1 + \sigma^2)^2} \cdot \sigma = \frac{\epsilon}{1 + \beta^2}$ Minimum variance model

Table 2.2 Actual Parameters Measured for Various Models of the  $256 \times 256$  Image to Match the  $16 \times 16$  Covariance Matrix of the Image

Image	Model	Parameters	l.s.e.%
Girl	C1	$\rho = 0.962$	0.720
	SC1	$\alpha = 0.4275, \gamma = 0.1415, \beta^2 = 0.0198$	0.162
	SC2	$\rho = 0.962, \alpha = 0.49963, \beta^2 = 0.0029$	0.720
	NC1	$\alpha = 0.2494, \alpha_1 = 0.95\alpha, \beta^2 = 0.0744$	0.377
	NC2-A	$\alpha = 0.2494, \alpha_1 = \alpha, \beta^2 = 0.0053$	0.598
	NC2-B	$\alpha = 0.2476, \alpha_1 = 0, \beta^2 = 8 \times 10^{-6}$	1.697
	NC3	$\rho = 0.962, \alpha = 0.49963, \beta^2 = 0.0015$	0.720
Earth	C1	$\rho = 0.968$	0.891
	SC1	$\alpha = 0.4275, \gamma = 0.1420, \beta^2 = 0.0169$	0.572
	SC2	$\rho = 0.968, \gamma = 0.49974, \beta^2 = 0.0020$	0.891
	NC1	$\alpha = 0.24966, \alpha_1 = 0.95\alpha, \beta^2 = 0.00631$	0.303
	NC2-A	$\alpha = 0.24955, \alpha_1 = \alpha, \beta^2 = 0.0073$	1.353
	NC2-B	$\alpha = 0.2482, \alpha_1 = 0, \beta^2 = 3 \times 10^{-6}$	2.877
	NC3	$\rho = 0.968, \alpha = 0.49974, \beta^2 = 9.7 \times 10^{-4}$	0.891
Chemical Plant	C1	$\rho = 0.9536$	2.158
	SC1	$\alpha = 0.4275, \gamma = 0.1420, \beta^2 = 0.0169$	0.827
	SC2	$\rho = 0.9536, \alpha = 0.49944, \beta^2 = 0.0043$	2.158
	NC1	$\alpha = 0.24966, \alpha_1 = 0.95\alpha, \beta^2 = 0.0631$	0.401
	NC2-A	$\alpha = 0.02493, \alpha_1 = \alpha, \beta^2 = 0.0084$	3.677
	NC2-B	$\alpha = 0.24708, \alpha_1 = 0, \beta^2 = 1.5 \times 10^{-3}$	6.724
	NC3	$\rho = 0.9536, \alpha = 0.49944, \beta^2 = 0.00225$	2.158

Table 2.3 Basis Restriction Mean Square Error of the Girl Image Represented by:

Sample Reduction Ratio	Size of an Image Block			
	8 x 8	16 x 16	32 x 32	64 x 64
(a) Causal Image Model (CI)				
2	0.774%	0.693%	0.588%	0.569%
4	3.611%	2.226%	2.030%	1.914%
8	5.540%	8.984%	4.604%	4.656%
16	7.734%	11.133%	13.662%	7.760%
32		13.208%	14.975%	11.740%
64		16.553%	22.961%	17.758%
128			25.953%	23.151%
256			31.154%	30.795%
512				49.018%
1024				60.951%
(b) Semicausal Image Model (SC1)				
2	1.334%	1.398%	1.311%	0.943%
4	3.264%	3.677%	3.104%	2.463%
8	6.056%	5.989%	5.182%	4.133%
16	10.931%	9.258%	8.121%	6.543%
32		13.791%	12.521%	10.007%
64		19.430%	18.253%	14.530%
128			26.089%	22.249%
256			39.802%	32.243%
512				39.690%
1024				60.951%
(c) Noncausal Image Model (NC1 or NC2-A or NC2-B)				
2	1.195%	0.887%	0.684%	0.571%
4	3.062%	3.066%	2.573%	1.977%
8	6.232%	5.291%	4.909%	3.785%
16	7.734%	8.551%	8.189%	6.474%
32		13.791%	12.132%	10.002%
64		16.553%	17.553%	14.745%
128			26.089%	21.272%
256			31.154%	30.640%
512				39.690%
1024				51.726%



Table 2.4 Basis Restriction Mean Square Error of the Earth Image Represented by:

Sample Reduction Ratio	Size of an Image Block			
	8 x 8	16 x 16	32 x 32	64 x 64
(a) Causal Image Model (C1)				
2	1.989%	1.660%	1.510%	1.476%
4	7.166%	4.571%	4.596%	4.450%
8	10.141%	13.554%	8.307%	8.881%
16	12.093%	16.132%	18.504%	13.064%
32		17.797%	19.399%	18.863%
64		20.534%	25.325%	22.981%
128			27.703%	27.440%
256			31.288%	33.120%
512				37.983%
1024				46.098%
(b) Semicausal Image Model (SC1)				
2	2.126%	1.896%	1.765%	1.549%
4	5.773%	5.441%	4.746%	4.513%
8	10.263%	9.049%	7.732%	7.337%
16	16.062%	12.679%	11.122%	10.751%
32		17.338%	15.614%	14.916%
64		23.428%	21.699%	20.342%
128			27.784%	26.163%
256			33.762%	32.118%
512				38.608%
1024				44.813%
(c) Noncausal Image Model (NC1 or NC2-A or NC2-B)				
2	2.247%	1.723%	1.490%	1.389%
4	5.330%	4.752%	4.186%	3.939%
8	9.659%	7.914%	7.175%	6.725%
16	12.093%	11.884%	10.913%	10.346%
32		17.338%	15.445%	14.693%
64		20.510%	20.402%	19.845%
128			27.784%	25.977%
256			31.288%	31.340%
512				38.608%
1024				41.930%

## CHAPTER THREE

### SEMICAUSAL MODELS AND HYBRID CODING

#### 3.1 Introduction

In this chapter we consider image coding techniques which combine transform and predictive coding techniques. Such techniques have been called Hybrid coding [17] or, more generally, Hybrid processing. The basic idea behind hybrid processing is to first convert a two-dimensional discrete random field (an array of random variables) into a sequence of one-dimensional, independent, discrete random processes via a unitary transformation. Then each of these one-dimensional processes is processed independently by one-dimensional techniques such as recursive filtering (for image restoration applications) or predictive coding (such as DPCM, for image transmission/storage applications).

In this chapter we show the semicausal models considered earlier yield hybrid coding algorithms. Once the parameters of a semicausal model are identified, the entire hybrid coding scheme can be designed. Adaptive hybrid coding schemes can then be designed by simply adapting the semicausal model to changes in image statistics. Some practical adaptive hybrid coding methods which strike a balance between complexity and performance are studied. Application of these models to coding of noisy images are also considered.

#### 3.2 Semicausal Image Models and Hybrid Coding

Let  $\{u_{i,j}\}$  represent a zero mean, Gaussian, stationary random field whose covariance function is defined as

$$r(k,l) = E u_{i,j} u_{i+k,j+l} \quad \forall i,j. \quad (3.2-1)$$

Consider an  $N \times M$  segment of this random field where  $1 \leq i \leq N$  and  $1 \leq j \leq M$ , and let  $u_j$  denote the  $j$ th column of the image, i.e.,

$$u_j = [u_{1,j}, u_{2,j}, \dots, u_{N,j}]^T. \quad (3.2-2)$$

From (3.2-1) it follows that

$$Eu_j u_{j+l}^T = R_l \quad (3.2-3a)$$

where  $R_l$  is an  $N \times N$  Toeplitz matrix of elements

$$R_l(m,n) = r(m-n, l) \quad 1 \leq m, n \leq N. \quad (3.2-3b)$$

### 3.2.1 Hybrid Coding of Separable Covariance Image Fields

Consider the often used separable covariance model for images

$$r(k, l) = \sigma^2 \rho_v^{|k|} \rho_h^{|l|} \quad (3.2.1-1)$$

where  $\rho_v$  and  $\rho_h$  are the vertical and horizontal correlations, respectively.

This gives

$$R_l = \sigma^2 \rho_h^{|l|} R_v \quad (3.2.1-2a)$$

where

$$R_v = \{\rho_v^{|m-n|}\} \quad (3.2.1-2b)$$

It is well known that  $R_v$  is the covariance of a zero mean, first order stationary Markov process whose one step correlation is  $\rho_v$ . Let  $\Psi$  denote the Karhunen Loeve (KL) transform of this process (see Chapter 4), i.e.,



$\Psi$  is a unitary matrix that satisfies

$$\Psi R_v \Psi^T = \Lambda \quad \Psi \Psi^T = I \quad (3.2.1-3)$$

where  $\Lambda = \{\lambda_i\}$  is the diagonal matrix of eigenvalues of  $R_v$ . Define the transformation

$$v_j \stackrel{\Delta}{=} \Psi u_j. \quad (3.2.1-4)$$

Using (3.2.1-2a), (3.2.1-3) and (3.2.1-4), one obtains

$$E v_j v_{j+l}^T = \Psi R_{\ell} \Psi^T = \sigma_h^2 \rho_{\ell}^2 \Lambda \quad (3.2.1-5a)$$

$$\text{Or} \quad E v_j(i) v_{j+l}(i+k) = \sigma_h^2 \rho_{\ell}^2 \lambda_i \delta_{k,0}. \quad (3.2.1-5b)$$

Eqn. (3.2.1-5b) implies that i) the elements of the transformed column  $v_j$  are mutually uncorrelated and ii) for each  $i$ , the sequence  $\{v_j(i), 1 \leq j \leq M\}$  is a first order, stationary Markov process. Therefore, we can write

$$v_j(i) = \rho_h v_{j-1}(i) + e_j(i) \quad (3.2.1-6a)$$

where

$$E e_j(i) = 0 \quad E e_j(i) e_{j+l}(i+k) = \sigma^2 (1 - \rho_h^2) \lambda_i \delta_{\ell,0} \delta_{k,0} \quad (3.2.1-6b)$$

and  $\{v_j(i), 1 \leq i \leq N\}$  are the elements of the vector  $v_j$ . (3.2.1-6)

spells the so called Hybrid coding method for the random field  $\{u_{i,j}\}$ .

First, each column  $u_j$  is unitarily transformed (ideally by the KL transform) to obtain  $v_j$  and for each sequence  $\{v_j(i), j = 1, 2, \dots\}$  for  $1 \leq i \leq N$ , an independent DPCM channel is used. This overall scheme is shown in Fig. 3.1. Fig. 3.2 shows the details of the  $i$ th DPCM channel and the

reconstruction filter at the receiver. Often, a fast unitary transform is used to replace the KL transform to make the scheme more practical (see Chapter 4). For video image data where  $\rho_h \approx \rho_v \approx 0.95$ , the Cosine transform performs very close to the KL transform defined in (3.2.1-3) [1,31,34]

More generally, if any two-dimensional random field  $\{u_{i,j}\}$  can be transformed via a unitary transformation to a sequence of independent one-dimensional Markov processes, then a Hybrid coding scheme for transmissions of  $\{u_{i,j}\}$  can be designed.

### 3.2.2 Semicausal Representations as Two Source Models for Finite Random Fields

Consider the given image to be an  $N \times M$  segment of the infinite, stationary random field. Semicausal representations we have considered in the previous chapter [see (2.5.2-1) and 2.5.2-9)] when written in an  $N \times 1$  vector notation are of the form

$$Qu_j = Pu_{j-1} + e_j + b_j \quad (3.2.2-1)$$

where  $Q$  is a tridiagonal Toeplitz matrix defined by

$$q_{i,j} = \begin{cases} 1, & i = j \\ -\alpha, & |i-j| = 1 \\ 0, & \text{otherwise} \end{cases} \quad (3.2.2-2a)$$

and

$$P = \begin{cases} \gamma I, & \text{for SC1} \\ \rho_h Q, & \text{for SC2} \end{cases} \quad (3.2.2-2b)$$

$$b_j = \begin{cases} \alpha[u_{0,j}, 0, \dots, 0, u_{N+1,j}]^T, & \text{for SC1} \\ \alpha[b_{1,j}, 0, \dots, 0, b_{N,j}]^T, & \text{for SC2} \end{cases} \quad (3.2.2-2c)$$

$$b_{1,j} = u_{0,j} - \rho_h u_{0,j-1}.$$

$$b_{N,j} = u_{N+1,j} - \rho_h u_{N+1,j-1}. \quad (3.2.2-2d)$$

The  $N \times 1$  vector  $b_j$  contains only two nonzero entries which depend only on the boundary variables  $\{u_{0,j}\}$  and  $\{u_{N+1,j}\}$  of the  $j$ th image column. Note from (3.2-2) that the  $j$ th image column,  $u_j$  contains only  $N$  elements. The covariance of  $\epsilon_j$  is

$$R_\epsilon = E\epsilon_j \epsilon_k^T = \begin{cases} \beta^2 I \delta_{j,k}, & \text{for SC1} \\ \beta^2 Q \delta_{j,k}, & \text{for SC2} \end{cases} \quad (3.2.2-2e)$$

$$\text{where } \beta^2 = (1 - \rho_v^2)(1 - \rho_h^2) / (1 + \rho_v^2) \text{ for the SC2 model.} \quad (3.2.2-2f)$$

Eqn. (3.2.2-1) can be looked at, in general, as a two source model for the vector sequence  $\{u_j\}$ , whose statistics are specified by the statistics for the "source inputs",  $\{\epsilon_j\}$  and  $\{b_j\}$ . We note that (3.2.2-1) may not always qualify to be a vector Markov model

$$Qu_j = Pu_{j-1} = f_j \quad (3.2.2-3a)$$

by defining

$$f_j = \epsilon_j + b_j. \quad (3.2.2-3b)$$



This is because the sequence  $\{f_j\}$  is not guaranteed to be white, even though  $\{\epsilon_j\}$  is such. From the linearity of (3.2.2-1), the two source outputs can be identified by the solution of the equations

$$Qu_j^o = Pu_{j-1}^o + \epsilon_j \quad (3.2.2-4a)$$

$$Qu_j^b = Pu_{j-1}^b + b_j \quad (3.2.2-4b)$$

and the image field is the composition [ 31 ]

$$u_j = u_j^o + u_j^b. \quad (3.2.2-5)$$

The second source output  $u_j^b$  depends completely on the boundary variables. Hence, as the size of the image column gets larger, one would expect a smaller contribution of  $u_j^b$  in influencing the statistical properties of  $u_j$ . The  $N \times M$  random field will be stationary when the statistics of the boundary variables are consistent with those of  $\{u_{1,j}\}$ . In other words, the case of stationary statistics is only a special case of (3.2.2-5). For minimum variance representations, the orthogonality condition (2.3.1-1) implies that the two source outputs  $u_j^o$  and  $u_j^b$  are orthogonal. For stationary, white noise driven, semicausal models, one does not have this condition. If one starts by specifying the boundary variables to be orthogonal to the stationary white noise field  $\{\epsilon_{t,j}\}$ , then the finite  $N \times M$  field  $\{u_{1,j}\}$  need not be stationary. Asymptotically,  $(N, M \rightarrow \infty)$ , (3.2.2-4) and (3.2.2-5) will yield stationary random field  $\{u_{1,j}\}$  (assuming  $Q$  is always nonsingular and (3.2.2-1) is a stable recursive relation).

### 3.2.3 Stochastic Decoupling of Semicausal Models by the Cosine Transform

For a large number of image fields, the adjacent elements of a column (or a row) are highly correlated and often the correlation parameter has a value around 0.95. Thus, for a finite  $N \times M$  random field, it is reasonable to assume that the boundary variables that need to be specified in (3.2.2-1) satisfy the conditions

$$\begin{aligned} u_{0,j} &= u_{1,j} \\ u_{N+1,j} &= u_{N,j} \end{aligned} \quad (3.2.3-1)$$

This means the two outermost boundary rows of the  $(N+2) \times M$  field  $\{u_{i,j}; 0 \leq i \leq N+1, 1 \leq j \leq M\}$  are equal. This also means that (3.2.2-1) subject to (3.2.3-1) is no longer a stationary field on the  $(N+2) \times M$  array of points. Using (3.2.3-1) in (3.2.3-1) and rearranging terms, we get a one source model (the second source is deterministic, as defined by (3.2.3-1))

$$Q_c u_j = P u_{j-1} + \epsilon_j \quad (3.2.3-2)$$

where  $Q_c$  is defined as

$$Q_c \triangleq \begin{bmatrix} 1-\alpha & -\alpha & & \\ -\alpha & 1 & & \\ & & 1 & -\alpha \\ & & -\alpha & 1-\alpha \end{bmatrix} \quad (3.2.3-3a)$$

and

$$P = \begin{cases} \gamma I, & \text{for SC1} \\ \rho_h Q_c, & \text{for SC2.} \end{cases} \quad (3.2.3-3b)$$

For SC1 model,  $\{\epsilon_{i,j}\}$  is still assumed to be a stationary white noise field. For SC2 model, (3.2.3-2) should satisfy the minimum variance conditions of (2.3.1-1). When applied to (3.2.3-2), this implies

$$E\epsilon_j \epsilon_k^T = \beta^2 Q_c \delta_{j,k}.$$

Hence, the covariance of  $\epsilon_j$  is now given as

$$R_\epsilon = E\epsilon_j \epsilon_k^T = \begin{cases} \beta^2 I \delta_{j,k}, & \text{for SC1} \\ \beta^2 Q_c \sigma_{j,k}, & \text{for SC2.} \end{cases} \quad (3.2.3-4)$$

#### Proposition

The KL transform of any vector  $u_j$  of the random field of (3.2.3-2) is the discrete Cosine transform (DCT) [ 1 ] for SC1 as well as SC2 models. For proof, see [ 35 ].

The eigenvalues of  $Q_c$  are given by [see (4.2-11c)]

$$\lambda_{ci} = 1 - 2\alpha \cos \frac{(i-1)\pi}{N} \quad 1 \leq i \leq N. \quad (3.2.3-5)$$

Define  $\Psi_c$  to be the DCT matrix. Since it diagonalizes the matrices  $Q_c$  and  $P$  we have

$$\Psi_c Q_c \Psi_c^T = \Lambda_c = \text{Diagonal } \{\lambda_{ci}\} \quad (3.2.3-6a)$$



$$\Psi_c P \Psi_c^T = \Gamma_c = \{\gamma_i\} \quad \gamma_i = \begin{cases} \gamma & , \text{ for SC1} \\ \rho_h \lambda_{ci} & , \text{ for SC2} \end{cases} \quad (3.2.3-6b)$$

Also, define

$$v_j = \Psi_c u_j. \quad (3.2.3-7)$$

Multiplying both sides of (3.2.3-2) by  $\Psi_c$  and using (3.2.3-6) and (3.2.3-7) we obtain

$$\Lambda_c v_j = \Gamma v_{j-1} + e_j \quad (3.2.3-8a)$$

where

$$e_j \triangleq \Psi_c \epsilon_j. \quad (3.2.3-8b)$$

Since  $\Lambda_c$  and  $\Gamma$  are diagonal, (3.2.3-8a) is a set of decoupled equations

$$\lambda_{ci} v_j(i) = \gamma_i v_{j-1}(i) + e_j(i) \quad 1 \leq i \leq N. \quad (3.2.3-9)$$

From (3.2.3-4) and (3.2.3-6a) and (3.2.3-8b),  $\{e_j(i)\}$  is a white noise field which satisfies the equation

$$E e_j(i) e_k(l) = \begin{cases} \beta^2 \delta_{j,k} \delta_{i,l} & , \text{ for SC1} \\ \beta^2 \lambda_{ci} \delta_{j,k} \delta_{i,l} & , \text{ for SC2} \end{cases} \quad (3.2.3-10)$$

Hence, for each  $i$ , the sequence  $\{v_j(i), \forall j\}$  is a first order Markov sequence. Moreover, if the initial variables  $\{v_0(i), 1 \leq i \leq N\}$  are uncorrelated then for  $\forall j > 0$ ,  $\{v_j(i), 1 \leq i \leq N\}$  will be uncorrelated elements of the vector  $v_j$ . Also, for  $u_0 = 0$  or  $u_0 = u_\infty$  (i.e., steady state in  $j$ ), the above condition will always be satisfied. For arbitrary

initial conditions, say  $u_0 = c$ , where  $c$  is an arbitrary random vector,  $u_j$  will have a decomposition

$$u_j = u_j^o + u_j^c \quad (3.2.3-11a)$$

where  $Q_c u_j^o = P u_{j-1}^o + \epsilon_j \quad u_0^o = 0 \quad (3.2.3-11b)$

and  $Q_c u_j^c = P u_{j-1}^c \quad u_0^c = c. \quad (3.2.3-11c)$

The KL transform of  $u_j^o$  now will be the DCT. In a practical DPCM system, the statistics of the initial condition do not affect the ultimate system performance because the initial vector can always be quantized accurately and transmitted before starting the DPCM transmission.

#### 3.2.4 Stochastic Decoupling of Stationary Semicausal Fields

Random fields for which (3.2.3-1) is not a reasonable assumption (i.e., one step correlation in the "j" direction is not close to 1) or when stationarity of the random field is an essential requirement of the model, we have to restrict ourselves to (3.2.2-1). The boundary variables (elements of  $b_j$ ) are random variables which are samples from the stationary random field  $\{u_{1,j}\}$  and cannot be specified independently. In that case, (3.2.2-1) admits the decomposition [see (3.2.2-4) - (3.2.2-5)]

$$Q u_j^o = P u_{j-1}^o + \epsilon_j \quad u_0^o = 0 \quad j \geq 1 \quad (3.2.4-1a)$$

$$Q u_j^b = P u_{j-1}^b + b_j \quad u_0^b = u_0 \quad j \geq 1 \quad (3.2.4-1b)$$

where

$$u_j = u_j^o + u_j^b \quad j \geq 1 \quad (3.2.4-2)$$

and  $u_0$  is the initial value of the sequence  $\{u_j\}$ .

### Proposition

The KL transform of any column vector  $u_j^0$ ,  $j \geq 1$  of the random field  $\{u_{i,j}^0\}$  of (3.2.4-1a) is the Sine transform for SC1 as well as the SC2 models. For proof see [35].

Let  $\Psi_s$  be the Sine transform. Then

$$\Psi_s Q \Psi_s = \Lambda_s = \text{Diagonal } \{\lambda_i\} \quad \lambda_i = 1 - 2\alpha \cos \frac{i\pi}{N+1} \quad 1 \leq i \leq N \quad (3.2.4-3)$$

$$\Psi_s P \Psi_s = \Gamma = \{\gamma_i\} \quad \gamma_i = \begin{cases} \gamma & , \text{ for SC1} \\ \rho_h \lambda_i & , \text{ for SC2} \end{cases} \quad (3.2.4-4)$$

Defining

$$v_j = \Psi_s u_j^0 \quad e_j = \Psi_s \epsilon_j \quad (3.2.4-5)$$

and multiplying both sides of (3.2.4-1a) by  $\Psi_s$  and using (3.2.4-3), (3.2.4-4) and (3.2.4-5) we get a sequence of decoupled equations

$$\lambda_i v_j(i) = \gamma_i v_{j-1}(i) + e_j(i) \quad v_0(i) = 0 \quad 1 \leq i \leq N, j \geq 1 \quad (3.2.4-6a)$$

$$E e_j(i) e_k(l) = \begin{cases} \beta^2 \delta_{i,l} \delta_{j,k} & , \text{ for SC1} \\ \beta^2 \lambda_i \delta_{i,l} \delta_{j,k} & , \text{ for SC2} \end{cases} \quad (3.2.4-6b)$$

From (3.2.4-6a) and (3.2.4-6b) it is evident that  $\{v_j(i)\}$  is a sequence of  $N$ , first order Markov processes and for any  $j \geq 1$  the elements  $\{v_j(i), 1 \leq i \leq N\}$  are uncorrelated. Hence,  $\Psi_s$  is the KL transform of  $u_j^0$ .

Figure 3.3 shows the realization of decomposition of (3.2.4-2) and stochastic decoupling of (3.2.4-6).



### 3.3 Hybrid Coder Design for Semicausal Random Fields

For the sake of simplicity of presentation, we will only consider the semicausal models of (3.2.3-2) which are decoupled by the Cosine transform. The sequence of decoupled equations (3.2.3-9) and (3.2.3-10) can be rewritten as

$$v_j(i) = \rho_i v_{j-1}(i) + e_j(i) \quad 1 \leq i \leq N \quad (3.3-1)$$

where

$$\rho_i = \frac{\gamma_i}{\lambda_{ci}} = \begin{cases} \gamma/\lambda_{ci} & , \text{ for SC1} \\ \rho_h & , \text{ for SC2} \end{cases} \quad (3.3-2a)$$

and  $\{e_j(i)\}$  is a white noise field whose covariances are given by

$$E e_j(i) e_k(l) \triangleq \beta^2(i) \delta_{j,k} \delta_{i,l}$$

$$\beta^2(i) \triangleq \begin{cases} \beta^2/\lambda_{ci}^2 & , \text{ for SC1} \\ \beta^2/\lambda_{ci} & , \text{ for SC2} . \end{cases} \quad (3.3-2b)$$

#### 3.3.1 DPCM Equations

Since (3.3-1) is a sequence of  $N$  independent Markov processes, each of these sequences could be transmitted via an independent DPCM channel, as shown in Fig. 3.2. The equation at the transmitter and receiver are simply as follows:

Predictor:  $\bar{v}_j(i) = \rho_i v_{j-1}^*(i) \quad (3.3.1-1a)$

Differential Signal:  $\hat{e}_j(i) = v_j(i) - \bar{v}_j(i) \quad (3.3.1-1b)$

$$\text{Quantizer Output: } e_j^*(i) \quad (3.3.1-1c)$$

$$\text{Reconstruction Filter: } v_j^*(i) = \rho_1 v_{j-1}^*(i) + e_j^*(i) \quad (3.3.1-1d)$$

The encoding scheme requires, first, to take the Cosine transform of each column vector  $u_j$ . The DCT is a fast transform and is also the KL transform of each column of the semicausal image fields characterized by (3.2.3-2). This is followed by N DPCM channels for predictive coding of successive Cosine transformed vectors. The receiver simply reconstructs the transformed vectors according to (3.3.1-1d) and performs the inverse Cosine transformation. To complete the design, we now need to specify the quantizers in the various DPCM channels.

### 3.3.2 Bit Allocation

We will assume all the quantizers are identical in their characteristics (i.e., bit rate vs. distortion). Let

$P$  = Average desired bit rate in bits/pixel of the image field.

$f(n)$  = Mean square distortion of a quantizer with  $2^n$  levels for unit variance input random variables. This is a positive, monotonically decreasing convex function. We will assume  $f(n)$  has a continuous first derivative.

$0 \leq n_i$  = Number of bits per pixel, allocated to the  $i$ th DPCM channel.

From the definition of  $P$ , we have

$$\frac{1}{N} \sum_{i=1}^N n_i = P \quad n_i \geq 0. \quad (3.3.2-1)$$

The average mean square distortion in encoding of the image vector  $u_j$  is given by

$$D = \frac{1}{N} E \delta u_j^T \delta u_j \quad (3.3.2-2)$$

where  $\delta u_j \triangleq u_j - u_j^*$ .

Since  $v_j = \Psi_c u_j$  is a unitary transformation and  $v_j(i)$  are coded via DPCM, we have

$$\begin{aligned} \delta v_j(i) &= v_j(i) - v_j^*(i) \\ &= v_j(i) - \rho_i v_{j-1}^*(i) - e_j^*(i) \\ &= \hat{e}_j(i) - e_j^*(i) \\ &= \delta \hat{e}_j(i) \end{aligned} \quad (3.3.2-3)$$

i.e., the reconstruction error in  $v_j(i)$  (assuming noiseless channel) equals the quantization error in the  $i$ th channel. This gives

$$\begin{aligned} D &= \frac{1}{N} E \delta v_j^T \delta v_j \\ &= \frac{1}{N} \sum_{i=1}^N E (\delta e_j(i))^2. \end{aligned} \quad (3.3.2-4)$$

Thus, the average distortion per pixel is the average quantizer distortion. If  $\hat{\beta}_j^2(i)$  denotes the variance of the  $j$ th quantizer input in the  $i$ th DPCM channel, then

$$E(\delta \hat{e}_j(i))^2 = \hat{\beta}_j^2(i) f(n_i) \quad \forall j. \quad (3.3.2-5)$$

Using (3.3-1), (3.3.1-1a) and (3.3.2-4) in (3.3.1-1b) and simplifying, we get



$$\begin{aligned}\hat{e}_j(i) &= v_j(i) - \bar{v}_j(i) \\ &= e_j(i) + \rho_1 \hat{e}_{j-1}(i) .\end{aligned}\quad (3.3.2-6)$$

Eqs. (3.3.2-5) and (3.3.2-6) together give a recursive relation for the variance of  $\hat{e}_j(i)$  as

$$\hat{\beta}_j^2(i) = \beta^2(i) + \rho_1^2 \hat{\beta}_{j-1}^2(i) f(n_1) \quad \hat{\beta}_0^2 = 0 \quad (3.3.2-7)$$

where we have used the fact that  $e_j(i)$  is uncorrelated with the quantization error at step  $j-1$ . In steady state

$$\hat{\beta}_j^2(i) \triangleq \hat{\beta}^2(i) = \frac{\beta^2(i)}{1 - \rho_1^2 f(n_1)} . \quad (3.3.2-8)$$

Hence, (3.3.2-5) becomes

$$E(\delta \hat{e}_j(i))^2 = \frac{\beta^2(i) f(n_1)}{1 - \rho_1^2 f(n_1)} \quad (3.3.2-9)$$

giving

$$D = \frac{1}{N} \sum_{i=1}^N g_i(n_i) \beta^2(i) \quad (3.3.2-10a)$$

where

$$g_i(x) = \frac{f(x)}{1 - \rho_1^2 f(x)} \quad x \geq 0 . \quad (3.3.2-10b)$$

The function  $g_i(x)$  represents the mean square distortion of the  $i$ th DPCM loop of a Markov process whose prediction error variance is unity. Like the function  $f(x)$ , for  $|\rho_1| < 1$ , each  $g_i(x)$  is also a positive, monotonically decreasing, convex function with a continuous first derivative.

The bit allocation problem is to minimize (3.3.2-10a) subject to the constraints of (3.3.2-1). This is equivalent to finding

$$D' = \min_{\substack{n_i \geq 0 \\ \lambda}} \left\{ \lambda P - \frac{1}{N} \sum_{i=1}^N [g_i(n_i) \beta^2(i) + \lambda n_i] \right\} \\ = \min_{\lambda} \left\{ \lambda P - \frac{1}{N} \sum_{i=1}^N \max_{n_i \geq 0} [g_i(n_i) \beta^2(i) + \lambda n_i] \right\}. \quad (3.3.2-11)$$

Solution of constrained minimization problems of this type are well known in optimization theory. Recently, Segall [ 66 ] has considered a similar bit allocation problem [with  $g_i(x) = g(x)$ ,  $\forall i$ ] for encoding of vector sources. The solution is given by

$$g'_i(n_i) \beta^2(i) + \lambda = 0 \quad \lambda \leq -g'_i(0) \beta^2(i) \\ n_i = 0 \quad \lambda > -g'_i(0) \beta^2(i). \quad (3.3.2-12)$$

Denoting  $h_i(x) = g_i^{-1}(x)$  (3.3.2-13)

we can solve (3.3.2-12) for  $n_i$  as

$$n_i = \begin{cases} h_i \left( \frac{-\lambda}{\beta^2(i)} \right), & \lambda \leq -g'_i(0) \beta^2(i) \\ 0, & \lambda > -g'_i(0) \beta^2(i) \end{cases} \quad (3.3.2-14)$$

where  $\lambda$  is the root of the nonlinear equation

$$\sum_{i: \lambda \leq -g'_i(0) \beta^2(i)} h \left( -\frac{\lambda}{\beta^2(i)} \right) = NP. \quad (3.3.2-15)$$

The value of the minimum distortion is

$$D_{\min} = \frac{1}{N} \left[ \sum_{\lambda \leq -g_1'(0)} g_1(n_1) \beta^2(i) + \sum_{\lambda > -g_1'(0)} \beta^2(i) \right]. \quad (3.3.2-16)$$

Now consider the following special cases.

1.  $\hat{\beta}^2(i) \approx \beta^2(i)$ , i.e., the effect of quantization on the variance of the prediction error is ignored. This gives

$$g_1(n) \approx f(n) \quad \forall i. \quad (3.3.2-17)$$

When the quantizer in the DPCM loop is the ideal optimal block encoder (Shannon quantizer) that achieves the rate distortion bound we have

$$f(n) = 2^{-2n} \quad (3.3.2-18)$$

which gives

$$f'(x) = (-2 \log_e 2) 2^{-2x}$$

$$\text{or } h(x) = f'^{-1}(x) = -\frac{1}{2} \log_2 \left( \frac{x}{-2 \log_e 2} \right). \quad (3.3.2-19)$$

Defining

$$\theta = \lambda / (2 \log_e 2) \quad (3.3.2-20)$$

and using (3.3.2-18) in (3.3.2-14) to (3.3.2-16), we get

$$n_1 = \begin{cases} \frac{1}{2} \log_2 \left( \frac{\beta^2(i)}{\theta} \right), & 0 < \theta \leq \beta^2(i) \\ 0, & \theta > \beta^2(i) \end{cases} \quad (3.3.2-21a)$$



where  $\theta$  is the solution of

$$\sum_{i=1}^N \max \left[ 0, \frac{1}{2} \log_2 \frac{\beta^2(i)}{\theta} \right] = NP \quad (3.3.2-21b)$$

and the minimized distortion is

$$D_{\min} = \frac{1}{N} \sum_{i=1}^N \min[\beta^2(i), \theta] \quad (3.3.2-21c)$$

Eqs. (3.3.2-21) are valid for both SC1 and SC2 models, where  $\beta^2(i)$  is defined by (3.3-2b).

2. Consider the case when  $f(\cdot)$  and  $g_1(\cdot)$  are given by (3.3.2-18) and (3.3.2-10b) respectively. Then

$$\begin{aligned} g_1'(x) &= \frac{f'(x)}{(1 - \rho_1^2 f(x))^2} \\ &= \frac{(-2 \log_e 2) 2^{-2x}}{(1 - \rho_1^2 2^{-2x})^2} \end{aligned} \quad (3.3.2-22)$$

From this equation one can obtain a unique inverse (note that  $g_1'(x)$  must be nonpositive for all  $x \geq 0$ ), as (see Appendix C)

$$g_1'^{-1}(x) \triangleq h_1(x) = \begin{cases} -\frac{1}{2} \log_2 \left[ \frac{-\log_e 2 + \rho_1^2 x + \sqrt{(\log_e 2)^2 - (2 \log_e 2) \rho_1^2 x}}{\rho_1^4 x} \right], & \rho_1 \neq 0 \\ -\frac{1}{2} \log_2 \left( \frac{-x}{2 \log_e 2} \right), & \rho_1 = 0 \end{cases} \quad (3.3.2-23)$$

For SC1 model, defining

$$\theta = \frac{\lambda}{(2 \log_e 2)} \quad (3.3.2-24)$$

and using (3.3.2-23) in (3.3.2-14), (3.3.2-15) and (3.3.2-16) we get

$$n_i = \begin{cases} k_2 \log_2 \frac{\beta^2(i)}{\theta} w(i, \theta) & , \quad 0 < \theta \leq \frac{\beta^2(i)}{(1 - \rho_i^2)^2} \\ 0 & , \quad \theta > \frac{\beta^2(i)}{(1 - \rho_i^2)^2} \end{cases} \quad (3.3.2-25a)$$

where

$$w(i, \theta) \triangleq \begin{cases} 1 & , \quad \rho_i = 0 \\ \frac{1}{2\rho_i^4} \left[ 1 + \frac{2\rho_i^2 \theta}{\beta^2(i)} - \left( 1 + \frac{4\rho_i^2 \theta}{\beta^2(i)} \right)^{k_2} \right] & , \quad \rho_i \neq 0 \end{cases} \quad (3.3.2-25b)$$

$\theta$  is the solution of

$$\sum_{i: 0 < \theta \leq \frac{\beta^2(i)}{(1 - \rho_i^2)^2}} k_2 \log_2 \frac{\beta^2(i) w(i, \theta)}{\theta} = NP \quad (3.3.2-25c)$$

and the minimum distortion is

$$D_{\min} = \frac{1}{N} \sum_{i=1}^N \min[\beta^2(i), \theta/w(i, \theta)] \quad (3.3.2-25d)$$

In the case of SC2 model, substitution of  $\rho_i = \rho_h = \text{constant}$ , (3.3.2-25) above gives the desired bit allocation and distortion formulas. The bit allocations are obtained by first solving (3.3.2-25c) iteratively (by Newton's method, for example) to obtain  $\theta$ , for a fixed rate  $P$ . Given  $\theta$ , (3.3.2-25a) and (3.3.2-25b) yield the desired allocations  $\{n_i\}$  and (3.3.2-25d) gives the corresponding distortion.

### 3.3.3 Integer Bit Allocation

In the above, we assumed  $n_i$  to be a real number. In many practical situations  $n_i$  is required to be an integer. An approximate integer bit allocation can be obtained via the foregoing method by rounding  $n_i$  to the nearest integer. The actual bit rate then would be

$$P_a = \frac{1}{N} \sum_{i=1}^N [n_i]$$

where  $[x]$  indicates the nearest integer to  $x$ . To obtain the exact solution, the minimization of (3.3.2-10a) is subject to the constraint that  $\{n_i\}$  be a set of nonnegative integers. The solution is obtained via an iterative algorithm due to Fox [ 11 ] as follows.

Let  $\underline{n}$  denote a vector of elements  $\{n_i, 1 \leq i \leq N\}$ .

1. Start with the allocation  $\underline{n}^0 = \underline{0}$ .
2. Set  $\ell = 1$ .
3.  $\underline{n}^\ell + \underline{n}^\ell + \underline{e}_i$  where  $\underline{e}_i$  is the  $i$ th unit vector and  $i$  is any index for which

$$\Delta_{i,\ell} = \beta^2(i)g_i(n_i^{\ell-1}) - \beta^2(i)g_i(n_i^{\ell-1} + 1)$$

is maximum. The quantity  $\Delta_{i,\ell}$  is called the marginal return of increasing the  $i$ th allocation in  $\ell$ th step by one bit.

4. If  $\sum_{i=1}^N n_i^\ell \geq PN$ , terminate; otherwise  $\ell \rightarrow \ell + 1$  and go to step 3.

This algorithm simply means the marginal returns  $\Delta_{i,\ell}$  are calculated for  $1 \leq i \leq N$  and  $\ell = 1, 2, \dots$ , and are arranged in a decreasing order until all the bits are exhausted. Tables 3.1 and 3.2 show the bit



allocations for the SC1, SC2 and separable covariance models for Girl image obtained via real bit allocation and integer bit allocation algorithms described above.

### 3.4 Adaptive Hybrid Coding

The coding scheme of the previous section can be adapted to image fields whose spatial statistics vary slowly by updating the various coefficients of the image model with variations of the statistics. A complete update of the image model parameters could often increase the complexity of the coder to make it impractical. In the sequel we consider two adaptive schemes which offer reasonable improvement in coder performance with only a marginal increase in its complexity.

#### 3.4.1 Adaptive Variance Estimation

For a fixed predictor in the feedback loop of a DPCM channel, the variance of the prediction error will fluctuate with changes in image statistics. In this scheme we update the variance of the prediction error at each step  $j$ . This updated variance is used to adjust the spacing of the quantizer levels in each DPCM channel. For mean square error criterion, the decision and reconstruction levels of a quantizer are directly proportional to the standard deviation of the input random variables. Hence, the above mentioned adaptation can be achieved by simply normalizing the prediction error by its updated standard deviation. The quantizer levels are then fixed and correspond to unit variance random variables. Fig. 3.4 shows this scheme.

Let

$$\hat{\sigma}_j^2(i) \triangleq \text{Variance of } e_j(i), \text{ the prediction error at step } j \text{ of the } i\text{th DPCM loop} = E[e_j(i)]^2 \quad (3.4.1-1a)$$

$$\sigma_j^{*2}(i) \triangleq \text{Variance of the quantized values} = E[e_j^*(i)]^2. \quad (3.4.1-1b)$$

Since the quantized variables  $e_j^*(i)$  are available both at the receiver and the transmitter, it is easy to estimate  $\sigma_j^{*2}(i)$ . Castellino et al [ 8 ] have suggested a formula for an estimate of  $\sigma_j^{*2}(i)$  (for single channel DPCM system) as

$$\hat{\sigma}_j^2(i) = \frac{1-\gamma}{\gamma} \sum_{m=1}^j \gamma^m e_{j-m+1}^{*2}(i) + \gamma^j \sigma_1^{*2}(i) \quad 0 < \gamma < 1. \quad (3.4.1-2)$$

This has been called an exponential average variance estimator. A more convenient form of (3.4.1-2) is the recursion

$$\hat{\sigma}_{j+1}^{*2}(i) = (1-\gamma) e_j^{*2}(i) + \gamma \hat{\sigma}_j^{*2}(i) \quad j = 1, 2, \dots \quad (3.4.1-3)$$

For small quantization errors one may take  $\hat{\sigma}_j$  to be equal to  $\hat{\sigma}_j$ . For Lloyd-Max quantizers [ 44 ] a more accurate estimate of  $\hat{\sigma}_j$  is possible. Since the variance of a Lloyd-Max quantizer input equals the sum of the variances of the quantizer output and the quantization error, we have

$$\begin{aligned} \hat{\sigma}_j^2(i) &= \sigma_j^{*2}(i) + f(n_1) \hat{\sigma}_j^2(i) \\ \text{or} \quad \hat{\sigma}_j^2(i) &= \frac{\sigma_j^{*2}(i)}{1-f(n_1)} \quad n_1 \geq 1 \end{aligned} \quad (3.4.1-4)$$

where  $n_1$  is the number of bits allocated to the  $i$ th channel. Using (3.4.1-4) in (3.4.1-3) we get

$$\hat{\sigma}_{j+1}^2(i) = \frac{1-\gamma}{1-f(n_i)} e_j^{*2}(i) + \gamma \hat{\sigma}_j^2(i) \quad n_i > 1 \quad 0 < \gamma < 1. \quad (3.4.1-5)$$

The above estimate become poor for DPCM channels which are assigned small number of bits ( $n_i \approx 1$ ). For these channels  $\hat{\sigma}_j(i)$  could be estimated by some sort of extrapolation of the already estimated  $\hat{\sigma}_j(i)$ . For example, for the SC1 model, we know

$$\hat{\sigma}_j^2(i) \approx E \hat{e}_j^2(i) = \frac{\beta^2}{[1-\rho_i^{2f(n_i)}]\lambda_{ci}^2} \quad i \in I \quad (3.4.1-6)$$

where  $I$  is the set of, say,  $m$  channels for which  $n_i > 1$ . From (3.4.1-6) an estimate of  $\beta^2$  at step  $j$ , denoted by  $\tilde{\beta}_j^2$  is given by

$$\tilde{\beta}_j^2 = \frac{1}{m} \sum_{i \in I} \hat{\sigma}_j^2(i) \lambda_{ci}^2 [1 - \rho_i^{2f(n_i)}]. \quad (3.4.1-7)$$

This gives the extrapolated estimates as

$$\hat{\sigma}_j^2(i) = \frac{\tilde{\beta}_j^2}{\lambda_{ci}^2 [1 - \rho_i^{2f(n_i)}]} \quad i \notin I. \quad (3.4.1-8)$$

For SC2 model, the equations corresponding to (3.4.1-7) and (3.4.1-8) become

$$\tilde{\beta}_j^2 = \frac{1}{m} \sum_{i \in I} \hat{\sigma}_j^2(i) \lambda_{ci} [1 - \rho_h^{2f(n_i)}] \quad (3.4.1-9)$$

$$\hat{\sigma}_j^2(i) = \frac{\tilde{\beta}_j^2}{\lambda_{ci} [1 - \rho_h^{2f(n_i)}]} \quad i \notin I. \quad (3.4.1-10)$$

The adaptive variance estimator only needs to solve Eqns. (3.4.1-5), (3.4.1-7) and (3.4.1-8) for SC1 model and (3.4.1-5), (3.4.1-9) and



(3.4.1-10) for SC2 model. We finally note that this adaptive scheme maintains the same constant data rate in each DPCM channel as in the nonadaptive scheme of the previous section.

### 3.4.2 Adaptive Classification

In this method each image column is classified as belonging to one of  $K$  predetermined classes. Each of these classes is determined according to the activity in that image column. The activity in an image column is measured by the variance of that column. For a given class of images the probability distribution function of the variances of all the columns can be pre-determined. (Note that this probability distribution function could depend on the size of the image column used in hybrid coding.)

In the DPCM loop, the transformed signal in each DPCM channel is processed as before except that the differential signal is quantized according to the classification of that image column. Thus, the quantizer in the DPCM loop is adapted to the image activity in each column. The number of quantization levels (or bits) depend on the variance of a class so that columns of high dynamic activity are assigned more bits than those of low activity. In this way quantizing bits are employed more efficiently. However, the classification information for each column needs to be transmitted. This can be done by sending an extra  $\log_2 K$  bits per column of  $\frac{1}{N} \log_2 K$  bits/pixel. Fig. 3.5 shows the adaptive classification scheme. Experimentally it was found that the variance of successive columns, denoted by  $\{\epsilon_j\}$  (say), are highly correlated. Instead of transmitting the classification map, a DPCM loop for transmission of  $\{\epsilon_j^*\}$  are used for classification at the receiver as well as the transmitter. A two bit quantizer was found to give very accurate reproduction of  $\{\epsilon_j\}$ .

Let  $p(\xi)$  = probability density of the variances  $\xi$  of a column.

Suppose the  $K$  classes have been predetermined and let  $(t_k, t_{k+1})$ ,  $1 \leq k \leq K$  denote the decision boundaries for the  $k$ th class. Since  $\xi \geq 0$ ,  $t_0 = 0$ ,  $t_{K+1} = \infty$ . Then

$$p_k = \int_{t_k}^{t_{k+1}} p(\xi) d\xi = \text{probability of the } k\text{th class} \quad (3.4.2-1)$$

$$\bar{\xi}_k = \frac{1}{p_k} \int_{t_k}^{t_{k+1}} \xi p(\xi) d\xi = \text{variance of the } k\text{th class.} \quad (3.4.2-2)$$

First assume that the thresholds  $\{t_k\}$  has been somehow predetermined and  $p_k$  and  $\bar{\xi}_k$  are known. Also, we will assume that for each class  $k$ , the image model parameters have been predetermined and are known. To this end, let us denote by  $\rho_{i,k}$ ,  $\beta^2(i,k)$ ,  $n_{i,k}$ , etc., the quantities for the  $i$ th DPCM channel and  $k$ th class corresponding to the definitions of  $\rho_i$ ,  $\beta^2(i)$ ,  $n_i$ , etc., respectively. Then, following the development of the foregoing sections, we can write the expected average distortion for any image column (in steady state DPCM) as

$$D = \frac{1}{N} \sum_{i=1}^N \sum_{k=1}^K \beta^2(i,k) g_{i,k}(n_{i,k}) p_k \quad (3.4.2-3)$$

where  $n_{i,k} \geq 0$  are such that the expected average bit rate must be constant, i.e.,

$$\frac{1}{N} \sum_{i=1}^N \sum_{k=1}^K n_{i,k} p_k = P. \quad (3.4.2-4)$$

The bit allocation problem associated with (3.4.2-3) and (3.4.2-4) can be solved along the same lines as in section 3.3. As an example, consider

the case when

$$g_{i,k}(x) \approx f(x) = 2^{-2x}$$

then one obtains

$$n_{i,k} = \max \left[ 0, \frac{1}{2} \log_2 \frac{\beta^2(i,k)}{\theta} \right] \quad (3.4.2-5a)$$

where  $\theta$  is the solution of

$$\sum_{i=1}^N \sum_{k=1}^K \max \left[ 0, \frac{1}{2} \log_2 \frac{\beta^2(i,k)}{\theta} \right] p_k = NP \quad (3.4.2-5b)$$

and the minimum achievable distortion is

$$D_{\min} = \sum_{i=1}^N \sum_{k=1}^K \min[\theta, \beta^2(i,k)] p_k. \quad (3.4.2-5c)$$

This method of adaptive hybrid coding requires i) measurement of variance of each column and its transmission by an extra DPCM channel, ii) classification of each column to one of  $K$  classes based on thresholds  $\{t_k\}$ , and iii) storing of  $K$  bit allocation tables, one for each class.

### 3.5 Experimental Results

Several computer experiments have been performed on the Girl and Chemical Plant images to simulate the hybrid coding schemes discussed in the previous sections. Table 3.3 shows the parameters of the various image models used here. In all the experiments, the Cosine transform based semicausal models were used. A  $256 \times 256$  image was divided into 16 strips, each of size  $16 \times 256$ . Each strip was hybrid coded independently. This way only a 16 step Cosine transform is needed which makes the scheme



feasible for a real time implementation [ 46 ]. In all the performance measurements, the signal to noise ratio (SNR) is defined as

$$\text{SNR} = 20 \log_{10} \left( \frac{\text{Peak to Peak Value of the Signal}}{\text{r.m.s. error}} \right) . \quad (3.5-1)$$

For an eight bit original data this becomes

$$\text{SNR} = 20 \log_{10} \frac{255}{\text{r.m.s. error}} . \quad (3.5-2)$$

The normalized mean square error is measured over the entire  $256 \times 256$  image and is defined as

$$\text{NMSE} = \frac{\sum_{i=1}^{256} \sum_{j=1}^{256} (u_{i,j} - u_{i,j}^*)^2}{\sum_{i=1}^{256} \sum_{j=1}^{256} u_{i,j}^2} . \quad (3.5-3)$$

In each DPCM channel a compandor is used as an approximation to the Max quantizer (see Appendix A).

### 3.5.1 Nonadaptive Hybrid Coding

Figure 3.6 shows the SNR vs. bit rate and rate distortion curve for the SC1, SC2 and the separable covariance image models for the girl image. As expected, the performances of SC2 and separable covariance models are very close. The SC1 model performs better than the other two by about 1.5 to 2 dB, in general, above rates of 1 bit/pixel. The same set of plots for Chemical Plant image is shown in Fig. 3.7. Since the performances of SC2 and separable covariance models are close, for simplicity, the curve for the separable covariance model is not shown in Fig. 3.7.

### 3.5.2 Adaptive Variance Estimation

Figure 3.8 shows the SNR vs. bit rate and rate distortion curve for the various models of the Girl Image for this case. In these experiments, the variance estimates were updated only for channels for which  $n_i \geq 2$  bits/pixel.

The performance of SC2 and separable covariance model improves by about 1.5 dB at 1 bit rate and about 4 dB at 2 bit rate. These values can be found from Table 3.4, which gives the quantitative comparisons on a model by model basis. The reason for larger improvement at 2 bit rate is that the variance estimates (based on quantized data) are more accurate since many more channels have  $n_i \geq 2$  bits/pixel. The performance improvement for SC1 model is less (only 0.5 dB at 1 bit rate and 1.5 dB at 2 bit rate). This could be because the SC1 model performance was already better (than SC2) to start with and the margin of improvement by updating prediction error variance is small. As the size of the image column (N) is increased, the performance of the adaptive variance estimator was found to improve. This is, again, because the number of channels (for a fixed average rate) with bit allocation  $n_i \geq 2$  would increase giving a better estimate of the variances (as well as of the extrapolated values). Similar conclusions can be made for the Chemical Plant Image. The corresponding results are shown in Fig. 3.9 and Table 3.5.

### 3.5.3 Adaptive Classification

Two different experiments utilizing this method were performed. In the first experiment, a probability distribution function of the column

variances was determined from the histogram of their sample variances. Classification thresholds  $\{t_k\}$  were determined for a  $K = 4$  case assuming equal probability for each class. Then each column of the image was classified. The actual measurements model for the Cosine transformed vectors was assumed, as

$$v_j(i,k) = \rho_{i,k} v_{j-1}(i,k) + e_j(i,k), \quad 1 \leq i \leq N, \quad k = 1, \dots, 4 \quad (3.5.3-1)$$

with

$$E e_j^2(i,k) \triangleq \beta^2(i,k) \quad (3.5.3-2)$$

$$\triangleq (1 - \rho_{i,k}^2) E[v_j(i,k)]^2.$$

The parameters  $\rho_{i,k}$  and  $\beta^2(i,k)$  were measured for each class and bit allocation was done according to the method described in the previous chapter. Fig. 3.5 shows the adaptive classification hybrid coding scheme. Fig. 3.10 shows the  $16 \times 32$  classification map of  $16 \times 256$  portion of the image with 16 element columns. (Recall that the given  $256 \times 256$  image was divided into sixteen  $16 \times 256$ , rectangular subimages.)

This method gave a large improvement (see Fig. 3.11 for the Girl Image and Fig. 3.12 for the Chemical Plant Image) in SNR over the previous two schemes (about 5.5 dB at 1 bit rate and 8 dB at 2 bit rate over nonadaptive). However, the above procedure is somewhat impractical for online transmission (could be acceptable for storage) because it requires identification of the  $2NK = 8N$  parameters,  $\rho_{i,k}$  and  $E[v_j(i,k)]^2$  for each image. These parameters are then used to determine the bit allocations for various classifications. Assuming eight bits are required to transmit each of these parameters (this is actually a pessimistic estimate), the additional overhead for their transmission is only



$\frac{8 \times 16 \times 8}{256 \times 256} = \frac{1}{64}$  bit/pixel. The overhead for transmission of the class of the column variance is only 2 bits per column or  $\frac{1}{8}$  bit/pixel. Thus, the total overhead is always less than 0.14 bit/pixel. However, the complexity of the scheme at the transmitter is increased substantially.

The complexity of the foregoing method can be reduced considerably by using models for  $\rho_{i,k}$  and  $\beta^2(i,k)$  according to SC1 or SC2 representations. In our experiments here we assumed

$$\rho_{i,k} = \rho_i \quad \forall k \quad \rho_i = \begin{cases} \gamma/\lambda_{ci}, & \text{for SC1} \\ \rho_h, & \text{for SC2} \end{cases}$$

$$\beta^2(i,k) = \beta_0^2(i) \sigma_k^2 \quad \forall k \quad \beta_0^2(i) = \begin{cases} \beta_0^2/\lambda_{ci}^2, & \text{for SC1} \\ \beta_0^2/\lambda_{ci}, & \text{for SC2} \end{cases}$$

where  $\sigma_k^2$  is the variance of the columns belonging to the  $k$ th class,  $\beta_0^2(i)$  represents the prediction error variance of the  $i$ th, unit variance Markov process. Compared to the nonadaptive case, the only additional computation this model requires is the measurement of the sample variance of an image column and classifying it. Figs. 3.13 and 3.14 show the bit allocations for various models used for adaptive classification hybrid coding. Since the first DPCM channel in the Cosine transform represents the d.c. value (or sample mean of the columns), the number of bits allocated to this channel (for a given bit rate and class) were kept the same for all different models. The bit allocation algorithm of previous sections was thus used only for  $i = 2, \dots, N$  in the case of SC1 and SC2 models. Figs. 3.11 and 3.12 show the performance of these models when used for adaptive

classification. Generally, the performance of the SC1 model is superior to that of the SC2. For the Girl Image, it is better than nonadaptive (separable covariance model) hybrid coding by about 3 dB, but is worse than the previous adaptive classification experiment by 2 to 3 dB. This, of course, is the price the designer has to pay for a simplified system. However, for the Chemical Plant image, the adaptive classification scheme does not give much SNR improvement over the nonadaptive scheme, it is worse than the adaptive variance scheme. This is understood by referring to Figs. 3.15 and 3.16, which are the histograms of image column variances. For the Girl image, the variances have a large dynamical range, whereas the variance of the Chemical Plant image are nearly equal. Hence image column activities of the Chemical Plant image remain invariant and therefore classification does not help. Finally, note that this scheme will produce variable bit rate from one image column to the next because of a possible change in classification.

Figs. 3.17-3.19 show the results of various hybrid coding schemes on a model by model basis for the Girl image. Figs. 3.20 and 3.21 are those for the Chemical Plant image. Tables 3.4 and 3.5 give the quantitative comparisons of the above mentioned results. Figs. 3.22 and 3.23 show the encoded Girl image at approximate bit rates of 1 and 2 bits/pixel, and the corresponding figures for the encoded Chemical Plant image are shown in Figs. 3.24 and 3.25. Fig. 3.26 compares the original and the adaptive classified (based on actual measurement model) hybrid encoded images at 1 and 2 bits/pixel.

Finally, observe that as an image column size is increased, the ambiguity in classifying it into different classes will also go up because the activity in a large image column is not likely to be uniform so as to be represented by its variance.

### 3.6 Extensions of Hybrid Coding

Hybrid coding techniques can be generalized and extended to higher order semicausal models and for coding of noisy images. In this section we briefly discuss the formulations and simulation results.

#### 3.6.1 Hybrid Encoded Image with Channel Error

Since practical communication channels are noisy, it is worthwhile to study the channel noise effects on the Hybrid encoded images. A binary symmetric channel is used here as the noisy communication channel. Fig. 3.27 shows the representation of such a channel, where the probability of receiving an incorrect symbol is  $P_e$  and a correct one is  $1 - P_e$ , regardless of which symbol is transmitted.

Fig. 3.28 shows the effect of channel errors on hybrid coding schemes. Generally, the adaptive classification is quite robust. The nonadaptive and adaptive variance schemes can be made less sensitive to channel errors by reducing somewhat the horizontal correlation parameter. The SC1 model adaptive variance estimation seems to be less sensitive than the SC2 model. Figs. 3.29 and 3.30 show the encoded images in the presence of channel errors. Table 3.6 gives the quantitative comparisons of these results.



### 3.6.2 Higher Order Predictor in DPCM Loop of Hybrid Coding

This experiment is designed to have a  $n$ th order predictor instead of a first order predictor in the DPCM loop. Table 3.7 shows the results of using various predictors. Table 3.8 shows the numerical values of the predictor coefficients which are precalculated on the basis of the statistics of the transformed image strips.

These coefficients,  $\alpha_i$ , appear in the  $n$ th order autoregressive process (one for each channel)

$$v_j = \sum_{i=1}^n \alpha_i v_{j-i} + e_j \quad (3.6.2-1)$$

and are evaluated by solving the linear, Toeplitz equations

$$r_k = \sum_{i=1}^n r_{k-i} \alpha_i \quad (3.6.2-2)$$

where  $r_k = E v_j v_{j+k}$  is the covariance of the  $i$ th channel process in Hybrid coding.

The variance of the differential signal  $e_j$  is

$$\sigma_j^2 = \sigma^2 - \sum_{i=1}^n \alpha_i r_i \quad (3.6.2-3)$$

where  $\sigma^2$  is the variance of the input image.

A block diagram of this scheme is shown in Fig. 3.31 and Table 3.7 shows clearly that first order predictor is a reasonable choice for Hybrid Coding, since the signal to noise ratio improvement is small even though the order of the predictor goes up to four.

### 3.6.3 Hybrid Coding of Noisy Images

In many image transmission applications, the source image may happen to be noisy. This is because of the image spot pick-up sensor characteristics or due to some inherent limitations inside the mechanism. The foregoing developed coding methods can be modified to encode noisy images, if we know the statistics of noisy images beforehand. Let us assume a given noisy image degraded by additive white Gaussian noise with known signal to noise ratio (S/N) a priori, where S/N is defined as

$$S/N = \frac{\text{Standard deviation of the noise-free signal}}{\text{Standard deviation of the adding noise}}.$$

The additive noise in the given image can be filtered by replacing a predictor in the DPCM loop of Hybrid coder by a discrete Kalman filter. This design allows one to do the joint filtering and coding simultaneously. Fig. 3.32 is the block diagram of this scheme. The message and observation models in the  $i$ th channel of Hybrid coder after the transformation are as follows.

$$\text{Message:} \quad v_j(i) = p_h(i)v_{j-1}(i) + \epsilon_j(i) \quad (3.6.3-1)$$

$$\text{Observation:} \quad z_j(i) = v_j(i) + \eta_j(i) \quad (3.6.3-2)$$

and

$$E\epsilon_j(i)\epsilon_j(i+k) = \sigma^2(1-\rho_h(i))^2\lambda_{1,0}\delta_{k,0} \quad (3.6.3-3)$$

$$E\eta_j(i)\eta_j(i+k) = (S/N)^2\delta_{1,0}\delta_{k,0} \quad (3.6.3-4)$$

$\{\lambda_i\}$  are the diagonal entries of eigenvalue of  $R_v = \{\rho_v^{|m-n|}\}$ ,  $\rho_h$  and  $\rho_v$  are the horizontal and vertical corrections respectively.

The encoding scheme requires first taking the Cosine transform of each noisy image column  $u_j$ , then applying a bank of discrete Kalman filter DPCM on each row of the resulting image. Other necessary equations used in this scheme are as follows.

Predicted Observation:  $z_{j/j-1}(i) = \rho_h(i) \bar{v}_{j-1}(i)$  (3.6.3-5)

Innovation:  $e_j(i) = z_j(i) - z_{j/j-1}(i)$  (3.6.3-6)

Quantizer Output:  $e_j^*(i)$  (3.6.3-7)

Current Estimate:  $\bar{v}_j(i) = \rho_h(i) \bar{v}_{j-1}(i) + k_j(i) e_j^*(i)$  (3.6.3-8)

The above equations are very similar to the DPCM equations (page 46).

Furthermore,  $k_j(i)$  appears in (3.6.3-8), is called the Kalman gain and often referred to as a correction factor to the innovation  $\hat{e}_j(i)$ , (it is  $\hat{e}_j^*(i)$  essentially in this scheme) and can be obtained recursively as follows.

Gain:  $k_j(i) = \bar{v}_{j/j-1}(i) [\bar{v}_{j/j-1}(i) + \bar{v}_{v_j}(i)]^{-1}$  (3.6.3-9)

A priori Variance:  $\bar{v}_{j+1/j}(i) = \rho_h(i) \bar{v}_{v_j}(i) \rho_h(i) + \Psi_e$  (3.6.3-10)

A posteriori Variance:  $\bar{v}_{v_j}(i) = [1 - k_j(i)] \bar{v}_{j/j-1}(i)$  (3.6.3-11)

where

$$\tilde{v}_{j+1/j}(i) \triangleq v_{j+1}(i) - \bar{v}_{j+1/j}(i) \quad (3.6.3-12)$$

$$\tilde{v}_j(i) \triangleq v_j(i) - \bar{v}_j(i) \quad (3.6.3-13)$$



$$\bar{v}_{v_{j+1/j}}(i) = \text{var } v_{j+1/j}(i) \quad (3.6.3-14)$$

$$\bar{v}_{v_j}(i) = \text{var } v_j(i) \quad (3.6.3-15)$$

For easy reference, the eqns (3.6.3-5) through (3.6.3-15) are summarized in Table 3.9

Since we have a unity variance fixed level quantizer in the DPCM loop, it is required to know the variances of the innovations  $\epsilon_j(i)$  beforehand. These can be calculated approximately by summing the variances of  $\epsilon_j(i)$  and  $\eta_j(i)$ . A proper choice of initial conditions  $\bar{v}_{0/0}(i)$  and  $\bar{v}_{v_{0/0}}(i)$  is required. For simplicity, both are assumed to be zero. This means the initial value of  $i$ th DPCM channel is available to the receiver without distortion.

Three different values of S/N of noisy image were simulated in this study. Fig. 3.33 shows the restored images of implementing this scheme in a noisy Girl image. Table 3.10 tabulates the corresponding experimental results. The first entry of each category gives the improvement of signal to noise ratio in decibels,  $\text{SNR}_1$ , the second entry gives the actual signal to ratio,  $\text{SNR}_2$ , of the filtered image. These two quantities are related as follows.

$$\text{SNR}_2 \triangleq 10 \log_{10} \frac{(\text{Peak to Peak Value of Noise-free Image})^2}{\text{Error Variance of Filtered Image}} = 10 \log_{10} \frac{(255)^2}{\sigma_e^2}$$

$$\text{SNR}_1 \triangleq 10 \log_{10} \frac{\text{Error Variance of Noisy Image}}{\text{Error Variance of Filtered Image}} = 10 \log_{10} \frac{\sigma_b^2}{\sigma_e^2}$$

$$\begin{aligned}
\text{SNR}_2 &= 10 \log_{10} \frac{(255)^2}{\sigma_e^2} \\
&= 10 \log_{10} \frac{(255)^2}{\sigma_a^2} + 10 \log_{10} \frac{\sigma_a^2}{\sigma_b^2} + 10 \log_{10} \frac{\sigma_b^2}{\sigma_e^2} \\
&= 10 \log_{10} \frac{(255)^2}{\sigma_a^2} + 20 \log_{10} \frac{S}{N} + \text{SNR}_1
\end{aligned}$$

where  $\sigma_a^2$  is the variance of noise-free Girl image (in our example it equals 1816.21). Therefore, the above equation becomes

$$\text{SNR}_2 = 10 \log_{10} \frac{(255)^2}{1816.21} + 20 \log_{10} \frac{S}{N} + \text{SNR}_1 \quad (3.6.3-16)$$

In [34] it has shown that semicausal image models can be used to formulate and solve problems in image restoration. Here various hybrid coding schemes based on these models have been extended to encode noisy images. Due to the knowledge of image models, hybrid coding schemes can be successfully applied to encode both noisy and noiseless images. The results of this section promise the effectiveness of previously developed hybrid coding schemes in image data compression applications.

### 3.7 Summary of Results and Conclusions

Based on the above experiments and the theory discussed in this chapter, the following conclusions are made.

- 1) It was found that the performance of conventional nonadaptive hybrid coding can be improved up to 5.5 dB at low bit rates ( $\approx 1$  bit/pixel) by improved statistical characterization of the image via more accurate models and/or via adapting the parameters of the

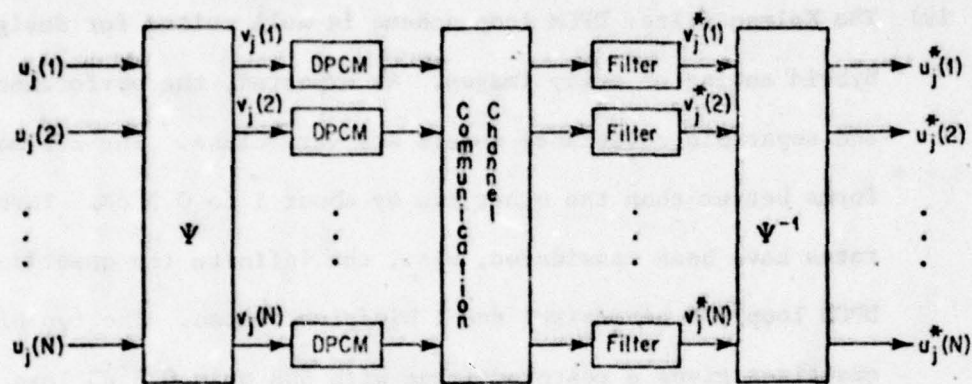
chosen model to changes in image statistics. The actual measurements model applied in the adaptive classification coding scheme gave the best results. However, this model requires identification of a large number of parameters. In general, the SC1 model performed better than SC2 and separable covariance models by 2 to 3 dB. As expected from theoretical considerations, the SC2 and separable covariance models performed almost identically.

- ii) The adaptive variance estimation technique is useful when it is desired to maintain the performance of a hybrid coder, designed for a nominal statistics, in the face of changing statistics (e.g., the correlation parameter). If the image data statistics is close to the design parameters, then the improvement over nonadaptive scheme is marginal (1 to 1.5 dB at 1 bit/pixel). This technique is effective at relatively higher bit rates  $\geq 1$  bit/pixel and for relatively larger image column sizes. It should be considered not so much for achieving low transmission rates as for achieving higher SNR at moderate rates. The complexity over a nonadaptive scheme is marginal, and it can be hardware implemented very easily. Finally, it maintains a constant bit rate from one image column to the next and its performance in the presence of channel errors is no worse than the nonadaptive schemes.
- iii) The adaptive classification scheme is a variable bit rate technique (average bit rate from one column to the next can vary) which is robust (with respect to channel errors) and can yield varying degree of performances depending upon the coder complexity. It is relatively



more effective at low bit rates ( $\leq 1$  bit/pixel) and its performance is degraded as the image column size increases.

- iv) The Kalman filter DPCM loop scheme is well suited for designing Hybrid coding of noisy images. As expected, the performance of SC2 and separable covariance models are very close. The SC1 model performs better than the other two by about 1 to 0.5 dB. Three different rates have been considered, viz., the infinite (no quantizer in the DPCM loop), 2 bits/pixel and 1 bit/pixel rates. The two bit rate quantizer gives a restored image with SNR only 0.5 dB less than the infinite rate.
- v) The overall Kalman filter DPCM coder performance depends on additive noise vs. quantizer noise (bit rate) considerations. At low signal to noise ratios, the additive noise dominates, and moderate changes in bit rates have only marginal effect on improving the SNR of the encoded signal. (Note that the SNR is bounded by the Kalman filter performance without any quantizer noise). At high signal to noise ratios, the effect of quantization is more visible.



$\Psi$  = One Dimensional Unitary Transform

Figure 3.1 Hybrid Coding System

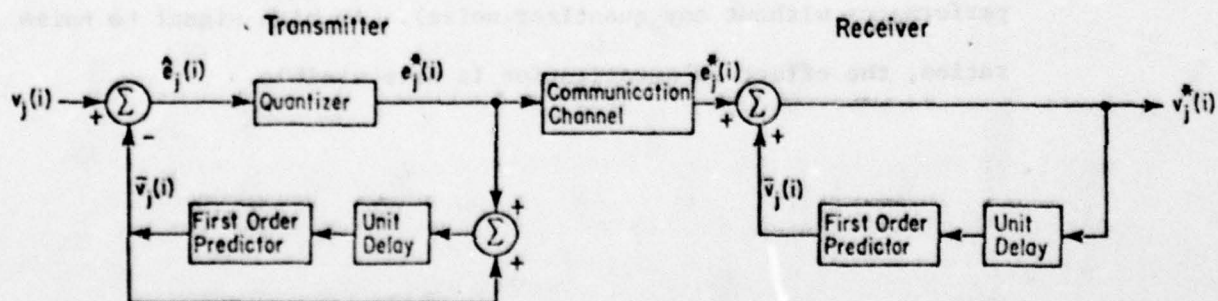


Figure 3.2 The i-th DPCM Channel

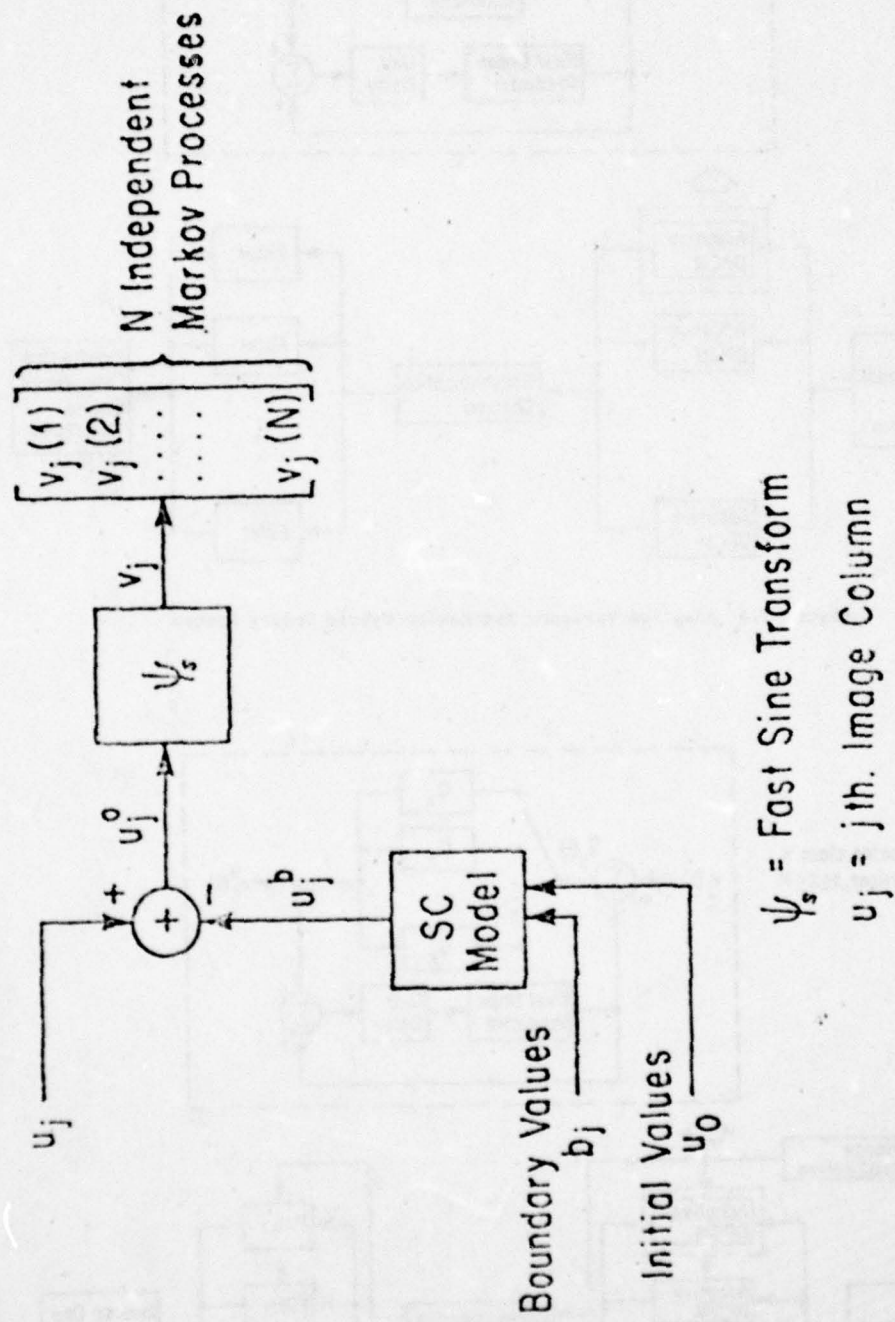


Figure 3.3 Realization of Semicausal Model Decomposition



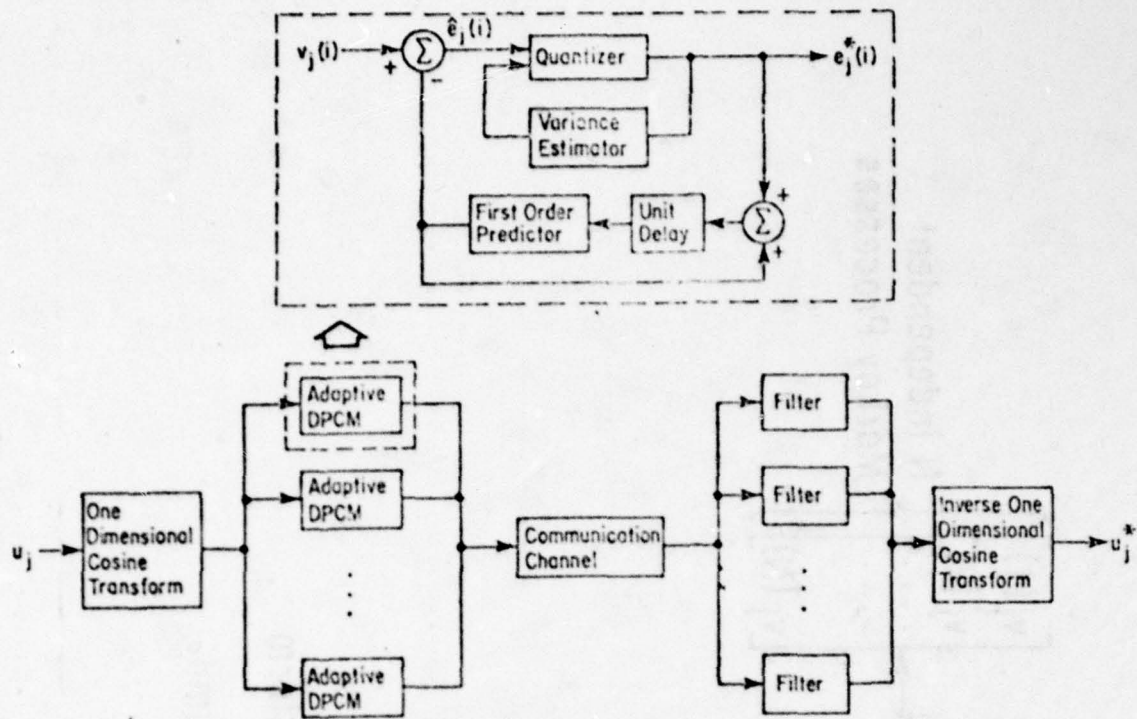


Figure 3.4 Adaptive Variance Estimation Hybrid Coding System

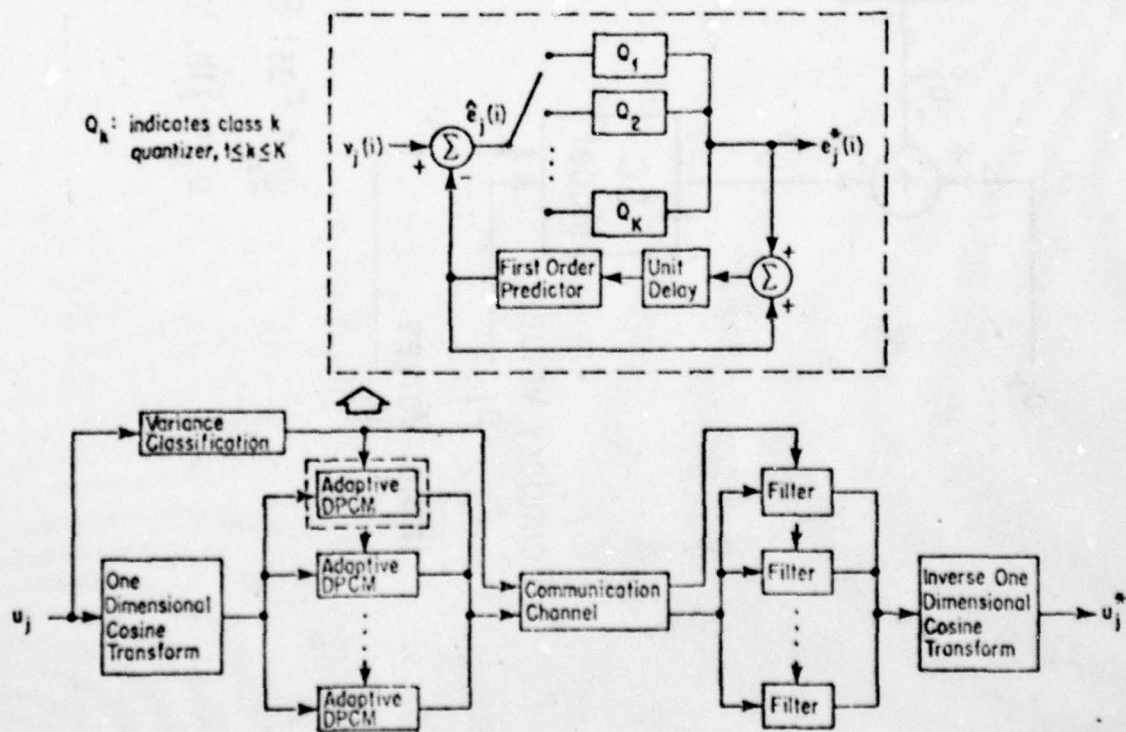


Figure 3.5 Adaptive Classification Hybrid Coding System

AD-A078 781

CALIFORNIA UNIV DAVIS SIGNAL AND IMAGE PROCESSING LAB F/G 9/4  
APPLICATIONS OF STOCHASTIC MODELS FOR IMAGE DATA COMPRESSION.(U)  
SEP 79 S WANG , A K JAIN DAAG29-78-G-0206

ARO-16222.3-EL

NL

UNCLASSIFIED

2 OF 3  
AD-A078781



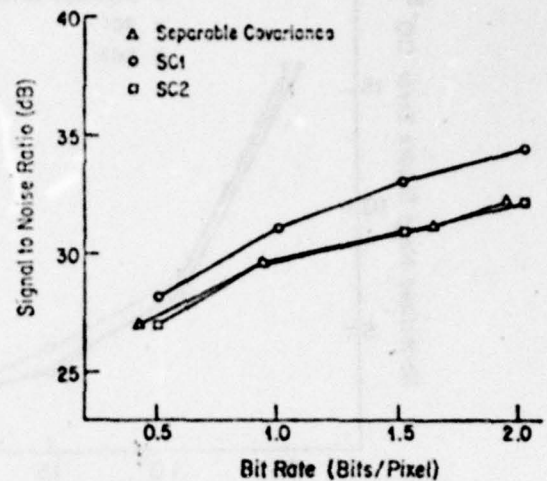
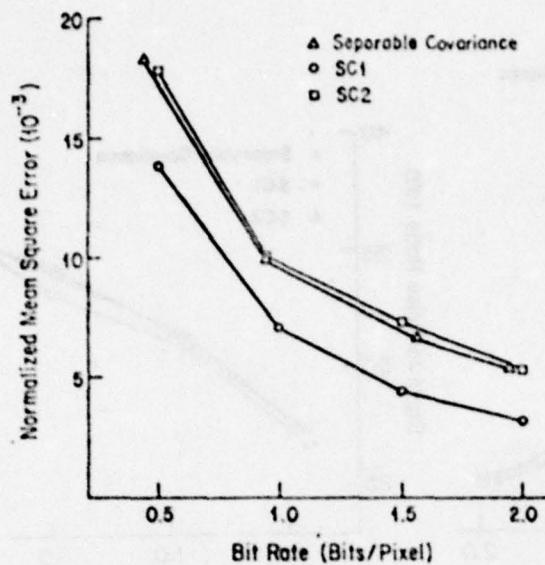


Figure 3.6 Nonadaptive Hybrid Coding Scheme for Various Image Models of the Girl Image . Encoded via 16 x 256 Image Strip, (a) Rate Distortion Curve (b) Signal to Noise Ratio versus Bit Rate

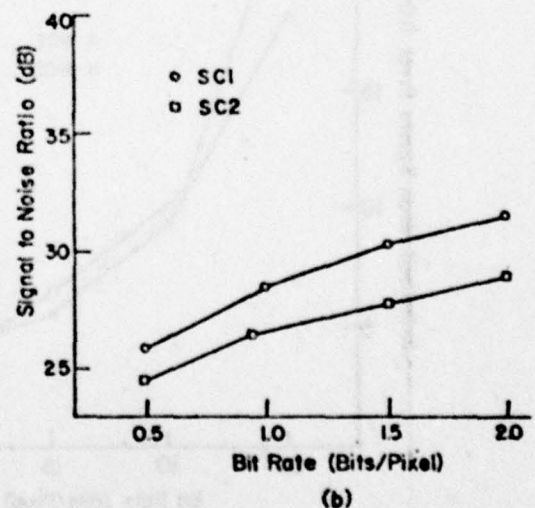
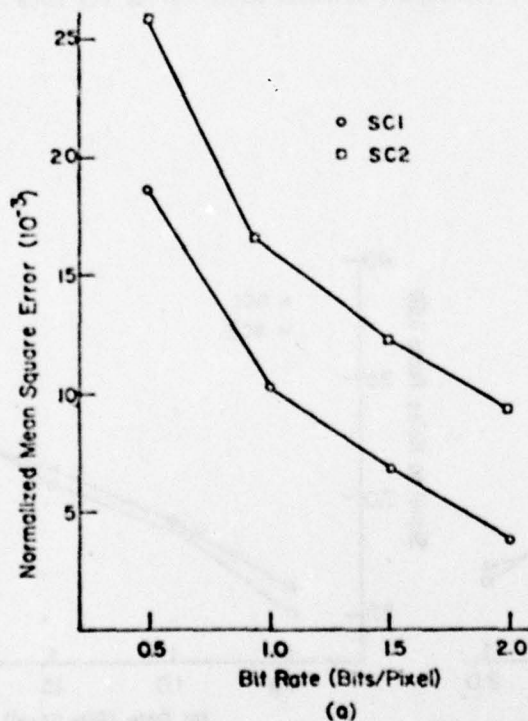


Figure 3.7 Nonadaptive Hybrid Coding Scheme for Various Image Models of the Chemical Plant Image Encoded via 16 x 256 Image Strip, (a) Rate Distortion Curve (b) Signal to Noise Ratio versus Bit Rate



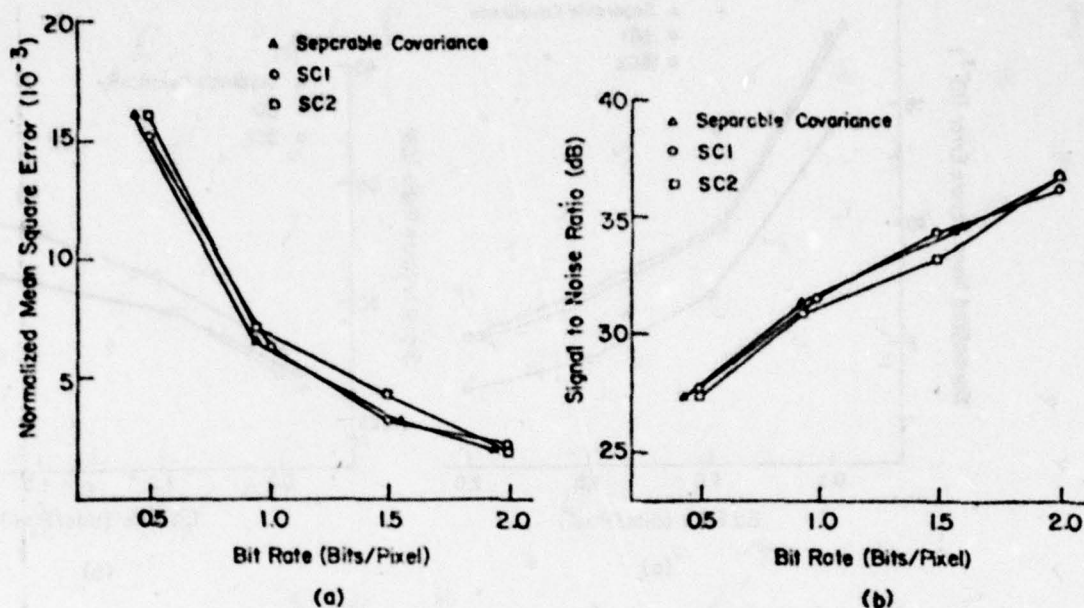


Figure 3.8 Comparison of Adaptive Variance Estimation Hybrid Coding Scheme for Various Image Models of the Girl Image Encoded via  $16 \times 256$  Image Strip.  
(a) Rate Distortion Curve (b) Signal to Noise Ratio versus Bit Rate

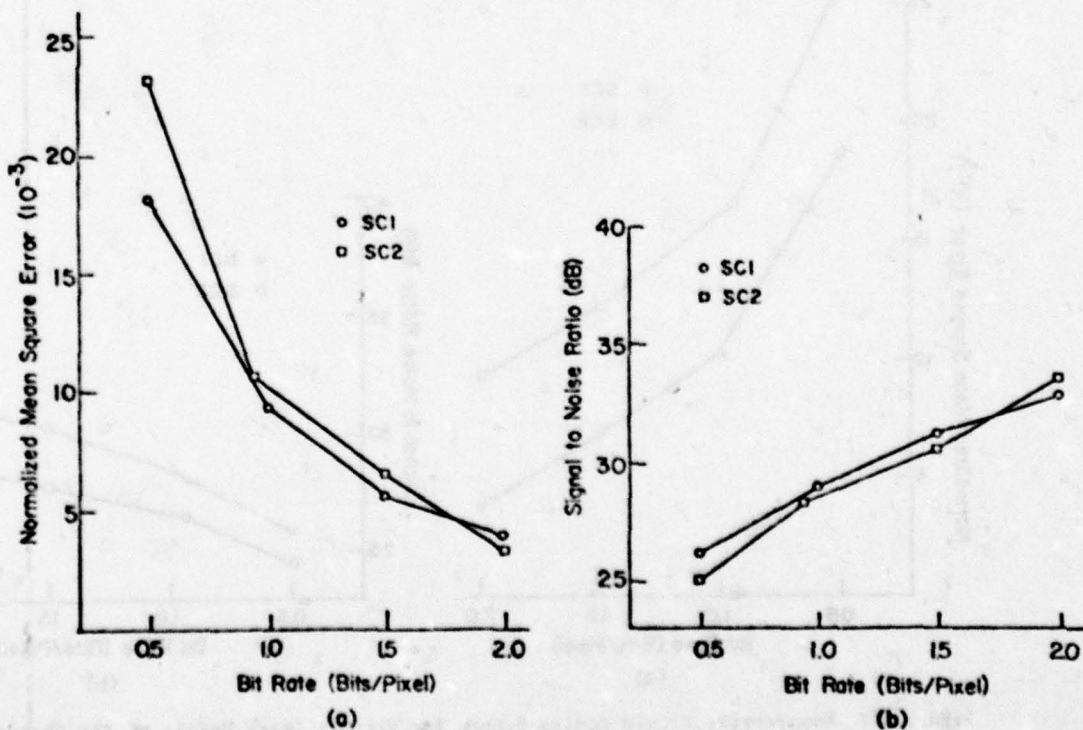
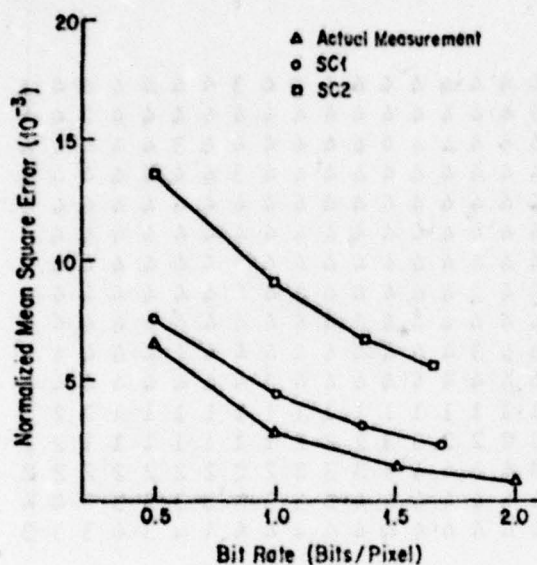


Figure 3.9 Comparison of Adaptive Variance Estimation Hybrid Coding Scheme for Various Image Models of the Chemical Plant Image Encoded via  $16 \times 256$  Image Strip.  
(a) Rate Distortion Curve (b) Signal to Noise Ratio versus Bit Rate

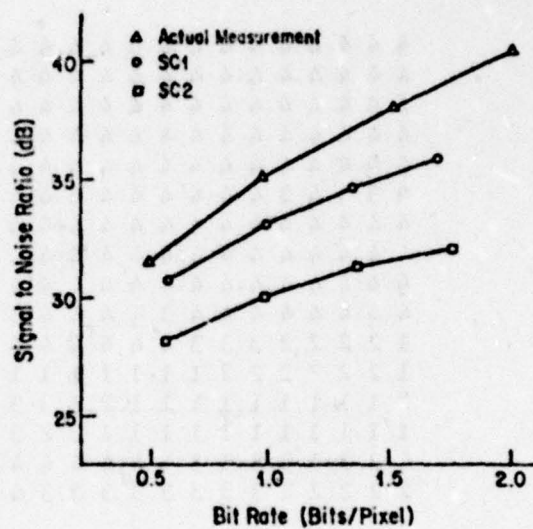
(a)

(b)

79

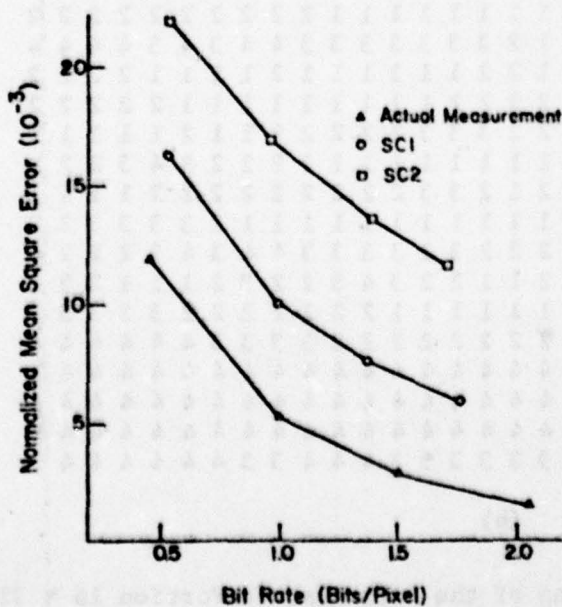


(a)

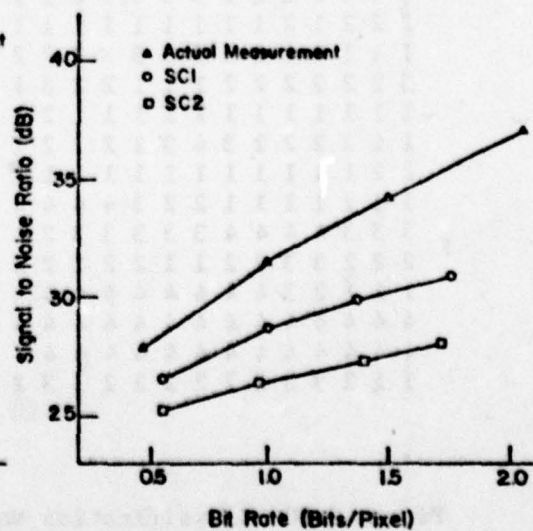


(b)

Figure 3.11 Comparison of Adaptive Classification Hybrid Coding Scheme for Various Image Models of the Girl Image Encoded via  $16 \times 256$  Image Strip, (a) Rate Distortion Curve (b) Signal to Noise Ratio versus Bit Rate



(a)



(b)

Figure 3.12 Comparison of Adaptive Classification Hybrid Coding Results for Various Image Models of the Chemical Plant Image Encoded via  $16 \times 256$  Image Strip, (a) Rate Distortion Curve (b) Signal to Noise Ratio Versus Bit Rate



[illegible][illegible]

Figure 3.13 Bar Allocations for Adaptive Classification,  $K = 4$ , Girl Image  
(a) Actual Measurement Model (b) SC1 Model (c) SC2 Model



MAXIMUM = .2230E+05 + 1.1E+01 = .2194E+01 RANGE = .2235E+05  
 VARIANCE = .0619E+01 MEAN = .1068E+04 STANDARD DEVIATION = .2413E+01

PSEUDO LEVEL      LOWER LEVEL      OCCURRENCES      EACH STAR REPRESENTS      16 OCCURRENCES

			100	200	400	600	800
1	.9194E+01	703	1				
2	.3204E+03	766	1				
3	.7077E+03	574	1				
4	.10570E+04	427	1				
5	.1406E+04	319	1				
6	.1755E+04	247	1				
7	.2104E+04	162	1				
8	.2454E+04	143	1				
9	.2803E+04	130	1				
10	.3152E+04	155	1				
11	.3501E+04	73	1				
12	.3851E+04	53	1				
13	.4200E+04	47	1				
14	.4549E+04	33	1				
15	.4899E+04	26	1				
16	.5248E+04	25	1				
17	.5597E+04	21	1				
18	.5946E+04	17	1				
19	.6296E+04	11	1				
20	.6645E+04	10	1				
21	.6994E+04	10	1				
22	.7343E+04	14	1				
23	.7693E+04	9	1				
24	.8042E+04	12	1				
25	.8391E+04	6	1				
26	.8740E+04	6	1				
27	.9089E+04	7	1				
28	.9438E+04	4	1				
29	.9787E+04	6	1				
30	.10136E+05	3	1				
31	.10487E+05	4	1				
32	.10837E+05	2	1				
33	.11186E+05	4	1				
34	.11535E+05	4	1				
35	.11884E+05	2	1				
36	.12234E+05	2	1				
37	.12583E+05	2	1				
38	.12932E+05	4	1				
39	.13281E+05	1	1				
40	.13631E+05	4	1				
41	.13980E+05	20	1				
42	.14329E+05	2	1				
43	.14679E+05	4	1				
44	.15028E+05	1	1				
45	.15377E+05	2	1				
46	.15726E+05	1	1				
47	.16076E+05	3	1				
48	.16425E+05	2	1				
49	.16774E+05	2	1				
50	.17123E+05	5	1				
51	.17473E+05	4	1				
52	.17822E+05	4	1				
53	.18171E+05	6	1				
54	.18521E+05	2	1				
55	.18870E+05	2	1				
56	.19219E+05	1	1				
57	.19568E+05	4	1				
58	.19918E+05	3	1				
59	.20267E+05	6	1				
60	.20616E+05	9	1				
61	.20965E+05	1	1				
62	.21315E+05	6	1				
63	.21664E+05	6	1				
64	.22013E+05	6	1				

Figure 3.15 Histogram of Image Column Activities (Variances), Girl Image Is Used



MAXIMUM= .10713E+05 MINIMUM= .28970E+02 RANGE= .10684E+05  
 VARIANCE= .20560E+07 MEAN= .1688E+04 STANDARD DEVIATION= .1427E+04

PSEUDO LEVEL LOWER OCCURRENCES EACH STAR REPRESENTS 16 OCCURRENCES

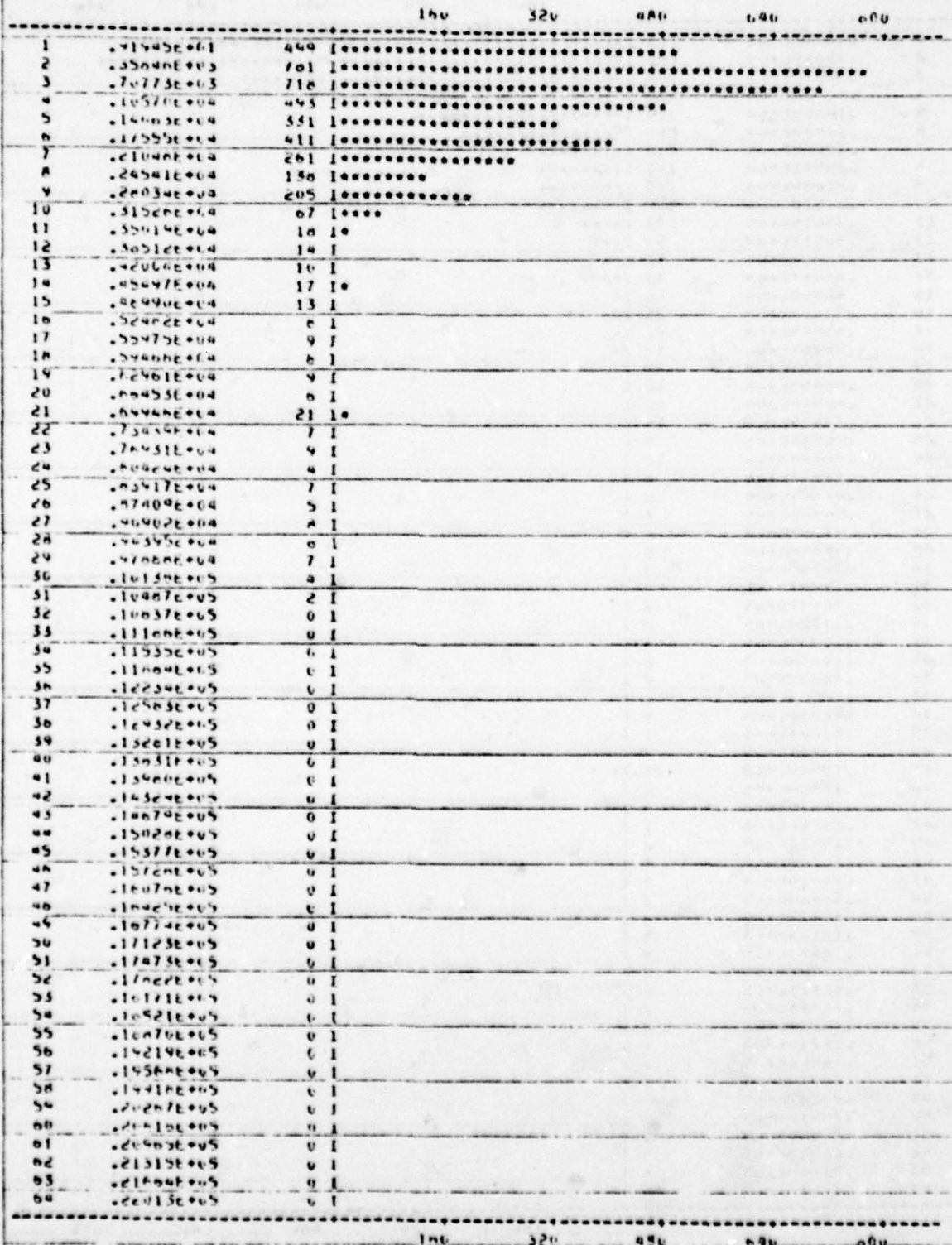


Figure 3.16 Histogram of Image Column Activities (Variances), Chemical Plant Image Is Used

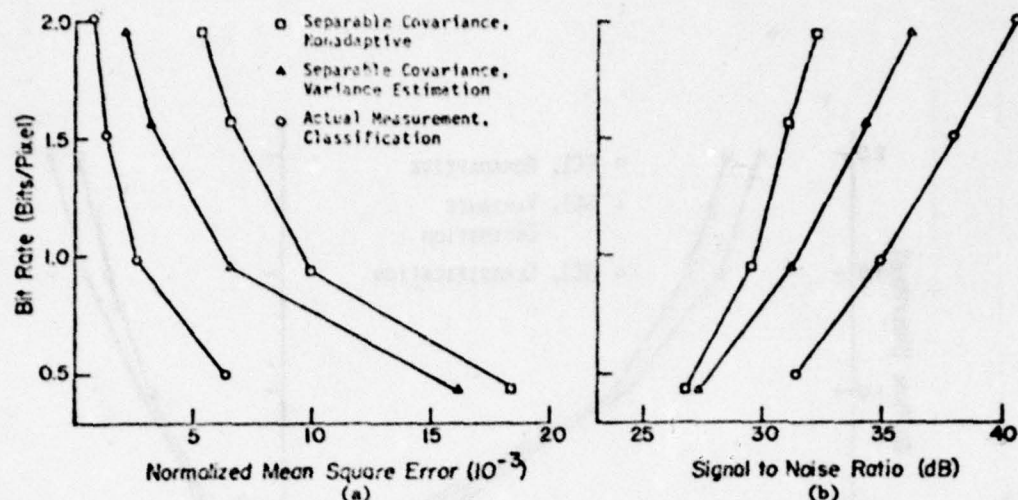


Figure 3.17 Hybrid Coding Results for Separable Covariance Model of the Girl Image Encoded via  $16 \times 256$  Image Strip. (a) Rate Distortion Curve (Bit Rate versus Normalized Mean Square Error) (b) Bit Rate versus Signal to Noise Ratio

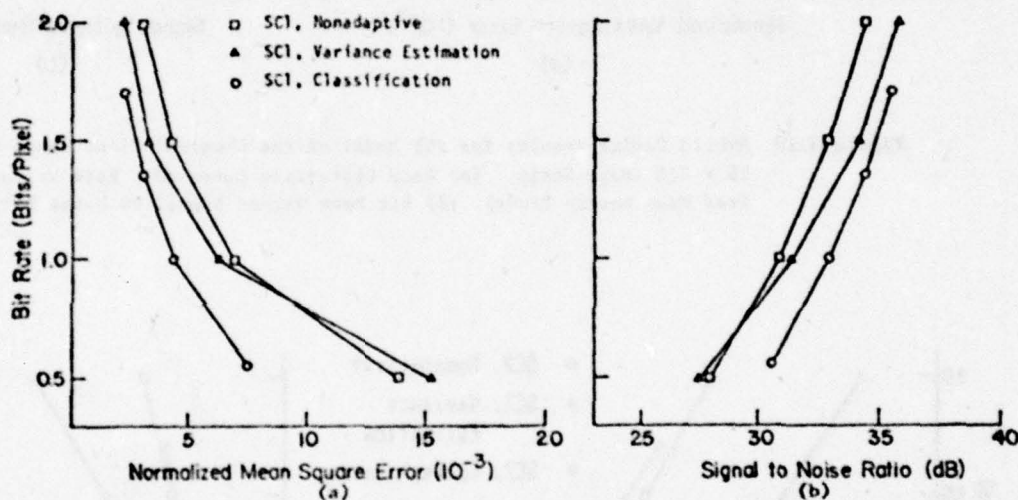


Figure 3.18 Hybrid Coding Results for SC1 Model of the Girl Image Encoded via  $16 \times 256$  Image Strip. (a) Rate Distortion Curve (Bit Rate versus Normalized Mean Square Error) (b) Bit Rate versus Signal to Noise Ratio

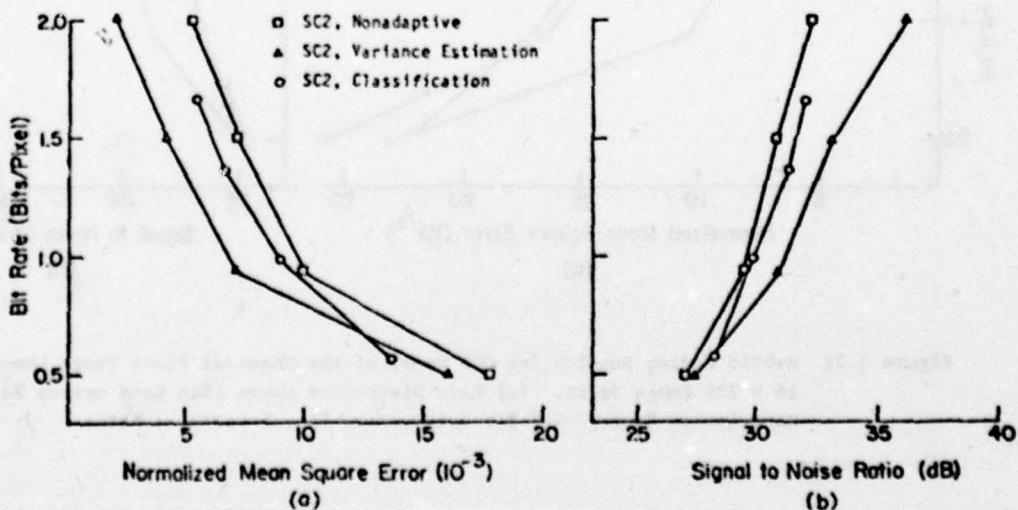


Figure 3.19 Hybrid Coding Results for SC2 Model of the Girl Image Encoded via  $16 \times 256$  Image Strip. (a) Rate Distortion Curve (Bit Rate versus Normalized Mean Square Error) (b) Bit Rate versus Signal to Noise Ratio

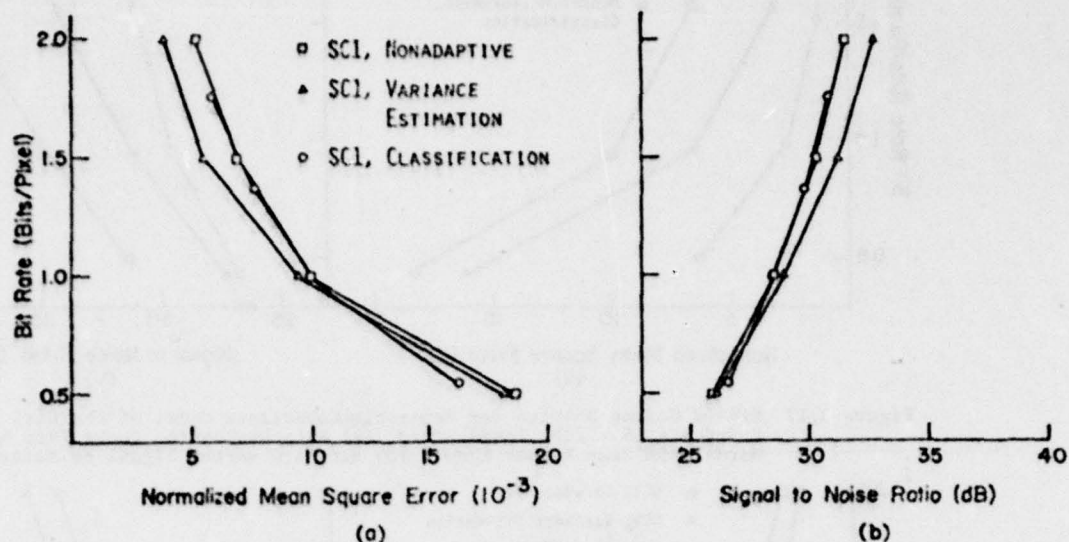


Figure 3.20 Hybrid Coding Results for SC1 Model of the Chemical Plant Image Encoded via  $16 \times 256$  Image Strip. (a) Rate Distortion Curve (Bit Rate versus Normalized Mean Square Error) (b) Bit Rate versus Signal to Noise Ratio

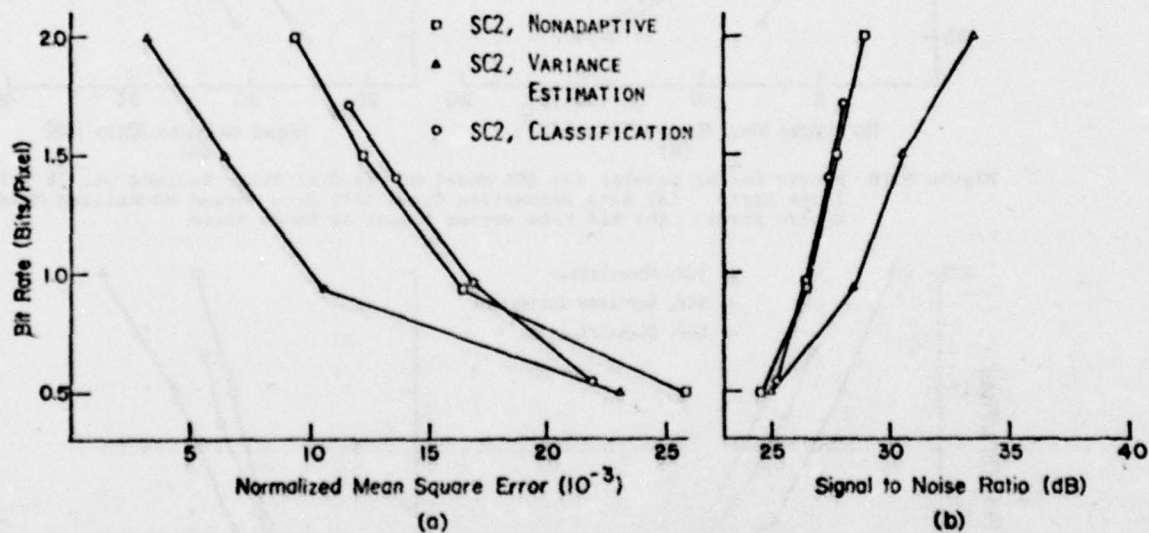


Figure 3.21 Hybrid Coding Results for SC2 Model of the Chemical Plant Image Encoded via  $16 \times 256$  Image Strip. (a) Rate Distortion Curve (Bit Rate versus Normalized Mean Square Error) (b) Bit Rate versus Signal to Noise Ratio





(a) SC1 Model, Nonadaptive



(d) SC2 Model, Nonadaptive



(b) SC1 Model, Adaptive  
Variance Estimation



(e) SC2 Model, Adaptive  
Variance Estimation



(c) SC1 Model, Adaptive  
Classification



(e) SC2 Model, Adaptive  
Classification

Figure 3.22 Hybrid Encoded Girl Image at 1 Bit/Pixel Approximately



(a) SC1 Model, Nonadaptive  
(2 Bits/Pixel)



(d) SC2 Model, Nonadaptive  
(2 Bits/Pixel)



(b) SC1 Model, Adaptive Variance  
Estimation (2 Bits/Pixel)



(e) SC2 Model, Adaptive Variance  
Estimation (2 Bits/Pixel)



(c) SC1 Model, Adaptive Classi-  
fication (1.7 Bits/Pixel)



(f) SC2 Model, Adaptive Classi-  
fication (1.67 Bits/Pixel)

Figure 3.23 Hybrid Encoded Girl Image at 1.7 to 2 Bits/Pixel Approximately



(a) SC1 Model, Nonadaptive



(d) SC2 Model, Nonadaptive



(b) SC1 Model, Adaptive  
Variance Estimation



(e) SC2 Model, Adaptive  
Variance Estimation



(c) SC1 Model, Adaptive  
Classification



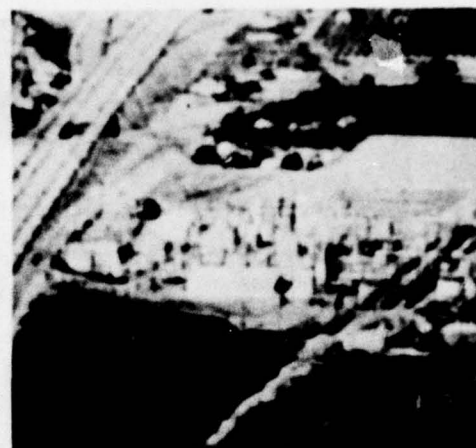
(f) SC2 Model, Adaptive  
Classification

Figure 3.24 Hybrid Encoded Chemical Plant Image at 1 Bit/Pixel  
Approximately





(a) SC1 Model, Nonadaptive  
(2 Bits/Pixel)



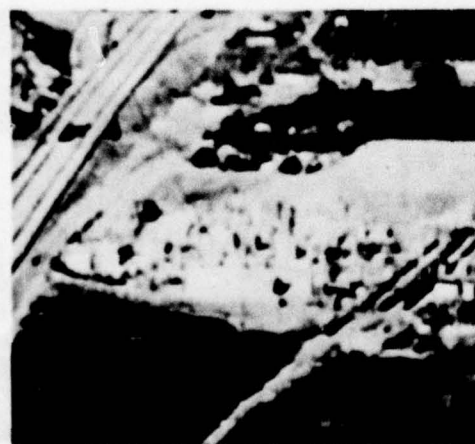
(d) SC2 Model, Nonadaptive  
(2 Bits/Pixel)



(b) SC1 Model, Adaptive  
Variance Estimation  
(2 Bits/Pixel)



(e) SC2 Model, Adaptive  
Variance Estimation  
(2 Bits/Pixel)



(c) SC1 Model, Adaptive Classi-  
fication (1.77 Bits/Pixel)



(f) SC2 Model, Adaptive Classi-  
fication (1.72 Bits/Pixel)

Figure 3.25 Hybrid Encoded Chemical Plant Image at 1.7 to 2 Bits/Pixel  
Approximately



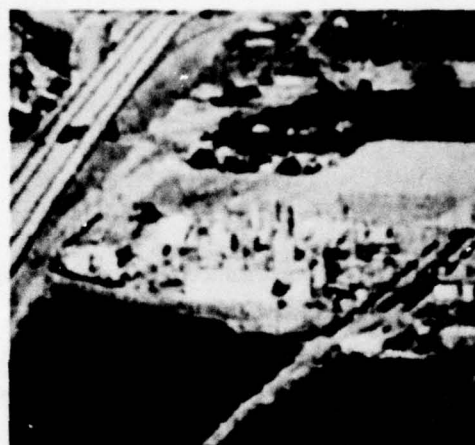
(a) Original Girl



(d) Original Chemical Plant



(b) Actual Measurement Model,  
0.97 Bit/Pixel



(e) Actual Measurement Model,  
1.02 Bits/Pixel



(c) Actual Measurement Model,  
2.02 Bits/Pixel



(f) Actual Measurement Model,  
2.06 Bits/Pixel

Figure 3.26 Actual Measurement Model Hybrid Encoded Image at 1 and 2 Bits/Pixel Approximately

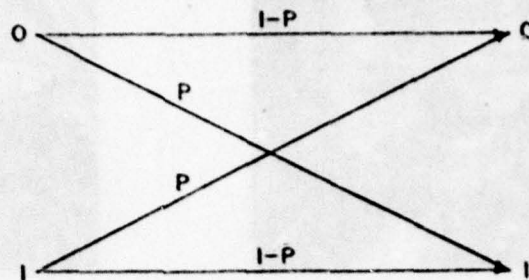


Figure 3.27 Model of a Binary Symmetric Channel

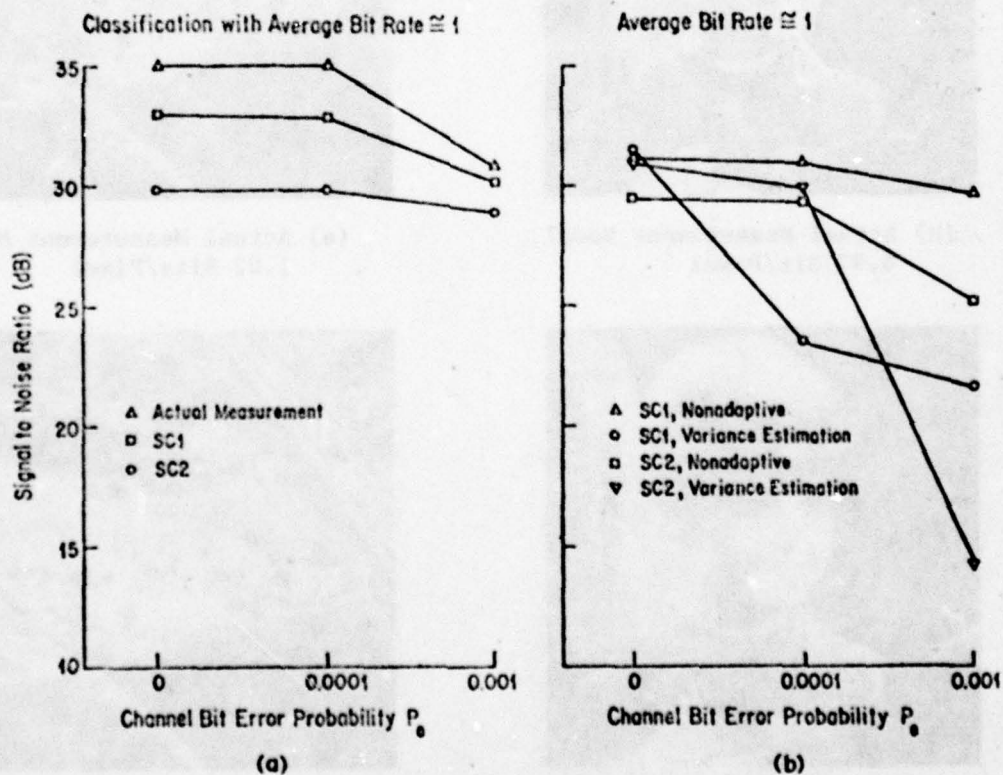


Figure 3.28 Effect of Channel Error





(a) SC1 Model, Nonadaptive



(d) SC2 Model, Nonadaptive



(b) SC1 Model, Adaptive  
Variance Estimation



(e) SC2 Model, Adaptive  
Variance Estimation



(c) SC1 Model, Adaptive  
Classification



(f) SC2 Model, Adaptive  
Classification

Figure 3.29 Hybrid Encoded Girl Image with Channel Error  $P_e = 0.0001$  at 1 Bit/Pixel Approximately



(a) SC1 Model, Nonadaptive



(d) SC2 Model, Nonadaptive



(b) SC1 Model, Adaptive  
Variance Estimation



(e) SC2 Model, Adaptive  
Variance Estimation



(c) SC1 Model, Adaptive  
Classification



(f) SC2 Model, Adaptive  
Classification

Figure 3.30 Hybrid Encoded Girl Image with Channel Error  $P_e = 0.001$  at 1 Bit/Pixel Approximately

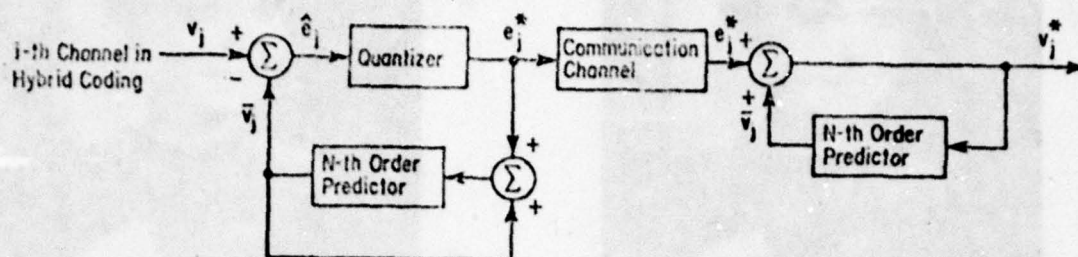


Figure 3.31 Higher Order Predictor and DPCM Channel

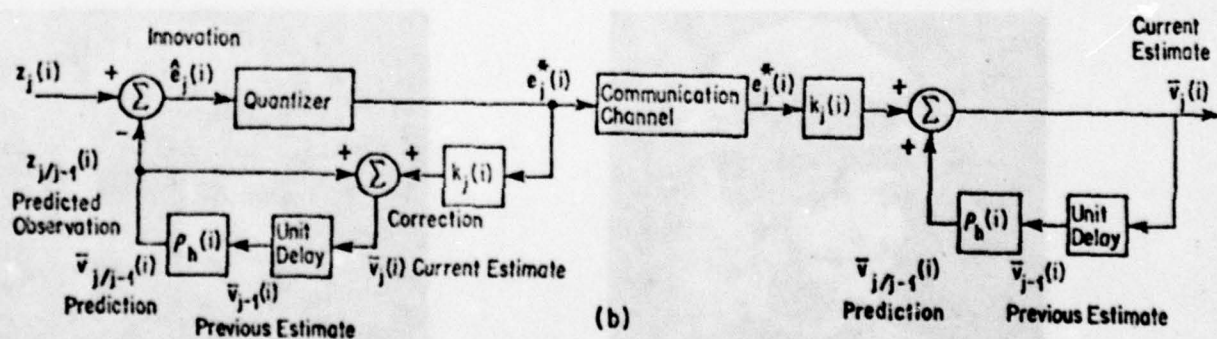
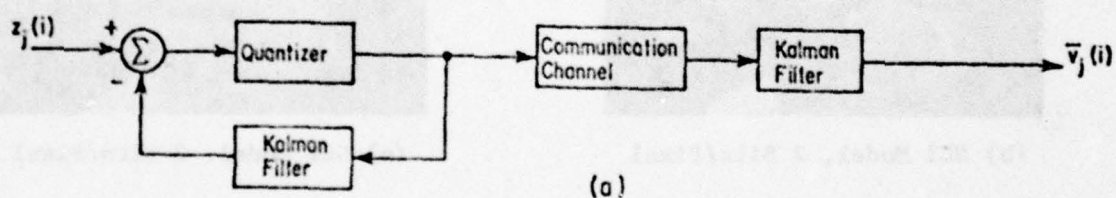


Figure 3.32 Kalman Filter DPCM Loop for the i-th Channel in Hybrid Coding





(a) SC1 Model, Infinite Rate



(d) SC2 Model, Infinite Rate



(b) SC1 Model, 2 Bits/Pixel



(e) SC2 Model, 2 Bits/Pixel



(c) SC1 Model, 1 Bit/Pixel



(f) SC2 Model, 1 Bit/Pixel

Figure 3.33 Restored Images of the Kalman Filter DPCM Loop Scheme Implemented on a Noisy Girl Image ( $S/N = 5$ )

Table 3.1 Bit Allocation Patterns Based on Equation (3.3.2-25), Girl Image

Desired Average Bit Rate	2			1.5			1			0.5		
Type of Bit Allocation	n	[n]	n*	n	[n]	n*	n	[n]	n*	n	[n]	n*
DPCM Channel No.												

(a) SC1 Model

1	4.27	4	4	3.77	4	4	3.15	3	3	2.16	2	2
2	4.12	4	4	3.62	4	4	3.00	3	3	2.01	2	2
3	3.74	4	4	3.24	3	3	2.62	3	3	1.63	2	2
4	3.28	3	3	2.78	3	3	2.16	2	2	1.17	1	1
5	2.83	3	3	2.33	2	2	1.70	2	2	0.72	1	1
6	2.42	2	2	1.92	2	2	1.30	1	1	0.31	0	0
7	2.06	2	2	1.56	2	2	0.95	1	1	0	0	0
8	1.75	2	2	1.25	1	1	0.63	1	1	0	0	0
9	1.49	1	1	0.99	1	1	0.37	0	0	0	0	0
10	1.27	1	1	0.77	1	1	0.14	0	0	0	0	0
11	1.08	1	1	0.58	1	1	0	0	0	0	0	0
12	0.93	1	1	0.43	0	0	0	0	0	0	0	0
13	0.81	1	1	0.31	0	0	0	0	0	0	0	0
14	0.71	1	1	0.21	0	0	0	0	0	0	0	0
15	0.65	1	1	0.15	0	0	0	0	0	0	0	0
16	0.61	1	1	0.11	0	0	0	0	0	0	0	0
Average Bit Rate	2.00	2	2	0.15	1.5	1.5	1.00	1.0	1.0	0.50	0.5	0.5

(b) SC2 Model

1	5.97	6	6	5.30	5	5	4.45	4	4	3.19	3	3
2	3.99	4	4	3.33	3	3	2.51	3	2	1.39	1	1
3	3.05	3	3	2.40	2	2	1.65	2	1	0.77	1	1
4	2.50	3	3	1.89	2	2	1.21	1	1	0.51	1	1
5	2.13	2	2	1.55	2	1	0.95	1	1	0.38	0	1
6	1.87	2	2	1.32	1	1	0.78	1	1	0.29	0	1
7	1.67	2	2	1.15	1	1	0.66	1	1	0.24	0	0
8	1.51	2	2	1.02	1	1	0.57	1	1	0.20	0	0
9	1.39	1	1	0.92	1	1	0.51	1	1	0.17	0	0
10	1.29	1	1	0.85	1	1	0.45	0	1	0.15	0	0
11	1.21	1	1	0.79	1	1	0.43	0	1	0.14	0	0
12	1.15	1	1	0.75	1	1	0.40	0	1	0.12	0	0
13	1.11	1	1	0.71	1	1	0.38	0	0	0.12	0	0
14	1.07	1	1	0.69	1	1	0.36	0	0	0.11	0	0
15	1.05	1	1	0.67	1	1	0.35	0	0	0.10	0	0
16	1.04	1	1	0.66	1	1	0.35	0	0	0.10	0	0
Average Bit Rate	2.00	2	2	1.50	1.5	1.5	1.00	0.94	1	0.50	0.38	0.5

where n: real bit allocation

[n]: Indicates the nearest integer of n

n\*: Integer bit calculated via integer bit allocation algorithm

Table 3.2 Bit Allocation Patterns Based on Equation (3.3-21), Girl Image

Desired Average Bit Rate	2			1.5			1			0.5		
Type of Bit Allocation	n	[n]	n*	n	[n]	n*	n	[n]	n*	n	[n]	n*
DPCM Channel No.												
(a) Separable Covariance Model												
1	5.39	5	5	4.89	5	5	4.38	4	4	3.44	3	4
2	4.05	4	4	3.56	4	4	3.04	3	3	2.10	2	2
3	3.26	3	3	2.76	3	3	2.25	2	2	1.31	1	1
4	2.70	3	3	2.20	2	2	1.68	2	2	0.74	1	1
5	2.31	2	2	1.81	2	2	1.30	1	1	0.36	0	0
6	2.01	2	2	1.51	2	1	1.00	1	1	0.06	0	0
7	1.78	2	2	1.28	1	1	0.76	1	1	0	0	0
8	1.59	2	2	1.09	1	1	0.57	1	1	0	0	0
9	1.43	1	2	0.93	1	1	0.42	0	1	0	0	0
10	1.31	1	1	0.81	1	1	0.29	0	0	0	0	0
11	1.20	1	1	0.70	1	1	0.18	0	0	0	0	0
12	1.11	1	1	0.62	1	1	0.10	0	0	0	0	0
13	1.05	1	1	0.55	1	1	0.03	0	0	0	0	0
14	1.00	1	1	0.50	0	0	0	0	0	0	0	0
15	0.96	1	1	0.46	0	0	0	0	0	0	0	0
16	0.94	1	1	0.44	0	0	0	0	0	0	0	0
Average Bit Rate	2.10	1.94	2	1.51	1.57	1.5	1.00	0.94	1	0.50	0.44	0.5
(b) SC1 Model												
1	4.27	4	4	3.77	4	4	3.15	3	3	2.16	2	2
2	4.12	4	4	3.62	4	4	3.00	3	3	2.01	2	2
3	3.74	4	4	3.24	3	3	2.62	3	3	1.63	2	2
4	3.28	3	3	2.78	3	3	2.16	2	2	1.17	1	1
5	2.83	3	3	2.33	2	2	1.70	2	2	0.72	1	1
6	2.42	2	2	1.92	2	2	1.30	1	1	0.31	0	0
7	2.06	2	2	1.56	2	2	0.94	1	1	0	0	0
8	1.75	2	2	1.25	1	1	0.63	1	1	0	0	0
9	1.48	1	1	0.99	1	1	0.37	0	0	0	0	0
10	1.27	1	1	0.77	1	1	0.14	0	0	0	0	0
11	1.08	1	1	0.58	1	1	0	0	0	0	0	0
12	0.93	1	1	0.43	0	0	0	0	0	0	0	0
13	0.81	1	1	0.31	0	0	0	0	0	0	0	0
14	0.71	1	1	0.21	0	0	0	0	0	0	0	0
15	0.65	1	1	0.15	0	0	0	0	0	0	0	0
16	0.61	1	1	0.11	0	0	0	0	0	0	0	0
Average Bit Rate	2.00	2	2	1.50	1.5	1.5	1.00	1	1	0.50	0.5	0.5
(c) SC2 Model												
1	6.15	6	6	5.65	6	6	5.12	5	5	4.07	4	4
2	4.17	4	4	3.67	4	4	3.14	3	3	2.08	2	2
3	3.21	3	3	2.71	3	3	2.18	2	2	1.13	1	1
4	2.64	3	3	2.14	2	2	1.61	2	2	0.56	1	1
5	2.24	2	2	1.74	2	2	1.22	1	1	0.16	0	0
6	1.95	2	2	1.45	1	1	0.92	1	1	0	0	0
7	1.71	2	2	1.21	1	1	0.68	1	1	0	0	0
8	1.52	2	2	1.02	1	1	0.49	0	1	0	0	0
9	1.36	1	1	0.86	1	1	0.33	0	0	0	0	0
10	1.23	1	1	0.73	1	1	0.20	0	0	0	0	0
11	1.13	1	1	0.63	1	1	0.10	0	0	0	0	0
12	1.04	1	1	0.54	1	1	0.01	0	0	0	0	0
13	0.98	1	1	0.48	0	0	0	0	0	0	0	0
14	0.93	1	1	0.43	0	0	0	0	0	0	0	0
15	0.89	1	1	0.39	0	0	0	0	0	0	0	0
16	0.87	1	1	0.37	0	0	0	0	0	0	0	0
Average Bit Rate	2.00	2	2	1.50	1.5	1.5	1.00	0.94	1	0.50	0.5	0.5

where  $n$  : real bit allocation[n]: indicates the nearest integer of  $n$  $n^*$ : integer bit calculated via integer bit allocation algorithm



Table 3.3 Parameters of Image Models Used in Hybrid Coding

Separable Covariance Model

$$\rho_h = \rho_v = 0.95$$

$$\beta^2(i) = (1 - \rho_h^2) / \lambda_i$$

$$\lambda_i = [\Psi R \Psi]_{i,i}$$

Semicausal Model SC1

$$\alpha = .4275, \gamma = 0.1415, \beta^2 = 0.0198 \quad (\text{Girl Image})$$

$$\alpha = .4275, \gamma = 0.1420, \beta^2 = 0.0169 \quad (\text{Chemical Plant Image})$$

$$\lambda_{ci} = 1 - 2\alpha \cos \frac{(i-1)\pi}{N}, \quad 1 \leq i \leq N$$

$$\beta^2(i) = \beta^2 / \lambda_{ci}^2$$

$$\rho_i = \gamma / \lambda_{ci}$$

Semicausal Model SC2

$$\rho_h = \rho_v = 0.95, \quad \alpha = \rho_v / (1 + \rho_v^2)$$

$$\lambda_{ci} = 1 - 2\alpha \cos \frac{(i-1)\pi}{N}, \quad 1 \leq i \leq N$$

$$\beta^2 = (1 - \rho_h^2)(1 - \rho_v^2) / (1 + \rho_v^2)$$

$$\beta^2(i) = \beta^2 / \lambda_{ci}$$

$$\rho_i = \rho_h$$

Actual Measurement Model

$$v_j(i) = \rho_i v_{j-1}(i) + e_j(i)$$

$$\rho_i = E v_j(i) v_{j-1}(i) \approx \frac{1}{16M} \sum_{j=2}^M \sum_{k=1}^{16} v_j^k(i) v_{j-1}^k(i)$$

$$\beta^2(i) = E e_j^2(i) = (1 - \rho_i^2) E v_j^2(i) \approx \frac{(1 - \rho_i^2)}{16M} \sum_{j=1}^M \sum_{k=1}^{16} [v_j^k(i)]^2$$

where  $v_j^k(i)$  =  $i$ th element of the  $j$ th column of the  $k$ th  $16 \times M$  size image strip ( $k=1, \dots, 16$  here).

Table 3.4 Hybrid Coding Results of the Girl Image Encoded via 16 × 256 Image Strip

Desired Average Bit Rate	2			1.5			1			0.5		
Method	SNR	N.M.S.E.	Actual Rate	SNR	N.M.S.E.	Actual Rate	SNR	N.M.S.E.	Actual Rate	SNR	N.M.S.E.	Actual Rate
(a) Separable Covariance Model												
Nonadaptive	32.26	0.535%	1.94	31.26	0.674%	1.56	29.57	0.993%	0.94	26.91	1.833%	0.44
Adaptive Variance Estimation	36.24	0.214%	1.94	34.33	0.332%	1.56	31.31	0.666%	0.94	27.47	1.612%	0.44
(b) SC1 Model												
Nonadaptive	34.55	0.316%	2	33.07	0.444%	1.5	31.05	0.707%	1	28.13	1.384%	0.5
Adaptive Variance Estimation	35.97	0.228%	2	34.25	0.338%	1.5	31.48	0.640%	1	27.73	1.518%	0.5
Adaptive Classification	35.80	0.236%	1.70	34.55	0.316%	1.36	33.07	0.444%	1	30.74	0.758%	0.5
(c) SC2 Model												
Nonadaptive	32.30	0.529%	2	30.91	0.730%	1.5	29.53	1.003%	0.94	27.03	1.783%	0.5
Adaptive Variance Estimation	36.25	0.213%	2	33.17	0.434%	1.5	31.00	.715%	0.94	27.48	1.608%	0.5
Adaptive Classification	32.05	0.561%	1.67	31.31	0.666%	1.38	29.97	.906%	0.98	28.20	1.362%	0.5
(d) Actual Measurement Model												
Adaptive Classification	40.59	0.079%	2.02	38.07	0.140%	1.52	35.01	0.284%	0.97	31.42	0.649%	0.5

Table 3.5 Hybrid Coding Results of the Chemical Plant Image Encoded via 16 x 256 Image Strip

Desired Average Bit Rate	2			1.5			1			-0.5		
Method	SNR	N.M.S.E.	Actual Rate	SNR	N.M.S.E.	Actual Rate	SNR	N.M.S.E.	Actual Rate	SNR	N.M.S.E.	Actual Rate
(a) SC1 Model												
Nonadaptive	31.54	0.520%	2	30.29	0.693%	1.5	28.55	1.034%	1	25.98	1.867%	0.5
Adaptive Variance Estimation	32.82	0.387%	2	31.23	0.558%	1.5	28.98	0.938%	1	26.09	1.820%	0.5
Adaptive Classification	30.93	0.592%	1.77	29.87	0.764%	1.38	28.66	1.009%	1.02	26.58	1.630%	0.55
(b) SC2 Model												
Nonadaptive	28.96	0.941%	2	27.80	1.228%	1.5	26.50	1.658%	0.94	24.56	2.590%	0.5
Adaptive Variance Estimation	33.55	0.327%	2	30.55	0.653%	1.5	28.41	1.069%	0.94	25.05	2.318%	0.5
Adaptive Classification	28.01	1.171%	1.72	27.336	1.368%	1.41	26.40	1.699%	0.97	25.27	2.199%	0.55
(c) Actual Measurement Model												
Adaptive Classification	37.03	0.147%	2.06	34.22	0.280%	1.52	31.48	0.527%	1.02	27.92	1.196%	0.47



Table 3.6 Hybrid Coding Results with Communication Errors, Girl Image Encoded via 16 × 256 Image Strip

Bit Error Probability $P_e$	0			0.0001			0.001		
Method	SNR	N.M.S.E.	Actual Rate	SNR	N.M.S.E.	Actual Rate	SNR	N.M.S.E.	Actual Rate
(a) Separable Covariance Model									
Nonadaptive	29.57	0.993%	0.94	29.38	1.039%	0.94	27.99	1.430%	0.94
Adaptive Variance Estimation	31.31	0.666%	0.94	28.17	1.373%	0.94	11.77	59.90%	0.94
(b) SC1 Model									
Nonadaptive	31.05	0.707%	1	30.97	0.720%	1	29.60	0.987%	1
Adaptive Variance Estimation	31.48	0.640%	1	23.45	4.064%	1	21.60	6.229%	1
Adaptive Classification	33.07	0.444%	1	32.95	0.456%	1	30.24	0.851%	1
(c) SC2 Model									
Nonadaptive	29.53	1.003%	0.94	29.31	0.105%	0.94	25.17	2.738%	0.94
Adaptive Variance Estimation	31.00	0.715%	0.94	29.95	0.910%	0.94	14.33	33.22%	0.94
Adaptive Classification	29.97	0.906%	0.98	29.97	0.906%	0.98	28.97	1.139%	0.98
(d) Actual Measurement Model									
Adaptive Classification	35.01	0.284%	0.97	35.00	0.285%	0.97	30.88	0.736%	0.97

Table 3.7 The Experimental Results of Higher Order Predictor Implemented on the Girl Image with 16 DPCM Channels

Order of the Predictor	1	2	3	4
Signal to Noise Ratio (dB)	31.202	31.748	31.796	31.792

Table 3.8 Predictor Coefficients of Various Orders for Different Channels in Hybrid Coding

Order of the Predictor	1			2			3			4			
Channel Number	$\alpha_1$	$\alpha_1$	$\alpha_2$	$\alpha_1$	$\alpha_2$	$\alpha_3$	$\alpha_1$	$\alpha_2$	$\alpha_3$	$\alpha_4$			
1	0.989	1.457	-0.473	1.465	-0.498	0.017	1.465	-0.508	0.048	-0.021			
2	0.967	1.424	-0.472	1.480	-0.643	0.120	1.486	-0.672	0.188	-0.046			
3	0.926	1.313	-0.418	1.369	-0.592	0.133	1.372	-0.605	0.164	-0.023			
4	0.866	1.815	-0.368	1.220	-0.483	0.097	1.220	-0.482	0.094	0.003			
5	0.851	1.100	-0.292	1.130	-0.406	0.104	1.129	-0.400	0.086	0.016			
6	0.820	1.076	-0.251	1.039	-0.305	0.053	1.041	-0.317	0.092	-0.038			
7	0.742	0.915	-0.233	0.915	-0.233	-0.001	0.915	-0.240	0.029	-0.033			
8	0.666	0.786	-0.179	0.788	-0.191	0.143	0.788	-0.192	0.020	-0.007			
9	0.614	0.699	-0.138	0.698	-0.132	-0.009	0.697	-0.133	-0.004	-0.008			
10	0.617	0.660	-0.070	0.661	-0.075	0.009	0.660	-0.075	0.004	0.007			
11	0.512	0.551	-0.098	0.548	-0.083	-0.027	0.547	-0.084	-0.018	-0.017			
12	0.458	0.500	-0.091	0.501	-0.096	0.011	0.501	-0.093	-0.002	0.026			
13	0.401	0.413	-0.032	0.414	-0.042	0.025	0.413	-0.040	0.006	0.047			
14	0.326	0.337	-0.035	0.339	-0.052	0.050	0.338	-0.051	0.046	0.012			
15	0.283	0.284	-0.007	0.284	-0.003	-0.015	0.285	-0.003	-0.024	0.031			
16	0.227	0.236	-0.040	0.236	-0.043	0.011	0.236	-0.044	0.014	-0.015			

Table 3.9 Discrete Kalman Filter and DPCM Algorithms

Message Model	$v_{j+1}(i) = \rho_h(i)v_j(i) + \epsilon_{j+1}(i)$
Observation Model	$z_j(i) = v_j(i) + \eta_j(i)$
Prior Statistics	$E\epsilon_j(i) = 0, E\eta(i) = 0, Ev_0(i) = \mu_{v_0}(i) = 0$ $E\eta_j(i)\eta_{j+l}(i+k) = (S/N)^2 \delta_{l,0} \delta_{k,0} = \Psi_{\eta} \delta_{l,0} \delta_{k,0}$ $E\epsilon_j(i)\epsilon_{j+l}(i+k) = \sigma^2(1-\rho_h(i))\lambda_i \delta_{l,0} \delta_{k,0} = \Psi_{\epsilon} \delta_{l,0} \delta_{k,0}$ $E\epsilon_j(i)\eta_{j+l}(i+k) = E\epsilon_j(i)v_0(i+k) = E\eta_j(i)v_0(i+k) = 0$ $\text{var}[v_0(i)] = v_{v_0}(i)$
Innovation	$\hat{e}_j(i) = z_j(i) - \rho_h(i)\tilde{v}_{j-1}(i)$
Filter	$\tilde{v}_j(i) = \rho_h(i)\tilde{v}_{j-1}(i) + k_j(i)e_j^*(i)$
Gain	$k_j(i) = v_{\tilde{v}_{j/j-1}}(i) \left[ v_{\tilde{v}_{j/j-1}}(i) + v_{v_j}(i) \right]^{-1}$
A Priori Variance	$v_{\tilde{v}_{j+1/j}} = \rho_h(i)v_{\tilde{v}_j}(i)\rho_h(i) + \Psi_{\epsilon}$
A Posteriori Variance	$v_{\tilde{v}_j}(i) = [1-k_j(i)]v_{\tilde{v}_{j/j-1}}(i)$
Initial Conditions	$\hat{v}_{0/0}(i) = \hat{v}_0(i) = \mu_{v_0}(i) = 0$ $v_{\tilde{v}_{0/0}}(i) = v_{\tilde{v}_0}(i) = v_{v_0}(i)$



Table 3.10 The Experimental Results of Kalman Filter DPCM Loop Implemented on the Noisy Girl Image. The First Entry of Each Category Shows the Improvement of Signal to Noise Ratio in Decibels and the Second Entry Shows Signal to Noise Ratio in Decibels of the Noisy Encoded Image.

Image Model	Kalman Filter DPCM Loop with Quantizer at Average Rate = (.) Bits/Pixel, Where (.) Is				
	∞	2	1.5	1	0.5
(a) S/N = 1					
Separable Covariance Model	9.1058	8.3765	8.4023	7.5003	7.5231
	24.6652	23.9359	23.9617	23.0597	23.0825
Semicausal Model SC1	9.1327	8.4537	8.4517	8.1968	8.1660
	24.6921	24.0131	24.0111	23.7562	23.7454
Semicausal Model SC2	8.7611	8.1918	8.2143	7.4203	7.4409
	24.3205	23.7512	23.7737	22.9802	23.0003
(b) S/N = 2					
Separable Covariance Model	5.8183	4.5647	4.5878	3.8615	3.8129
	27.3983	26.1447	26.1678	25.4415	25.3929
Semicausal Model SC1	5.8895	5.2081	5.0295	4.6383	4.0781
	27.4695	26.7881	26.6095	26.2183	25.6581
Semicausal Model SC2	5.7026	4.6184	4.6257	3.9068	3.7119
	27.2826	26.1984	26.2057	25.4868	25.2919
(c) S/N = 5					
Separable Covariance Model	2.2492	-0.5675	-0.9584	-1.6039	-3.0860
	31.7880	28.9713	28.5804	27.9349	26.4528
Semicausal Model SC1	2.6618	1.1673	0.7125	-0.1349	-2.1458
	32.2006	30.7061	30.2513	29.4039	27.3930
Semicausal Model SC2	2.2390	-0.5083	-1.1176	-1.5362	-3.3641
	31.7778	29.0305	28.4212	23.0026	26.1747

\* : without quantizer in the DPCM loop

## CHAPTER FOUR

### NONCAUSAL MODELS AND TRANSFORM CODING

#### 4.1 Introduction

Transform coding has attracted considerable attention in the recent years due to its applications in image storage and transmission. This scheme is different from the classical forms of image coding where either the image samples are directly coded (PCM) or the result of a local operation on pixels is coded (DPCM and predictive coding) [9]. In transform coding the image is first unitary transformed and then the transformed samples are quantized and coded for transmission or storage. Fig. 4.1 shows a typical image transform coding system.

Transform coding has some special characteristics, viz.,

(a) Energy Packing: The energy of samples in the transform domain is generally concentrated near the low spatial frequencies. This property is exploited to achieve data compression.

(b) Channel Error Immunity: Transform coded images are robust with respect to channel errors. This results from the inherent averaging operation of the transform. Each reconstructed image sample is a weighted function of all transform samples. Hence, the channel error is distributed over all of the reconstructed image samples so that it is less objectionable to a human viewer.

In this chapter, noncausal image representations discussed in Chapter 2 are shown to yield transform coding algorithms. Adaptive transform coding scheme analogous to the classification Hybrid coding method can be designed to account for changes in image statistics.

## 4.2 Image Transform

Consider an  $N \times N$  image,  $\{u_{i,j}, i,j = 1, \dots, N\}$ . Let  $A$  be a transform operator with elements  $\{a_{i,j,k,\ell}, i,j,k,\ell = 1, \dots, N\}$  which operates on  $\{u_{i,j}\}$  to give

$$v_{k,\ell} = \sum_{i=1}^N \sum_{j=1}^N a_{i,j,k,\ell} u_{i,j}. \quad (4.2-1)$$

The operator  $A$  is said to be separable if

$$a_{i,j,k,\ell} = a_{i,k} a_{j,\ell} \quad (4.2-2)$$

so that (4.2-1) becomes

$$v_{k,\ell} = \sum_{i=1}^N \sum_{j=1}^N a_{i,k} a_{j,\ell} u_{i,j}. \quad (4.2-3)$$

The above equation can be implemented in two steps. First, a one-dimensional transform is taken along each row (or column) of the image  $\{u_{i,j}\}$ . Then, a one-dimensional transform is taken along each column (or row) of the resulting image. In matrix notation, this becomes

$$V = A U A^T. \quad (4.2-4)$$

Generally, the matrix operator  $A$  is further restricted to be unitary, i.e.,

$$A^{-1} = A^* \cdot T \quad (4.2-5)$$

where  $\cdot$  denotes complex conjugate and  $T$  denotes transpose. This means the image matrix  $U$  can be recovered as

$$U = A^{-1} V (A^T)^{-1} = A^* \cdot T V A^* \quad (4.2-6)$$



and the Parseval's energy conservation rule

$$\sum_{i=1}^N \sum_{j=1}^N |u_{i,j}|^2 = \sum_{k=1}^N \sum_{\ell=1}^N |v_{k,\ell}|^2 \quad (4.2-7)$$

is satisfied. Common examples of transform matrices are the discrete Fourier (F), Sine ( $\Psi_s$ ), Cosine ( $\Psi_c$ ), Hadamard (H), Slant (SL), Karhunen Loeve ( $\Psi$ ), etc. These are defined as follows:

- a. Fourier Transform [ 3 ]. The Fourier transform matrix is defined as

$$F_{k,\ell} = \frac{1}{\sqrt{N}} \exp \left\{ \frac{-2\pi i (k-1)(\ell-1)}{N} \right\} \quad 1 \leq k, \ell \leq N \quad (4.2-8)$$

where  $i = \sqrt{-1}$ , and the discrete Fourier transform of an image is given by

$$v_{m,n} = \frac{1}{N} \sum_{k=1}^N \sum_{\ell=1}^N u_{k,\ell} \exp \left\{ -\frac{2\pi i}{N} [(m-1)(k-1) + (n-1)(\ell-1)] \right\}. \quad (4.2-9a)$$

Its inverse transform is

$$u_{k,\ell} = \frac{1}{N} \sum_{m=1}^N \sum_{n=1}^N v_{m,n} \exp \left\{ \frac{2\pi i}{N} [(m-1)(k-1) + (n-1)(\ell-1)] \right\}. \quad (4.2-9b)$$

- b. Sine Transform [ 27 ]. The Sine transform matrix  $\Psi_s$  is symmetric and is defined as

$$\Psi_{s_{k,\ell}} = \sqrt{\frac{2}{N+1}} \sin \frac{k\ell\pi}{N+1} \quad 1 \leq k, \ell \leq N. \quad (4.2-10)$$

It has been shown [ 30 ], if  $Q_s$  is an arbitrary, symmetric, tridiagonal, Toeplitz matrix

$$Q_s = \begin{bmatrix} a & b & \circ \\ b & a & b \\ \circ & b & a \end{bmatrix} \quad (4.2-10a)$$

then  $\Psi_s$  contains the eigenvectors of  $Q_s$  and satisfies the relation

$$Q_s \Psi_s = \Psi_s \Lambda_s \quad (4.2-10b)$$

where  $\Lambda_s$  is a diagonal matrix whose entries are the eigenvalues of  $Q_s$ , given by

$$\lambda_{s_i} = a + 2b \cos \frac{i\pi}{N+1} \quad 1 \leq i \leq N. \quad (4.2-10c)$$

c. Cosine Transform [ 1 ]. The Cosine transform matrix  $\Psi_c$  is defined as

$$\Psi_{c,k,\ell} = \begin{cases} \frac{1}{\sqrt{N}}, & k = 1, 1 \leq \ell \leq N \\ \sqrt{\frac{2}{N}} \cos \frac{(2\ell-1)(k-1)\pi}{2N}, & 2 \leq k \leq N, 1 \leq \ell \leq N. \end{cases} \quad (4.2-11)$$

It has been shown [ 29 ], the Cosine transform matrix contains the eigenvectors of an arbitrary symmetric tridiagonal matrix  $Q_c$  of order  $N$ .

$$Q_c = \begin{bmatrix} a-b & b & \circ \\ b & a & b \\ \circ & b & a-b \end{bmatrix} \quad (4.2-11a)$$

and satisfies the relation

$$Q_c \Psi_c = \Psi_c \Lambda_c \quad (4.2-11b)$$

where  $\Lambda_c$  is a diagonal matrix whose entries are given by

$$\lambda_{c_i} = a + 2b \cos \frac{(i-1)\pi}{N} \quad 1 \leq i \leq N. \quad (4.2-11c)$$

- d. Hadamard Transform [ 54 ]. The Hadamard transform matrix is a square array whose entry takes only binary values  $\pm 1$  and rows and columns are orthogonal. The lowest size  $2 \times 2$  orthogonal Hadamard matrix is given by

$$H_2 = \frac{1}{\sqrt{2}} \begin{bmatrix} 1 & 1 \\ 1 & -1 \end{bmatrix}. \quad (4.2-12)$$

The construction rule for a Hadamard matrix of size  $N = 2^n$ , where  $n$  is an integer, is simple. Let  $H_N$  be a Hadamard matrix of size  $N$ , the matrix

$$H_{2N} = \frac{1}{\sqrt{2}} \begin{bmatrix} H_N & H_N \\ H_N & -H_N \end{bmatrix} \quad (4.2-13)$$

is a Hadamard matrix of size  $2N$ .

- e. Slant Transform [ 55 ]. For matrix size of  $N = 2$ , the Slant transform matrix is identical to the Hadamard transform of order two. That is,

$$SL_2 = \frac{1}{\sqrt{2}} \begin{bmatrix} 1 & 1 \\ 1 & -1 \end{bmatrix}. \quad (4.2-14)$$

The Slant matrix of order  $N$  ( $N=2^n, n=3,4,5,\dots$ ) can be generated in terms of the Slant matrix of order  $\frac{N}{2}$  by the recursive relation



$$SL_N = \frac{1}{\sqrt{2}} \begin{bmatrix} 1 & 0 & & 0 & 1 & 0 & & 0 \\ a_N & b_N & & 0 & -a_N & b_N & & 0 \\ \hline 0 & & I_{(N/2)-2} & & 0 & & II_{(N/2)-2} & \\ 0 & 1 & & 0 & 0 & -1 & & 0 \\ \hline -b_N & a_N & & 0 & b_N & a_N & & 0 \\ \hline 0 & & I_{(N/2)-2} & & 0 & & -II_{(N/2)-2} & \end{bmatrix} \begin{bmatrix} SL_{\frac{N}{2}} & 0 \\ \hline 0 & SL_{\frac{N}{2}} \end{bmatrix} \quad (4.2-15)$$

where  $II_k$  represents a  $k \times k$  identity matrix. The constants  $a_N$  and  $b_N$  may be computed from the recursive relation

$$a_2 = 1$$

$$b_N = [1 + 4(a_{N/2})^2]^{-1/2} \quad (4.2-16)$$

$$a_N = 2b_N a_{N/2}$$

f. Karhunen Loeve Transform [ 37,42 ]. Here, we consider a special transform which depends on the image statistics.

If  $\{x_i, i=1, \dots, N\}$  is a one-dimensional first-order Markov process with covariance matrix  $R$ , where

$$R = \begin{bmatrix} 1 & \rho & \rho^2 & \dots & \rho^{N-1} \\ \rho & 1 & \rho & & \\ \rho^2 & \rho & 1 & & \\ . & & & . & \\ . & & & & . \\ \rho^{N-1} & & & & 1 \end{bmatrix} \quad (4.2-17)$$

Then the elements of the KL transform matrix  $\Psi$  are given by [ 56 ]

(N = even)

$$\Psi_{i,j} = \sqrt{\frac{2}{N+\gamma_i^2}} \sin \left[ \omega_i \left( j - \frac{N+1}{2} \right) + \frac{j\pi}{2} \right] \quad (4.2-18a)$$

where 
$$\gamma_i^2 = \frac{1 - \rho^2}{1 - 2\rho \cos \omega_i + \rho^2} \quad (4.2-18b)$$

and  $\{\omega_i\}$  are the positive roots of the transcendental equation

$$\tan n\omega = - \frac{(1 - \rho^2) \sin n\omega}{\cos \omega - 2\rho + \rho^2 \cos \omega} . \quad (4.2-18c)$$

Due to the non-periodicity of the sine terms in (4.2-18a), there is no fast algorithm available for implementing the KL transform matrix.

In matrix form,  $\Psi$  satisfies

$$R\Psi = \Psi\Gamma \quad (4.2-19)$$

where  $\Gamma = \{\gamma_i\}$  is the diagonal matrix of eigenvalues of  $R$ , which can be calculated via (4.2-18c).

#### 4.3 Stochastic Decoupling of Noncausal Models by Sine Transform [ 31 ]

In Chapter 2 we discussed three different noncausal models. Their spatial structures are depicted in Fig. 4.2 together with the boundary elements needed in representation of an  $N \times N$  square image. Now we show that each model yields a stochastic decomposition by the Sine transform.

#### 4.3.1 NCI Model

From Chapter 2, we can write the NCI model (2.5.3-1) in matrix form, as

$$U Q_s + Q_s U = \epsilon + B \quad (4.3.1-1)$$

where  $U$  and  $\epsilon$  are  $N \times N$  matrices, and  $Q_s$  is a tridiagonal, symmetric, Toeplitz matrix defined in (4.2-10a) with  $a = \frac{1}{2}$ ,  $b = -\alpha$ . From (4.2-10c), its eigenvalues are

$$\lambda_{s_i} = \frac{1}{2} - 2\alpha \cos \frac{i\pi}{N+1} \quad 1 \leq i \leq N. \quad (4.3.1-2)$$

The matrix  $B$  is a sparse matrix of the form

$$B = \alpha \begin{bmatrix} u_{01} + u_{10} & u_{02} & u_{03} & \cdots & u_{0,N-1} & u_{0,N} + u_{1,N+1} \\ u_{20} & \boxed{\phantom{\text{matrix}}} & & & & u_{2,N+1} \\ u_{30} & & \bigcirc & & & u_{3,N+1} \\ \vdots & & & & & \vdots \\ u_{N-1,0} & & & & & u_{N-1,N+1} \\ u_{N+1,1} + u_{N,0} & u_{N+1,2} & u_{N+1,3} & \cdots & u_{N+1,N-1} & u_{N+1,N} + u_{N,N+1} \end{bmatrix} \quad (4.3.1-3)$$

Note that the four corner boundary elements  $u_{00}$ ,  $u_{0,N+1}$ ,  $u_{N+1,0}$  and  $u_{N+1,N+1}$  are not needed in  $B$  (see Fig. 4.2). Alternatively we write



$$B \in S_1^+(u). \quad (4.3.1-4)$$

Let us denote  $\bar{A}$  as an  $N^2 \times 1$  vector of lexicographic ordered elements of an  $N \times N$  matrix  $A$ . Then (4.3.1-1) has a Kronecker product form

$$J \bar{U} \stackrel{\Delta}{=} (I \otimes Q_s + Q_s \otimes I) \bar{U} = \bar{\epsilon} + \bar{B}. \quad (4.3.1-5)$$

From (2.5.3-2), the covariance matrix of  $\{\epsilon_{i,j}\}$  (see Table 2.1 under NC1) can be written as

$$R_\epsilon \stackrel{\Delta}{=} E \bar{\epsilon} \bar{\epsilon}^T = \beta^2 (I \otimes Q_{s_1} + Q_{s_1} \otimes I) \stackrel{\Delta}{=} \beta^2 J_1 \quad (4.3.1-6)$$

where  $Q_{s_1}$  is defined in (4.2-10a) with  $a = \frac{1}{2}$ ,  $b = -\alpha_1$ . Now from (4.3.1-5) we obtain the decomposition

$$\bar{U} = \bar{U}^o + \bar{U}_b \quad \text{or} \quad U = U^o + U_b \quad (4.3.1-7)$$

$$\text{where} \quad \bar{U}^o \stackrel{\Delta}{=} J^{-1} \bar{\epsilon}, \quad \bar{U}_b \stackrel{\Delta}{=} J^{-1} \bar{B}. \quad (4.3.1-7a)$$

It is clear that  $\bar{U}_b$  is obtained by passing the boundary elements  $B$  through a noncausal filter  $J^{-1}$ . Therefore (4.3.1-7) shows that a discrete random field defined by a noncausal representation has a stochastic decomposition in which  $U_b$  is a random field completely determined by

---

Let  $S_k$  denote the space of all linear boundary elements of a random field  $\{x_{i,j}\}$  which is described as

$$S_k(x) = \{\mathcal{L}[x_{1-k,j}, x_{N+k,j}, x_{i,1-k}, x_{i,N+k}] : 1-k \leq i,j \leq N+k\}$$

where  $\mathcal{L}$  denotes any linear operator.

the boundary elements. Fig. 4.3 shows the realization algorithm for noncausal model decomposition of (4.3.1-7).

The covariance matrix of  $\bar{U}^0$  is obtained as

$$\begin{aligned} R_o &\triangleq E \bar{U}^0 \bar{U}^{0T} = J^{-1} E[\bar{\epsilon} \bar{\epsilon}^T] J^{-1} = J^{-1} R_{\epsilon} J^{-1} = \beta^2 J^{-1} J_1 J^{-1} \quad (4.3.1-8) \\ &= \beta^2 [I \otimes Q_s + Q_s \otimes I]^{-1} [I \otimes Q_{s_1} + Q_{s_1} \otimes I] [I \otimes Q_s + Q_s \otimes I]^{-1}. \end{aligned}$$

If we denote  $\Psi_s$  to be the Sine transform matrix, then from (4.2-10) it diagonalizes  $Q_s$ . It follows that  $\Psi_s$  should also reduce  $J$ ,  $J_1$ ,  $R_o$ , etc. all to their diagonal form. In fact, it is trivial to check that

$$D = (\Psi_s \otimes \Psi_s) X (\Psi_s \otimes \Psi_s) , \quad \text{for } X = J, J_1, R_o, R_{\epsilon} \quad (4.3.1-9)$$

where  $D$  is an  $N^2 \times N^2$  diagonal matrix.

Hence  $(\Psi_s \otimes \Psi_s)$  is the KL transform of  $\bar{U}^0$ , i.e.,

$$\bar{V}^0 = (\Psi_s \otimes \Psi_s) \bar{U}^0 \quad \text{or} \quad V^0 = \Psi_s U^0 \Psi_s . \quad (4.3.1-10)$$

Then  $V^0$  is the KL transformed matrix and its elements are uncorrelated, i.e.,

$$E V_{i,j}^0 V_{k,l}^0 = d_{i,j} \delta_{i,k} \delta_{j,l} \quad 1 \leq i, j \leq N . \quad (4.3.1-11)$$

Therefore, it is obvious that one can write [ 7 ]

$$D = \beta^2 (I \otimes \Lambda_s + \Lambda_s \otimes I)^{-1} (I \otimes \Lambda_{s_1} + \Lambda_{s_1} \otimes I) (I \otimes \Lambda_s + \Lambda_s \otimes I)^{-1} \quad (4.3.1-12)$$

which gives

$$E V_{i,j}^0 = d_{ij} = \beta^2 \frac{[\lambda_{s_1 i} + \lambda_{s_1 j}]}{[\lambda_{s_i} + \lambda_{s_j}]^2} \quad 1 \leq i, j \leq N \quad (4.3.1-13)$$

where  $\lambda_{s_1}$  is obtained from (4.3.1-2) with  $\alpha$  replaced by  $\alpha_1$ .

For a given image the elements  $V_{i,j}^0$  can be easily realized via the equation

$$V_{i,j}^0 = \frac{e_{i,j}}{\lambda_{s_i} + \lambda_{s_j}} \quad (4.3.1-14)$$

where  $e = \Psi_s \epsilon \Psi_s$ ,  $V^0 = \Psi_s U^0 \Psi_s$ . (4.3.1-14a)

Using the representation (2.5.3-1) and boundary matrix  $\{B_{i,j}\}$ , find the matrix  $\{\epsilon_{i,j}\}$ , then from (4.3.1-2) find the values of  $\lambda_{s_i}$  and  $\lambda_{s_j}$ , and compute the values of  $e_{i,j}$  via  $e = \Psi_s \epsilon \Psi_s$ . Since  $\Psi_s$  is the Sine transform, a fast algorithm can be used in computing all the equations discussed in the above.

#### 4.3.2 NC2 Model

NC2 representation (2.5.3-6) can be written in matrix form as

$$UH + HU + 2Q_s U Q_s = \epsilon + B \quad (4.3.2-1)$$

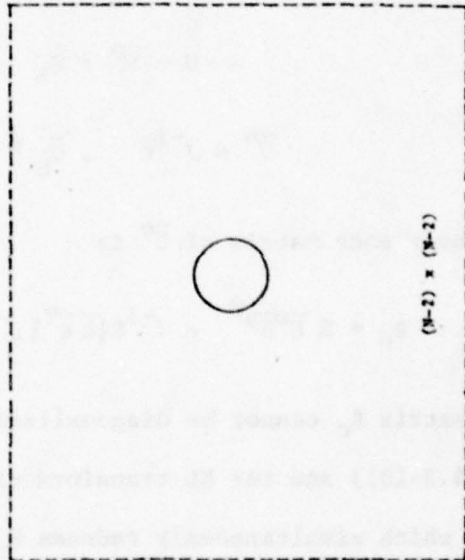
where

$$H_{i,j} = \begin{cases} \frac{1}{2} + 2\alpha^2, & i = j \\ -\alpha, & |i-j| = 1 \\ \alpha^2, & |i-j| = 2 \\ 0, & \text{otherwise} \end{cases} \quad (4.3.2-2)$$

and  $Q_s$  is a tridiagonal, symmetric, Toeplitz matrix defined in (4.2-10a) with  $a = \frac{1}{2}$ ,  $b = -\alpha$ , and  $B$  is an  $N \times N$  sparse matrix which contains the boundary elements and is defined in the following equation.



$2\alpha(u_{01}^{+u_1})$	$2\alpha u_{02}$	$2\alpha u_{03}$	$2\alpha u_{04}$	$2\alpha u_{0, N-2}$	$2\alpha(u_{0, N-1}^{+u_1, N+1})$	$2\alpha(u_{0, N}^{+u_1, N+1})$
$-2\alpha^2(u_{00}^{+u_1, 20})$	$-2\alpha^2(u_{01}^{+u_1, 20})$	$-2\alpha^2(u_{02}^{+u_1, 20})$	$-2\alpha^2(u_{03}^{+u_1, 20})$	$-2\alpha^2(u_{0, N-2}^{+u_1, N+1})$	$-2\alpha^2(u_{0, N-1}^{+u_1, N+1})$	$-2\alpha^2(u_{0, N}^{+u_1, N+1})$
$-\alpha^2(u_{-1, 1}^{+u_1, 1})$	$-\alpha^2(u_{-1, 2}^{+u_1, 2})$	$-\alpha^2(u_{-1, 3}^{+u_1, 3})$	$-\alpha^2(u_{-1, 4}^{+u_1, 4})$	$-\alpha^2(u_{-1, N-2}^{+u_1, N+1})$	$-\alpha^2(u_{-1, N-1}^{+u_1, N+1})$	$-\alpha^2(u_{-1, N}^{+u_1, N+1})$
$2\alpha u_{20}$						$2\alpha u_{2, N+1}$
$-2\alpha^2(u_{10}^{+u_1, 20})$						$-2\alpha^2(u_{1, N+1}^{+u_1, 20, N+1})$
$-\alpha^2(u_{01}^{+u_1, 2, -1})$						$-\alpha^2(u_{0, N+2, N+2})$
$2\alpha u_{30}$						$2\alpha u_{3, N+1}$
$-2\alpha^2(u_{20}^{+u_1, 30})$						$-2\alpha^2(u_{2, N+1}^{+u_1, 30, N+1})$
$-\alpha^2(u_{1, -1}^{+u_1, -1})$						$-\alpha^2(u_{1, N+2, N+2})$
$2\alpha u_{40}$						$2\alpha u_{4, N+1}$
$-2\alpha^2(u_{30}^{+u_1, 40})$						$-2\alpha^2(u_{3, N+1}^{+u_1, 40, N+1})$
$-\alpha^2(u_{4, -1}^{+u_1, -1})$						$-\alpha^2(u_{4, N+2, N+2})$
$2\alpha u_{N-2, 0}$						$2\alpha u_{N-2, N+1}$
$-2\alpha^2(u_{N-3, 0}^{+u_1, N-1, 0})$						$-2\alpha^2(u_{N-3, N+1}^{+u_1, N-1, N+1})$
$-\alpha^2(u_{N-2, -1}^{+u_1, N-1, -1})$						$-\alpha^2(u_{N-2, N+2, N+2})$
$2\alpha u_{N-1, 0}$						$2\alpha u_{N-1, N+1}$
$-2\alpha^2(u_{N-2, 0}^{+u_1, N-1, 0})$						$-2\alpha^2(u_{N-2, N+1}^{+u_1, N-1, N+1})$
$-\alpha^2(u_{N-1, -1}^{+u_1, N-1, -1})$						$-\alpha^2(u_{N-1, N+2, N+2})$
$2\alpha(u_{N+1, 1}^{+u_1, 0})$	$2\alpha u_{N+1, 2}$	$2\alpha u_{N+1, 3}$	$2\alpha u_{N+1, 4}$	$2\alpha u_{N+1, N-2}$	$2\alpha(u_{N+1, N-1}^{+u_1, N+1})$	$2\alpha(u_{N+1, N}^{+u_1, N+1})$
$-2\alpha^2(u_{N-1, 0}^{+u_1, N+1, 0})$	$-2\alpha^2(u_{N+1, 1}^{+u_1, N+1, 1})$	$-2\alpha^2(u_{N+1, 2}^{+u_1, N+1, 2})$	$-2\alpha^2(u_{N+1, 3}^{+u_1, N+1, 3})$	$-2\alpha^2(u_{N+1, N-3}^{+u_1, N+1, N-1})$	$-2\alpha^2(u_{N+1, N-2}^{+u_1, N+1, N})$	$-2\alpha^2(u_{N+1, N-1}^{+u_1, N+1, N+1})$
$-\alpha^2(u_{N+2, 1}^{+u_1, N+1, -1})$	$-\alpha^2(u_{N, 0}^{+u_1, N+2, 2})$	$-\alpha^2(u_{N+2, 3})$	$-\alpha^2(u_{N+2, 4})$	$-\alpha^2(u_{N+2, N-2})$	$-\alpha^2(u_{N+2, N-1}^{+u_1, N+1})$	$-\alpha^2(u_{N+2, N}^{+u_1, N+2})$



An easier notation for B is  $B \in S_2(u)$  (see page 114 footnote).

In Kronecker product notation, (4.3.2-1) becomes

$$[I \otimes H + H \otimes I + 2Q_s \otimes Q_s] \bar{U} = \bar{\epsilon} + \bar{B} \quad (4.3.2-4)$$

$$J \bar{U} = \bar{\epsilon} + \bar{B} \quad (4.3.2-4a)$$

where  $J \triangleq [I \otimes H + H \otimes I + 2Q_s \otimes Q_s]$  and the covariance matrix of  $\bar{\epsilon}$  is

$$R_{\epsilon} = E \bar{\epsilon} \bar{\epsilon}^T = \beta^2 J_1 \quad (4.3.2-5)$$

where  $\alpha$  is replaced by  $\alpha_1$  in  $J_1$  and Eqn. (4.3.2-4) can be rewritten as

$$\bar{U} = \bar{U}^o + \bar{U}_b \quad (4.3.2-6)$$

where  $\bar{U}^o = J^{-1} \bar{\epsilon}$  ,  $\bar{U}_b \triangleq J^{-1} \bar{B}$  (4.3.2-6a)

and the covariance matrix of  $\bar{U}^o$  is

$$R_o = E \bar{U}^o \bar{U}^{oT} = J^{-1} E[\bar{\epsilon} \bar{\epsilon}^T] J^{-1} = \beta^2 J^{-1} J_1 J^{-1} . \quad (4.3.2-7)$$

Now, the matrix  $R_o$  cannot be diagonalized by the Sine transform matrix  $\psi_s$  (see (4.2-10)) and the KL transform of  $\bar{U}^o$  has to be the biorthogonal transform which simultaneously reduces H and  $Q_s$  matrices to their diagonal form.

It is noted that H can be further decomposed as

$$H = Q_s^2 + H^b \quad (4.3.2-8)$$

where  $H^b$  is a sparse matrix of only two nonzero elements

$$H^b = \begin{bmatrix} \alpha^2 & & \\ & \bigcirc & \\ & & \alpha^2 \end{bmatrix} . \quad (4.3.2-9)$$

Recalling the requirement of  $|\alpha| < \frac{1}{4}$  for NC2 model (see (2.5.3-6)), we may assume  $H^b \approx [0]$  and a reasonable approximation of  $H$  is

$$H \approx Q_s^2 . \quad (4.3.2-10)$$

Substituting (4.3.2-10) into (4.3.2-14a) yields

$$\begin{aligned} J &= I \otimes H + H \otimes I + 2Q_s \otimes Q_s \\ &\approx I \otimes Q_s^2 + Q_s^2 \otimes I + 2Q_s \otimes Q_s \\ &= J' . \end{aligned} \quad (4.3.2-11)$$

If  $\Psi_s$  denotes the Sine transform, it is trivial to prove that

$$(\Psi_s \otimes \Psi_s) J' (\Psi_s \otimes \Psi_s) = I \otimes \Lambda_s^2 + \Lambda_s^2 \otimes I + 2\Lambda_s \otimes \Lambda_s \quad (4.3.2-12)$$

where  $\Lambda_s$  is an  $N \times N$  diagonal matrix with entries defined in (4.3.2-2).

Following the same steps as we developed in the case of NC1 model, the Sine transform is a good approximation to the biorthogonal transformation in the case of NC2 model.

$$E V_{ij}^{o2} \approx \beta^2 \frac{[\lambda_{s1_i} + \lambda_{s1_j}]^2}{[\lambda_{s1_i} + \lambda_{s1_j}]^4} \quad (4.3.2-13)$$



Furthermore, since  $\Psi_s$  is independent of  $\alpha$ , a fast Sine transform exists and the values of  $V_{i,j}$  can be easily realized.

#### 4.3.3 NC3 Model

NC3 representation is shown in (2.5.3-10). In matrix notation, it becomes

$$Q_s U Q_s = \epsilon + B \quad (4.3.3-1)$$

where  $Q_s$  is a tridiagonal, symmetric, Toeplitz matrix defined in (4.2-10a) with  $a = 1$ ,  $b = -\alpha$ , and eigenvalues  $\lambda_s$  as defined in (4.3.1-2)

$$\text{and} \quad B = \alpha Q_s B_1 + \alpha B_2 Q_s - \alpha^2 B_3 \quad (4.3.3-2)$$

where

$$B_1 = \begin{bmatrix} u_{01} & u_{02} & \cdots & u_{0,N} \\ \hline & \bigcirc & & \\ \hline u_{N+1,1} & u_{N+1,2} & \cdots & u_{N+1,N} \end{bmatrix} \quad (4.3.3-3a)$$

$$B_2 = \begin{bmatrix} u_{10} \\ u_{20} \\ \vdots \\ u_{N,0} \end{bmatrix} \bigcirc \begin{bmatrix} u_{1,N+1} \\ u_{2,N+1} \\ \vdots \\ u_{N,N+1} \end{bmatrix} \quad (4.3.3-3b)$$

$$B_3 = \begin{bmatrix} u_{00} \\ \hline u_{0,N+1} \end{bmatrix} \bigcirc \begin{bmatrix} u_{0,N+1} \\ \hline u_{N+1,N+1} \end{bmatrix} \quad (4.3.3-3c)$$

Thus

$$B \in S_1(u) \quad (4.3.3-4)$$

where the definition of  $S_1$  see page 114 footnote.

Rewriting (4.3.3-1) in Kronecker product form, we have

$$(Q_s \otimes Q_s) \bar{U} = J \bar{U} = \bar{\epsilon} + \bar{B} \quad (4.3.3-5)$$

where

$$J \triangleq Q_s \otimes Q_s \quad (4.3.2-6)$$

so that

$$\bar{U} = \bar{U}^0 + \bar{U}_b \quad (4.3.3-7)$$

where

$$\bar{U}^0 \triangleq J^{-1} \bar{\epsilon}, \quad \bar{U}_b \triangleq J^{-1} \bar{B}. \quad (4.3.3-7a)$$

From Table 2-1, it is noted that the covariance matrix of  $\bar{\epsilon}$  can be written as

$$R_{\bar{\epsilon}} = E \bar{\epsilon} \bar{\epsilon}^T = \beta^2 (Q_s \otimes Q_s). \quad (4.3.3-8)$$

Thus the covariance matrix of  $\bar{U}^0$  is

$$R_0 = E \bar{U}^0 \bar{U}^{0T} = J^{-1} E [\bar{\epsilon} \bar{\epsilon}^T] J^{-1} = \beta^2 J^{-1} J J^{-1} = \beta^2 J^{-1}. \quad (4.3.3-9)$$

Let  $\Psi_s$  be the Sine transform independent of  $\alpha$ , recalling the mathematical development described for NC1 and NC2 models, it is seen that  $(\Psi_s \otimes \Psi_s)$  is the KL transform of  $\bar{U}^0$ . Let us define

$$\bar{V}^0 = (\Psi_s \otimes \Psi_s) \bar{U}^0, \text{ which implies } V^0 = \Psi_s U^0 \Psi_s. \quad (4.3.3-10)$$

Then

$$E V_{i,j}^{02} = \frac{\beta^2}{\lambda_{s_i} \lambda_{s_j}}. \quad (4.3.3-11)$$

Thus the above equation is in a form which is easily realizable. For a given image, the matrix  $\{B_{i,j}\}$  is first computed and leads to the matrix  $\{U_{i,j}^0\}$ . Then from (4.3.1-2) the values of  $\lambda_i$  and  $\lambda_j$  are found. A two-dimensional fast Sine transform is performed over  $\{u_{i,j}^0\}$ . (4.3.3-11) is used to evaluate the variances of each point of the transformed image  $\{v_{i,j}^0\}$ .

#### 4.4 Stochastic Formulation of Noncausal Models by Cosine Transform

The Sine transform could be used to analyze the noncausal representations as described in the previous section. For certain special conditions on the outmost boundary variables (refer to Fig. 4.2), the resulting representations could also be analyzed by the Cosine transform.

For many image fields, the adjacent elements of a column (or a row) are highly correlated and often the correlation parameter has a value close to unity. Let us first consider the NC1 model.

For a finite  $N \times N$  image random field, the boundary elements of NC1 model that need to be specified in (2.5.3-1) satisfy the conditions

$$\begin{aligned} u_{0,j} &= u_{1,j} & 1 \leq j \leq N \\ u_{N+1,j} &= u_{N,j} & 1 \leq j \leq N \\ u_{i,0} &= u_{i,1} & 1 \leq i \leq N \\ u_{i,N+1} &= u_{i,N} & 1 \leq i \leq N \end{aligned} \quad (4.4-1)$$

This means the two outmost boundary rows of four edges of the  $(N+2) \times (N+2)$  field are equal. The NC1 image field subject to (4.4-1) is no longer a stationary field. Rewriting (2.5.3-1) in matrix form with the constraint (4.4-1), we have

$$Q_c U + U Q_c = \epsilon \quad (4.4-2)$$



where

$$Q_c = \begin{bmatrix} \frac{1}{2} - \alpha & -\alpha & & & \\ -\alpha & \frac{1}{2} & & & \\ & & \ddots & & \\ & & & \frac{1}{2} & -\alpha \\ & & & -\alpha & \frac{1}{2} - \alpha \end{bmatrix} \quad (4.4-3)$$

and eigenvalues of  $Q_c$  are given by

$$\lambda_c = \frac{1}{2} - 2\alpha \cos \frac{(i-1)\pi}{N} \quad 1 \leq i \leq N. \quad (4.4-3a)$$

The subscript c indicates  $Q_c$  is now diagonalized by the Cosine transform. In Kronecker product form (4.4-2) becomes

$$(I \otimes Q_c + Q_c \otimes I) \bar{U} = \bar{\epsilon}. \quad (4.4-4)$$

Therefore

$$\bar{U} = J^{-1} \bar{\epsilon} \quad (4.4-5)$$

where

$$J \triangleq (I \otimes Q_c + Q_c \otimes I). \quad (4.4-5a)$$

The covariance matrix of  $R$  is

$$R = E \bar{U} \bar{U}^T = J^{-1} E [\bar{\epsilon} \bar{\epsilon}^T] J^{-1} = J^{-1} R J^{-1} \quad (4.4-6)$$

where

$$R = E \bar{\epsilon} \bar{\epsilon}^T. \quad (4.4-6a)$$

Eqn. (4.4-5) does not involve a term in  $\bar{U}_b$ , compare with (4.3.1-7), any more.

Since we have used the boundary conditions of (4.4-1) in deriving (4.4-2), it means that the error signal  $\{\epsilon_{i,j}\}$  along the four boundary edges is no longer a completely arbitrary random variable. For stationary NC1 model, the covariance matrix of  $\bar{\epsilon}$  was defined in (4.3.1-6), where

$$Q_{s_1} = \begin{bmatrix} \frac{1}{2} & -\alpha_1 & & & \\ -\alpha_1 & \frac{1}{2} & & & \\ & & \frac{1}{2} & -\alpha_1 & \\ & & & & \frac{1}{2} & -\alpha_1 \\ & & & & -\alpha_1 & \frac{1}{2} \end{bmatrix} \quad (4.4-7)$$

Imposition of the boundary conditions also implies the  $Q_{s_1}$  could be approximated as  $Q_{c_1}$  where

$$Q_{s_1} \approx Q_{c_1} = \begin{bmatrix} \frac{1}{2} - \alpha_1 & -\alpha_1 & & & \\ -\alpha_1 & \frac{1}{2} & & & \\ & & \frac{1}{2} & -\alpha_1 & \\ & & & & \frac{1}{2} & -\alpha_1 \\ & & & & -\alpha_1 & \frac{1}{2} - \alpha_1 \end{bmatrix} \quad (4.4-8)$$

The above equation could be diagonalized by Cosine transform, and the following expression is obtained for  $R_c$

$$R_c \approx \beta^2 (Q_{c_1} \otimes I + I \otimes Q_{c_1}) = \beta^2 J_1 \quad (4.4-9)$$

where

$$J_1 \triangleq (Q_{c_1} \otimes I + I \otimes Q_{c_1}) \quad (4.4.9a)$$

Substituting (4.4-9) to (4.4-6), yields

$$R \approx \beta^2 J^{-1} J_1 J^{-1} \quad (4.4-10)$$

Following the same procedure as we did in section 4.3.1, it is easy to show  $(\Psi_c \otimes \Psi_c)$ , where  $\Psi_c$  is the Cosine transform matrix, could reduce  $J$  and  $J_1$  to their diagonal forms. Therefore

$$E \bar{V} \bar{V}^T \approx \beta^2 (\Lambda_c \otimes I + I \otimes \Lambda_c)^{-1} (\Lambda_{c_1} \otimes I + I \otimes \Lambda_{c_1}) (\Lambda_c \otimes I + I \otimes \Lambda_c)^{-1} \quad (4.4-11)$$

which implies

$$E v_{i,j}^2 \approx \beta^2 \frac{(\lambda_{c_{1_i}} + \lambda_{c_{1_j}})}{(\lambda_{c_i} + \lambda_{c_j})^2} \quad 1 \leq i, j \leq N \quad (4.4-12)$$

where  $\{\lambda_{c_{1_i}}\}$  and  $\{\lambda_{c_i}\}$  could be computed from (4.4-3a). It is obvious that the elements  $v_{i,j}$  can be quite easily realized and given by

$$v_{i,j} \approx \frac{e_{i,j}}{\lambda_{c_i} + \lambda_{c_j}} \quad (4.4-13)$$

where  $e \approx \Psi_c^T e \Psi_c$ ,  $V \approx \Psi_c^T U \Psi_c$ . (4.4-13a)

Once again, fast algorithm can be used to implement the Cosine transform in the above equations.

For NC2 and NC3, similar models can be obtained by simply assuming the outermost boundary values to be equal. Table 4.1 summarizes the formulas for the three models which are useful in the design of transform coders for random fields represented by noncausal models.

#### 4.5 Transform Coder Design for Noncausal Models via Cosine Transform

In coding problems, one would like to find the minimum number of bits required to represent a random field subject to the specific amount of distortion. A common approach of evaluating the performance of a coding scheme is to obtain its distortion vs. rate characteristics. Referring to Fig. 4.1, which shows the overall transform coding system, an image  $U$  is unitarily transformed to obtain  $V$ . Each element of  $V$  is then quantized independently by a zero memory quantizer and is used for



transmission and/or storage. For reconstruction of the original image, one simply performs the inverse transformation of the quantized samples.

One basic property of the KL transform is that it completely decorrelates the transform samples. Other unitary transforms reduce the inter-sample correlation. The transform coder efficiency is maximized when the transformed samples are uncorrelated. The quantizer design depends on the probability distribution of the transformed samples. In our study, we have found the transform sample  $v_{i,j}$  can be modeled quite well by the Gaussian density model

$$p(x) = \frac{1}{\sqrt{2\pi}\sigma} \exp[-(x-\mu)^2/2\sigma^2] \quad (4.5-1)$$

where  $\mu$  and  $\sigma$  are the mean and standard deviation of the random variable  $x$ . Many times the first sample  $v_{11}$  is modeled by a Rayleigh density, because, for many transforms, it is proportional to the average value (or the so called d.c) of the image data, which for non-negative image data would be a non-negative random variable. However, if the image data has been converted to a zero mean data before processing, then the Gaussian density model suffices. In the sequel, without loss of generality, we will assume  $\{u_{i,j}\}$  to be zero mean random variables, therefore,  $\{v_{m,n}\}$  are also zero mean random variables. Let

$$\sigma_{v_{m,n}}^2 \triangleq E v_{m,n}^2 \quad (4.5-2)$$

be the variance of the transformed sample  $v_{m,n}$ . In Fig. 4.1 if there are no channel errors, then the coder/decoder will generate a perfect transaction and we will have  $\hat{v}_{m,n}^* = v_{m,n}^*$ . The average mean square distortion in encoding entire  $N \times N$  image is defined as

$$D = \frac{1}{N^2} \sum_{i=1}^N \sum_{j=1}^N E (\hat{u}_{i,j}^* - u_{i,j})^2. \quad (4.5-3)$$

Since the transformation is unitary, the Parseval's relation implies

$$D = \frac{1}{N^2} \sum_{m=1}^N \sum_{n=1}^N E (\hat{v}_{m,n}^* - v_{m,n})^2 \quad (4.5-4)$$

and in the absence of channel errors

$$D = \frac{1}{N^2} \sum_{m=1}^N \sum_{n=1}^N E (v_{m,n}^* - v_{m,n})^2. \quad (4.5-4)$$

Assuming all the quantizers are identical in their characteristics,  $f(b)$ , where

$f(b)$  = mean square distortion of a quantizer with  $2^b$  levels for unit variance input random variable

$p$  = desired average bit rate in bits/pixel of the image random field

we can write

$$D = \frac{1}{N^2} \sum_{m=1}^N \sum_{n=1}^N f(b_{m,n}) \sigma_v^2(m,n) \quad (4.5-5)$$

where  $b_{m,n}$  = number of bits allocated to the sample  $v_{m,n}$ . Now, since the total number of bits available is fixed, i.e.,

$$\sum_{m=1}^N \sum_{n=1}^N b_{m,n} = N^2 p \quad (4.5-6)$$

and

$$b_{m,n} \geq 0 \quad (4.5-7)$$

the overall distortion given by (4.5-5) is minimized by finding the optimal bit allocation among the various samples subject to the constraints

of (4.5-6) and (4.5-7). Following Chapter 3, section 3.3.2, and Appendix A, the bit allocation problem can be solved as before and the distortion vs. rate characteristics can be determined. For the noncausal models considered here,  $\sigma_v^2(m,n)$  are obtained from Table 4.1 for Cosine transform coding. The overall coding system is shown in Fig. 4.4(a). In general when the conditions of (4.4-1) are invalid, boundary variables are arbitrary, we can use the following method.

#### 4.6 Fast KL (Sine) Transform Data Compression

In either noncausal model (NC1, NC2 or NC3), the decomposition  $U = U^0 + U_b$  plays an important role in the analysis. Fig. 4.4(b) illustrates a Sine transform data compression scheme. First the boundary samples are quantized and the boundary response  $U_b^*$  is computed. Subtracting  $U_b^*$  from  $U$  gives  $\tilde{U}^0$ , which is nearly equal to  $U^0$ , if quantization errors in boundary samples are small. The covariance matrix of  $U^0$  is a function of  $Q$  for NC1 and NC3 models and a function of  $Q$  and  $H$  for NC2 model. It has been shown that Sine transform serves as the exact KLT for NC1 and NC3 models and a good approximation to the NC2 model.  $\tilde{U}^0$  is therefore quantized with a bank of noncausal model influenced quantizers and transmitted over the channel.

In actual implementation, a large image would be first divided into small blocks and each block is coded independently. Since the noncausal models require separate coding of image boundaries, the number of boundary samples that are needed to be quantized for each block can be minimized by overlapping the boundaries of the various image blocks, namely, only the right vertical and lower horizontal need to be quantized. Rate



distortion calculations for one-dimensional noncausal models (with one overlapping boundary point) have shown to give lower bit rates than the conventional KLT or other unitary transform coding without any overlap. Details of these aspects and comparisons with conventional transform coding techniques are given in [ 36 ].

#### 4.7 Experimental Results

Several computer experiments have been performed to simulate the transform coding schemes discussed in the previous sections. In all the experiments only Cosine transform based scheme was implemented. A  $256 \times 256$  image was divided into 16 image blocks, each of size  $64 \times 64$ . Each block was transform coded independently. The size of image block could be chosen arbitrarily, the size  $64 \times 64$  being chosen for comparison with the methods of the next chapter.

Figure 4.5 shows a typical bit allocation pattern of a NC1 Cosine transform image. Tables 4.2 and 4.3 summarize the results for the Girl and Chemical Plant images respectively. Figure 4.6 shows rate distortion curve and rate vs. SNR for the Girl image. The corresponding characteristics for the Chemical Plant image are shown in Figure 4.7. Figure 4.8(a)-(c) show encoded Girl images at 0.5 bit/pixel, 1 bit/pixel and 2 bits/pixel. Figure 4.9(a)-(c) show encoded Chemical Plant images at 0.5 bit/pixel, 1 bit/pixel and 2 bits/pixel. As expected, the performance of this model (NC1) is consistent with the conventional transform coding methods.

#### 4.8 Classification Transform Coding

We have mentioned in the last section that in order to increase the transmission efficiency and ease the burden of buffer storage, the test image is divided into small image blocks. Then each image block is transform coded independently. In the classification transform coding, one additional step is added to allocate flexible bits to each transform channel quantizer. It says each image block is classified as belonging to one of  $K$  predetermined classes according to its own activity. The activity in the image block is measured by the variance of that image block. For a given class of images the probability distribution function of all the image block variances can be predetermined. Note that this probability distribution function would depend on the size of the image block used in transform coding.

The transform signal in each transform channel is processed as before except that the signal in the transform domain is quantized according to the classification of that image block. In this way, the transform channel quantizer is adapted to the changes of activity in the image blocks. Image blocks with high activity are assigned more quantizer bits than those of low activity. Therefore the quantizer bits are employed more efficiently. This scheme is somewhat analogous to the adaptive classification hybrid coding described in Chapter three.

This scheme also requires the classification information to be transmitted to the receiver. This can be done by sending an extra  $\log_2 K$  bits per image block or  $\frac{1}{N^2} \log_2 K$  bits/pixel (where  $K$  stands for the number of classes and  $N$  is the size of an image block). Experimentally, this value turns out to be very small. For example, in the case of  $K = 4$  and  $M = 16$ ,

the overhead for its transmission is only  $\frac{\log_2 4}{16 \times 16} = \frac{1}{128}$  bit / pixel.

Let us define  $p_k$   $\triangleq$  probability of the  $k$ th class and also assume for each class  $k$ , the image model parameters have been predetermined and are known. Then following the same development of adaptive classification hybrid coding, we can write the expected average distortion for each image block as

$$D = \frac{1}{N^2} \sum_{i=1}^N \sum_{j=1}^N \sum_{k=1}^K \sigma_{v_{i,j}}^2 (k) f(b_{i,j,k}) p_k \quad (4.8-1)$$

where  $b_{i,j,k} \geq 0$  and represents the  $ij$ th transform channel quantizer bit and  $k$ th class.

Another constraint could be the expected average bit rate must be constant, i.e.,

$$\frac{1}{N^2} \sum_{i=1}^N \sum_{j=1}^N \sum_{k=1}^K b_{i,j,k} p_k = P. \quad (4.8-2)$$

The above bit allocation problem can be solved along the same lines in the previous section.

Figure 4.10 shows a typical bit allocation pattern for two-class problem with equal probabilities ( $p_k = 0.5$ ) for each class and size of the image block was  $64 \times 64$ . Figure 4.11(a) shows the corresponding  $4 \times 4$  classification map and image block measure variances. Classification map and image block measure variances for the Chemical Plant image with same kind of strategy is shown in Figure 4.12(b).

The scheme requires the following additional steps compared to ordinary transform coding.



1. Measurement of the variance of each image block.
2. Classification of each image block to one of K classes based on the assumption of  $p_k$ .
3. Storing of K bit allocation tables, one for each class.

Results from several simulations show that this scheme gives, relatively, a large improvement in SNR for lower bit rates  $\approx 0.5$  bit/pixel and relatively smaller image block sizes. At higher bit rates ( $\approx 2$  bits/pixel) and larger image block sizes, the improvement in SNR becomes less significant if at all, and is evidenced by appearance of a "blocking" effect in the encoded image. This is because as the image block size is increased, the ambiguity in classifying it into different classes increases since the activity in a large image block is no longer uniform. Generally, the following conclusions can be made.

1. Classification transform coding scheme can improve the SNR over the standard transform coding (based on NC1 model) for simple structured image (like Girl image).
2. The complexity of implementing this scheme is marginal. Bit allocation is wholly determined by the model with a proper adjustment of the actual image block variance.
3. As the number of classes goes up, the quality of the reconstructed image improves if the size of image block is much less than the actual size of the test image.

Tables 4.2 and 4.3 list the results of classification transform encoded Girl and Chemical Plant images, both with  $64 \times 64$  image block size and two classes. The rate distortion curves of this scheme are shown in Figures 4.6 and 4.7. Finally, the encoded images at 0.5 bit/pixel, 1 bit/pixel and 2 bits/pixel are shown in Figures 4.8 and 4.9.

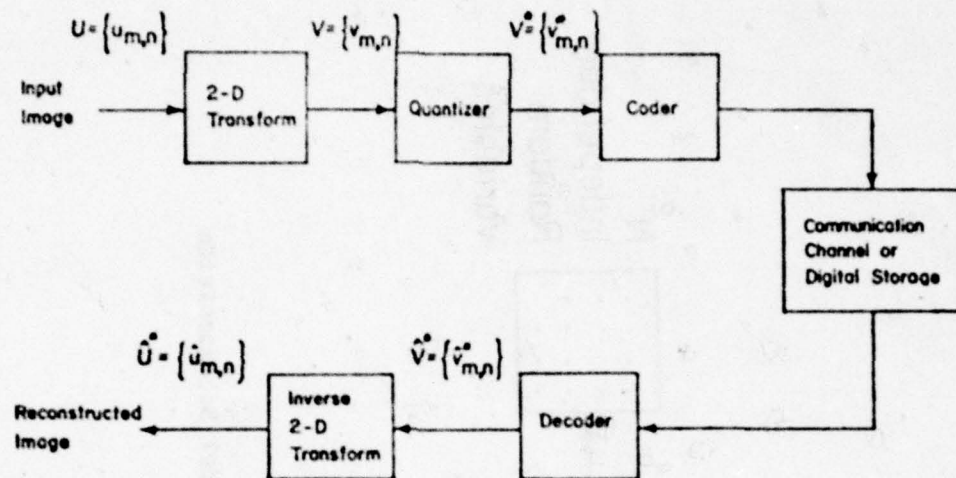


Figure 4.1 Conventional Image Transform Coding System

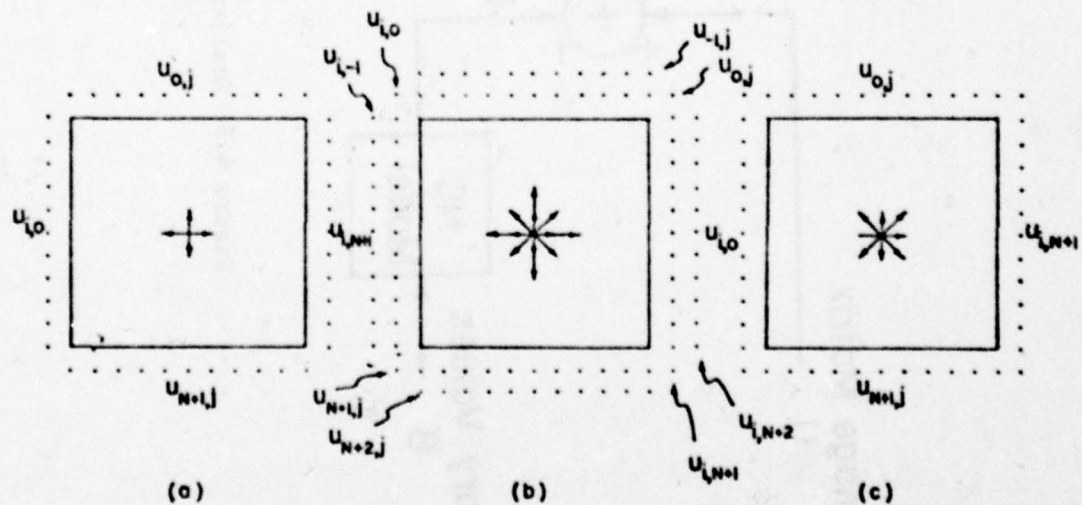


Figure 4.2 Spatial Structures of Three Noncausal Image Representations  
(a) NC1 (b) NC2 (c) NC3

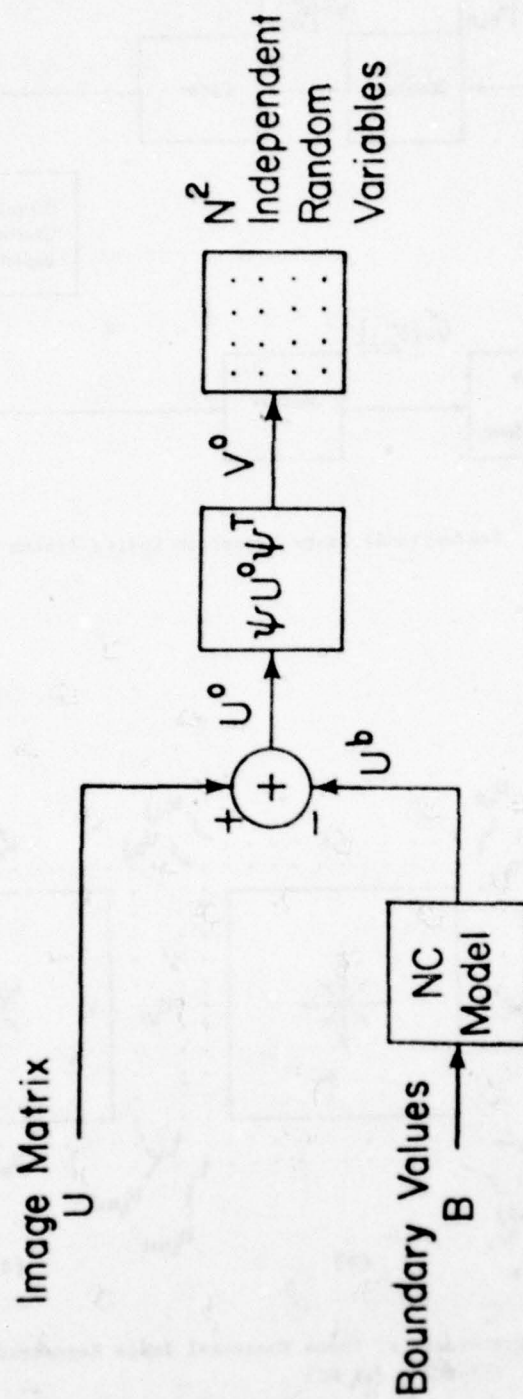


Figure 4.3 Realization of Noncausal Model Decomposition



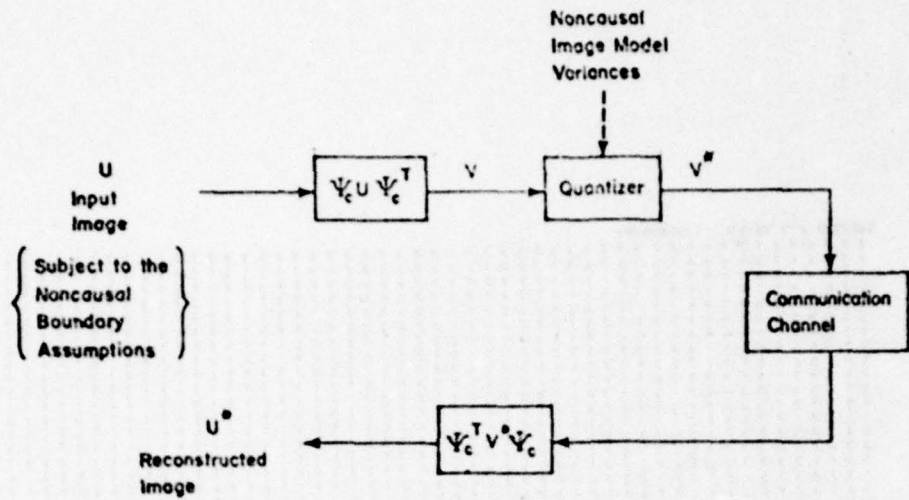


Figure 4.4(a) Cosine Transform Coding via Two-Dimensional Noncausal Model

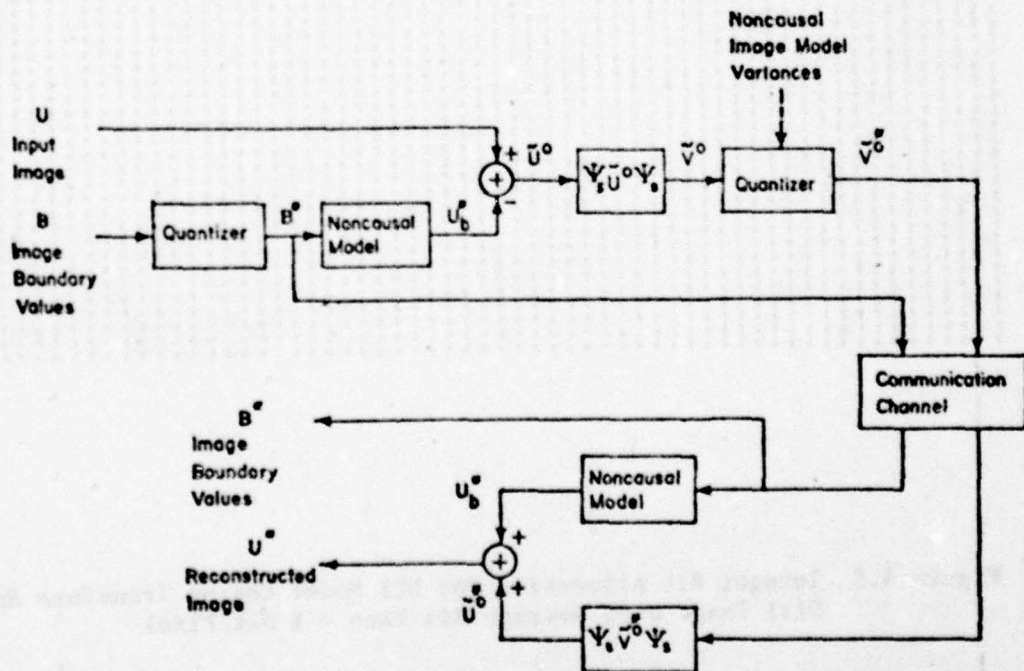


Figure 4.4(b) Fast KL (Sine) Transform Coding via Two-Dimensional Noncausal Model

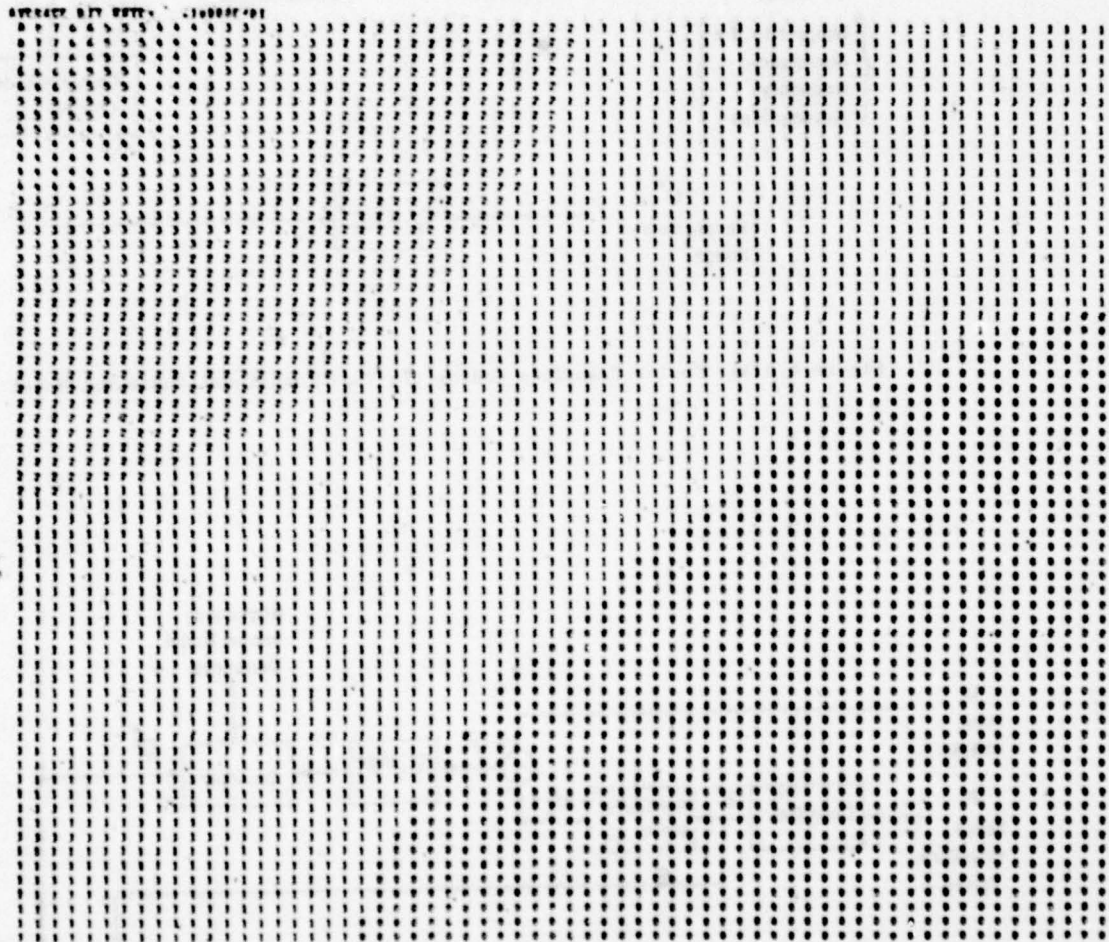


Figure 4.5 Integer Bit Allocation for NCI Model Cosine Transform Encoded Girl Image with Average Bit Rate = 1 Bit/Pixel

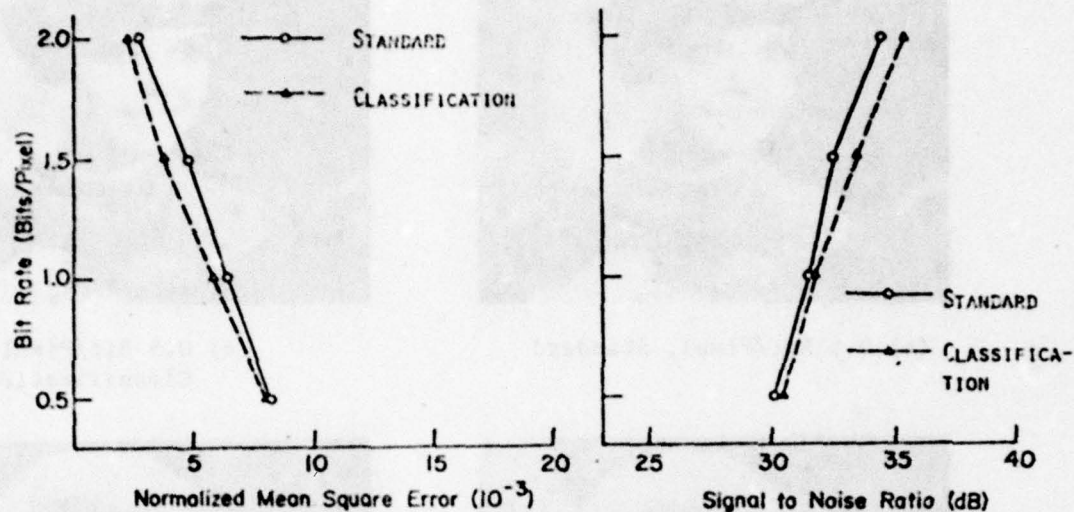


Figure 4.6 Transform Coding Results of NCI Model of the Girl Image with Image Block Size  $64 \times 64$  (a) Rate Distortion Curve (b) Bit Rate versus SNR

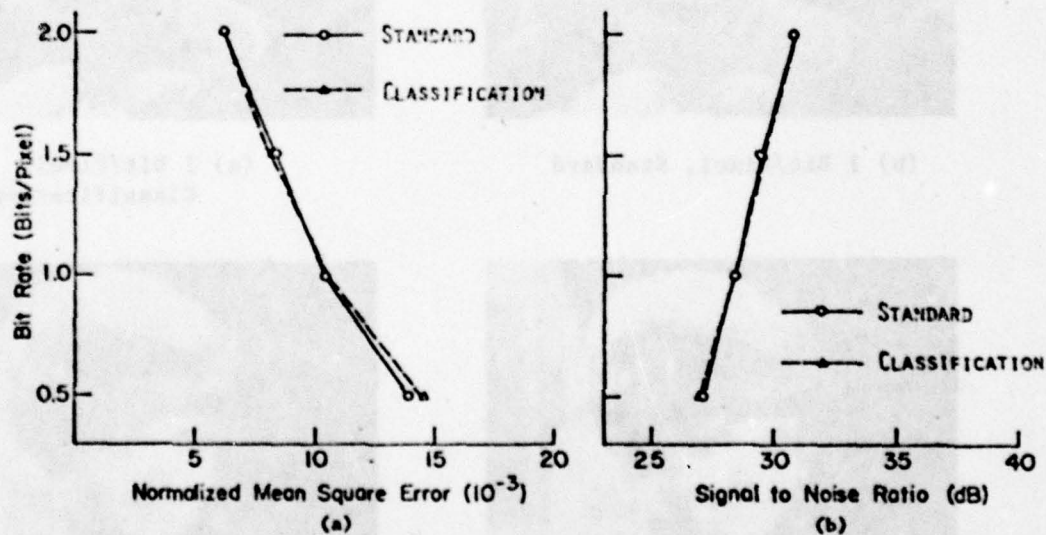


Figure 4.7 Transform Coding Results of NCI Model of the Chemical Plant Image with Image Block Size  $64 \times 64$  (a) Rate Distortion Curve (b) Bit Rate versus SNR





(a) 0.5 Bit/Pixel, Standard



(d) 0.5 Bit/Pixel,  
Classification



(b) 1 Bit/Pixel, Standard



(e) 1 Bit/Pixel,  
Classification

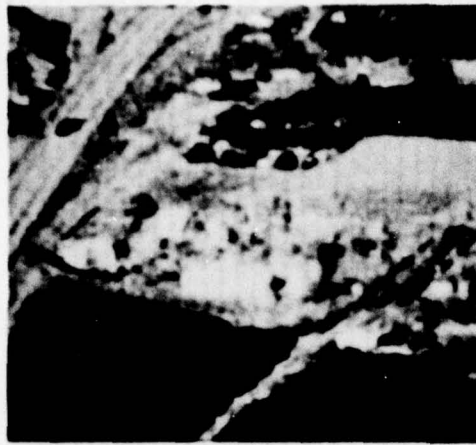


(c) 2 Bits/Pixel, Standard

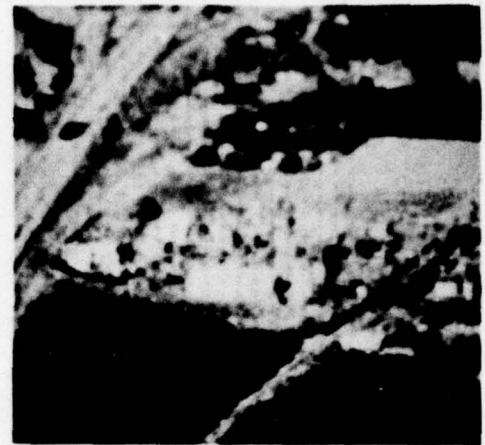


(f) 2 Bits/Pixel,  
Classification

Figure 4.8 Cosine Transform Encoded Girl Image



(a) 0.5 Bit/Pixel, Standard



(d) 0.5 Bit/Pixel,  
Classification



(b) 1 Bit/Pixel, Standard



(e) 1 Bit/Pixel,  
Classification

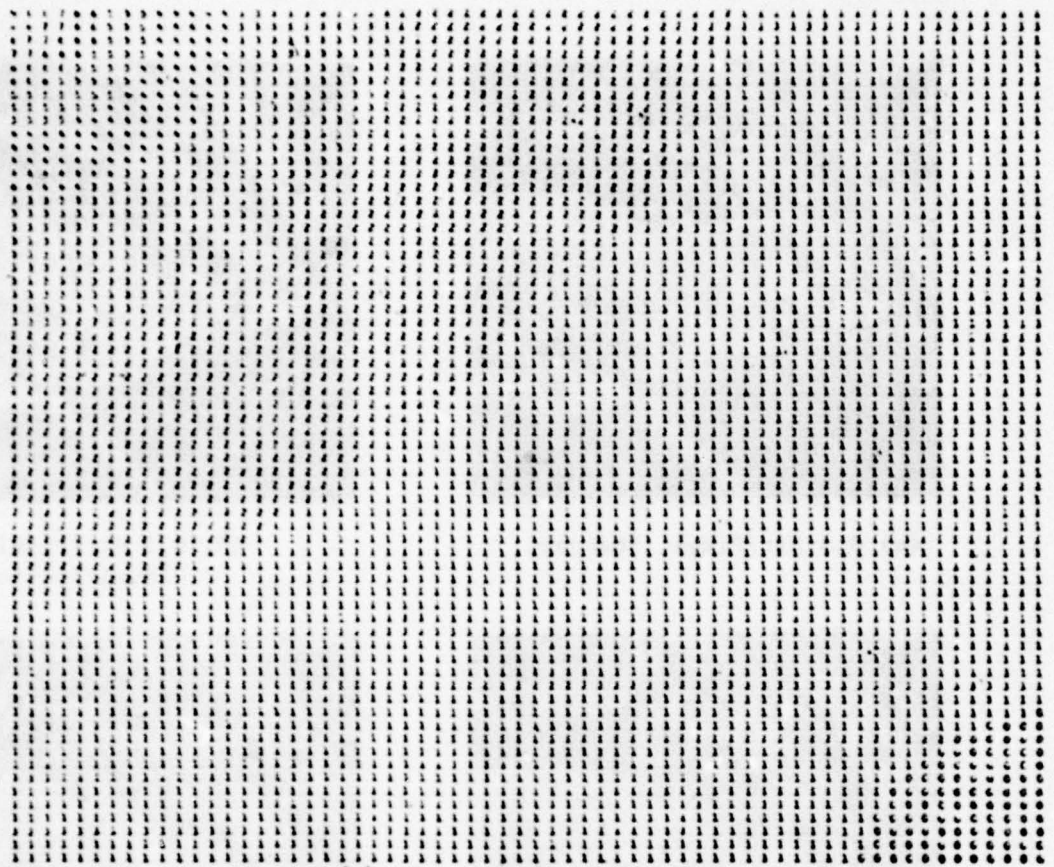


(c) 2 Bits/Pixel, Standard

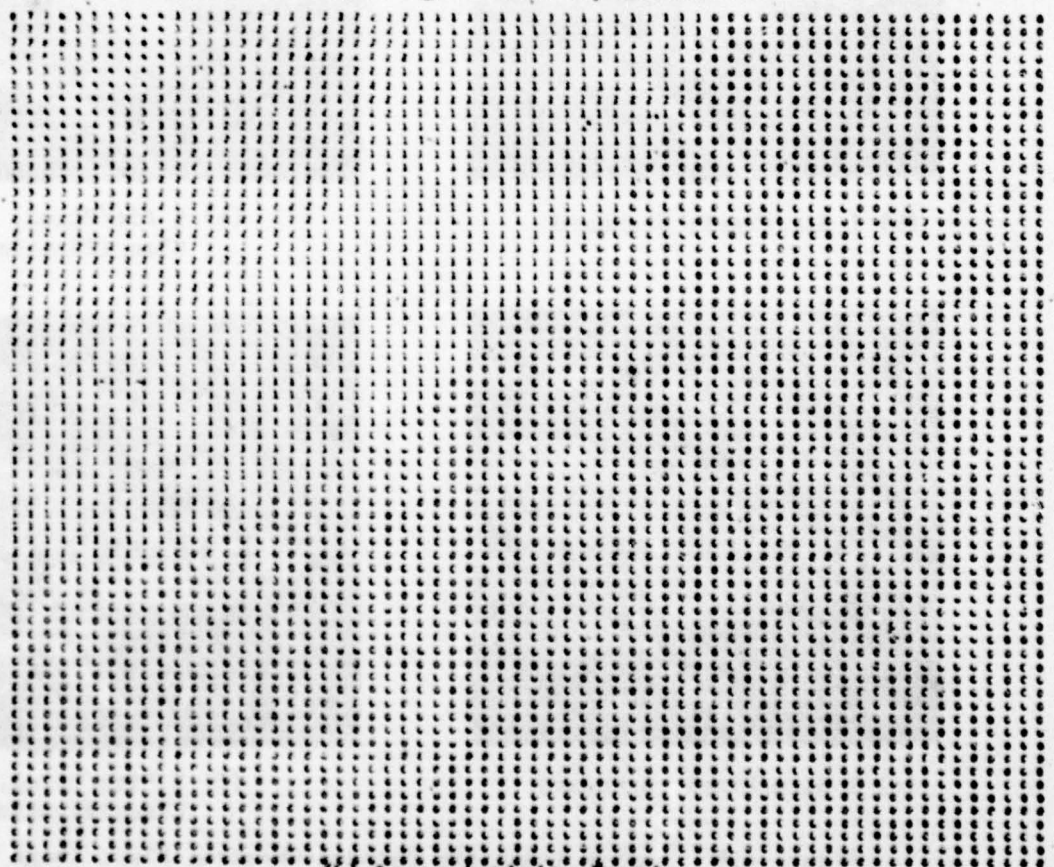


(f) 2 Bits/Pixel,  
Classification

Figure 4.9 Cosine Transform Encoded Chemical Plant Image



(a) Higher Activity Portion



(b) Lower Activity Portion

Figure 4.10 Bit Allocation with Classification at Bit Rate = 1 Bit/Pixel  
(k=2, Girl Image and 64 x 64 Image Block Size)



2	1	1	1	572.26	2166.34	3136.82	1878.98
2	1	2	2	659.34	1639.23	1199.76	929.15
2	1	2	2	1237.50	1649.39	1190.22	1404.61
1	2	1	1	1988.18	1066.08	5779.13	3405.83

(a)

2	2	2	2	1250.41	780.69	646.67	856.33
2	2	2	1	1209.60	984.43	1171.79	1540.41
1	1	1	1	1462.82	2897.02	2053.08	1366.84
1	1	1	2	2596.36	2464.29	1517.38	1051.94

(b)

Figure 4.11 Classification Map and Image Block Measurement Variances

with Two Classes (Equal Probabilities  $P_k = 0.5$ )

(a) Girl Image (b) Chemical Plant Image.

where 2 indicates lower activity and 1 indicates higher activity, size of the classification map is obtained as  $(\frac{256}{N}) \times (\frac{256}{N})$  and  $N = 64$  in this example.

Table 4.1 Summary of Important Formulas of Noncausal Represented Image Random Fields

Model	Cosine	Sine
NC1 ARMA Model	$\bar{U} = J^{-1} \bar{C} \quad (4.4-5)$ $J = (I \otimes Q_c + Q_c \otimes I) \quad (4.4-5a)$ $Q_c = \begin{bmatrix} \lambda_2 - \alpha & -\alpha & & & \\ & \lambda_2 & & & \\ & -\alpha & \lambda_2 & & \\ & & & \lambda_2 & -\alpha \\ & & & -\alpha & \lambda_2 - \alpha \end{bmatrix} \quad (4.4-3)$ $\bar{V} = (\bar{V}_s \otimes \bar{V}_c) \bar{U}$ $E[v_{ij}^2] = \beta^2 \frac{(\lambda_{c1i} + \lambda_{c1j})}{(\lambda_{c1} + \lambda_{c1j})^2} \quad (4.4-12)$ $\lambda_{c1} = \lambda_2 - 2\alpha \cos \frac{(i-1)\pi}{N} \quad (4.4-3a)$	$\bar{U} = \bar{U}^0 + \bar{U}_b = J^{-1} \bar{C} + J^{-1} \bar{B} \quad (4.3.1-7)$ $\bar{B} \quad (4.3.1-3)$ $J = I \otimes Q_s + Q_s \otimes I \quad (4.3.1-5)$ $Q_s = \begin{bmatrix} \lambda_2 & -\alpha & & & \\ & -\alpha & & & \\ & -\alpha & \lambda_2 & & \\ & & & \lambda_2 & -\alpha \\ & & & -\alpha & \lambda_2 \end{bmatrix} \quad (4.3.1-10)$ $\bar{V}^0 = (\bar{V}_s \otimes \bar{V}_s) \bar{U}^0 \quad (4.3.1-8)$ $E[v_{ij}^{02}] = \beta^2 \frac{(\lambda_{s1i} + \lambda_{s1j})}{(\lambda_{s1} + \lambda_{s1j})^2} \quad (4.3.1-13)$ $\lambda_{s1} = \lambda_2 - 2\alpha \cos \frac{i\pi}{N+1} \quad (4.3.1-2)$
NC2 ARMA Model	$\bar{U} = J^{-1} \bar{C}$ $J = I \otimes H + H \otimes I + 2Q_c \otimes Q_c$ $H = Q_c^2 + H^b$ $\bar{V} = (\bar{V}_c \otimes \bar{V}_c) \bar{U}$ $E[v_{ij}^2] = \beta^2 \frac{(\lambda_{c1i} + \lambda_{c1j})^2}{(\lambda_{c1} + \lambda_{c1j})^4}$ $Q_c, \lambda_{c1} \text{ same as NC1 ARMA Model}$	$\bar{U} = \bar{U}^0 + \bar{U}_b = J^{-1} \bar{C} + J^{-1} \bar{B} \quad (4.3.2-6)$ $\bar{B} \quad (4.3.2-3)$ $J = I \otimes H + H \otimes I + 2Q_s \otimes Q_s \quad (4.3.2-4a)$ $H = Q_s^2 + H^b \quad (4.3.2-8)$ $\bar{V}^0 = (\bar{V}_s \otimes \bar{V}_s) \bar{U}^0$ $E[v_{ij}^{02}] = \beta^2 \frac{(\lambda_{s1i} + \lambda_{s1j})^2}{(\lambda_{s1} + \lambda_{s1j})^4} \quad (4.3.2-13)$ $Q_s, \lambda_{s1} \text{ same as NC1 ARMA Model}$
NC3 Minimum Variance Model	$\bar{U} = J^{-1} \bar{C}$ $J = Q_c \otimes Q_c$ $Q_c = \begin{bmatrix} 1-\alpha & -\alpha & & & \\ & -\alpha & 1 & & \\ & & & 1 & -\alpha \\ & & & -\alpha & 1-\alpha \end{bmatrix}$ $\bar{V} = (\bar{V}_c \otimes \bar{V}_c) \bar{U}$ $E[v_{ij}^2] = \frac{\beta^2}{\lambda_{c1} \lambda_{c1j}}$ $\lambda_{c1} = 1 - 2\alpha \cos \frac{(i-1)\pi}{N}$	$\bar{U} = \bar{U}^0 + \bar{U}_b = J^{-1} \bar{C} + J^{-1} \bar{B} \quad (4.3.3-7)$ $\bar{B} \quad (4.3.3-2)$ $J = Q_s \otimes Q_s \quad (4.3.3-6)$ $Q_s = \begin{bmatrix} 1 & -\alpha & & & \\ & -\alpha & & & \\ & -\alpha & & & \\ & & & -\alpha & 1 \end{bmatrix}$ $\bar{V}^0 = (\bar{V}_s \otimes \bar{V}_s) \bar{U}^0 \quad (4.3.3-10)$ $E[v_{ij}^{02}] = \frac{\beta^2}{\lambda_{s1} \lambda_{s1j}} \quad (4.3.3-11)$ $\lambda_{s1} = 1 - 2\alpha \cos \frac{i\pi}{N+1} \quad (4.3.1-2)$

Table 4.2 Girl Image, Cosine Transform Coding Results,  
NCl Model with 64 x 64 Image Block

Bit Rate	Standard		Classification	
	N.M.S.E. (%)	SNR	N.M.S.E. (%)	SNR
0.5	0.8213	30.396	0.8208	30.399
1.0	0.6399	31.480	0.5906	31.828
1.5	0.4929	32.614	0.3956	33.569
2.0	0.3075	34.662	0.2556	35.465

Table 4.3 Chemical Plant Image, Cosine Transform Coding Results,  
NCl Model with 64 x 64 Image Block

Bit Rate	Standard		Classification	
	N.M.S.E. (%)	SNR	N.M.S.E. (%)	SNR
0.5	1.4067	27.214	1.4711	27.020
1.0	1.0443	28.508	1.0699	28.403
1.5	0.8320	29.495	0.8087	29.619
2.0	0.6106	30.830	0.6244	30.742



## CHAPTER FIVE

### IMAGE MODELS FOR FEATURE CODING

#### 5.1 Introduction

In this chapter we consider an image coding technique which preserves the attractive characteristics of standard transform coding, i.e., energy packing and channel error immunity, as well as improves the visual appearance of an encoded image. This technique is called Feature transform coding. The basic idea behind this technique lies in segmenting an image which is considered to be a composition of two parts, deterministic and stochastic, where the stochastic part is dealt with by known statistical analysis according to the image model algorithms developed in Chapter 4 and the deterministic part (which could be called features) is obtained as the residual after the stochastic part is removed.

Other two source modeling of images has been considered earlier by Schreiber [ 62 ], Yan and Sakrison [ 74 ]. The present approach is somewhat more general and is based on stochastic models of images by partial difference equations.

In section 5.2 we demonstrate the concept of feature extraction via image model operators. In section 5.3 we then relate the transform coding scheme with the feature extraction concept and a set of operations performed with this new technique is described in detail. Finally, in section 5.4, we present results of encoded images and compare them with standard NCl Cosine transform encoded image at the same bit rate.

#### 5.2 Feature Extraction via Image Models

The problem of feature extraction is to determine the rough profile of an object within a given image. It is noted that most important

informations of an image lie on features which contribute the visual appearance of an image. Here a new technique is presented in which the edge points (feature) is detected from the knowledge of image models.

#### 5.2.1 Image Modeling Operator

A given image,  $U$ , can be treated as a sample function of a two-dimensional random field. We consider the random field as a composition of two parts, the first part representing the relatively smooth variations within the image which can be described by stochastic image models and the other representing the unpredictable part or deterministic part called the features or edges. Thus, we can write the image  $U$  as

$$U = U_s + U_d \quad (5.2.1-1)$$

where  $U_s$  and  $U_d$  represent the stochastic and deterministic parts respectively.

Typically, the stochastic part representing smooth variations consists of background and low spatial frequency information and the deterministic part describes the abrupt changes (large variations) usually caused by the distinct edges of an object. Therefore, a more effective coding method would be to segment the image into the said parts and code them efficiently.

Typically, an infinite, stationary random field may be represented by its spectral density function (SDF). Several candidates have been proposed in Table 2.1. Let  $\mathcal{Z}$  denote an operator acting on a discrete image.

Denoting  $\epsilon$  as the output signal after applying this operator, we can write

$$\epsilon_s \triangleq \mathcal{Z}[U_s], \quad \epsilon_d \triangleq \mathcal{Z}[U_d]. \quad (5.2.1-2)$$

A common example of  $\mathcal{L}$  is the Laplacian operator<sup>†</sup>, which takes the difference of an image element with an algebraic average of its nearest four neighbors. Most feature extraction (or edge detection) problems could be formulated as a segmentation of  $U_s$  and  $U_d$  in the above equation, of course, with different operators.

Letting  $t$  be the arbitrary selected threshold which is employed to classify  $\epsilon(i,j)$ , the  $(i,j)$ th component of  $\epsilon$ , the segmentation criterion is

$$\epsilon_s(i,j) = \begin{cases} \epsilon(i,j) & \text{if } |\epsilon(i,j)| < t \\ t & \text{if } |\epsilon(i,j)| \geq t \end{cases} \quad (5.2.1-3)$$

$$\epsilon_d(i,j) = \begin{cases} 0 & \text{if } |\epsilon(i,j)| < t \\ \epsilon(i,j) - \text{Sign } \epsilon(i,j) & \text{if } |\epsilon(i,j)| \geq t \end{cases} \quad (5.2.1-4)$$

Thus we compare  $|\epsilon(i,j)|$  with  $t$ , and if  $|\epsilon(i,j)| \geq t$ , then the point  $(i,j)$  belongs to the set of boundary points; otherwise, it belongs to the stationary part. The values assigned to  $\epsilon_s$  and  $\epsilon_d$  are according to the above equations.

---

† The Laplacian of a continuous function  $f(x,y)$  is defined as

$$\epsilon(x,y) \triangleq \nabla^2 f = \frac{\partial^2 f}{\partial x^2} + \frac{\partial^2 f}{\partial y^2}$$

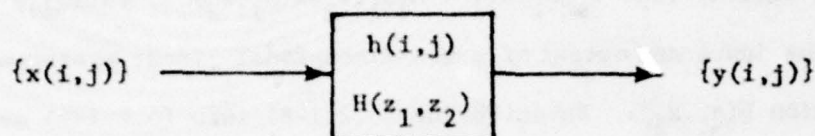
and its discrete equivalent is given by the difference equation

$$\epsilon_{i,j} = (f_{i+1,j} + f_{i-1,j} + f_{i,j+1} + f_{i,j-1}) - 4f_{i,j}$$

where  $f_{i,j} \approx f(x_i, y_j)$ ,  $\epsilon_{i,j} \approx \epsilon(x,y)\Delta x\Delta y$ ,  $\Delta x$  and  $\Delta y$  are the finite difference intervals in the  $x$  and  $y$  coordinates respectively.



There are two simple ways of selecting the threshold  $t$ . First, using the histogram of  $|\epsilon(i,j)|$ , a threshold value is picked such that a desired percentage of total image elements would be detected as edge points. Second, we could let  $t = c\sigma$ ,  $c = \text{constant}$ ,  $\sigma = \text{standard deviation of } |\epsilon(i,j)|$ . Now, let us consider the selection of  $\mathcal{L}$ .



Let  $\{x(i,j)\}$  and  $\{y(i,j)\}$  be the input and output sequences, respectively, of a two-dimensional linear system with transfer function  $H(z_1, z_2)$ . The SDFs of  $\{x(i,j)\}$  and  $\{y(i,j)\}$  are related by

$$S_y(z_1, z_2) = H(z_1, z_2)H(z_1^{-1}, z_2^{-1})S_x(z_1, z_2) . \quad (5.2.1-5)$$

For an input white noise field  $\{w(i,j)\}$ , the output would be a stationary random field, say  $\{s(i,j)\}$ , such that its SDF is given by

$$S_s(z_1, z_2) = H(z_1, z_2)H(z_1^{-1}, z_2^{-1})S_w(z_1, z_2) . \quad (5.2.1-6)$$

For the sake of simplicity, the SDF of the white noise field is taken to be unity. Then (5.3.1-6) becomes

$$S_s(z_1, z_2) = H(z_1, z_2)H(z_1^{-1}, z_2^{-1}) . \quad (5.2.1-7)$$

Therefore the transfer function can be viewed as

$$H(z_1, z_2) = [S_s(z_1, z_2)]^{1/2} . \quad (5.2.1-8)$$

Taking a two-dimensional Z transform on both sides of (5.2.1-1) yields

$$V(z_1, z_2) = V_s(z_1, z_2) + V_d(z_1, z_2), \quad (5.2.1-9)$$

where  $V \triangleq Z\{U\}$ ,  $V_s \triangleq Z\{U_s\}$  and  $V_d \triangleq Z\{U_d\}$ . (5.2.1-9a)

It is obvious that  $V_s(z_1, z_2) = H(z_1, z_2)W(z_1, z_2)$  if  $\{w(i, j)\}$  and  $\{u_s(i, j)\}$  are the input and output of a two-dimensional linear system with transfer function  $H(z_1, z_2)$ . Substituting (5.2.1-8) into (5.2.1-9) we get

$$V(z_1, z_2) = [S_s(z_1, z_2)]^k W(z_1, z_2) + V_d(z_1, z_2) \quad (5.2.1-10)$$

where  $W(z_1, z_2)$  is the two-dimensional Z transform of the white noise field.

Rearranging the terms of (5.2.1-10), we have

$$[S_s(z_1, z_2)]^{-k} V(z_1, z_2) = W(z_1, z_2) + [S_s(z_1, z_2)]^{-k} V_d(z_1, z_2) \quad (5.2.1-11)$$

Denoting  $\epsilon(z_1, z_2) \triangleq [S_s(z_1, z_2)]^{-k} V(z_1, z_2)$  and taking inverse two-dimensional Z transform on both sides of (5.2.1-11), we get

$$\epsilon(i, j) = \epsilon_s(i, j) + \epsilon_d(i, j) \quad \forall i, j \quad (5.2.1-12)$$

where  $\epsilon_d$  is the inverse Z transform of  $[S_s]^{-k} V_d$ , and  $\epsilon_s$  is the white noise field. For finite image, we define a two-dimensional transform of the image as

$$V \triangleq \bar{\Psi}[U] = \Psi U \Psi^T \quad (5.2.1-13)$$

where superscript T indicates conjugate and transpose operations and  $\bar{\Psi}$  is the unitary KL transform of U. (The above equation implies  $\bar{\Psi}$  is a

separable transform, which will be true for our image models). From the foregoing discussion, if we define

$$\mathcal{Z} = \bar{\Psi}^{-1} S_s^{-1/2} \bar{\Psi} \quad (5.2.1-14)$$

where superscript  $-1$  indicates inverse operation and  $S_s$  is the SDF of stationary random field, then  $\mathcal{Z}$  would be the desired edge detection operator.

### 5.2.2 Approximate Rational Function Operator

The SDF of NCI image model is given by

$$S_s(z_1, z_2) = \frac{1 - r\alpha(z_1 + z_1^{-1} + z_2 + z_2^{-1})}{[1 - \alpha(z_1 + z_1^{-1} + z_2 + z_2^{-1})]^2} \quad (5.2.2-1)$$

where  $r\alpha = \alpha_1$  and  $\beta^2 = 1$ , to be consistent with the formula given in Table 2.1. If we assume  $R(z_1, z_2) = [S_s(z_1, z_2)]^{-1/2}$  then the alternative expression for  $R(z_1, z_2)$  is given by (see Appendix B)

$$R(z_1, z_2) = 1 - \sum_{n=1}^{\infty} \frac{1 \cdot 3 \cdot 5 \cdots (2n-3)}{2^{n-1} (n-1)!} \left(1 - r + \frac{r}{2n}\right) r^{n-1} x^n. \quad (5.2.2-2)$$

By picking different values of  $n$ , we obtain various orders of  $R(z_1, z_2)$  with which the edge detection operator could be defined as

$$\mathcal{Z} = R^{(n)}(z_1, z_2) \quad n = 1, 2, \dots \quad (5.2.2-3)$$

This implies  $\mathcal{Z}$  is a two-dimensional  $n$ th order difference operator.

### 5.2.3 Edge Information Subtraction Procedure

We have stated the concepts of image modeling operator and edge points segmentation criterion in the preceding sections. The sequence



of operations needed to be performed may now be listed as follows:

1. Take discrete unitary transform of the input image,  $V = \Psi U \Psi^T$ , where  $\Psi$  denotes the chosen discrete unitary transform.
2. Based on the image model, find the proper representation for the SDF,  $S_s$ , in the  $\Psi$  domain.
3. Calculate  $S_s^{-1/2}$  and multiply it with  $V$ , yielding  $\epsilon = S_s^{-1/2} V$ .
4. Take inverse discrete unitary transform of  $\epsilon$ , obtaining  $\epsilon_d = \Psi^{-1} \epsilon \Psi^{-T}$ .
5. Pick a reasonable threshold to segment  $\epsilon_d$  from  $\epsilon_s$  according to equations (5.2.1-3) and (5.2.1-4).
6. Generate edge address map  $\mathcal{J}_d$  which is the set of  $(i,j)$  coordinates of each detected edge point.

Once the edge information is known, the stationary field  $U_s$  and deterministic field  $U_d$  of the given image can be obtained by the following fairly obvious way:

7. Take discrete unitary transform of  $\epsilon_d$ , getting  $\epsilon_d = \Psi \epsilon_d \Psi^T$ .
8. Premultiply  $S_s^{1/2}$  with  $\epsilon_d$ , and define  $V_d = S_s^{1/2} \epsilon_d$ .
9. Take inverse discrete unitary transform of  $V_d$  to obtain  $U_d = \Psi^T V_d \Psi$ .
10. Subtracting  $U_d$  from the input image  $U$ , gives the stationary field as  $U_s = U - U_d$ .

We have considered two transforms, i.e., discrete Fourier transform and discrete Cosine transform as the two-dimensional unitary transform operators in our preliminary feature extraction study. The experiments were performed on the  $256 \times 256$  Girl image in  $64 \times 64$  image blocks. For

comparison, the thresholds for different methods of edge detection were chosen to yield approximately equal number of detected edge points. The formulas for evaluating the value  $S_s(k, \ell)$  will be different according to which transform is actually implemented and the image model used. The NCl model was chosen for all experiments. First we let

$$S_s(k, \ell) = S_s \left( z_1 = e^{\frac{-2\pi k}{N}}, z_2 = e^{\frac{-2\pi \ell}{N}} \right)$$

be the approximation of the SDF in the discrete Fourier transform domain when  $N$  is sufficiently large. However, in the case of Cosine transform, the numerical value of  $S_s(k, \ell)$  is taken from the cosine transform variance formula (see Table 4.1). Figures 5.1(a) and 5.1(b) show the resulting images of these two experiments. A significant visual difference can be observed from these two figures. The block effect obtained with the discrete Fourier transform approximation is not present in using the Cosine transform. Hence, it is preferable to use the Cosine transform in the study of feature extraction concepts.

If the approximate rational operator  $R^{(n)}$  is used, rather than  $S_s^{-k}$ ,  $\epsilon(i, j)$  could be calculated directly in the spatial domain (because  $R^{(n)}$  becomes a two-dimensional  $n$ th order difference operator). Segmentation of  $\epsilon(i, j)$  could be performed as before. The spatial structure of  $R^{(n)}$  as a difference operator is shown for various values of  $n$  in Appendix B.

#### 5.2.4 Image Enhancement

A typical image is usually made up of objects having edges at which the brightness changes abruptly. It has been known to investigators in the image processing field that the human visual system is sensitive to these edges. By this argument a "good" image should result if these

edge points can be isolated and emphasized so as to make the image appear sharp. We have initiated a study towards this end. Following the concept developed in the previous sections, the stationary (stochastic) field and deterministic (feature) field of any given image can be easily generated. The way to "sharpen" the image can be done by the following equation

$$U' = \alpha U_s + \beta U_d \quad \forall i,j \quad (5.2.4-1)$$

where  $U_s$  represents the stationary field which contains mostly background information, and  $U_d$  represents the deterministic field which results from the edge information.

Using (5.2.4-1), one can change various values of  $\alpha$  and  $\beta$  and achieve different enhancement (sharp or blur) images  $U'$ . Figures 5.3II and 5.4II demonstrate the results. The thresholds used in these experiments are given in Table 5.1. It is seen that  $U_s + 1.5U_d$  gives the best enhancement image among the six combinations in our study.

The overall block diagram of this system is shown in Fig. 5.2, which consists of two functions, decomposition and synthesis. The stochastic modeling operator  $\mathcal{Z}$  is determined by a chosen image model, and (5.2.4-1) is implemented by adjusting the two values  $\alpha$  and  $\beta$ .

### 5.3 Transform Coding Using Nonstationary Image Representation

In the foregoing presentation, we considered a new concept of image decomposition, an image can be separated into its stochastic (stationary) and deterministic (feature) components, i.e.,

$$U = U_s + U_d \quad (5.2.1-1)$$



One of the possible applications of (5.2.1-1) is to extend it to image coding or data compression. In comparison with current existing coding schemes, including the one presented in Chapter 4, this scheme is found to give better performance in terms of resolution for the same bit rate, and gives more pleasing encoded images to the human viewer.

Let us give an overview of this coding scheme and then describe the various operations in detail. The block diagram of this scheme is given in Figure 5.5. First,  $U$  is transformed by a two-dimensional unitary transform. There is a tradeoff between a large image block size to extract sufficient edge information and a small size to save memory and computational effort. We find that a good compromise is achieved by  $64 \times 64$  blocks. Next, applying operator  $\mathcal{Z}'$  on  $V$  (see Fig. 5.5) where  $V$  is the transformed image. The output of this operation,  $\epsilon$ , is segmented next according to (5.2.1-3) and (5.2.1-4). If  $|\epsilon(i,j)| \geq t$ , the location  $(i,j)$  is recorded as one of the edge addresses, otherwise it is rejected. The value of  $\epsilon$  at the detected edge point is quantized before transmission to the receiver. This quantized version of  $\epsilon$ ,  $\epsilon^*$ , is also needed to calculate  $V_d^*$  as  $\mathcal{Z}^{-1}\epsilon^*$ , where  $V_d^*$  is viewed as the deterministic part of the transformed image. Subtracting  $V_d^*$  from  $V$ , we have  $V_s$ , the stochastic part of the transformed image. A conventional transform coding scheme is then implemented on  $V_s$ . Finally,  $V_s^*$ ,  $\epsilon_d^*$  together with edge address map,  $J_d$ , are used for coding and transmission over the communication channel.

At the receiver, the process proceeds in a fairly obvious way. First, we reconstruct  $V_d^*$  based on the received  $\epsilon_d^*$  and  $J_d$ . Then summing it with  $V_s^*$ , yields  $V^*$ . Finally, the inverse unitary transform is operated on  $V^*$  to recover the input image.

We now describe details of some of the operations that need to be performed.

1) Run Length Coding

The purpose of this operation is to efficiently transmit the edge address map. The entropy of the run length serves as a measure of bit rate required to recover the original edge address map without distortion. For higher threshold,  $t$ , fewer pixels are detected as edge points. In this situation, in order to prevent excessively long runs, pseudo runs are inserted if run length exceeds a fixed number (64 in our experiment).

2) Fixed Level Quantization

Essentially we have only one quantizer at this stage and  $\epsilon_d(i,j)$  is assumed to have a Laplacian distribution with mean zero and variance  $\sigma_{\epsilon_d}^2$  which has to be calculated for each value of  $t$ , since the values of  $\epsilon_d(i,j)$  would vary with  $t$ . Due to the fact that the values of  $\epsilon_d(i,j)$  are usually small, it has been found that a two bit quantizer gives a very accurate reproduction of  $\epsilon_d(i,j)$ . We have studied the effect of assigning different bits to the quantizer. Notice that if the number of detected edge points increases, then assigning too many bits to the quantizer would mean that we are not able to allocate sufficient bits to the transform domain quantizers, and this would cause the objectionable low spatial frequency quantization errors in the encoded image.

3) Transform Domain Quantization

In order to accomplish the task of data compression, we must allocate unequal number of bits to the quantizers for each element of  $V_g$ . The

fundamental idea of transform coding is that high energy (activity) samples are quantized more accurately than low energy samples. The variances of each element of  $V_s$ , the stochastic part of the transformed image, can be estimated from the SDF corresponding to the transform used. The quantization scheme used here is the Lloyd-Max quantizer with the assumption that each element of  $V_s$  is Gaussian in distribution.

#### 4) Function of $\mathcal{Z}'$

Referring to Fig. 5.5, it is seen that

$$e = \mathcal{Z}'V = \psi^{-1} S_s^{-\frac{1}{2}} V. \quad (5.3-1)$$

From the above equation, clearly, we have defined  $\mathcal{Z}'$  as

$$\mathcal{Z}' = \psi^{-1} S_s^{-\frac{1}{2}}. \quad (5.3-2)$$

Comparing (5.3-2) with (5.2.1-4), it can be seen that  $\mathcal{Z}'$  is slightly different from  $\mathcal{Z}$ , the way presented in Fig. 5.5 is easily realizable.

#### 5) Considerations in Deleting Isolated Point

Edge detection is often affected by noise contained in the original image. If we examine the edge picture (picture composed of the detected edge points only) closely, see Fig. 5.1, we would find many isolated spots spread over the scene. Actually, we have no sharp distinction between a "true edge point" or a "noise" point. A simple edge detection scheme in the presence of small amount of noise is to first implement the edge extraction algorithm, then followed by an algorithm that removes the isolated edges (noise) from the scene. In this way, one could get a much



clearer edge profile. We have included this scheme inside edge detection logic box of Figure 5.5.

An advantage of this transform coding method is that it gives us a flexible way to meet any requirement of getting a good visual image subject to a fixed bit rate. There are three adjustable parameters associated with the entire process, viz,

a. Edge point selection threshold

The basic formula is given by  $t = c\sigma$ , where  $\sigma$  is the rms value of  $\epsilon(i,j)$ , and  $c$  is an adjustable constant. When  $c \rightarrow \infty$  no pixel will be detected as an edge point. Some of the operations in Figure 5.5 could be bypassed in this case and a conventional transform coding method is directly performed on the image  $U$ .

b. Edge quantizer's bit ( $n_e$  bits/edge)

We have made experiments concerning this fixed integer bit's effect on a bit allocation strategy. The various bit rates used are 1, 2, 3 and 4. The results will be presented in the next section. Experimentally, it has been found that 2 bits (4 levels) gives a proper bit selection.

c. Desired bit rate ( $n$ )

It is the desired overall average bit rate in bits/pixel in the final encoded image.

The above mentioned parameters are related by

$$n = n_1 + n_2 + n_3 \quad (5.3-3)$$

$n_1$  : Average bit rate for transform coding of  $V_s^*$

$n_2$  : Average bit rate for coding the amplitudes of detected edge points

$$= \frac{n_e \times (\text{Number of Detected Edge Points})}{(\text{Number of Image Pixels})} \quad (5.3-4)$$

$n_3$  : Bit rate required to recover the edge address map,  $\mathcal{J}_d$ .

$$= \frac{(\text{Entropy of } \mathcal{J}_d) \times (\text{Number of Detected Edge Points})}{(\text{Number of Image Pixels})} \quad (5.3-5)$$

Once the edge point selection threshold is given, the number of detected edge points is automatically determined. For a fixed  $n_e$ ,  $n_2$  and  $n_3$  can be calculated via (5.3-4) and (5.3-5), respectively. If we desire to have bit rate of  $n$  (or  $\frac{8}{n}$  data compression) in the final encoded image,  $n_1$  has to be calculated via (5.3-3).

#### 5.4 Experimental Results and Comparisons

A series of computer simulations has been conducted to evaluate the performance of this scheme called Feature transform coding. A  $256 \times 256$  image was first divided into 16 equal-sized image blocks, each of size  $64 \times 64$ . Each image block was feature transform coded independently. In all the experiments, Cosine transform based NCI model was used and several definitions of performance measurements, i.e., SNR, NMSE, etc., are defined in section 3.5 of Chapter 3. Two images of different category (statistics) were used in order to test how sensitive the scheme was to the image content.

The quantities  $n_e$  and  $t$  are the major parameters in the design of Feature transform coding. In our study, it is done experimentally as presented in the next section.

#### 5.4.1 Feature Transform Coding

In order to find the proper choice of  $n_e$  (edge quantizer's bit) for different values of  $t$  (threshold), we plot the curves of SNR and NMSE versus various settings of  $n_e$  for  $t = 1.5\sigma$  and  $t = 2\sigma$ . Figures 5.6-5.7 and Figures 5.10-5.11 are the results for Girl and Chemical Plant images, respectively. It can be seen from these figures that  $n_e$  must be equal to 2, since it gives the minimum NMSE or maximum SNR of all the bit rates. After determining  $n_e$ , we also plot the curves of SNR and NMSE versus various thresholds. Figure 5.8 demonstrates the curve for the Girl image, and Figure 5.12 is for the Chemical Plant image. It is observed that the SNR increases, while the threshold decreases for moderate bit rate (1~1.5) of both images. For high bit rate ( $=2$ ) this phenomenon is still observed for Chemical Plant image, but not for Girl image. This could be because the Chemical Plant image is a complicated scene in which more edge points must be separated from the background and encoded adequately. For low bit rate ( $=0.5$ ), as expected, this scheme performs slightly better than the standard transform coding (in our case NCI Cosine transform coding) for higher thresholds only. Based on these observations, it seems that  $t = 1.5\sigma$  and  $n_e = 2$  serve as the best parameters to be used to encode any given image at rate greater than 0.5 bit / pixel.

The comparisons of Feature transform encoded and standard transform encoded images are shown in Figure 5.14 for the Girl image and corresponding ones for the Chemical Plant image are shown in Figure 5.15. In all the images the Feature transform coder produces a "better" appearing image (at bit rate  $> 0.5$ ) than the standard transform coder. It is easily seen that there is a significant difference around the Girl's face and at the sides of the freeway in the Chemical Plant image. In general, the edges



are more clearly defined on the Feature transform encoded image. The above discussion is also supported by referring to the coding results shown in Tables 5.2 through 5.9, which give quantitative comparisons of the above two mentioned schemes. For easy reference, the performances of the standard transform coder at different bit rates are listed along with the Feature transform coder. The performance improves by about 1.5 dB at 1 bit rate for both images and by 2dB at 2 bit rate for Chemical Plant only. It is of interest to note that at 2 bit rate Figure 5.14(f) has less SNR value than Figure 5.14(c). However, by directly looking at the pictures, one can say that Figure 5.14(f) gives a better appearing image since the edges are more sharp regardless of the contrast of the background.

#### 5.4.2 Classification Feature Transform Coding

In this method the edge information map  $g_d$  and edge point  $e_d$  are encoded and transmitted as before, except that the stochastic portion of the transformed image,  $V_s$ , is classified as belonging to one of  $K$  pre-determined classes. In our case,  $K = 2$  and each class is assumed to be equiprobable. The classification maps for the Girl and Chemical Plant images are shown in Fig. 4.11(a) and Fig. 4.11(b). The block diagram of this scheme is analogous to Figure 5.5. However, the Transform Domain Quantization box now contains two types of bit allocation maps, one for each class.

This method gives an additional improvement of SNR over the Feature transform coder about 1 dB at bit rate  $\geq 1.5$  for the Girl image. But it failed for the Chemical Plant image. Figures 5.9 and 5.13 show the coding results versus various thresholds with  $n_e = 2$  assigned to the edge point quantizer. The reason for the discrepancy could be that the Chemical Plant

image is a complicated scene, and once enough detected edge point information has been subtracted from the original nonstationary image field, the resultant image field, i.e.  $V_s$ , would tend to have equal variances for each image block, i.e., the corresponding pixels of the remaining field  $V_s$  of each image block have approximately equal variances. However, this kind of property is violated for a simple structure image, i.e., Girl image, where after the edge point information is subtracted, some refined work, for example classification, could be applied on  $V_s$  if the ultimate goal of coding scheme is to get higher SNR in the final encoded image. We have shown the encoded images of this scheme along with Feature transform encoded images in Figures 5.16 and 5.17.

#### 5.4.3 Conclusions

Based on the above experiments and the theory discussed in Chapter 4, the following conclusions are made:

- (1) Regardless of the computational complexity, Feature transform coding scheme can improve the signal to noise ratio over the standard transform coding scheme (based on NCI Cosine transform model) by 1 to 2 dB at bit rates above 1 bit/pixel for usual images.
- (2) The complexity of Feature transform coding scheme is simpler than the technique proposed by Yen et al [ 74 ] where they ignored the problem of computation time, complexity, and storage. Meanwhile, they had more image dependent parameters that need to be identified. In our case, only two parameters, i.e.,  $n_e$  and  $t$ , are sufficient.
- (3) The Feature transform coding scheme is useful when it is desired to maintain the attractive characteristics of the transform coding

scheme, i.e., less sensitivity to the image statistics (scene to scene variation), as well as to incorporate the physiological reaction of the human visual system in the overall communication system design.

- (4) The Classification Feature transform coding scheme is suited for simple structured images at bit rate  $\geq 1$  bit/pixel. The complexity over the Feature transform code is marginal and its performance is improved by reducing the size of the image block or, in other words, the number of image blocks is increased.



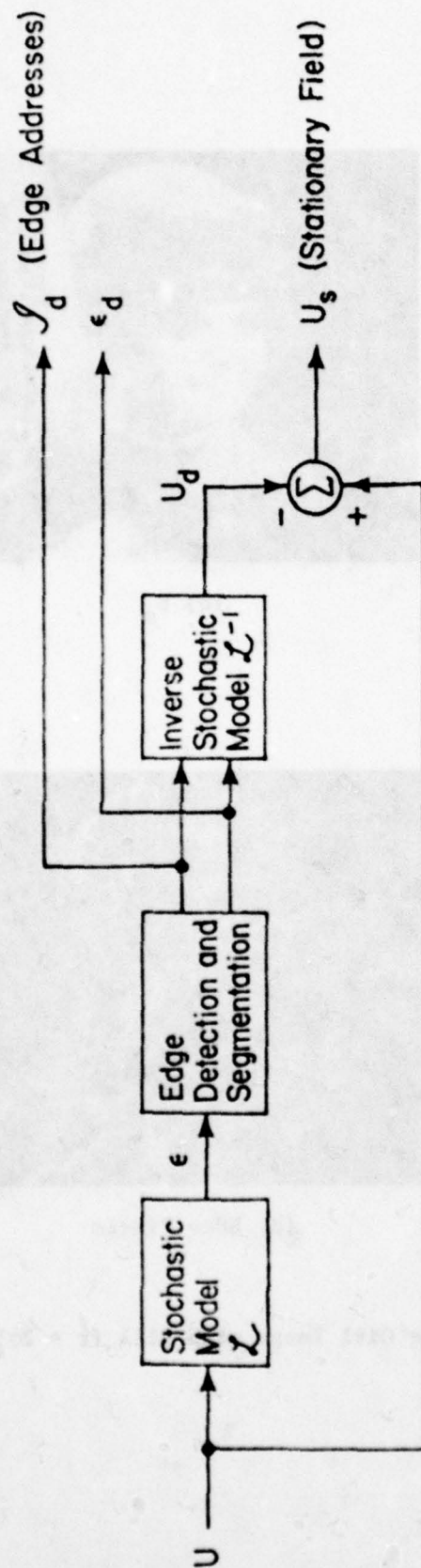


(a)

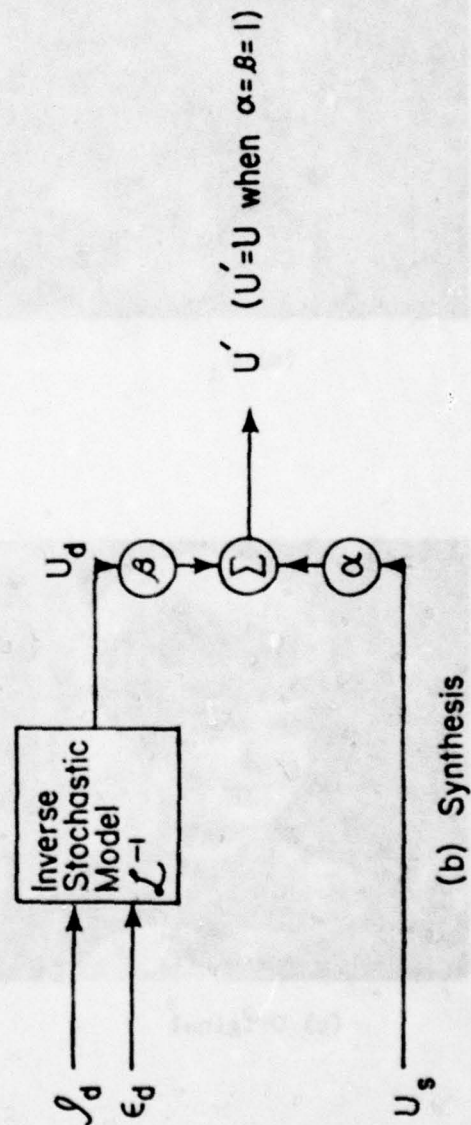


(b)

Figure 5.1 Edge Pictures with  $t = 2\sigma$  (a) Discrete Fourier Transform  
(b) Discrete Cosine Transform, where  $\sigma$  is the rms Value  
of  $c(i,j)$ , and the Total Detected Edge Points are 3612  
and 3587 for (a) and (b), respectively.



(a) Decomposition



(b) Synthesis

Figure 5.2 Realization of Stochastic Decomposition



(a)  $U_d$



(b)  $U_s$



(c) Original



(d) Edge Pixels

Figure 5.3I Image Decomposition of the Girl Image with 3111 ( $t = 2\sigma$ )  
Detected Edge Points





(a)  $0.5U_s + 1.5U_d$



(b)  $0.75U_s + 1.25U_d$



(c)  $U_s + 1.5U_d$



(d)  $U_s + 2U_d$



(e)  $U_s + 2.5U_d$



(f)  $U_s + 3U_d$

Figure 5.3II Image Enhancement of the Girl Image with 3111 ( $t = 2\sigma$ )  
Detected Edge Points



(a)  $U_d$



(b)  $U_s$



(c) Original



(d) Edge Pixels

Figure 5.4I Image Decomposition of the Chemical Plant Image with 3653  
( $t = 2\sigma$ ) Detected Edge Points



(a)  $0.5U_s + 1.5U_d$



(b)  $0.75U_s + 1.25U_d$



(c)  $U_s + 1.5U_d$



(d)  $U_s + 2U_d$



(e)  $U_s + 2.5U_d$



$U_s + 3U_d$

Figure 5.4II Image Enhancement of the Chemical Plant Image with 3653  
( $t = 2\sigma$ ) Detected Edge Points



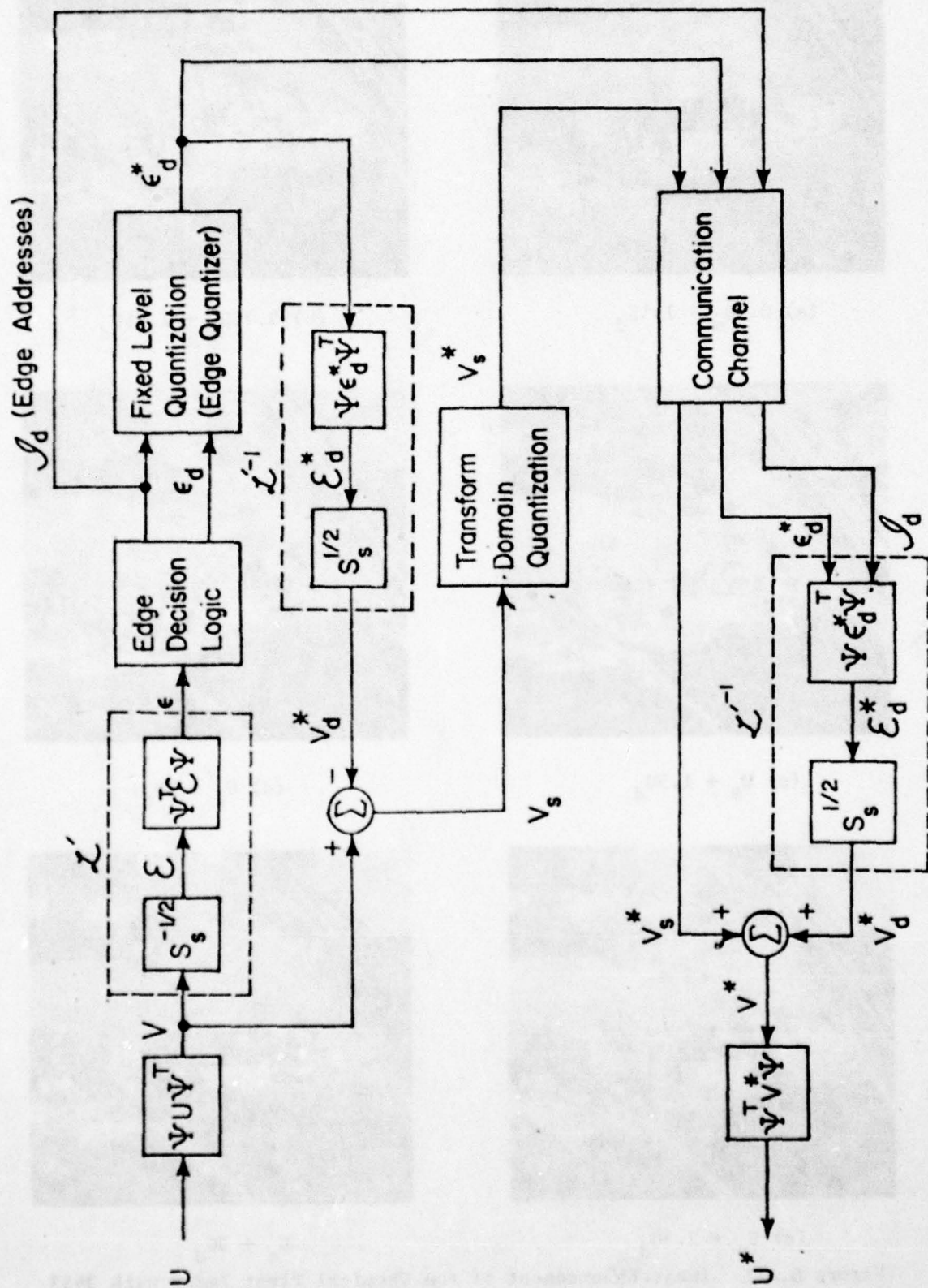


Figure 5.5 Transform Coding Based on Stochastic Segmentation

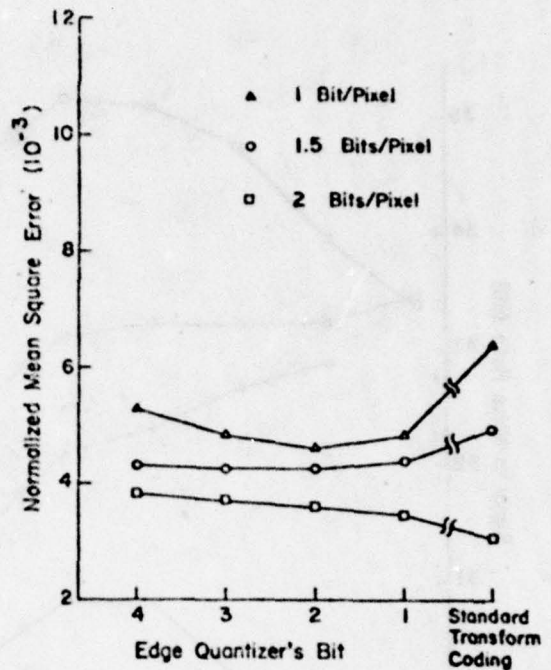
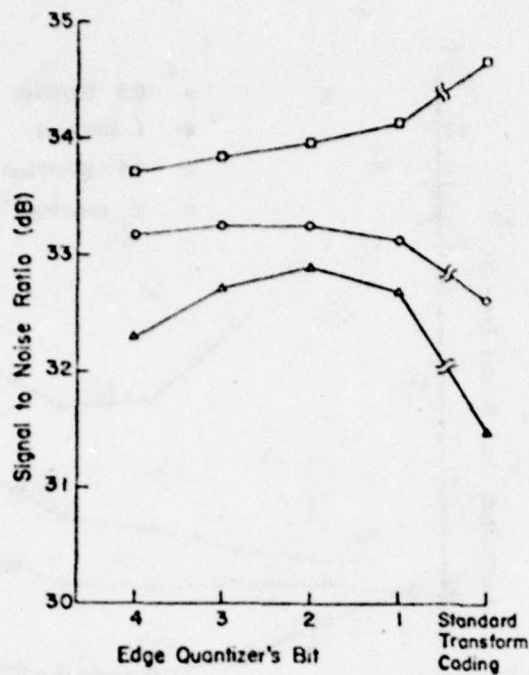


Figure 5.6 Feature Transform Coding Results for the Girl Image versus Various Edge Quantizer's Bits with 5737 ( $t=1.5\sigma$ ) Detected Edge Points

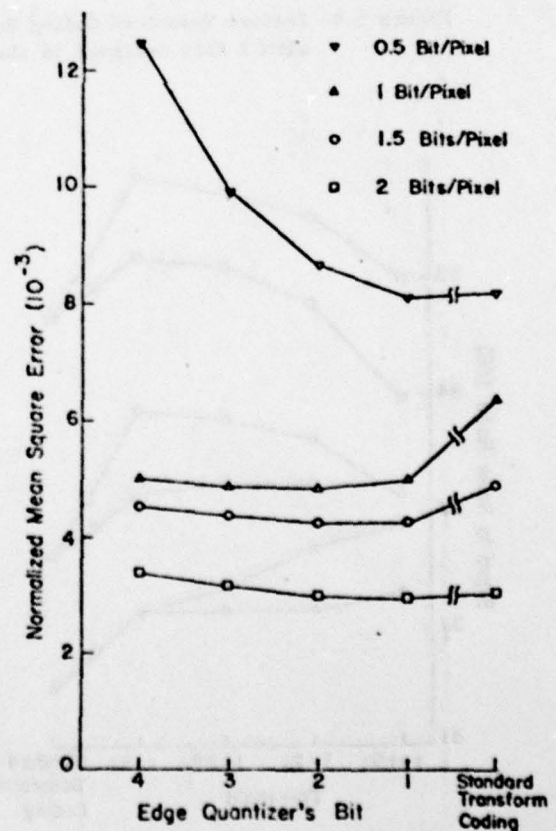
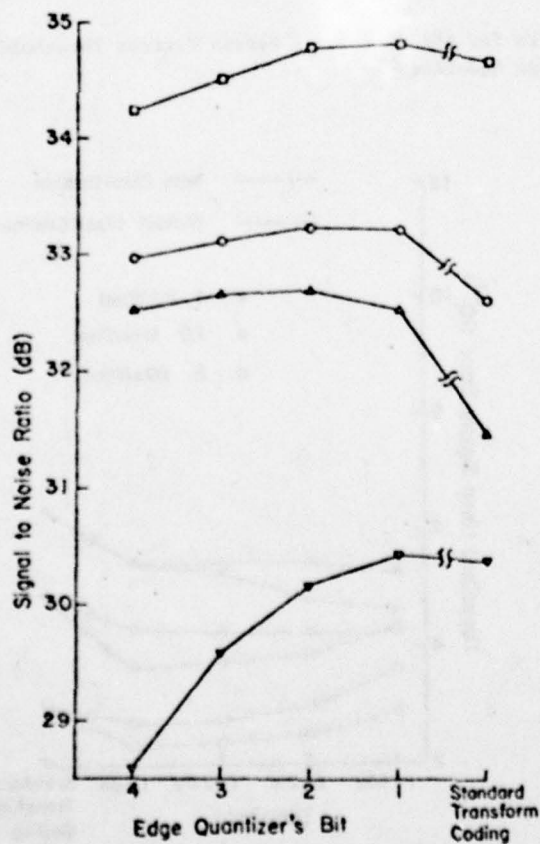


Figure 5.7 Feature Transform Coding Results for the Girl Image versus Various Edge Quantizer's Bits with 3111 ( $t=2\sigma$ ) Detected Edge Points

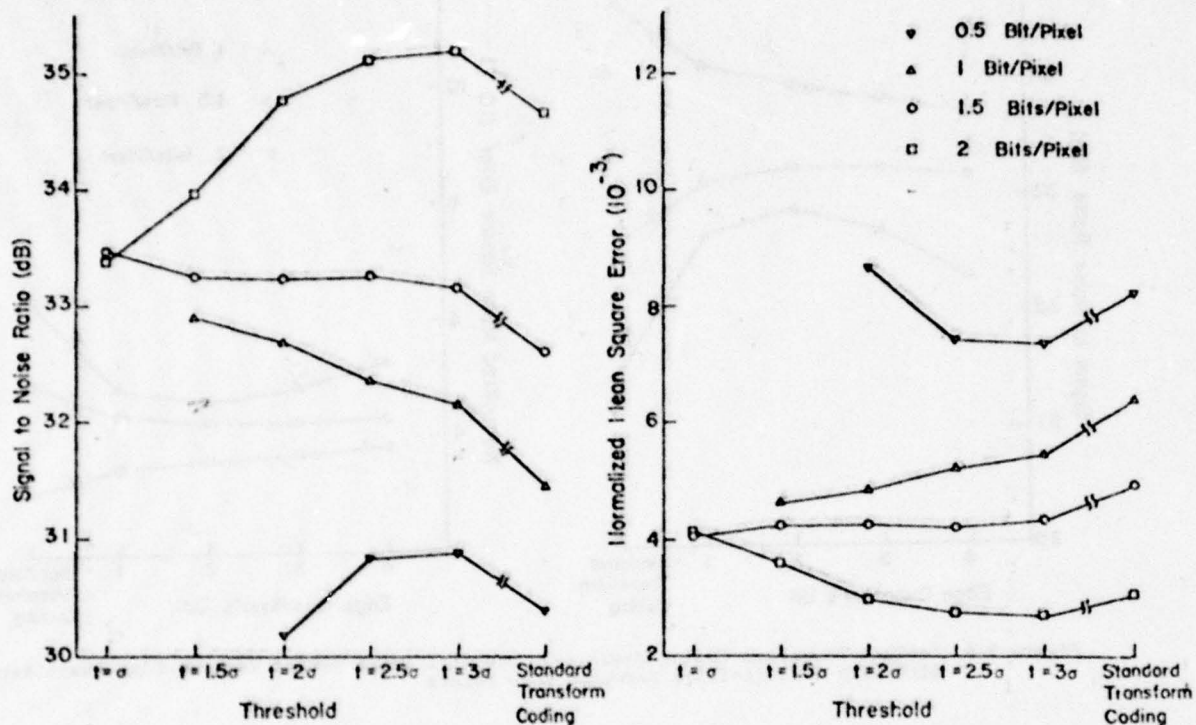


Figure 5.8 Feature Transform Coding Results for the Girl Image versus Various Thresholds with 2 Bits Assigned to the Edge Quantizer

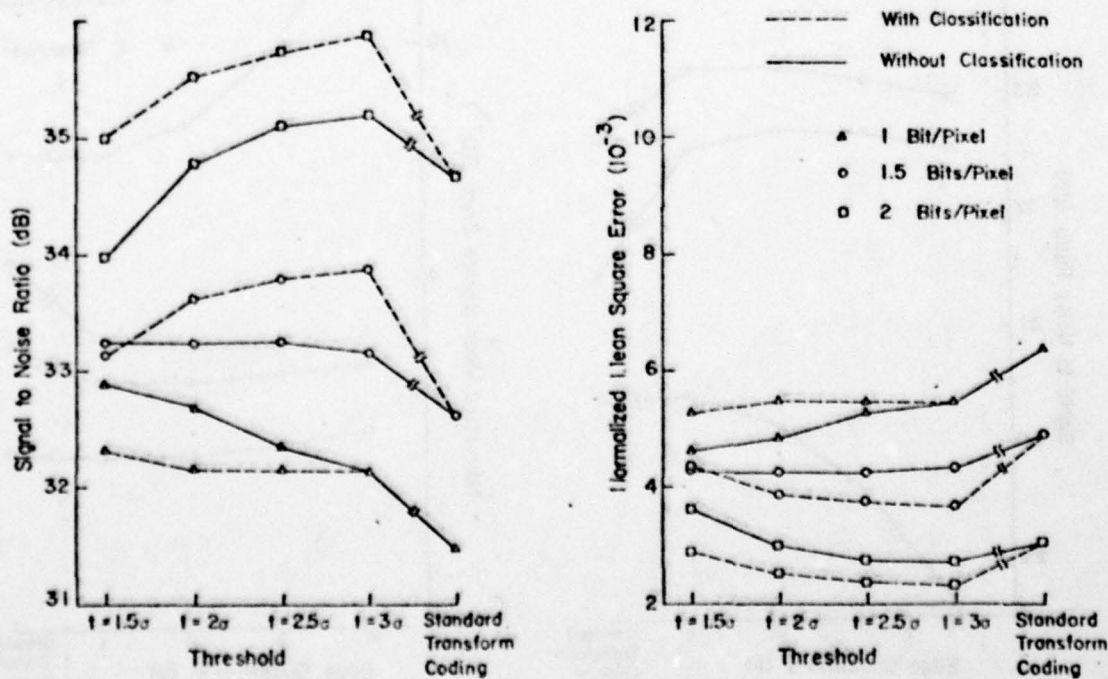


Figure 5.9 Classification Feature Transform Coding Results for the Girl Image versus Various Thresholds with 2 Bits Assigned to the Edge Quantizer



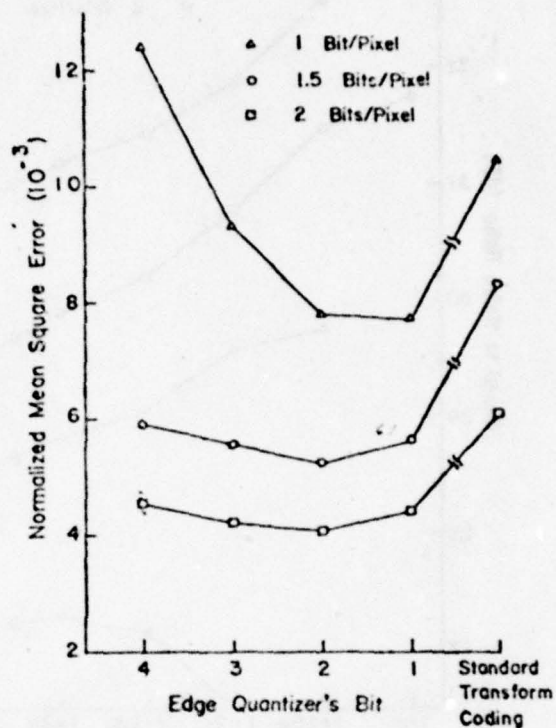
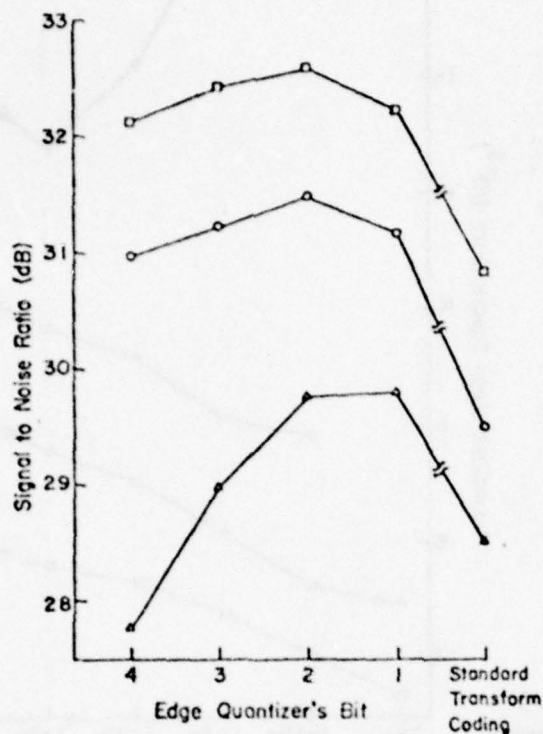


Figure 5.10 Feature Transform Coding Results for the Chemical Plant Image versus Various Edge Quantizer's Bits with 7079 ( $t = 1.5\sigma$ ) Detected Edge Points

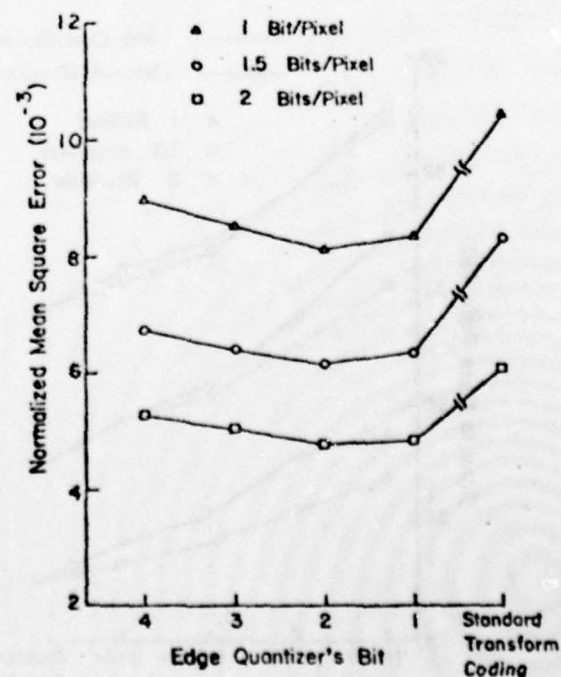
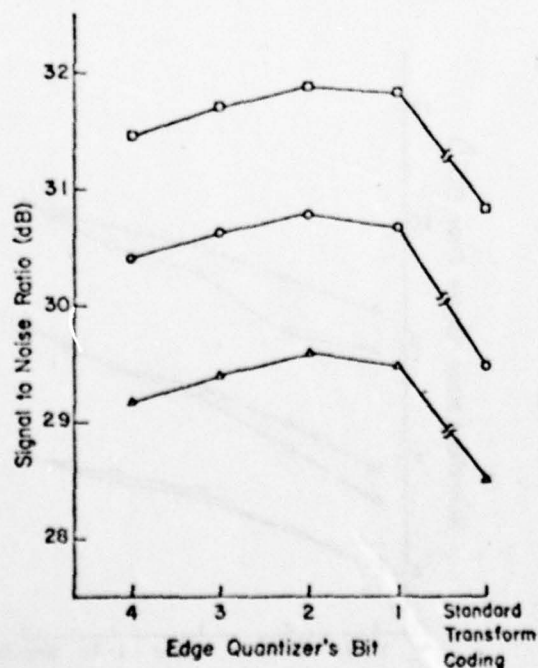


Figure 5.11 Feature Transform Coding Results for the Chemical Plant Image versus Various Edge Quantizer's Bits with 3653 ( $t = 2\sigma$ ) Detected Edge Points

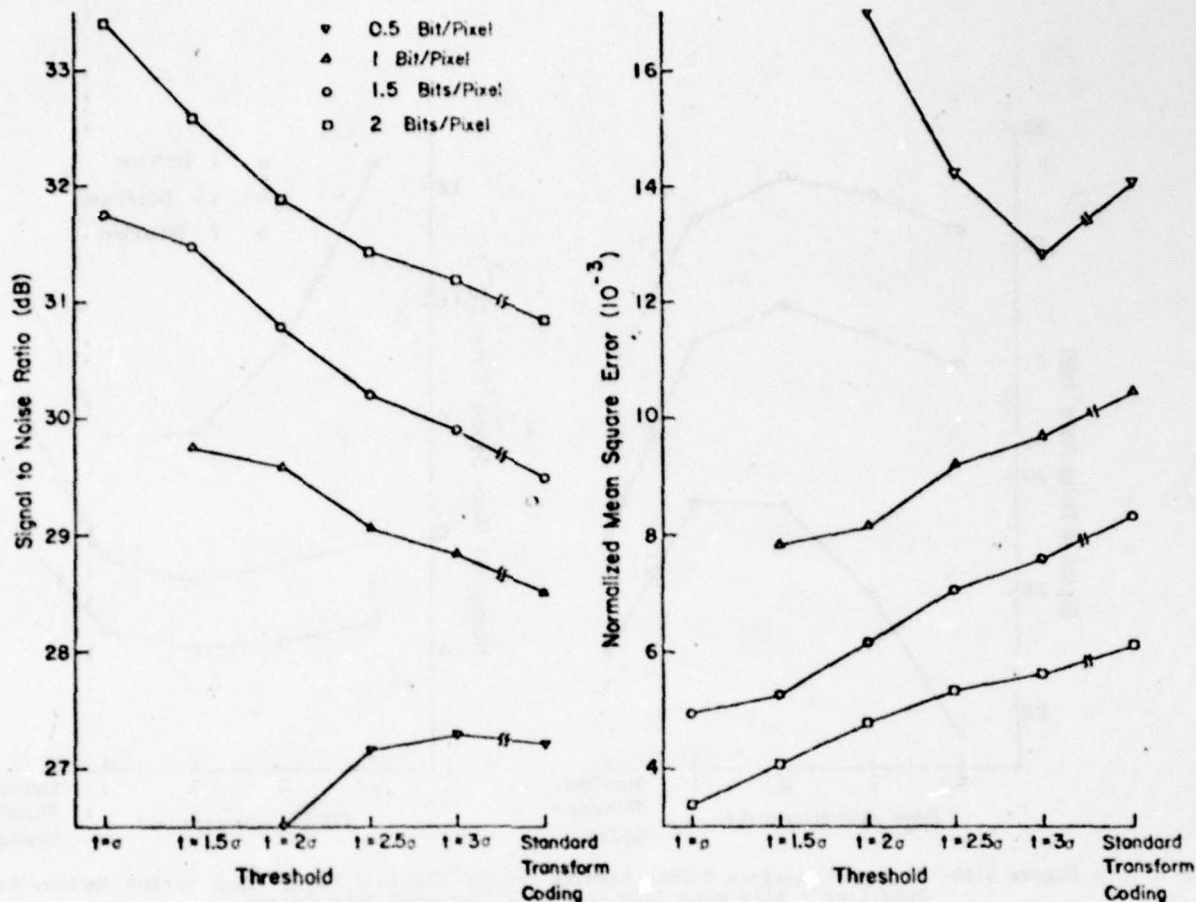


Figure 5.12 Feature Transform Coding Results for the Chemical Plant Image vs. Various Thresholds with 2 Bits Assigned to the Edge Quantizer

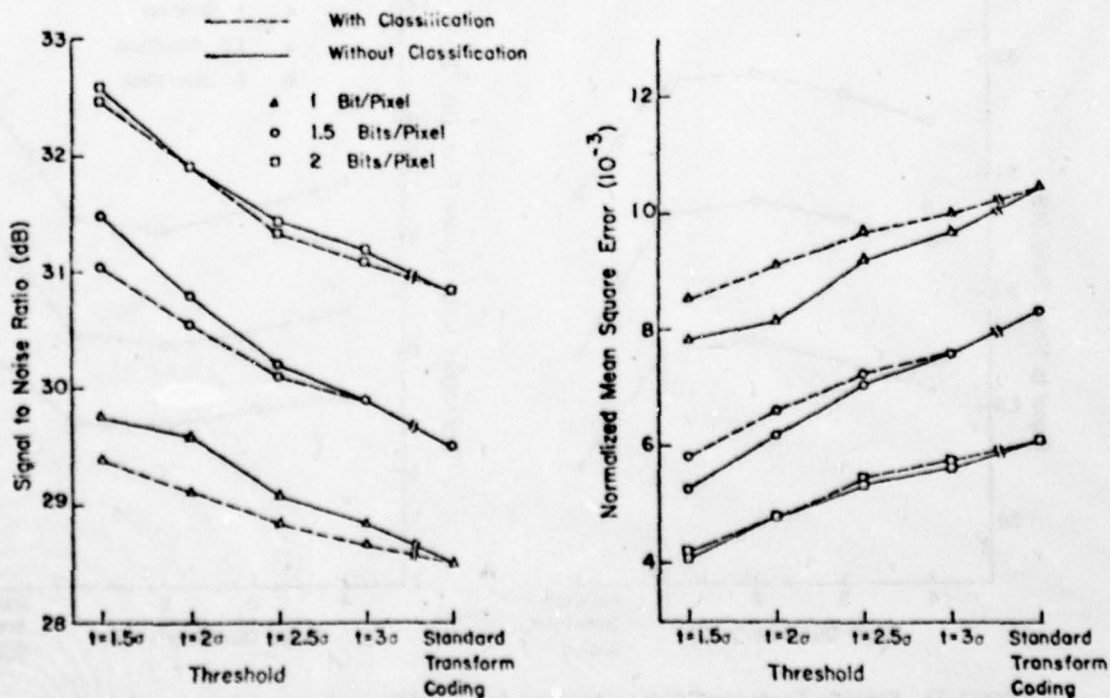


Figure 5.13 Classification Feature Transform Coding Results for the Chemical Plant Image vs. Various Thresholds with 2 Bits Assigned to the Edge Quantizer

AD-A078 781

CALIFORNIA UNIV DAVIS SIGNAL AND IMAGE PROCESSING LAB F/G 9/4  
APPLICATIONS OF STOCHASTIC MODELS FOR IMAGE DATA COMPRESSION.(U)  
SEP 79 S WANG , A K JAIN DAA629-78-G-0206

ARO-16222.3-EL

NL

UNCLASSIFIED

3 OF 3

AD-A078781



END  
DATE  
FILMED  
1-80  
DDC





(a) 1 Bit/Pixel,  
Standard Transform



(d) 1 Bit/Pixel,  
Feature Transform



(b) 1.5 Bits/Pixel,  
Standard Transform



(e) 1.5 Bits/Pixel,  
Feature Transform



(c) 2 Bits/Pixel,  
Standard Transform



(f) 2 Bits/Pixel,  
Feature Transform

Figure 5.14 Comparison of Standard Transform Encoded and Feature Transform Encoded ( $n = 2$  Bits,  $t = 1.5\sigma$ , 5737 Detected Edge Points) Girl Images



(a) 1 Bit/Pixel  
Standard Transform



(d) 1 Bit/Pixel,  
Feature Transform



(b) 1.5 Bits/Pixel,  
Standard Transform



(e) 1.5 Bits/Pixel  
Feature Transform



(c) 2 Bits/Pixel,  
Standard Transform



(f) 2 Bits/Pixel,  
Feature Transform

Figure 5.15 Comparison of Standard Transform Encoded and Feature Transform Encoded ( $n_s = 2$  Bits,  $t = 1.5\sigma$ , 7079 Detected Edge Points) Chemical Plant Images



(a) 1 Bit/Pixel



(d) 1 Bit/Pixel,  
Classification



(b) 1.5 Bits/Pixel



(e) 1.5 Bits/Pixel,  
Classification



(c) 2 Bits/Pixel



(f) 2 Bits/Pixel,  
Classification

Figure 5.16 Feature Transform Encoded Girl Image with  $n_e = 2$  Bits and  $t = 1.5\sigma$  (5737 Detected Edge Points)





(a) 1 Bit/Pixel



(d) 1 Bit/Pixel,  
Classification



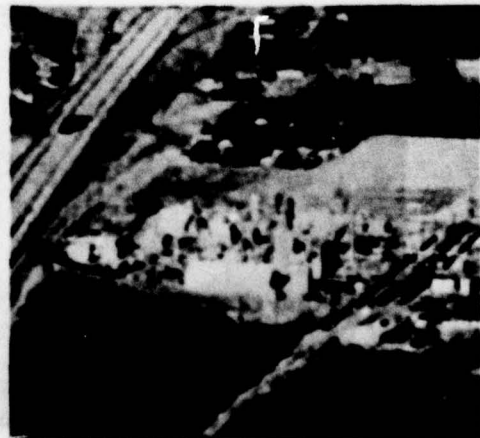
(b) 1.5 Bits/Pixel



(e) 1.5 Bits/Pixel,  
Classification



(c) 2 Bits/Pixel



(f) 2 Bits/Pixel,  
Classification

Figure 5.17 Feature Transform Encoded Chemical Plant Image with  $n_e = 2$  Bits and  $t = 1.5\sigma$  (7079 Detected Edge Points)

Table 5.1(a) Girl Image Thresholds and No. of  
Detected Edge Points

Threshold	No. of Edge Points	Entropy
$t = \sigma$	11624	3.190
$t = 1.5\sigma$	5737	3.626
$t = 2\sigma$	3111	3.949
$t = 2.5\sigma$	1768	3.957
$t = 3\sigma$	1063	3.698

Table 5.1(b) Chemical Plant Image Thresholds and  
No. of Detected Edge Points

Threshold	No. of Edge Points	Entropy
$t = \sigma$	14138	3.102
$t = 1.5\sigma$	7079	3.446
$t = 2\sigma$	3653	3.778
$t = 2.5\sigma$	1843	3.905
$t = 3\sigma$	923	3.585

Table 5.2 Feature Transform Coding Results for the Girl Image with 5737 ( $t = 1.5\sigma$ ) Detected Edge Points

Average Rate	2		1.5		1	
Edge Quantizer's Bit	SNR(dB)	NMSE(%)	SNR(dB)	NMSE(%)	SNR(dB)	NMSE(%)
$n_e = 4$	33.714	0.382	33.187	0.432	32.300	0.530
$n_e = 3$	33.844	0.371	33.252	0.426	32.710	0.482
$n_e = 2$	33.966	0.361	33.252	0.426	32.899	0.462
$n_e = 1$	34.133	0.347	33.126	0.438	32.687	0.485
Standard Xform Coding	34.662	0.308	2.614	0.493	31.480	0.640

Table 5.3 Feature Transform Coding Results for the Girl Image with 3111 ( $t = 2\sigma$ ) Detected Edge Points

Average Rate	2		1.5		1		0.5	
Edge Quantizer's Bit	SNR(dB)	NMSE(%)	SNR(dB)	NMSE(%)	SNR(dB)	NMSE(%)	SNR(dB)	NMSE(%)
$n_e = 4$	34.245	0.339	32.964	0.455	32.509	0.505	28.584	1.247
$n_e = 3$	34.511	0.318	33.121	0.438	32.659	0.488	29.583	0.990
$n_e = 2$	34.784	0.299	33.238	0.427	32.699	0.483	30.162	0.867
$n_e = 1$	34.814	0.297	33.213	0.429	32.543	0.501	30.441	0.813
Standard Xform Coding	34.662	0.308	32.614	0.493	31.480	0.640	30.396	0.821

Table 5.4 Feature Transform Coding Results for the Girl Image with 2 Bits Assigned to the Edge Quantizer

Average Rate	2		1.5		1		0.5	
Threshold	SNR(dB)	NMSE(%)	SNR(dB)	NMSE(%)	SNR(dB)	NMSE(%)	SNR(dB)	NMSE(%)
$t = 0$	33.378	0.413	33.470	0.405	-	-	-	-
$t = 1.5\sigma$	33.966	0.361	33.252	0.426	32.899	0.462	-	-
$t = 2\sigma$	34.784	0.299	33.238	0.427	32.699	0.483	30.162	0.867
$t = 2.5\sigma$	35.127	0.276	33.261	0.425	32.358	0.523	30.839	0.742
$t = 3\sigma$	35.209	0.271	33.162	0.434	32.159	0.547	30.870	0.736
Standard Xform Coding	34.662	0.308	32.614	0.493	31.480	0.640	30.396	0.821

Table 5.5 Classification Feature Transform Coding Results for the Girl Image with 2 Bits Assigned to the Edge Quantizer

Average Rate	2		1.5		1	
Threshold	SNR(dB)	NMSE(%)	SNR(dB)	NMSE(%)	SNR(dB)	NMSE(%)
$t = 1.5\sigma$	35.019	0.283	33.142	0.436	32.323	0.527
$t = 2\sigma$	35.537	0.251	33.632	0.390	32.163	0.547
$t = 2.5\sigma$	35.750	0.239	33.802	0.375	32.149	0.549
$t = 3\sigma$	35.873	0.233	33.875	0.369	32.148	0.549
Standard Xform Coding	34.662	0.308	32.614	0.493	31.480	0.640



Table 5.6 Feature Transform Coding Results for the Chemical Plant Image with 7079 ( $t = 1.5\sigma$ ) Detected Edge Points

Average Rate	2		1.5		1	
Edge Quantizer's Bit	SNR(dB)	NMSE(%)	SNR(dB)	NMSE(%)	SNR(dB)	NMSE(%)
$n_e = 4$	32.123	0.454	30.971	0.592	27.761	1.240
$n_e = 3$	32.424	0.424	31.236	0.557	28.986	0.936
$n_e = 2$	32.586	0.408	31.482	0.527	29.758	0.783
$n_e = 1$	32.228	0.443	31.170	0.566	29.800	0.776
Standard Xform Coding	30.830	0.611	29.495	0.832	28.508	1.044

Table 5.7 Feature Transform Coding Results for the Chemical Plant Image with 3653 ( $t = 2\sigma$ ) Detected Edge Points

Average Rate	2		1.5		1		0.5	
Edge Quantizer's Bit	SNR(dB)	NMSE(%)	SNR(dB)	NMSE(%)	SNR(dB)	NMSE(%)	SNR(dB)	NMSE(%)
$n_e = 4$	31.457	0.530	30.405	0.675	29.169	0.897	24.372	2.706
$n_e = 3$	31.697	0.504	30.624	0.642	29.395	0.851	25.562	2.055
$n_e = 2$	31.885	0.480	30.791	0.617	29.592	0.814	26.394	1.699
$n_e = 1$	31.836	0.485	30.666	0.635	29.479	0.835	26.795	1.549
Standard Xform Coding	30.830	0.611	29.495	0.832	28.508	1.044	27.214	1.407

Table 5.8 Feature Transform Coding Results for the Chemical Image with 2 Bits Assigned to the Edge Quantizer

Average Rate	2		1.5		1		0.5	
Threshold	SNR(dB)	NMSE(%)	SNR(dB)	NMSE(%)	SNR(dB)	NMSE(%)	SNR(dB)	NMSE(%)
$t = 0$	33.402	0.338	31.751	0.495	-	-	-	-
$t = 1.5\sigma$	32.586	0.408	31.482	0.527	29.758	0.783	-	-
$t = 2\sigma$	31.885	0.480	30.791	0.617	29.592	0.814	26.394	1.699
$t = 2.5\sigma$	31.428	0.533	30.208	0.706	29.062	0.919	27.169	1.421
$t = 3\sigma$	31.189	0.563	29.894	0.759	28.837	0.968	27.291	1.382
Standard Xform Coding	30.830	0.611	29.495	0.832	28.508	1.044	27.214	1.407

Table 5.9 Classification Feature Transform Coding Results for the Chemical Plant Image with 2 Bits Assigned to the Edge Quantizer

Average Rate	2		1.5		1	
Threshold	SNR(dB)	NMSE(%)	SNR(dB)	NMSE(%)	SNR(dB)	NMSE(%)
$t = 1.5\sigma$	32.461	0.420	31.044	0.582	29.392	0.852
$t = 2\sigma$	31.902	0.478	30.546	0.661	29.106	0.910
$t = 2.5\sigma$	31.334	0.545	30.095	0.725	28.832	0.969
$t = 3\sigma$	31.061	0.577	29.893	0.759	28.669	1.066
Standard Xform Coding	30.830	0.611	29.495	0.832	28.508	1.044

## CHAPTER SIX

### SUMMARY AND RECOMMENDATIONS FOR FUTURE RESEARCH

This thesis has shown that the application of the stochastic image models based on PDEs to the problem of image data compression has achieved considerable success. The use of image models has shown the connection between predictive, hybrid and transform coding schemes. From the choice of an approximate image model which gives the best approximation to the actual statistics of a class of images being processed, one would be able to determine the most efficient data compression scheme.

Simple basis restriction error experiments were performed to compare the energy compaction property of various image models. The results show that both the noncausal and semicausal models give superior performance over the causal models. Evidently, different spectral density function shapes of image models were the dominating factor in this aspect of study.

The performance of the hybrid coding scheme was significantly improved by two very simple methods, i.e., (1) Adaptive Variance Estimation: Adapting the variance of the prediction error, in each DPCM channel, the updated variance was used to adjust the spacing of the quantizer levels. (2) Adaptive Classification: Adapting the bit rate to the local variance of each image column.

The adaptive variance estimation scheme was shown having the potential of maintaining the performance of a hybrid coder, designed for a nominal statistics, in the face of changing statistics. The adaptive classification scheme performed more effectively at low bit

rate and was robust with respect to channel errors. Hybrid coding of noisy images was achieved by replacing the predictor in the DPCM loop by a Kalman filter. Experimental results showed that the two bit rate quantizer gave a restored image with SNR slightly less than the infinite rate (without quantizer in the DPCM loop).

A new technique called feature transform coding for efficient transform coding of images was presented. The experimental results of applying this technique to actual image data (Girl and Chemical Plant images) show that it provides us a flexible way of getting a good visual image (subject to a fixed bit rate) while maintaining the mean square error performance. It is evidenced by referring to Figures 5.6 - 5.13. The incorporation of classification, a scheme analogous to the adaptive classification hybrid coding, results in further improvement in the performance for simple structured images at bit rate  $\geq 1$  bit/pixel. Moreover, its complexity over the feature transform coder is marginal.

From a practical point of view, the most important results of this research is that it provides a theoretical framework for optimizing the design of an intraframe coding system for two dimensional data modeled by random fields. The various coding algorithms developed here can be easily implemented for designing practical coding systems for images.

Areas in need of further investigation are:



- 1) Inclusion of NC2 and NC3 models to the design of feature transform coder. Since only NC1 model based feature transform coder has been fully explored.
- 2) Extension to the higher order stochastic image models which might be needed to represent image spectral density functions (SDFs) more accurately.
- 3) Application of data compression schemes to biomedical images.
- 4) Study the effects of incorporating variance estimation scheme in the feature transform coder.
- 5) Use of stochastic models in the design of coders in the presence of channel errors.

## APPENDIX A

### QUANTIZER CONSIDERATIONS

#### A.1 Introduction

The basic principle in designing a quantizer is to determine the optimum quantization levels so as to minimize the overall mean square error between the original signal and quantized signal. The exact approach to quantization problem can only be solved by wasting a considerable amount of computing time and gives little insight for someone who has a new quantization problem and needs it to be solved in a small period of time. The useful approximation to the optimum quantizer was first proposed by Algazi [ 2 ]. In this Appendix, we have modified his formulas slightly and tabulated the characteristics of the resulting quantizer (so called compandor) for Gaussian and Laplacian distributed signals together with the optimum nonuniform (in the minimum mean square error sense) and optimum uniform quantizers which have been considered by Max [ 44 ] and others. Also rate-distortion functions  $f(n)$  are listed which were obtained by a piecewise exponential curve fitting technique to the tabulated quantizer numerical results.

#### A.2 Quantizer Structures

A typical quantizer characteristic is shown in Fig. A.1. The quantizer output  $y$  is assigned to one of  $N$  discrete values (Fig. A.1(a) and Fig. A.1(b) are for  $N$  even and odd respectively) depending on the value of input  $x$ . The  $x_i$  and  $y_i$  are called the "decision levels" and "quantization levels" respectively. If the probability density function,  $p(x)$ , of the quantizer input is given and is assumed to be symmetric, one would

have different quantizers according to the diverse assumptions of design constraints. In this section, we briefly review some of the useful quantizer results. The interested reader can find detailed information in references [2,40,44,51,72]

#### A.2.1 Optimum Nonuniform Quantizer

In this quantizer, the design procedure is to find the  $N$   $y_i$ 's and associated  $x_i$ 's in Fig. A.1 so as to minimize the distortion,  $D$ , which is defined as the expected value of  $W(\epsilon)$ , where  $W$  is an error weighting function and  $\epsilon$  is the quantization error. For simplicity,  $W(\epsilon)$  is assumed to be  $\epsilon^2$ , the square value of the quantization error. The distortion is obtained as

Case 1:  $N = \text{even}$

$$D = 2 \sum_{i=1}^{N/2} \int_{x_{i-1}}^{x_i} (y_i - x)^2 p(x) dx \quad (\text{A.2.1-1})$$

where  $x_0 = 0$ ,  $x_{\frac{N}{2}} = \infty$ , and  $y_i$  lies between  $x_{i-1}$  and  $x_i$ .

Case 2:  $N = \text{odd}$

$$D = \int_{-x_1}^{x_1} (y_1 - x)^2 p(x) dx + 2 \sum_{i=1}^{\frac{N-1}{2}} \int_{x_i}^{x_{i+1}} (y_{i+1} - x) p(x) dx \quad (\text{A.2.1-2})$$

where  $y_1 = 0$ ,  $x_1 > 0$ ,  $x_{\frac{N+1}{2}} = \infty$ , and  $y_i$  lies between  $x_{i-1}$  and  $x_i$ .

In order to minimize  $D$  for a fixed  $N$ , the necessary conditions are obtained by differentiating  $D$  with respect to the  $x_i$ 's and  $y_i$ 's and setting



the results equal to zero. After simple numerical manipulation, we have

Case 1:  $N = \text{even}$

$$x_i = \frac{1}{2}(y_i + y_{i+1}) \quad i = 1, \dots, \frac{N}{2} - 1 \quad (\text{A.2.1-3a})$$

$$\int_{x_{i-1}}^{x_i} (y_i - x)p(x)dx = 0 \quad i = 1, \dots, \frac{N}{2} \quad (\text{A.2.1-3b})$$

Case 2:  $N = \text{odd}$

$$x_i = \frac{1}{2}(y_i + y_{i+1}) \quad i = 1, \dots, \frac{N-1}{2} \quad (\text{A.2.1-4a})$$

$$\int_{x_{i-1}}^{x_i} (y_i - x)p(x)dx = 0 \quad i = 2, \dots, \frac{N+1}{2} \quad (\text{A.2.1-4b})$$

The above equations mean that  $x_i$  lies midway between the adjacent quantization levels and  $y_i$  is the centroid of the area under  $p(x)$  and lies between the adjacent decision levels.

#### A.2.2 Optimum Uniform Quantizer

This quantizer gives the minimum distortion under the constraint

$$x_i - x_{i-1} = y_i - y_{i-1} = q \quad \forall i \quad (\text{A.2.2-1})$$

where  $q$  is the equal length spacing between adjacent decision levels or quantization levels.

This is an easier problem to be solved than the previous optimum non-uniform quantizer. For this case, the distortion,  $D$ , becomes a function of  $q$  and of any particular value of  $N$ . If the probability density function

of the quantizer input is assumed to be known and symmetric, then a symmetric answer for the decision levels and quantization levels will be obtained. The distortion,  $D$ , can be obtained as

Case 1:  $N = \text{even}$

$$D = 2 \sum_{i=1}^{\frac{N}{2}-1} \int_{(i-1)q}^{iq} \left[ \left( \frac{2i-1}{2} \right) q - x \right]^2 p(x) dx + 2 \int_{\left( \frac{N}{2}-1 \right) q}^{\infty} \left[ \left( \frac{N-1}{2} \right) q - x \right]^2 p(x) dx \quad (\text{A.2.2-2})$$

Case 2:  $N = \text{odd}$

$$D = \int_{-\frac{q}{2}}^{\frac{q}{2}} x^2 p(x) dx + 2 \sum_{i=1}^{\frac{N-3}{2}} \int_{(i-\frac{1}{2})q}^{(i+\frac{1}{2})q} (iq-x)^2 p(x) dx + 2 \int_{\left( \frac{N-2}{2} \right) q}^{\infty} \left[ \left( \frac{N-1}{2} \right) q - x \right]^2 p(x) dx \quad (\text{A.2.2-3})$$

The optimum uniform quantizer step size  $q$  can be obtained by differentiating  $D$  with respect to  $q$  and setting the results equal to zero. We have

Case 1:  $N = \text{even}$

$$\frac{dD}{dq} = 2 \sum_{i=1}^{\frac{N}{2}-1} (2i-1) \int_{(i-1)q}^{iq} \left[ \left( \frac{2i-1}{2} \right) q - x \right] p(x) dx + 2(N-1) \int_{\left( \frac{N}{2}-1 \right) q}^{\infty} \left[ \left( \frac{N-1}{2} \right) q - x \right] p(x) dx = 0 \quad (\text{A.2.2-4})$$

Case 2:  $N = \text{odd}$

$$\frac{dD}{dq} = 2 \sum_{i=1}^{\frac{N-3}{2}} i \int_{(i-\frac{1}{2})q}^{(i+\frac{1}{2})q} (iq-x) p(x) dx + (N-1) \int_{\left( \frac{N-2}{2} \right) q}^{\infty} \left[ \left( \frac{N-1}{2} \right) q - x \right] p(x) dx = 0 \quad (\text{A.2.2-5})$$

In either case, the problem is quite acceptable to machine computation when  $p(x)$  and  $N$  are specified.

### A.2.3 Useful Approximation to the Optimum Nonuniform Quantizer [ 2 ]

Since a quantizer is often easier to implement, we consider the nonuniform quantizer as the cascade of two nonlinear devices and of a uniform quantizer as shown in Fig. A.2. With a given uniform quantizer and a given probability density function,  $p(x)$ , the two nonlinear devices  $f(\cdot)$  and  $g(\cdot)$  in Fig. A.2 are chosen so as to minimize the distortion,  $D = E[W\{g(y)-x\}]$ , where  $W$  as defined in section A.2.1 is an error weighting function. The distortion is made up of two parts:

1. The distortion  $D_n$  obtained within the range of the uniform quantizer.
2. The distortion in the tails  $D_T$  for which the nonlinear devices  $f(\cdot)$  and  $g(\cdot)$  are completely ineffective.

The analog system is shown in Fig. A.3. The quantization noise due to uniform quantizer is assumed to be independent of the input signal for a large number of quantization levels, the effect of which has been discussed in detail by many researchers. Referring to Fig. A.3, the two extreme points of the output of the first nonlinear device is a dominating factor in the determination of the overall distortion, in other words,  $D$  is a function of  $f(x_{\max})$  and  $f(x_{\min})$ , and  $f(x_{\max}) - f(x_{\min}) = Nq$ ,  $q$  being the step size of the uniform quantizer. The output of the second nonlinear device,  $g(y)$ , is expressed in terms of  $n$  and  $f(x)$  as

$$g(y) = g[f(x) + n] \approx g[f(x)] + ng'[f(x)] \quad (\text{A.2.3-1})$$



If the quantization error is small, a Taylor series expression of  $g(y)$  gives the above equation directly. And the expression for  $D_n$  can be written as

$$D_n = \int_{-\frac{q}{2}}^{\frac{q}{2}} \int_{x_{\min}}^{x_{\max}} W\{q[f(\alpha) + \beta] - \alpha\} p_x(\alpha) p_n(\beta) d\alpha d\beta \quad (\text{A.2.3-2})$$

The limits on the integrals are  $-\frac{q}{2}$  to  $\frac{q}{2}$  for the integral in  $\beta$  and  $x_{\min}$  to  $x_{\max}$  ( $f(x_{\max}) - f(x_{\min}) = Nq$ ) for the integral in  $\alpha$ .

If we assume  $W(\epsilon) = \epsilon^2$  and  $g(y)$  is sufficiently smooth and the quantization error is small, then following the development in [2], one would be able to obtain

$$D_n = \frac{1}{12N^2} \left[ \int_{x_{\min}}^{x_{\max}} [p_x(\alpha)]^{\frac{1}{3}} d\alpha \right]^3 \quad (\text{A.2.3-3})$$

If we take into account the probability of occurrence of  $D_n$  and  $D_T$ , we have

$$\begin{aligned} D = D_n & \left[ 1 - \int_{-\infty}^{x_{\min}} p_x(\alpha) d\alpha - \int_{x_{\max}}^{\infty} p_x(\alpha) d\alpha \right] + \int_{-\infty}^{x_{\min}} \left[ (x_{\min} + \frac{q}{2}) - x \right]^2 p_x(\alpha) d\alpha \\ & + \int_{x_{\max}}^{\infty} \left[ (x_{\max} - \frac{q}{2}) - x \right]^2 p_x(\alpha) d\alpha \end{aligned} \quad (\text{A.2.3-4})$$

For a symmetric probability density function, we set  $x_{\max} = -x_{\min} = X$ , and

$$D = \frac{2}{3N^2} \left[ \int_0^X [p_x(\alpha)]^{\frac{1}{3}} d\alpha \right]^3 \left[ 1 - 2 \int_X^{\infty} p_x(\alpha) d\alpha \right] + 2 \int_X^{\infty} \left[ (X - \frac{q}{2}) - x \right]^2 p_x(\alpha) d\alpha \quad (\text{A.2.3-5})$$

Equation (A.2.3-5) has to be minimized by proper choice of  $X$ . Once  $X$  is determined, then it can be shown that

$$f(x) = \frac{Nq \int_0^x [p_x(\alpha)]^{\frac{1}{3}} d\alpha}{2 \int_0^X [p_x(\alpha)]^{\frac{1}{3}} d\alpha} . \quad (\text{A.2.3-6})$$

It is noted from the above equation that the step size of the uniform quantizer will not affect the resulting nonuniform quantizer.

The characteristic of this quantizer for  $2^m$  ( $m = 1, \dots, 9$ ) quantization levels is given and discussed in the next section. We mention here that the derivation given in [ 2 ] erred in assuming the two extremes of the uniform quantizer shown in Fig. A.3 to be  $\pm \left(\frac{N-1}{2}\right)q$  instead of  $\pm \left(\frac{N}{2}\right)q$ .

### A.3 Results and Comparisons

The structures for the optimum uniform, optimum nonuniform and approximate nonuniform (compandor) quantizers are described in the previous sections. In this section, we present some nice characteristics of the approximate nonuniform quantizer along with the optimum uniform and optimum nonuniform quantizers. The equations defining the optimum nonuniform quantizer yield closed-form solution only in certain special cases, depending solely on the probability density function of the quantizer input signal. For example, even for the Gaussian distributed signal, for lack of the closed-form solution for the  $x_i$  (decision levels) and  $y_i$  (reconstruction levels), some sort of numerical solution must be sought. Max [ 44 ] suggested an iterative procedure to calculate  $x_i$  and  $y_i$  and

tabulated the values of  $x_1$  and  $y_1$  for  $N$  (number of levels) up to 36, since the time required to determine the quantizer structure increases exponentially with the total number of levels of the quantizer, Max's [44] work cannot be extended beyond  $N = 36$ . Kurtenbach and Wintz [40] applied the same numerical approach and tabulated the value of  $x_1$  and  $y_1$  to  $N = 512$  ( $N = 2^n$ ,  $n = 9$ ,  $n$ : number of quantizer bits) for the Gaussian distributed signal. They confessed also that the determination of the quantizer structure for  $m = 6, 7, 8, 9$  is limited because of the computer time required for each case. Paez and Glisson [51] published the quantizer results for the Laplacian and Gamma distributed signals facing the same kind of difficulty, and tabulated the data only up to  $N = 32$ . So the exact approach to the optimum nonuniform quantizer gives little insight and sometimes presents someone who has a new quantization problem with a considerable amount of computation time to obtain a significant result. The second advantage of designing the approximate nonuniform quantizer is that it is easily implementable with only a marginal increase in its complexity compared to the optimum uniform quantizer.

Tables A.1 and A.2 list the approximate average amount of CDC CYBER 173 computer time required to determine the quantizer structure for the optimum nonuniform, optimum uniform and approximate nonuniform quantizers. A comparison of these three quantizers can be easily made from the entries of Tables A.1 and A.2 to conclude that the approximate nonuniform quantizer is the best choice as far as computation time is concerned.

Note that we have used our own numerical approach to solve the values of  $x_1$  and  $y_1$  for a given quantizer. The procedure is described as follows:



If the probability density function is known, we make an initial guess for  $x_i$  ( $i = 1, \dots, \frac{N}{2} - 1$ ), where the  $x_i$  are uniformly spaced.  $\frac{x_N}{2}$  is assumed to be equal to five times the standard deviation of the input signal. Then  $y_i$  is calculated ( $i = 1, \dots, \frac{N}{2}$ ) by solving (A.2.1-3b).  $x_i$  ( $i = 1, \dots, \frac{N}{2} - 1$ ) is updated, denoted as  $\hat{x}_i$ , by using Newton's numerical method on (A.2.1-3a) compute resulting error  $e = x_i - \hat{x}_i$ . If it satisfies the required error bound, then  $x_i$  was chosen correctly, otherwise the process is repeated. Fig. A.4 shows the flow chart of this numerical procedure.

The correctness of the computer program was checked by printing out the numerical value of each data entry to five digits after the decimal point. Comparing the results with Max's [ 44 ], we have precise value for each  $x_i$  and  $y_i$ , and furthermore our accuracy is extended to five digits instead of four digits after the decimal point.

As a by-product of determining the quantizer structures, most of the useful information quantities were obtained. There are (a) the mean square error (M.S.E.) introduced in the quantization process, (b) the entropy at the quantizer output, (c) the signal to noise ratio, (d) the rate distortion function or source information rate. In addition, all the data entries tabulated are constructed for quantizer input signal with unit standard deviation (r.m.s. value). To obtain the 'decision levels'  $x_i$  or "quantization levels'  $y_i$  for signals with standard deviation different from unity, we simply need multiply the given values of data entries by the actual standard deviation. The M.S.E. is found by multiplying the given M.S.E. by the variance of the signal.

In all the measurements, after obtaining the values of  $x_i$  and  $y_i$ , the mean square errors (M.S.E.) are calculated by (A.2.1-1), (A.2.2-2) and (A.2.3-5) for optimum nonuniform, optimum uniform and approximate nonuniform quantizer respectively. Here we assume that the distribution of the quantizer input signal and quantizer structure is symmetric and that the total number of quantizer output levels is even. This constraint is not restrictive. For example, we have plotted Tables A.10-A.15 for  $N = 2, \dots, 36$ , which has both cases  $N = \text{even}$  and  $N = \text{odd}$ .

For entropy it is possible to treat the quantizer output as a discrete data source and can be calculated from the following formula.

$$\text{Entropy} = -2 \sum_{i=1}^{\frac{N}{2}} p_i \log_2 p_i \text{ bits per sample} \quad (\text{A.3-1})$$

$$\text{where } p_i = p[y=y_i] = p[x_{i-1} \leq x \leq x_i] = \int_{x_{i-1}}^{x_i} p(x) dx \quad i = 1, \dots, \frac{N}{2}.$$

Gaussian and Laplacian signal distributions were considered. These are the two commonly used assumptions for the signal distribution in the image processing area.

$$\begin{aligned} \text{Guassian density: } p(x) &= \frac{1}{\sqrt{2\pi}\sigma} e^{-\frac{x^2}{2\sigma^2}} \\ \text{rms value} &= \sigma \end{aligned} \quad (\text{A.3-2})$$

$$\begin{aligned} \text{Laplacian density: } p(x) &= \frac{\alpha}{2} e^{-\alpha|x|} \\ \text{rms value} &= \sigma = \frac{\sqrt{2}}{\alpha} \end{aligned} \quad (\text{A.3-3})$$

The exact formula for  $p_i$  in either case can be expressed as follows:

Laplacian distributed:

$$p_i = \int_{x_{i-1}}^{x_i} p(x) dx = \int_{x_{i-1}}^{x_i} \frac{\alpha}{2} e^{-\alpha|x|} dx = -\frac{1}{2} \left[ e^{-\alpha x_i} - e^{-\alpha x_{i-1}} \right] \quad i = 1, \dots, \frac{N}{2}$$

(A.3-4)

Gaussian distributed:

$$p_i = \int_{x_{i-1}}^{x_i} p(x) dx = \int_{x_{i-1}}^{x_i} \frac{1}{\sqrt{2\pi}\sigma} e^{-\frac{x^2}{2\sigma^2}} dx = \frac{1}{2} \left[ \text{erf}(x_i/\sqrt{2}\sigma) - \text{erf}(x_{i-1}/\sqrt{2}\sigma) \right]^\dagger$$

$i = 1, \dots, \frac{N}{2}$   
(A.3-5)

The signal to noise ratio (S.N.R.) is defined as

$$\text{S.N.R. (dB)} = 10 \log_{10} \frac{1}{\text{mean square error (M.S.E.)}} \quad (\text{A.3-6})$$

where we assume unity variance for the quantizer input signal.

Tables A.3 - A.8 tabulate the characteristics of three different quantizers with Gaussian and Laplacian distributed quantizer input signal.

In order to better compare the performances of these three quantizers, we have plotted the curves of all three quantizers into one single graph according to different categories, i.e., mean square error, signal to noise ratio, and entropy. These are shown in Figs. A.5 - A.10. It is seen

<sup>†</sup> We use the National Bureau of Standards definition for the error function, i.e.,

$$\text{erf}(x) = \frac{2}{\sqrt{\pi}} \int_0^x e^{-t^2} dt$$



from these figures that approximate nonuniform quantizers (compandor) perform virtually as good as optimum nonuniform quantizers, since the characteristic curves of these two quantizers are so close together. Fig. A.11 shows the unequal probabilities of quantizer output levels for the case of  $N = 8$ . Again, the similarity of the compandor and the nonuniform quantizer can be easily observed. Another significant result that can be observed from Figs. A.5 - A.10 is that the advantage of the optimum nonuniform quantizer and approximate nonuniform quantizer (compandor) over the optimum uniform quantizer starts with  $n = 2$  and increases as  $n$  increases. This effect is due to the fact that both former quantizer structures have more quantization levels near the origin than the optimum uniform quantizer. Here we make the assumption that our quantizer structure is symmetric with respect to the origin. But the optimum uniform quantizer still has its own advantages. It is easily calculable for the  $x_i$  (decision levels) and  $y_i$  (quantization levels). Also Wood [72] showed that it gives the minimum distortion among the three quantizer structures if a fixed entropy of the quantizer output is required.

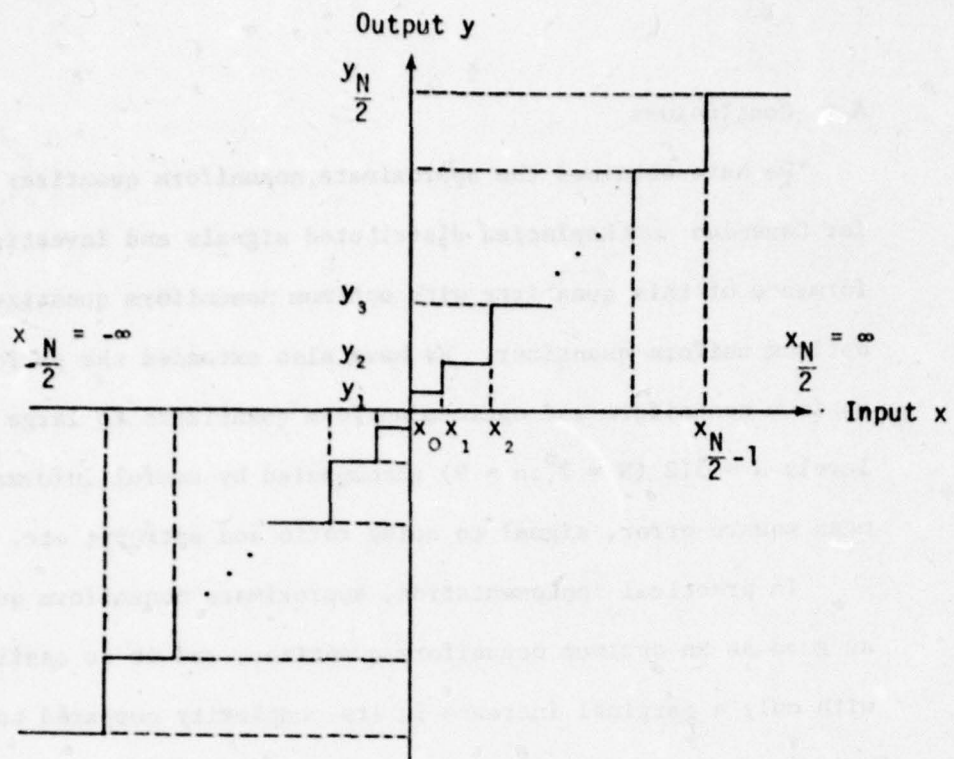
Since we have presented many tables for optimum nonuniform, optimum uniform and approximate nonuniform quantizers, all these tables are created under the assumption that we have a unity variance input signal. Using  $f(n)$  to denote M.S.E., there is no closed-form expression to relate  $f(n)$  and  $n$  ( $n$ : number of quantizer bits). However, one still can easily approximate the numerical results of  $f(n)$  by a piecewise exponential fitting numerical technique. Table A.9I shows the analytic models of  $f(n)$ . If we denote  $h(x) = f'^{-1}(x)$ , the corresponding analytic models of  $h(x)$  are shown in Table A.9II. Tables A.9I and A.9II serve as a useful tool for solving the Rate-Distortion problem in information theory.

#### A.4 Conclusions

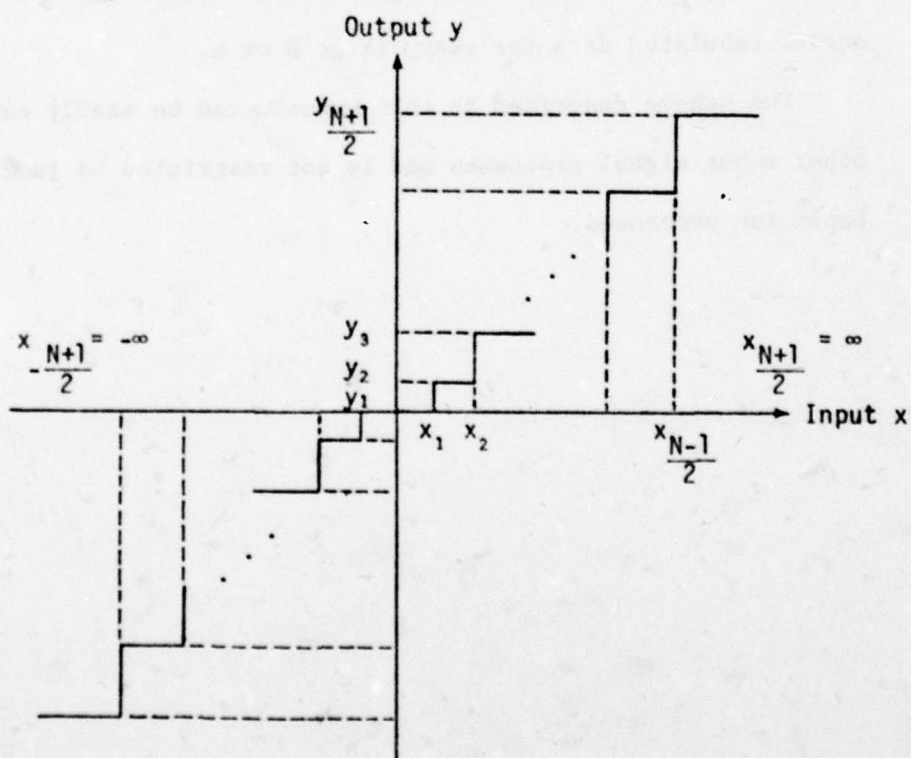
We have obtained the approximate nonuniform quantizer characteristics for Gaussian and Laplacian distributed signals and investigated the performance of this quantizer with optimum nonuniform quantizer as well as optimum uniform quantizer. We have also extended the performances of optimum nonuniform and optimum uniform quantizers to large quantization levels  $N = 512$  ( $N = 2^n: n = 9$ ) accompanied by useful information, viz., mean square error, signal to noise ratio and entropy, etc.

In practical implementation, approximate nonuniform quantizer seems as good as an optimum nonuniform quantizer, and it is easily calculable with only a marginal increase in its complexity compared to the optimum uniform quantizer. Also it is an acceptable and good quantizer structure if the computer system doesn't have enough buffer space to store the entire tabulated data for every large  $N$  or  $m$ .

The scheme described in this Appendix can be easily extended to other input signal processes and is not restricted to just Gaussian and Laplacian processes.



(a)  $N$  Even



(b)  $N$  Odd

Figure A.1 Quantizer Characteristics



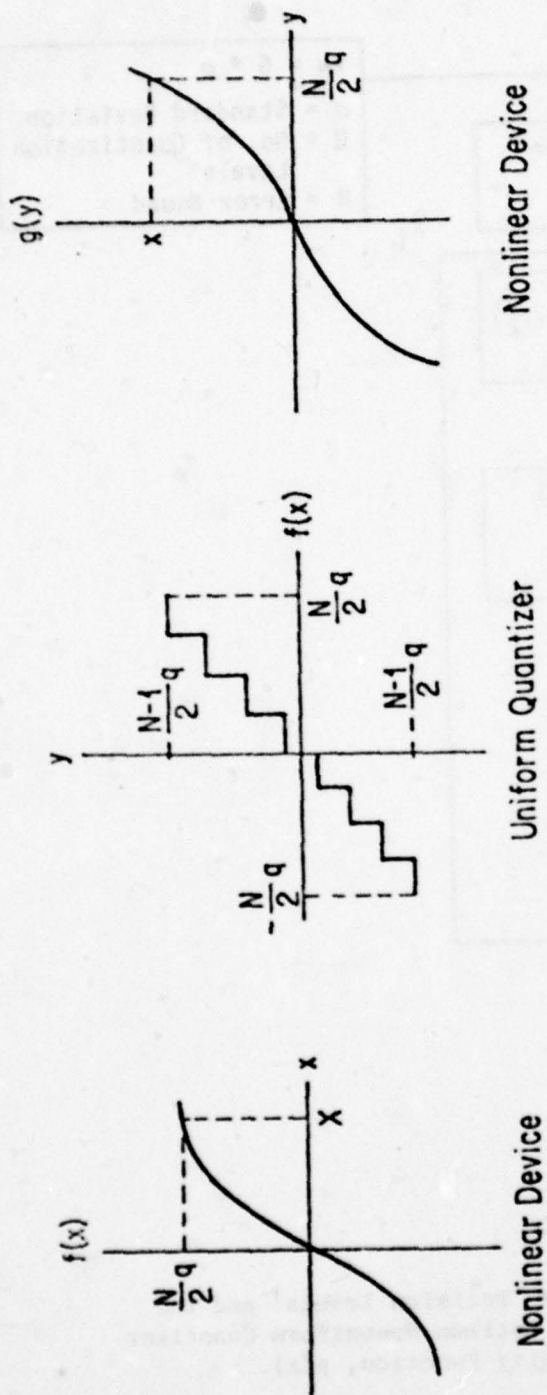


Figure A.2 Nonuniform Quantizer (Compandor)

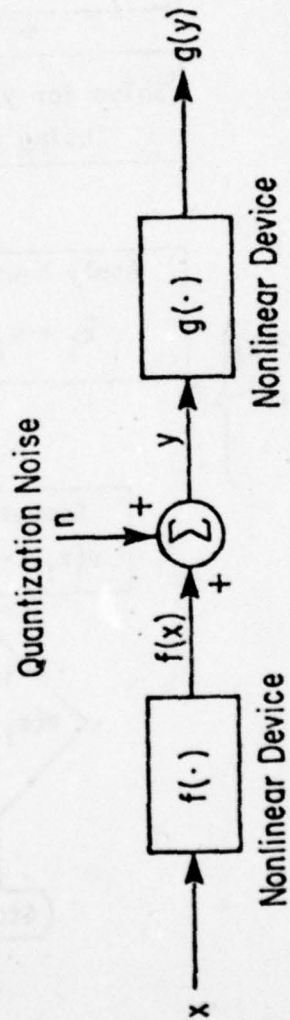


Figure A.3 Analog Model for Nonlinear Quantization

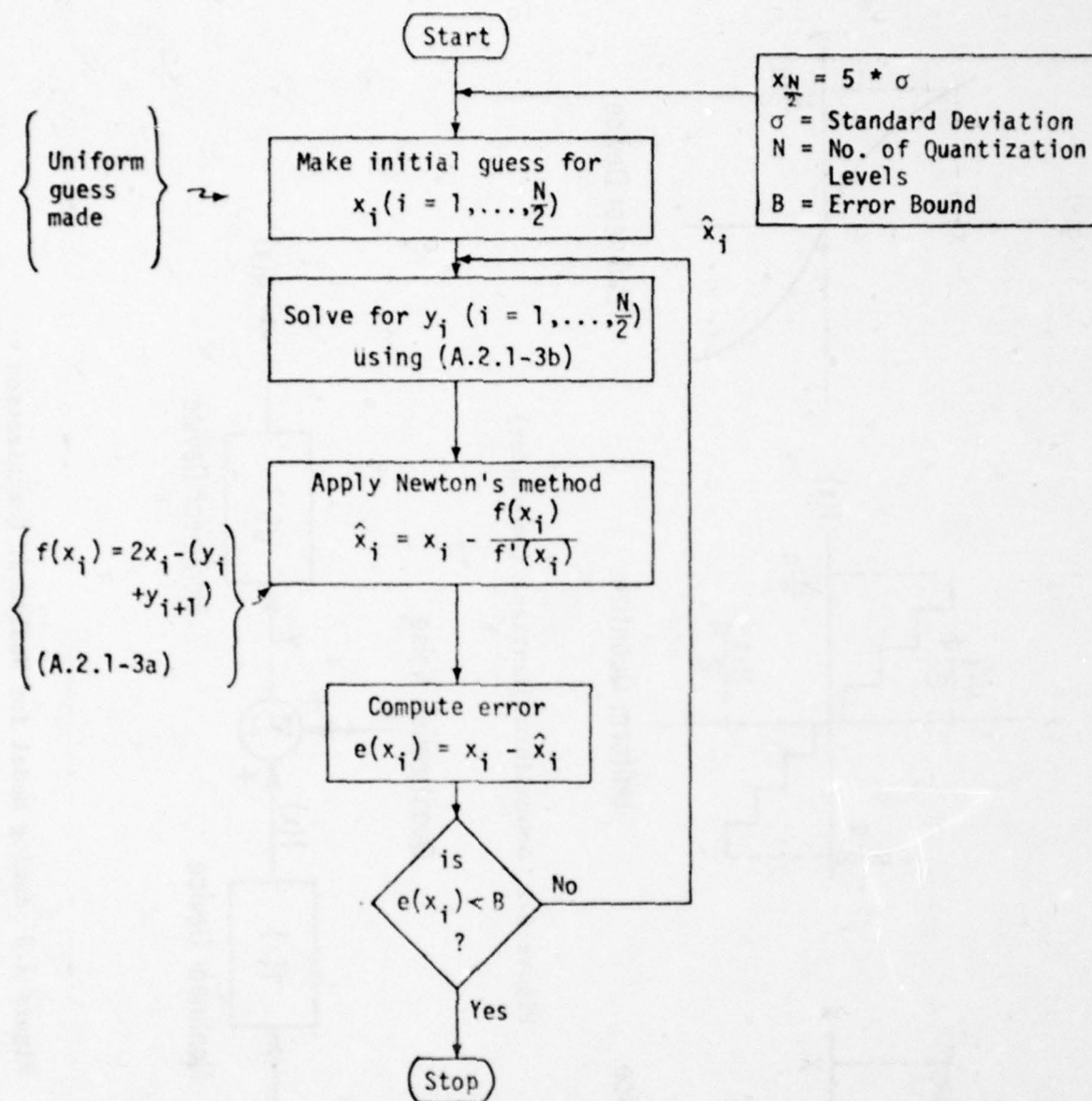


Figure A.4 Flow Chart of Determining the 'Decision Levels' and the 'Quantization Levels' for an Optimum Nonuniform Quantizer with a Given Probability Density Function,  $p(x)$ .

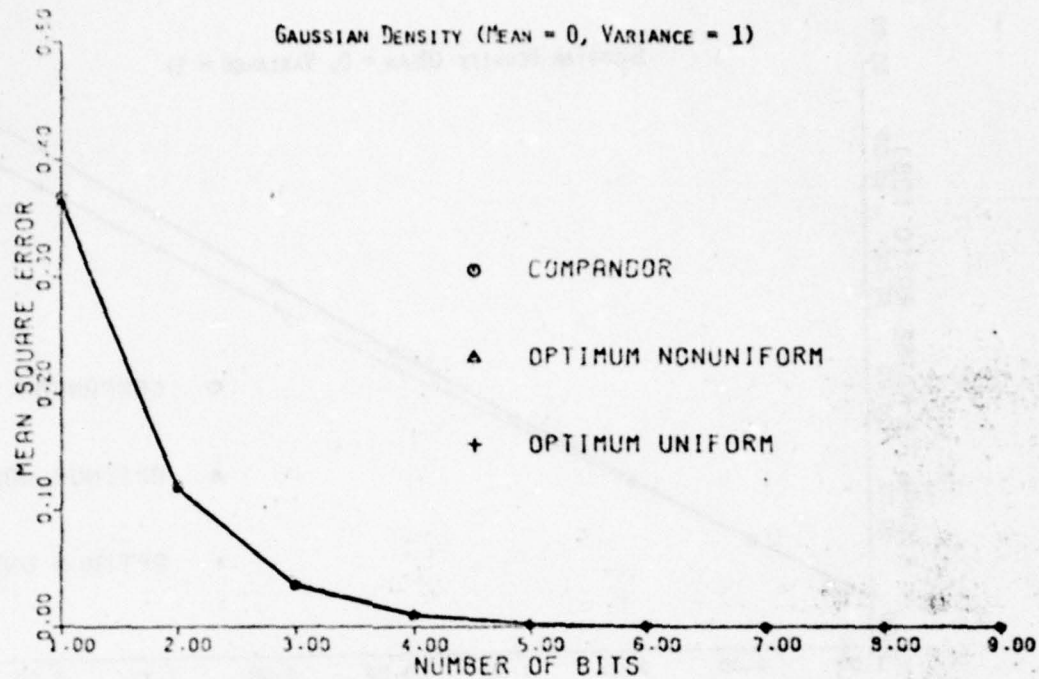


Figure A.5 Mean Square Error versus Number of Quantizer Bits for Signal with Gaussian Density (Mean = 0, Variance = 1)

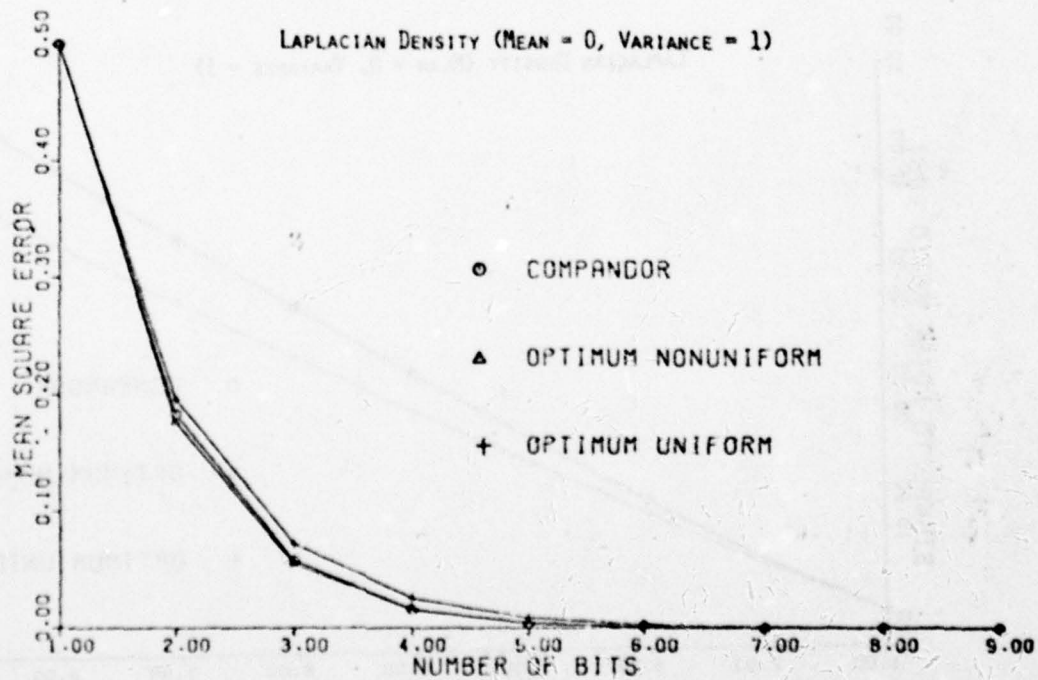


Figure A.6 Mean Square Error versus Number of Quantizer Bits for Signal with Laplacian Density (Mean = 0, Variance = 1)



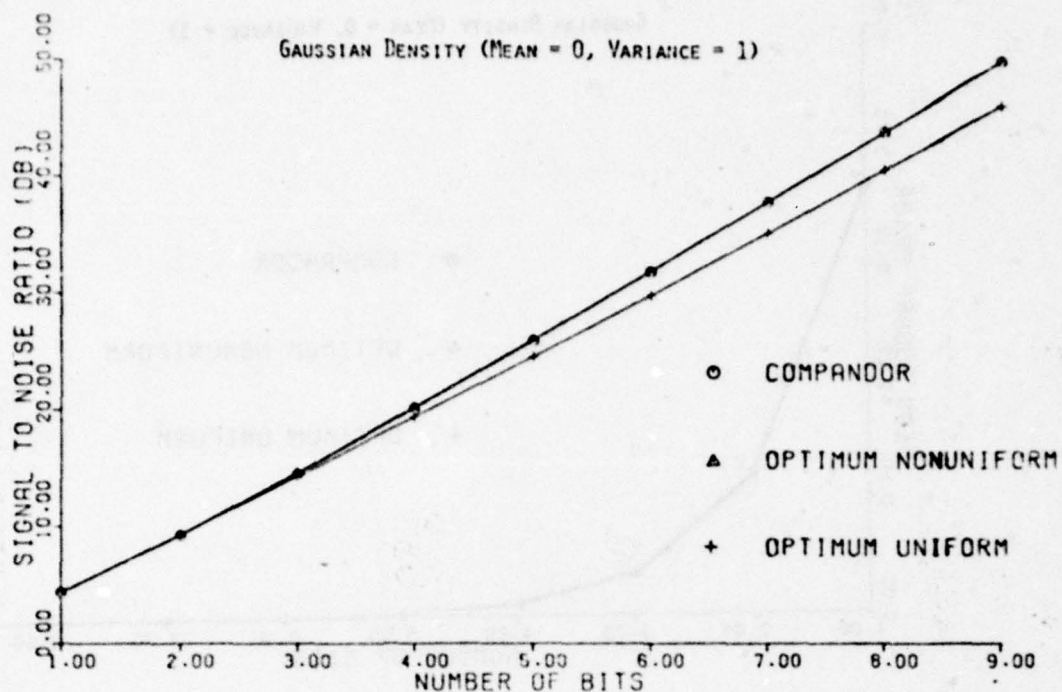


Figure A.7 Signal to Noise Ratio versus Number of Quantizer Bits for Signal with Gaussian Density (Mean = 0, Variance = 1)

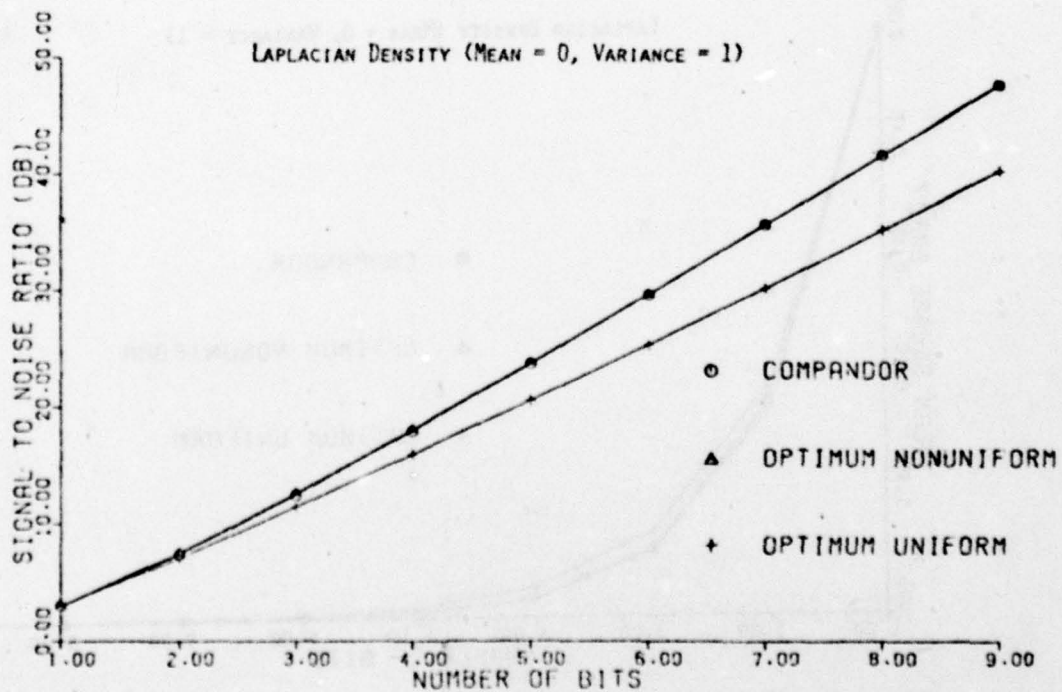


Figure A.8 Signal to Noise Ratio versus Number of Quantizer Bits for Signal with Laplacian Density (Mean = 0, Variance = 1)

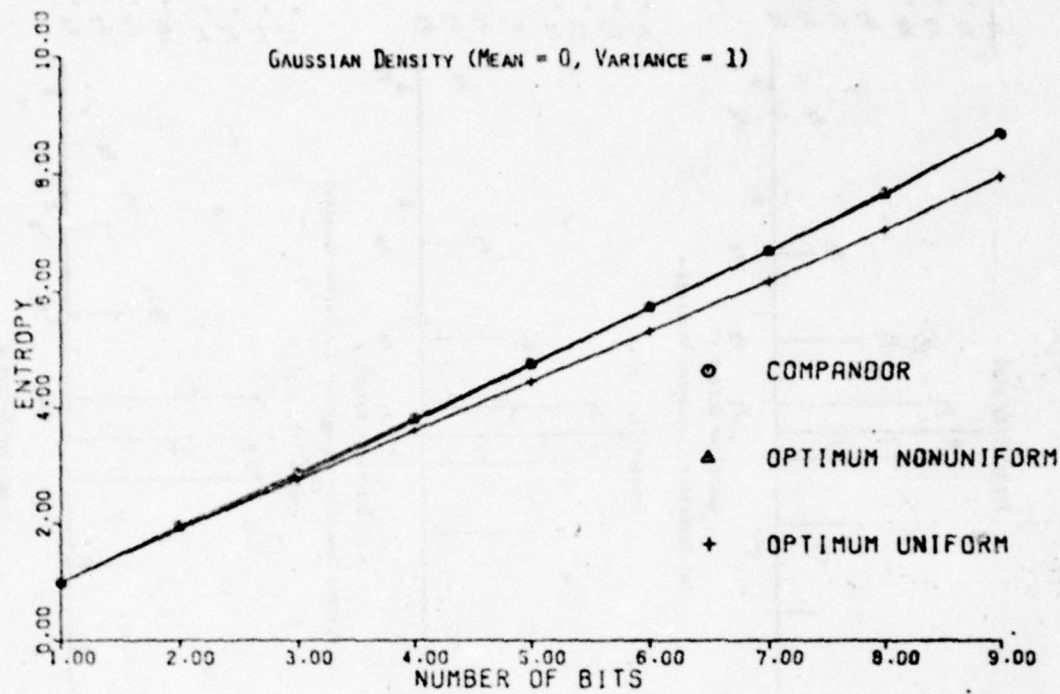


Figure A.9 Entropy versus Number of Quantizer Bits for Signal with Gaussian Density (Mean = 0, Variance = 1)

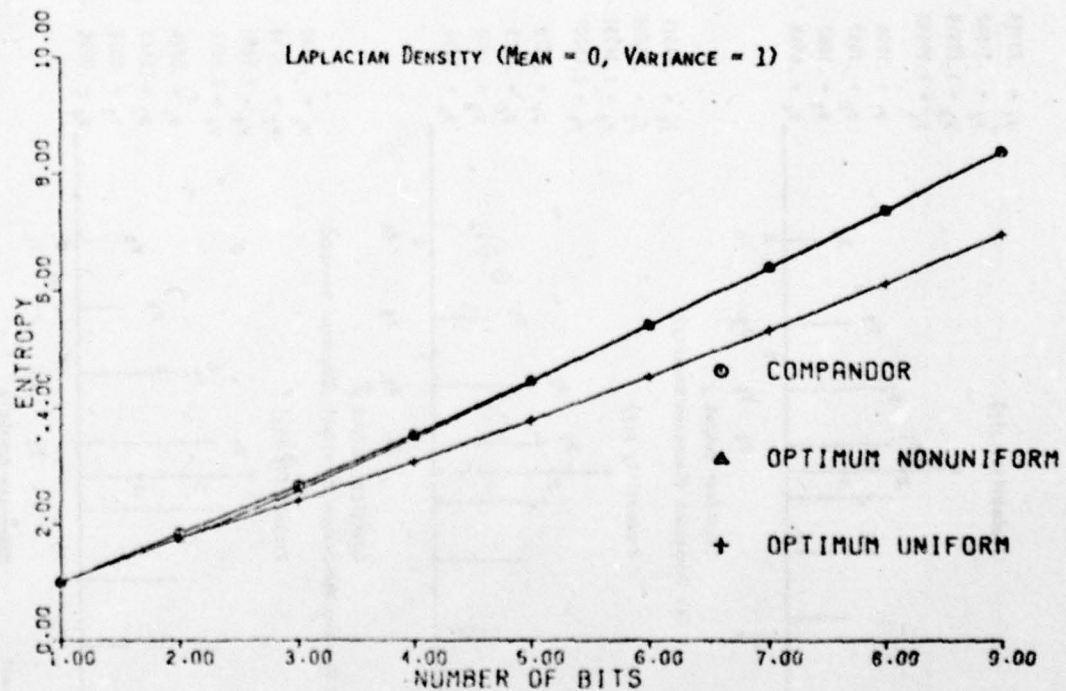


Figure A.10 Entropy versus Number of Quantizer Bits for Signal with Laplacian Density (Mean = 0, Variance = 1)

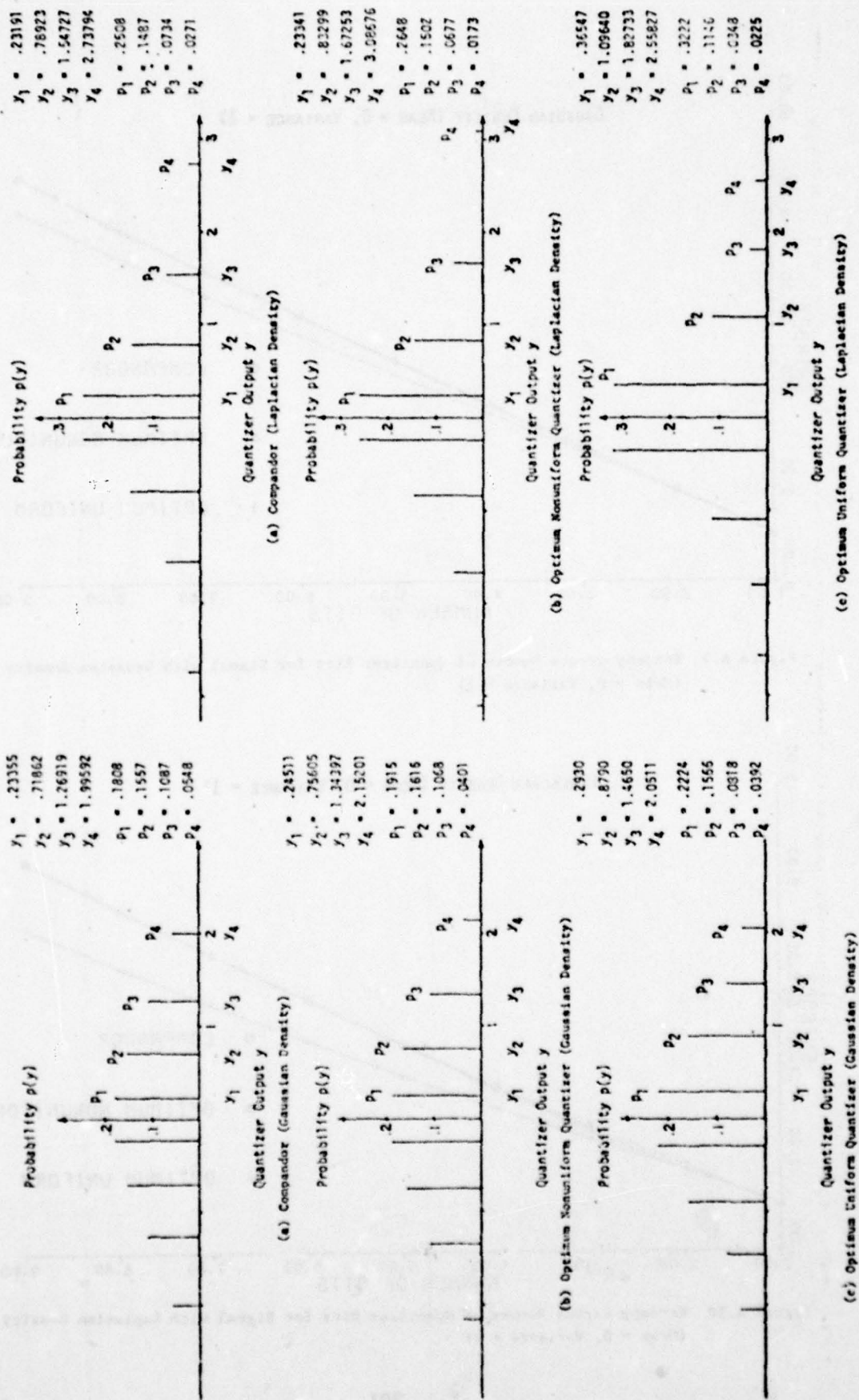


Figure A.11 Quantizer Output Levels and their Probability Distribution ( $N = 8$ )



Table A.1 Approximate Average Amount of CDC Cyber 173 Computer Time Required to Determine the Quantizer Structure with Gaussian Distributed Input Signal

No. of Quantizer Bit n	CDC Cyber 173 Computer Time (Seconds)		
	Optimum Uniform	Optimum Nonuniform	Approximate Nonuniform (Compandor)
1	↓	↓	↓
2			
3			
4			
5			
6			
7			
8			
9	10.193	382.331	4.816

The times shown are the cumulative computation times that are required to calculate the quantizers up to the corresponding value of n.

Table A.2 Approximate Average Amount of CDC Cyber 173 Computer Time Required to Determine the Quantizer Structure with Laplacian Distributed Input Signal

No. of Quantizer Bit n	CDC Cyber 173 Computer Time (Seconds)		
	Optimum Uniform	Optimum Nonuniform	Approximate Nonuniform (Compandor)
1	↓	↓	↓
2			
3			
4			
5			
6			
7			
8			
9	8.504	128.628	3.904

The times shown are the cumulative computation times that are required to calculate the quantizers up to the corresponding value of n.

Table A.3 Optimum Uniform Quantizers for Signal with Gaussian Density  
(Mean = 0, Variance = 1)

NO. OF BITS	NO. OF OUTPUT LEVELS	STEP SIZE	M.S.E.	S.N.R. (DB)	ENTROPY
1	2	1.59577	.36338	4.39639	1.00000
2	4	.99569	.11885	9.25015	1.90373
3	8	.58602	.03744	14.26668	2.76057
4	16	.33520	.01154	19.37696	3.60242
5	32	.18814	.00350	24.56527	4.44926
6	64	.10406	.00104	29.82948	5.30869
7	128	.05887	.00030	35.16651	6.18253
8	256	.03076	.00009	40.57869	7.06944
9	512	.01650	.00002	46.03469	7.96846

Table A.4 Optimum Uniform Quantizers for Signal with Laplacian Density  
(Mean = 0, Variance = 1)

NO. OF BITS	NO. OF OUTPUT LEVELS	STEP SIZE	M.S.E.	S.N.R. (DB)	ENTROPY
1	2	1.41421	.50000	3.01030	1.00000
2	4	1.05739	.19830	7.07075	1.75066
3	8	.73043	.07175	11.44191	2.39186
4	16	.48100	.02535	15.96005	3.06342
5	32	.27649	.00671	20.59821	3.78130
6	64	.16566	.00291	25.35595	4.53703
7	128	.09610	.00095	30.22918	5.32231
8	256	.05464	.00030	35.20827	6.13130
9	512	.03088	.00009	40.28120	6.95978

Table A.5 Optimum Nonuniform Quantizers for Signal with Gaussian Density  
(Mean = 0, Variance = 1)

BIT LEVEL	1	2	3	4	5	6	7
M.S.E.	.36338	.11748	.03859	.00950	.00290	.00084	.00016
S.N.R. (dB)	4.39619	9.30029	14.61540	20.22230	26.01249	31.90940	37.86342
ENTROPY	1.00000	1.91109	2.82443	3.76916	4.72911	5.70746	6.69916

I	X(I)	V(I)	X(I)	V(I)	X(I)	V(I)	X(I)	V(I)	X(I)	V(I)	X(I)	V(I)	X(I)	V(I)
1	0.00000	.79788	0.00000	.45279	0.00000	.24511	0.00000	.12643	0.00000	.06397	0.00000	.03356	0.00000	.01712
2			.98162	1.51043	.50059	.75605	.25630	.38616	.13212	.14628	.06716	.10072	.03425	.05137
3					1.05002	1.34397	.52255	.65693	.26502	.31175	.13439	.16004	.06091	.04504
4					1.76800	2.15201	.79975	.96256	.46721	.20182	.23560	.10279	.11994	
5							1.09953	1.25644	.53839	.60557	.26456	.30351	.13711	.15426
6							1.43741	1.61032	.67674	.74789	.33770	.37109	.17167	.18667
7							1.84381	2.06929	.82166	.89542	.40635	.44002	.20590	.22113
8							2.46016	2.73283	.97258	1.04972	.47564	.51065	.24640	.25767
9									1.13128	1.21281	.54567	.58089	.27499	.28231
10									1.30011	1.38740	.61659	.65228	.30908	.32720
11									1.46236	1.57731	.68853	.72478	.34448	.36190
12									1.60263	1.70832	.76166	.79853	.37940	.39669
13									1.70907	2.02960	.83615	.87374	.41447	.43203
14									2.17430	2.33877	.91218	.95060	.44966	.46733
15									2.30544	2.69288	.98994	1.02935	.48537	.50221
16									2.97684	3.26158	1.06981	1.11025	.52065	.53867
17											1.15194	1.19382	.55642	.57435
18											1.23672	1.27980	.59241	.61046
19											1.32453	1.36974	.62854	.64681
20											1.41585	1.46245	.66512	.68342
21											1.51126	1.56005	.70167	.72011
22											1.61146	1.66204	.73842	.75731
23											1.71733	1.77180	.77628	.79503
24											1.83002	1.88822	.81497	.83400
25											1.95103	2.01382	.85303	.87115
26											2.08440	2.15040	.89049	.90779
27											2.22701	2.30304	.92833	.94486
28											2.38916	2.47525	.96663	.98268
29											2.57567	2.67007	1.00440	1.02046
30											2.78656	2.89102	1.04400	1.05944
31											3.00242	3.11681	1.08449	1.10003
32											3.24957	3.37412	1.13089	1.15173
33													1.17291	1.19407
34													1.21559	1.23709
35													1.25896	1.28086
36													1.30315	1.32542
37													1.34816	1.37064
38													1.39402	1.41718
39													1.44066	1.46452
40													1.48807	1.51294
41													1.53775	1.56253
42													1.58797	1.61340
43													1.63954	1.66505
44													1.69255	1.71943
45													1.74716	1.77489
46													1.80353	1.83216
47													1.86163	1.88146
48													1.92220	1.95307
49													1.98514	2.01719
50													2.05068	2.08416
51													2.11926	2.15435
52													2.19130	2.22623
53													2.26731	2.30637
54													2.34782	2.38465
55													2.43303	2.47040
56													2.52304	2.57436
57													2.62064	2.67491
58													2.73056	2.78420
59													2.85070	2.90335
60													2.97224	3.07111
61													3.10022	3.24530
62													3.23276	3.40020
63													3.36359	3.76006
64													3.49361	4.26005



Table A.5 (cont'd) Optimum Nonuniform Quantizers for Signal with Gaussian Density  
(Mean = 0, Variance = 1)

BIT	8	9	10	11	12	13	14	15	16	17	18	19	20	21	22	23	24	25	26	27	28	29	30	31	32	33	34	35	36	37	38	39	40	41	42	43	44	45	46	47	48	49	50	51	52	53	54	55	56	57	58	59	60	61	62	63	64																																																																																																																																																																																																																																																																		
LEVEL	256	512	1024	2048	4096	8192	16384	32768	65536	131072	262144	524288	1048576	2097152	4194304	8388608	16777216	33554432	67108864	134217728	268435456	536870912	1073741824	2147483648	4294967296	8589934592	17179869184	34359738368	68719476736	137438953472	274877906944	549755813888	1099511627776	2199023255552	4398046511104	8796093022208	17592186044416	35184372088832	70368744177664	140737488355328	281474976710656	562949953421312	1125899906842624	2251799813685248	4503599627370496	9007199254740992	18014398509481984	36028797018963968	72057594037927936	144115188075855872	288230376151711744	576460752303423488	1152921504606846976	2305843009213693952	4611686018427387904	9223372036854775808	18446744073709551616	36893488147419103232	73786976294838206464	147573952589676412928	295147905179352825856	590295810358705651712	1180591620717411303424	2361183241434822606848	4722366482869645213696	9444732965739290427392	18889465931478580854784	37778931862957161709568	75557863725914323419136	151115727451828646838272	302231454903657293676544	604462909807314587353088	1208925819614629174706176	2417851639229258349412352	4835703278458516698824704	9671406556917033397649408	19342813113834066795298816	38685626227668133590597632	77371252455336267181195264	154742504910672534362390528	309485009821345068724781056	618970019642690137449562112	1237940039285380274899124224	2475880078570760549798248448	4951760157141521099596496896	9903520314283042199192993792	19807040628566084398385987584	39614081257132168796771975168	79228162514264337593543950336	158456325028528675187087900672	316912650057057350374175801344	633825300114114700748351602688	1267650600228229401496703205376	2535301200456458802993406410752	5070602400912917605986812821504	10141204801825835211973625643008	20282409603651670423947251286016	40564819207303340847894502572032	81129638414606681695789005144064	162259276829213363391578010288128	324518553658426726783156020576256	649037107316853453566312041152512	1298074214633706907132624082305024	2596148429267413814265248164610048	5192296858534827628530496329220096	10384593717069655257060992658440192	20769187434139310514121985316880384	41538374868278621028243970633760768	83076749736357242056487941267521536	166153499472714484112975882535042752	332306998945428968225951765070085504	664613997890857936451903530140171008	1329227995781715872903807060280342016	2658455991563431745807614120560684032	5316911983126863491607228241121368064	10633823966253726983214456482242736128	21267647932507453966428912964485472256	42535295865014907932857825928970944512	850705917300298158657156518579418880256	1701411834600596317314313137158837760512	3402823669201192634628626274317675521024	680564733840238526925725254863535104256	1361129467680477053851450509727070205056	2722258935360954107702901019454140410112	5444517870721908215405802038908280820224	10889035741443816430811604077816561640448	21778071482887632861623208155733123280896	43556142965775265723246416311466646561792	8711228593155053144649283262293333312358336	174224571863101062892985665245866666247168	348449143726202125785971330491733332473536	69689828745240425157194266098346666447168	139379657490480850314388532196693332473536	27875931498096170062877706439338666447168	55751862996192340125755412878677332473536	111503725992384680251510825757354666447168	223007451984769360503021651515711332473536	44601490396953872100604330303142666447168	89202980793907744201208660606285332473536	1784059615878154884024173212136666447168	3568119231756309768048346424273332473536	713623846351261953609669284854666447168	1427247692702523907219338569709332473536	2854495385405047814438677139418666447168	5708990770810095628877354278837332473536	11417981541620191257755412878677332473536	22835963083240382514510825757354666447168	45671926166480765029021651515711332473536	9134385233296153005804330303142666447168	18268770466592306011608660606285332473536	365375409331846120232173212136666447168	730750818663692240464346424273332473536	146150163732738448092868884854666447168	29230032746547689618573777139418666447168	58460065493095379237147554278837332473536	11692013098619075847429510515711332473536	2338402619723815169485902103142666447168	4676805239447630338971804206285332473536	93536104788952606779436084125711332473536	18707220957790521355887216515711332473536	37414441915580102715775412878677332473536	7482888383116020543155412878677332473536	149657767662320410863110825757354666447168	2993155353246408217270216515711332473536	59863107064928164345404330303142666447168	1197262141298563286888066606285332473536	23945242825971272737755412878677332473536	47890485651942545475510825757354666447168	957809713038850909510216515711332473536	1915619426077701819024330303142666447168	3831238852157603638048660606285332473536	76624777043152072760973212136666447168	1532495440863041455219338569709332473536	3064990881726082910438677139418666447168	6129981763452165820877354278837332473536	12259963526904331641755412878677332473536	24519927053808663283510825757354666447168	490398541076173265670216515711332473536	9807970821523465313404330303142666447168	19615941643046906226808660606285332473536	392318832860938124536173212136666447168	7846376657218762490723216515711332473536	156927533144375249814510825757354666447168	3138550662887514996285902103142666447168	6277101325775029992571804206285332473536	125542026515500599510216515711332473536	251084053031001199024330303142666447168	502168106062002398048660606285332473536	10043362121240047760973212136666447168	200867242424800955219338569709332473536	401734484849601910438677139418666447168	803468969699203820877354278837332473536	1606937939398407641755412878677332473536	3213875878796815283510825757354666447168	64277517575936305670216515711332473536	1285550351518726113404330303142666447168	2571100703037452226808660606285332473536	51422014060749044536173212136666447168	1028440281214980890723216515711332473536	20568805624299617814510825757354666447168	411376112485992356285902103142666447168	822752224971984712571804206285332473536	1645504449943969425510825757354666447168	32910088998879388510216515711332473536	65820177997758777024330303142666447168	131640355995517554048660606285332473536	2632807119910351080973212136666447168	526561423982070216194510825757354666447168	1053122847764140432908660606285332473536	210624569552828086180973212136666447168	42124913910565617237173212136666447168	842498278211312344743510825757354666447168	1684996576422624689485902103142666447168	3369993152845249378971804206285332473536	67399863056904987579436084125711332473536	13479972611380995159887216515711332473536	269599452227619903197755412878677332473536	539198904455239806395510825757354666447168	10783978089104796127910825757354666447168	21567956178209592255804330303142666447168	43135912356419184411608660606285332473536	862718247128383688232173212136666447168	1725436494256767376463110825757354666447168	3450872988513534752926216515711332473536	69017459770270695058524330303142666447168	13803491954054139011704330303142666447168	27606983908108278023408660606285332473536	552139678162165560468173212136666447168	1104279356324331200908660606285332473536	22085587126486624018173212136666447168	441711742529722480363510825757354666447168	8834234850594449607270216515711332473536	17668469001188898014510825757354666447168	353369380023777960290216515711332473536	7067387600475559205804330303142666447168	14134775200951118411608660606285332473536	282695504019022368232173212136666447168	565391008038044736464330303142666447168	113078201607608952908660606285332473536	2261564032152179058173212136666447168	45231280643043581163510825757354666447168	90462561286087162323216515711332473536	18092512257217432464510825757354666447168	3618502451443527492908660606285332473536	7237004902887054985804330303142666447168	14474009805774109971608660606285332473536	289480196115482199432173212136666447168	578960392230964398863510825757354666447168	1157920784261928797755412878677332473536	2315841568523857595510825757354666447168	4631683137047715191024330303142666447168	9263366274095430382048660606285332473536	18526732548190860764173212136666447168	370534650963817215283510825757354666447168	7410693019276344305670216515711332473536	148213860385526886113404330303142666447168	296427720771253772226808660606285332473536	5928554415425075444510825757354666447168	1185714803485015089024330303142666447168	2371429606970030178048660606285332473536	47428592139400603560973212136666447168	948571842788012071219338569709332473536	1897143645776024142438677139418666447168	3794287291572048284877354278837332473536	758857458314409656975510825757354666447168	15177148166280991139510825757354666447168	303542963325619822790216515711332473536	6070859266512396455804330303142666447168	121417185331123929108660606285332473536	2428343706622478582173212136666447168	48566874132449571643510825757354666447168	97133748264899143263510825757354666447168	1942674853297982865270216515711332473536	38853497065759657305404330303142666447168	777069941315193146108660606285332473536	155413988263038629219338569709332473536	310827976526077258438677139418666447168	621655953052154516877354278837332473536	1243311906104149033510825757354666447168	24866238122082980670216515711332473536	497324762441659613404330303142666447168	994649524883319227408660606285332473536	19892990497666384548173212136666447168	397859809953327690963510825757354666447168	795719619906655381926808660606285332473536	15914392398133117639510825757354666447168	3182878479626623527908660606285332473536	6365756959253247055804330303142666447168	127315139185064841173212136666447168	254630278370129682363510825757354666447168	5092605567402593647270216515711332473536	10185211134805187294510825757354666447168	20370422269610374589024330303142666447168	40740844539220749178048660606285332473536	814816890784414983560973212136666447168	16296337815688299671608660606285332473536	325926756313765993432173212136666447168	651853512627531986863510825757354666447168	1303707025255063973755412878677332473536	2607414050510127947510825757354666447168	5214828101020255895024330303142666447168	1042965620204051179008660606285332473536	20859312404081023580173212136666447168	417186248081620471603510825757354666447168	8343724961632409432048660606285332473536	166874498326648188640973212136666447168	3337489966532963772808660606285332473536	66749799330659275456173212136666447168	133499596661385550910825757354666447168	26699919332277110182173212136666447168	533998386645570203643510825757354666447168	1067996773291422407270216515711332473536	2135993546582844014510825757354666447168	42719870931656880290216515711332473536	85439741863313760280

Table A.6 Optimum Nonuniform Quantizers for Signal with Laplacian Density (Mean = 0, Variance = 1)

BIT LEVEL	1	2	3	4	5	6	7
P.S.F.	0.00000	0.17619	0.05468	0.01537	0.00418	0.00106	0.00027
S.A.R. (F)	3.01030	7.54307	12.63795	18.13255	23.06985	29.74381	35.68799
Entropy	1.00000	1.72024	2.56537	3.47671	4.42638	5.40032	6.38259

I	X(I)	Y(I)	X(I)	Y(I)	X(I)	Y(I)	X(I)	Y(I)	X(I)	Y(I)	X(I)	Y(I)	X(I)	Y(I)
1	0.000000	0.707107	0.000000	0.617702	0.000000	0.534400	0.000000	0.459890	0.000000	0.392630	0.000000	0.332630	0.000000	0.279558
2		1.12649	1.03393		0.53121	0.45299	0.36445	0.28498	0.22229	0.18049	0.14631	0.11999	0.09334	0.07026
3					0.46683	0.37676	0.27358	0.21377	0.16627	0.13077	0.10550	0.08105	0.06729	0.05436
4					0.41995	0.31114	0.22554	0.17281	0.13588	0.10550	0.08105	0.06729	0.05436	0.04312
5					0.38457	0.27798	0.19731	0.14781	0.11588	0.08950	0.07105	0.05729	0.04636	0.03712
6					0.35777	0.24778	0.17363	0.12945	0.10105	0.08105	0.06729	0.05436	0.04312	0.03436
7					0.33973	0.21713	0.15547	0.11548	0.08950	0.07105	0.05729	0.04636	0.03712	0.02836
8					0.32425	0.18716	0.14000	0.10000	0.07500	0.06000	0.04500	0.03500	0.02500	0.01500
9														
10														
11														
12														
13														
14														
15														
16														
17														
18														
19														
20														
21														
22														
23														
24														
25														
26														
27														
28														
29														
30														
31														
32														
33														
34														
35														
36														
37														
38														
39														
40														
41														
42														
43														
44														
45														
46														
47														
48														
49														
50														
51														
52														
53														
54														
55														
56														
57														
58														
59														
60														



Table A.6 (cont'd) Optimum Nonuniform Quantizer for Signal with Laplacian Density  
(Mean = 0, Variance = 1)

0			9			512			0.00002			0.65760			0.38272		
256			512			1024			1024			1024			1024		
0.0007			0.0007			0.0007			0.0007			0.0007			0.0007		
41.66436			41.66436			41.66436			41.66436			41.66436			41.66436		
7.35616			7.35616			7.35616			7.35616			7.35616			7.35616		
I	X(I)	Y(I)	I	X(I)	Y(I)	I	X(I)	Y(I)	I	X(I)	Y(I)	I	X(I)	Y(I)	I	X(I)	Y(I)
1	0.000000	.0055027	65	1.5027	1.5195	1	0.000000	.0055117	65	.88470	.89662	129	2.0368	2.0469	193	3.6705	3.6877
2	.017074	.025645	66	1.5165	1.5335	2	.011857	.017801	66	.90461	.91736	130	2.0572	2.0674	194	3.7052	3.7226
3	.034286	.042927	67	1.5708	1.5880	3	.023779	.029756	67	.92058	.93357	131	2.0777	2.0879	195	3.7403	3.7580
4	.051639	.060190	68	1.6056	1.6361	4	.035767	.041777	68	.93662	.94963	132	2.0982	2.1085	196	3.7760	3.7939
5	.069133	.077915	69	1.6410	1.6588	5	.047821	.053844	69	.95271	.96576	133	2.1189	2.1293	197	3.8122	3.8304
6	.086772	.095625	70	1.6769	1.6950	6	.059941	.066016	70	.96886	.98194	134	2.1397	2.1501	198	3.8489	3.8674
7	.10456	.11349	71	1.7135	1.7319	7	.072127	.078235	71	.98508	.99819	135	2.1606	2.1711	199	3.8862	3.9050
8	.12249	.13149	72	1.7506	1.7694	8	.084378	.090319	72	1.0014	1.0095	136	2.1816	2.1921	200	3.9241	3.9432
9	.14058	.14965	73	1.7884	1.8075	9	.096695	.102673	73	1.0177	1.0259	137	2.2027	2.2133	201	3.9626	3.9820
10	.15881	.16797	74	1.8269	1.8463	10	.10908	.11508	74	1.0341	1.0423	138	2.2240	2.2346	202	4.0017	4.0214
11	.17720	.18644	75	1.8660	1.8857	11	.12153	.12776	75	1.0505	1.0588	139	2.2453	2.2560	203	4.0415	4.0616
12	.19575	.20507	76	1.9058	1.9259	12	.13404	.14031	76	1.0671	1.0753	140	2.2667	2.2775	204	4.0820	4.1024
13	.21446	.22386	77	1.9464	1.9669	13	.14662	.15292	77	1.0838	1.0919	141	2.2883	2.2991	205	4.1232	4.1439
14	.23334	.24281	78	1.9878	2.0086	14	.15926	.16560	78	1.1003	1.1086	142	2.3100	2.3209	206	4.1641	4.1849
15	.25238	.26193	79	2.0299	2.0511	15	.17197	.17834	79	1.1170	1.1253	143	2.3318	2.3427	207	4.2058	4.2269
16	.27158	.28122	80	2.0728	2.0945	16	.18475	.19115	80	1.1337	1.1421	144	2.3538	2.3647	208	4.2473	4.2687
17	.29096	.30069	81	2.1166	2.1387	17	.19759	.20402	81	1.1506	1.1590	145	2.3758	2.3869	209	4.2896	4.3109
18	.31051	.32032	82	2.1613	2.1839	18	.21050	.21696	82	1.1674	1.1759	146	2.3980	2.4091	210	4.3328	4.3543
19	.33023	.34014	83	2.2069	2.2300	19	.22347	.22997	83	1.1844	1.1929	147	2.4204	2.4315	211	4.3760	4.3977
20	.35013	.36013	84	2.2535	2.2771	20	.23650	.24303	84	1.2014	1.2099	148	2.4428	2.4541	212	4.4196	4.4415
21	.37022	.38031	85	2.3011	2.3252	21	.24960	.25617	85	1.2185	1.2270	149	2.4654	2.4768	213	4.4637	4.4858
22	.39049	.40067	86	2.3498	2.3744	22	.26277	.26936	86	1.2356	1.2441	150	2.4882	2.4996	214	4.5082	4.5306
23	.41095	.42122	87	2.3996	2.4247	23	.27600	.28262	87	1.2528	1.2614	151	2.5111	2.5226	215	4.5531	4.5758
24	.43160	.44197	88	2.4505	2.4763	24	.28929	.29595	88	1.2700	1.2787	152	2.5342	2.5457	216	4.6002	4.6232
25	.45244	.46291	89	2.5027	2.5291	25	.30265	.30933	89	1.2873	1.2960	153	2.5574	2.5690	217	4.6475	4.6709
26	.47349	.48406	90	2.5561	2.5832	26	.31608	.32280	90	1.3047	1.3134	154	2.5807	2.5924	218	4.6952	4.7190
27	.49475	.50541	91	2.6109	2.6386	27	.32957	.33632	91	1.3222	1.3309	155	2.6042	2.6160	219	4.7432	4.7674
28	.51621	.52696	92	2.6671	2.6956	28	.34312	.34991	92	1.3397	1.3484	156	2.6279	2.6398	220	4.7916	4.8162
29	.53785	.54873	93	2.7248	2.7540	29	.35674	.36359	93	1.3572	1.3660	157	2.6518	2.6637	221	4.8403	4.8654
30	.55967	.57061	94	2.7841	2.8141	30	.37042	.37727	94	1.3748	1.3836	158	2.6758	2.6878	222	4.8894	4.9150
31	.58168	.59271	95	2.8450	2.8759	31	.38416	.39104	95	1.3926	1.4014	159	2.7000	2.7121	223	4.9390	4.9650
32	.60387	.61503	96	2.9077	2.9385	32	.39797	.40488	96	1.4103	1.4192	160	2.7244	2.7366	224	5.0002	5.0266
33	.62624	.63759	97	2.9723	3.0031	33	.41184	.41879	97	1.4282	1.4371	161	2.7490	2.7613	225	5.0519	5.0786
34	.64880	.66027	98	3.0389	3.0707	34	.42598	.43297	98	1.4460	1.4550	162	2.7737	2.7861	226	5.1042	5.1312
35	.67243	.68399	99	3.1076	3.1425	35	.43978	.44678	99	1.4640	1.4730	163	2.7987	2.8112	227	5.1571	5.1844
36	.69624	.70786	100	3.1786	3.2144	36	.45384	.46086	100	1.4820	1.4910	164	2.8238	2.8364	228	5.2106	5.2382
37	.72024	.73192	101	3.2515	3.2882	37	.46796	.47501	101	1.5001	1.5092	165	2.8492	2.8619	229	5.2646	5.2925
38	.74444	.75617	102	3.3279	3.3666	38	.48215	.48925	102	1.5183	1.5274	166	2.8748	2.8876	230	5.3191	5.3473
39	.76885	.78063	103	3.4067	3.4469	39	.49640	.50354	103	1.5365	1.5456	167	2.9005	2.9133	231	5.3742	5.4027
40	.79346	.80529	104	3.4880	3.5301	40	.51072	.51788	104	1.5548	1.5639	168	2.9265	2.9394	232	5.4298	5.4586
41	.81818	.83005	105	3.5714	3.6168	41	.52510	.53229	105	1.5732	1.5823	169	2.9528	2.9658	233	5.4859	5.5150
42	.84301	.85491	106	3.6569	3.7071	42	.53954	.54676	106	1.5916	1.6008	170	2.9792	2.9923	234	5.5425	5.5719
43	.86795	.87991	107	3.7443	3.8044	43	.55404	.56130	107	1.6101	1.6193	171	3.0060	3.0191	235	5.6006	5.6303
44	.89300	.90501	108	3.8337	3.9041	44	.56860	.57589	108	1.6287	1.6380	172	3.0329	3.0461	236	5.6592	5.6892
45	.91816	.93024	109	3.9251	4.0055	45	.58323	.59055	109	1.6473	1.6566	173	3.0601	3.0733	237	5.7184	5.7487
46	.94344	.95558	110	4.0185	4.1122	46	.59792	.60527	110	1.6660	1.6754	174	3.0876	3.1008	238	5.7781	5.8087
47	.96884	.98108	111	4.1139	4.2267	47	.61267	.62005	111	1.6848	1.6942	175	3.1153	3.1285	239	5.8384	5.8693
48	.99436	1.00666	112	4.2123	4.3478	48	.62748	.63490	112	1.7037	1.7131	176	3.1433	3.1565	240	5.8992	5.9304
49	1.02000	1.03234	113	4.3127	4.4761	49	.64236	.64983	113	1.7226	1.7321	177	3.1714	3.1846	241	5.9605	5.9919
50	1.04576	1.05810	114	4.4144	4.6128	50	.65730	.66477	114	1.7417	1.7512	178	3.2002	3.2134	242	6.0224	6.0540
51	1.07164	1.08402	115	4.5186	4.7585	51	.67230	.67977	115	1.7608	1.7703	179	3.2291	3.2423	243	6.0848	6.1166
52	1.10774	1.12017	116	4.6254	4.9151	52	.68736	.69483	116	1.7799	1.7894	180	3.2583	3.2715	244	6.1477	6.1797
53	1.13399	1.14641	117	4.7347	5.0842	53	.70248	.70995	117	1.7992	1.8087	181	3.2878	3.3010	245	6.2111	6.2433
54	1.16039	1.17281	118	4.8465	5.2679	54	.71766	.72513	118	1.8185	1.8280	182	3.3176	3.3308	246	6.2750	6.3074
55	1.18694	1.20936	119	4.9605	5.4605	55	.73290	.74037	119	1.8379	1.8474	183	3.3478	3.3610	247	6.3394	6.3720
56	1.21364	1.23606	120	5.0769	5.6611	56	.74821	.75568	120	1.8574	1.8669	184	3.3783	3.3915	248	6.4043	6.4371
57	1.24049	1.26291	121	5.1957	5.8702	57	.76358	.77105	121	1.8770	1.8865	185	3.4092	3.4224	249	6.4697	6.5026
58	1.26749	1.28993	122	5.3169	6.0889	58	.77900	.78647	122	1.8967	1.9062	186	3.4404	3.4536	250	6.5356	6.5687
59	1.29464	1.31711	123	5.4405	6.3165	59	.79449	.80196	123	1.9164	1.9259	187	3.4721	3.4853	251	6.6019	6.6352
60	1.32194	1.34427	124	5.5665	6.5531	60	.81004	.81751	124	1.9362	1.9457	188	3.5041	3.5173	252	6.6686	6.7021
61	1.34939	1.37171	125	5.6949	6.7987	61	.82565	.83312	125	1.9561	1.9656	189	3.5363	3.5495	253	6.7358	6.7694
62	1.37699	1.40426	126	5													



Table A.7 Companders for Signal with Gaussian Density  
(Mean = 0, Variance = 1)

*****TABLE A.7 COMPANDERS FOR SIGNAL WITH GAUSSIAN DENSITY*****													
BIT	1	2	3	4	5	6	7	8	9	10	11	12	13
LCuEL	2	4	8	16	32	64	128	256	512	1024	2048	4096	8192
M.S.E.	.36838	.12835	.03566	.00980	.00257	.00066	.00017	.00004	.00001	.00000	.00000	.00000	.00000
S.N.R. (dB)	4.33711	9.19543	14.46267	18.88816	22.92319	26.63331	30.01614	33.12119	36.01614	38.75939	41.38119	43.91614	46.38119
ENTROPY	1.00000	1.00000	1.00000	1.00000	1.00000	1.00000	1.00000	1.00000	1.00000	1.00000	1.00000	1.00000	1.00000

1	2	3	4	5	6	7	8	9	10	11	12	13	14
1	0.00000	.72728	0.00000	.42426	0.00000	.23355	0.00000	.12471	0.00000	.06453	0.00000	.03301	0.00000
2	1.62146		.87607	1.29829		.71642	.24967	.37524	.12916	.19396	.26602	.09907	.03343
3			2.05700		.98105	1.26419	.50343	.63445	.25903	.32448	.13214	.16527	.06688
4				1.55725	1.49592	.71520	.90879	.39239	.45687	.15846	.23172	.10235	.11710
5					2.54383	1.05455	1.20678	.52403	.59199	.26506	.29851	.13286	.15043
6						1.37281	1.54912	.64287	.73681	.33206	.36574	.16741	.18421
7							1.74414	1.96424	.80197	.87451	.39556	.43354	.20183
8								2.22165	2.54058	.94861	1.02450	.46748	.50208
9									2.91880	1.16240	1.18260	.53652	.57126
10										1.24543	1.35125	.60622	.64144
11										1.44852	1.53380	.67692	.71269
12										1.63176	1.73523	.74777	.78517
13										1.84530	1.96337	.82193	.85986
14										2.09136	2.23191	.89676	.93456
15										2.39892	2.56867	.97244	1.01184
16										2.78085	3.04586	1.05124	1.09120
17											3.41966	1.13175	1.17294
18												1.21479	1.25737
19												1.38071	1.34489
20												1.38997	1.43600
21												1.46567	1.53227
22												1.58068	1.63141
23												1.68358	1.73732
24												1.79279	1.85017
25												1.90965	1.97147
26												2.03591	2.10336
27												2.17403	2.24859
28												2.32756	2.41169
29												2.50193	2.59951
30												2.70616	2.82416
31												2.95694	3.10988
32												3.29160	3.51915
33													3.83115
34													1.14871
35													1.19070
36													1.23541
37													1.27688
38													1.32716
39													1.36633
40													1.41245
41													1.45959
42													1.50784
43													1.55729
44													1.60804
45													1.66022
46													1.71394
47													1.76936
48													1.82666
49													1.88603
50													1.94771
51													2.01195
52													2.07929
53													2.14952
54													2.22368
55													2.30216
56													2.38544
57													2.47514
58													2.57175
59													2.67709
60													2.79238
61													2.92353
62													3.07335
63													3.25087
64													3.46899
65													3.76327

Table A.7 (cont'd) Comparisons for Signal with Gaussian Density (Mean = 0, Variance = 1)

BIT				512				512				512			
LEVEL				0.000001				0.000001				0.000001			
M.S.E.				49.64151				49.64151				49.64151			
S.N.R. (dB)				7.94631				7.94631				7.94631			
ENTROPY				7.94631				7.94631				7.94631			
I	X(I)	Y(I)	I	X(I)	Y(I)	I	X(I)	Y(I)	I	X(I)	Y(I)	I	X(I)	Y(I)	I
1	0.000000	0.000000	65	1.1530	1.1530	1	0.000000	0.000000	65	1.1530	1.1530	193	1.9703	1.9703	1
2	0.16832	0.21279	66	1.1792	1.1792	2	0.008470	0.011671	66	1.1792	1.1792	194	1.9967	1.9967	2
3	0.31666	0.40203	67	1.2053	1.2053	3	0.016894	0.021118	67	1.2053	1.2053	195	2.0232	2.0232	3
4	0.46500	0.58724	68	1.2314	1.2314	4	0.025318	0.033666	68	1.2314	1.2314	196	2.0497	2.0497	4
5	0.61334	0.77245	69	1.2575	1.2575	5	0.033742	0.046214	69	1.2575	1.2575	197	2.0762	2.0762	5
6	0.76168	0.95766	70	1.2836	1.2836	6	0.042166	0.058762	70	1.2836	1.2836	198	2.1027	2.1027	6
7	0.91002	1.14287	71	1.3097	1.3097	7	0.050590	0.071310	71	1.3097	1.3097	199	2.1292	2.1292	7
8	1.05836	1.32808	72	1.3358	1.3358	8	0.059014	0.083858	72	1.3358	1.3358	200	2.1557	2.1557	8
9	1.20670	1.51329	73	1.3619	1.3619	9	0.067438	0.096406	73	1.3619	1.3619	201	2.1822	2.1822	9
10	1.35504	1.69850	74	1.3880	1.3880	10	0.075862	0.108954	74	1.3880	1.3880	202	2.2087	2.2087	10
11	1.50338	1.88371	75	1.4141	1.4141	11	0.084286	0.121502	75	1.4141	1.4141	203	2.2352	2.2352	11
12	1.65172	2.06892	76	1.4402	1.4402	12	0.092710	0.134050	76	1.4402	1.4402	204	2.2617	2.2617	12
13	1.80006	2.25413	77	1.4663	1.4663	13	0.101134	0.146598	77	1.4663	1.4663	205	2.2882	2.2882	13
14	1.94840	2.43934	78	1.4924	1.4924	14	0.109558	0.159146	78	1.4924	1.4924	206	2.3147	2.3147	14
15	2.09674	2.62455	79	1.5185	1.5185	15	0.117982	0.171694	79	1.5185	1.5185	207	2.3412	2.3412	15
16	2.24508	2.80976	80	1.5446	1.5446	16	0.126406	0.184242	80	1.5446	1.5446	208	2.3677	2.3677	16
17	2.39342	2.99497	81	1.5707	1.5707	17	0.134830	0.196790	81	1.5707	1.5707	209	2.3942	2.3942	17
18	2.54176	3.18018	82	1.5968	1.5968	18	0.143254	0.209338	82	1.5968	1.5968	210	2.4207	2.4207	18
19	2.69010	3.36539	83	1.6229	1.6229	19	0.151678	0.221886	83	1.6229	1.6229	211	2.4472	2.4472	19
20	2.83844	3.55060	84	1.6490	1.6490	20	0.160102	0.234434	84	1.6490	1.6490	212	2.4737	2.4737	20
21	2.98678	3.73581	85	1.6751	1.6751	21	0.168526	0.246982	85	1.6751	1.6751	213	2.5002	2.5002	21
22	3.13512	3.92102	86	1.7012	1.7012	22	0.176950	0.259530	86	1.7012	1.7012	214	2.5267	2.5267	22
23	3.28346	4.10623	87	1.7273	1.7273	23	0.185374	0.272078	87	1.7273	1.7273	215	2.5532	2.5532	23
24	3.43180	4.29144	88	1.7534	1.7534	24	0.193798	0.284626	88	1.7534	1.7534	216	2.5797	2.5797	24
25	3.58014	4.47665	89	1.7795	1.7795	25	0.202222	0.297174	89	1.7795	1.7795	217	2.6062	2.6062	25
26	3.72848	4.66186	90	1.8056	1.8056	26	0.210646	0.309722	90	1.8056	1.8056	218	2.6327	2.6327	26
27	3.87682	4.84707	91	1.8317	1.8317	27	0.219070	0.322270	91	1.8317	1.8317	219	2.6592	2.6592	27
28	4.02516	5.03228	92	1.8578	1.8578	28	0.227494	0.334818	92	1.8578	1.8578	220	2.6857	2.6857	28
29	4.17350	5.21749	93	1.8839	1.8839	29	0.235918	0.347366	93	1.8839	1.8839	221	2.7122	2.7122	29
30	4.32184	5.40270	94	1.9100	1.9100	30	0.244342	0.359914	94	1.9100	1.9100	222	2.7387	2.7387	30
31	4.47018	5.58791	95	1.9361	1.9361	31	0.252766	0.372462	95	1.9361	1.9361	223	2.7652	2.7652	31
32	4.61852	5.77312	96	1.9622	1.9622	32	0.261190	0.385010	96	1.9622	1.9622	224	2.7917	2.7917	32
33	4.76686	5.95833	97	1.9883	1.9883	33	0.269614	0.397558	97	1.9883	1.9883	225	2.8182	2.8182	33
34	4.91520	6.14354	98	2.0144	2.0144	34	0.278038	0.410106	98	2.0144	2.0144	226	2.8447	2.8447	34
35	5.06354	6.32875	99	2.0405	2.0405	35	0.286462	0.422654	99	2.0405	2.0405	227	2.8712	2.8712	35
36	5.21188	6.51396	100	2.0666	2.0666	36	0.294886	0.435202	100	2.0666	2.0666	228	2.8977	2.8977	36
37	5.36022	6.69917	101	2.0927	2.0927	37	0.303310	0.447750	101	2.0927	2.0927	229	2.9242	2.9242	37
38	5.50856	6.88438	102	2.1188	2.1188	38	0.311734	0.460298	102	2.1188	2.1188	230	2.9507	2.9507	38
39	5.65690	7.06959	103	2.1449	2.1449	39	0.320158	0.472846	103	2.1449	2.1449	231	2.9772	2.9772	39
40	5.80524	7.25480	104	2.1710	2.1710	40	0.328582	0.485394	104	2.1710	2.1710	232	3.0037	3.0037	40
41	5.95358	7.44001	105	2.1971	2.1971	41	0.337006	0.497942	105	2.1971	2.1971	233	3.0302	3.0302	41
42	6.10192	7.62522	106	2.2232	2.2232	42	0.345430	0.510490	106	2.2232	2.2232	234	3.0567	3.0567	42
43	6.25026	7.81043	107	2.2493	2.2493	43	0.353854	0.523038	107	2.2493	2.2493	235	3.0832	3.0832	43
44	6.39860	8.00000	108	2.2754	2.2754	44	0.362278	0.535586	108	2.2754	2.2754	236	3.1097	3.1097	44
45	6.54694	8.18957	109	2.3015	2.3015	45	0.370702	0.548134	109	2.3015	2.3015	237	3.1362	3.1362	45
46	6.69528	8.37914	110	2.3276	2.3276	46	0.379126	0.560682	110	2.3276	2.3276	238	3.1627	3.1627	46
47	6.84362	8.56871	111	2.3537	2.3537	47	0.387550	0.573230	111	2.3537	2.3537	239	3.1892	3.1892	47
48	6.99196	8.75828	112	2.3798	2.3798	48	0.395974	0.585778	112	2.3798	2.3798	240	3.2157	3.2157	48
49	7.14030	8.94785	113	2.4059	2.4059	49	0.404398	0.598326	113	2.4059	2.4059	241	3.2422	3.2422	49
50	7.28864	9.13742	114	2.4320	2.4320	50	0.412822	0.610874	114	2.4320	2.4320	242	3.2687	3.2687	50
51	7.43698	9.32699	115	2.4581	2.4581	51	0.421246	0.623422	115	2.4581	2.4581	243	3.2952	3.2952	51
52	7.58532	9.51656	116	2.4842	2.4842	52	0.429670	0.635970	116	2.4842	2.4842	244	3.3217	3.3217	52
53	7.73366	9.70613	117	2.5103	2.5103	53	0.438094	0.648518	117	2.5103	2.5103	245	3.3482	3.3482	53
54	7.88200	9.89570	118	2.5364	2.5364	54	0.446518	0.661066	118	2.5364	2.5364	246	3.3747	3.3747	54
55	8.03034	10.08527	119	2.5625	2.5625	55	0.454942	0.673614	119	2.5625	2.5625	247	3.4012	3.4012	55
56	8.17868	10.27484	120	2.5886	2.5886	56	0.463366	0.686162	120	2.5886	2.5886	248	3.4277	3.4277	56
57	8.32702	10.46441	121	2.6147	2.6147	57	0.471790	0.698710	121	2.6147	2.6147	249	3.4542	3.4542	57
58	8.47536	10.65398	122	2.6408	2.6408	58	0.480214	0.711258	122	2.6408	2.6408	250	3.4807	3.4807	58
59	8.62370	10.84355	123	2.6669	2.6669	59	0.488638	0.723806	123	2.6669	2.6669	251	3.5072	3.5072	59
60	8.77204	11.03312	124	2.6930	2.6930	60	0.497062	0.736354	124	2.6930	2.6930	252	3.5337	3.5337	60
61	8.92038	11.22269	125	2.7191	2.7191	61	0.505486	0.748902	125	2.7191	2.7191	253	3.5602	3.5602	61
62	9.06872	11.41226	126	2.7452	2.7452	62	0.513910	0.761450	126	2.7452	2.7452	254	3.5867	3.5867	62
63	9.21706	11.60183	127	2.7713	2.7713	63	0.522334	0.774000	127	2.7713	2.7713	255	3.6132	3.6132	63
64	9.36540	11.79140	128	2.7974	2.7974	64	0.530758	0.786548	128	2.7974	2.7974	256	3.6397	3.6397	64
			129	2.8235	2.8235							257	3.6662	3.6662	

Table A.8 Compandors for Signal with Laplacian Density  
(Mean = 0, Variance = 1)

BIT LEVEL	1	2	3	4	5	6	7
P.S.F.	.00000	.18346	.05714	.01403	.00423	.00108	.00027
S.N.R. (DB)	3.00000	7.36461	12.43290	17.95138	23.73534	29.65610	35.63734
ENTROPY	1.00000	1.83010	2.65434	3.53310	4.46120	5.42113	6.39967

I	X(I)	Y(I)	X(I)	Y(I)	X(I)	Y(I)	X(I)	Y(I)	X(I)	Y(I)	X(I)	Y(I)	X(I)	Y(I)
1	0.00000	.69827	0.00000	.42089	0.00000	.23191	0.00000	.12781	0.00000	.06354	0.00000	.03240	0.00000	.01634
2	1.74617		.94648	1.64677	.49132	.76923	.27310	.39208	.12935	.19664	.06531	.09873	.03286	.04952
3		2.65924			.54271	1.54727	.54271	.70006	.26846	.33865	.13269	.16720	.06628	.08318
4					.87343	2.86814	2.73794	.87343	1.06165	.41339	.49085	.20228	.23795	.11739
5					1.24822	1.44709	.57126	.65483	.27423	.31114	.13470	.15216	.07216	.08756
6					1.75367	2.04562	.74183	.83255	.34871	.38695	.16976	.18750	.09245	.10950
7					2.38425	2.78741	.92732	1.02653	.42590	.46557	.20540	.22345	.11266	.12966
8					3.20560	3.93790	1.13961	1.24005	.50420	.54722	.24166	.26002	.13088	.14750
9					4.08869		1.35545	1.47749	.58925	.63213	.27854	.29723	.15266	.16950
10							1.60699	1.74491	.67590	.72059	.31608	.33510	.17266	.18950
11							1.89241	2.05095	.76624	.81289	.35429	.37366	.19266	.20950
12							2.22231	2.40872	.86060	.90942	.39320	.41293	.21266	.22950
13							2.61312	2.83932	.95935	1.01050	.43285	.45295	.23266	.24950
14							3.06257	3.38019	1.06292	1.11667	.47324	.49375	.25266	.26950
15							3.57102	4.10797	1.17181	1.22863	.51442	.53522	.27266	.28950
16							4.13966	5.22465	1.28660	1.34641	.55462	.57573	.29266	.30950
17							6.12683		1.40795	1.47134	.59926	.62101	.31266	.32950
18									1.53667	1.60408	.64299	.66520	.33266	.34950
19									1.67371	1.74570	.68764	.71032	.35266	.36950
20									1.82021	1.89745	.73324	.75642	.37266	.38950
21									1.97759	2.06089	.77985	.80355	.39266	.40950
22									2.14759	2.25799	.82751	.85175	.41266	.42950
23									2.33241	2.43123	.87626	.89107	.43266	.44950
24									2.53488	2.64385	.92616	.94156	.45266	.46950
25									2.75673	2.88018	.97726	1.00329	.47266	.48950
26									3.00002	3.14619	1.02963	1.05630	.49266	.50950
27									3.26784	3.45039	1.08331	1.11049	.51266	.52950
28									3.56259	3.82565	1.13849	1.16649	.53266	.54950
29									4.00840	4.23260	1.19495	1.22340	.55266	.56950
30									4.48533	4.76771	1.25304	1.28270	.57266	.58950
31									5.00421	5.48507	1.31274	1.34329	.59266	.60950
32									5.56154	6.57711	1.37425	1.40566	.61266	.62950
33									7.44720		1.43755	1.46992	.63266	.64950
34											1.50079	1.53319	.65266	.66950
35											1.57011	1.60459	.67266	.68950
36											1.63964	1.67527	.69266	.70950
37											1.71152	1.74839	.71266	.72950
38											1.78592	1.82412	.73266	.74950
39											1.86303	1.90266	.75266	.76950
40											1.94384	1.98421	.77266	.78950
41											2.02820	2.06903	.79266	.80950
42											2.11274	2.15734	.81266	.82950
43											2.20297	2.24957	.83266	.84950
44											2.29721	2.34594	.85266	.86950
45											2.39583	2.44691	.87266	.88950
46											2.49925	2.55292	.89266	.90950
47											2.60798	2.66451	.91266	.92950
48											2.72259	2.78230	.93266	.94950
49											2.84374	2.90701	.95266	.96950
50											2.97223	3.03952	.97266	.98950
51											3.10901	3.18084	.99266	1.00950
52											3.25522	3.33224		
53											3.41226	3.49537		
54											3.58187	3.67204		
55											3.76621	3.86477		
56											3.96612	4.07677		
57											4.19129	4.31234		
58											4.44072	4.57734		
59											4.72344	4.88132		
60											5.04972	5.23284		
61											5.43547	5.65830		
62											5.88732	6.14950		
63											6.41586	6.75981		
64											7.03814	7.47539		
65											8.02549			



Table A.8 (cont'd) Comparators for Signal with Laplacian Density (Mean = 0, Variance = 1)

X			Y		
BIT	256		512		
LEVEL	0.00002		0.00002		
R.S.E.	41.64382		47.65160		
ENTROPY	7.35843		8.38272		

I	X(I)	Y(I)	I	X(I)	Y(I)	I	X(I)	Y(I)	I	X(I)	Y(I)	I	X(I)	Y(I)	I	X(I)	Y(I)
1	0.000000	.0082760	65	1.4535	1.4698	1	0.000000	.0041304	65	.60739	.61280	129	1.4618	1.4709	193	2.9151	2.9314
2	.016504	.024805	66	1.4863	1.5030	2	.0082688	.017415	66	.61841	.62394	130	1.4783	1.4866	194	2.9479	2.9646
3	.033138	.041504	67	1.5147	1.5366	3	.0165370	.020733	67	.62859	.63505	131	1.4949	1.5033	195	2.9813	2.9982
4	.049803	.058335	68	1.5537	1.5708	4	.024904	.027083	68	.64062	.64671	132	1.5117	1.5201	196	3.0152	3.0326
5	.066480	.075301	69	1.5881	1.6056	5	.033270	.037468	69	.65181	.65743	133	1.5286	1.5371	197	3.0497	3.0671
6	.083136	.092404	70	1.6237	1.6409	6	.041630	.045883	70	.66306	.66831	134	1.5456	1.5542	198	3.0847	3.1025
7	.10101	.10785	71	1.6588	1.6760	7	.050023	.054313	71	.67437	.67905	135	1.5628	1.5714	199	3.1204	3.1385
8	.11832	.12701	72	1.6933	1.7114	8	.058470	.062815	72	.68574	.69045	136	1.5801	1.5888	200	3.1566	3.1750
9	.13527	.14436	73	1.7319	1.7508	9	.066902	.071334	73	.69718	.70292	137	1.5975	1.6063	201	3.1935	3.2121
10	.15337	.16273	74	1.7694	1.7885	10	.075408	.079845	74	.70867	.71444	138	1.6151	1.6240	202	3.2310	3.2500
11	.17117	.18005	75	1.8078	1.8270	11	.084125	.088473	75	.72023	.72603	139	1.6329	1.6418	203	3.2692	3.2885
12	.18902	.19802	76	1.8465	1.8663	12	.092780	.097095	76	.73185	.73769	140	1.6508	1.6598	204	3.3081	3.3278
13	.20707	.21615	77	1.8862	1.9063	13	.10142	.10573	77	.74354	.74940	141	1.6688	1.6779	205	3.3477	3.3678
14	.22527	.23443	78	1.9266	1.9470	14	.11009	.11444	78	.75529	.76118	142	1.6870	1.6962	206	3.3881	3.4085
15	.24361	.25287	79	1.9677	1.9886	15	.11880	.12317	79	.76710	.77303	143	1.7054	1.7146	207	3.4292	3.4501
16	.26215	.27147	80	2.0097	2.0310	16	.12755	.13194	80	.77898	.78495	144	1.7239	1.7332	208	3.4717	3.4925
17	.28084	.29024	81	2.0525	2.0743	17	.13633	.14074	81	.79093	.79693	145	1.7426	1.7520	209	3.5160	3.5372
18	.29969	.30918	82	2.0962	2.1184	18	.14515	.14957	82	.80295	.80896	146	1.7614	1.7709	210	3.5617	3.5839
19	.31871	.32828	83	2.1409	2.1635	19	.15401	.15845	83	.81503	.82110	147	1.7805	1.7900	211	3.6083	3.6310
20	.33790	.34756	84	2.1865	2.2096	20	.16290	.16736	84	.82718	.83329	148	1.7997	1.8093	212	3.6567	3.6791
21	.35727	.36702	85	2.2331	2.2567	21	.17183	.17631	85	.83941	.84554	149	1.8190	1.8288	213	3.6965	3.7187
22	.37681	.38665	86	2.2807	2.3049	22	.18080	.18530	86	.85170	.85787	150	1.8385	1.8484	214	3.7421	3.7643
23	.39654	.40647	87	2.3294	2.3547	23	.18980	.19432	87	.86407	.87028	151	1.8580	1.8680	215	3.7908	3.8136
24	.41645	.42648	88	2.3793	2.4047	24	.19885	.20338	88	.87651	.88275	152	1.8777	1.8878	216	3.8407	3.8641
25	.43655	.44668	89	2.4304	2.4568	25	.20793	.21249	89	.88902	.89530	153	1.8973	1.9075	217	3.8917	3.9157
26	.45685	.46707	90	2.4827	2.5095	26	.21705	.22163	90	.90160	.90792	154	1.9186	1.9288	218	3.9441	3.9707
27	.47734	.48766	91	2.5364	2.5637	27	.22622	.23081	91	.91426	.92062	155	1.9399	1.9499	219	3.9977	4.0251
28	.49801	.50845	92	2.5914	2.6193	28	.23542	.24003	92	.92700	.93340	156	1.9598	1.9699	220	4.0528	4.0808
29	.51887	.52944	93	2.6480	2.6769	29	.24466	.24929	93	.93982	.94625	157	1.9806	1.9907	221	4.1093	4.1381
30	.53992	.55065	94	2.7060	2.7357	30	.25394	.25860	94	.95271	.95918	158	2.0017	2.0124	222	4.1673	4.1969
31	.56113	.57207	95	2.7657	2.7962	31	.26326	.26794	95	.96568	.97219	159	2.0231	2.0338	223	4.2270	4.2575
32	.58266	.59371	96	2.8272	2.8586	32	.27263	.27732	96	.97873	.98526	160	2.0446	2.0554	224	4.2884	4.3194
33	.60441	.61557	97	2.8904	2.9228	33	.28203	.28675	97	.99186	.99846	161	2.0663	2.0773	225	4.3517	4.3840
34	.62639	.63766	98	2.9556	2.9886	34	.29145	.29622	98	1.0051	1.0117	162	2.0883	2.0994	226	4.4168	4.4502
35	.64859	.65998	99	3.0229	3.0574	35	.30097	.30579	99	1.0184	1.0251	163	2.1105	2.1217	227	4.4841	4.5185
36	.67101	.68255	100	3.0924	3.1280	36	.31050	.31528	100	1.0318	1.0385	164	2.1329	2.1443	228	4.5535	4.5891
37	.69363	.70534	101	3.1642	3.2011	37	.32003	.32483	101	1.0453	1.0520	165	2.1556	2.1671	229	4.6254	4.6622
38	.71645	.72833	102	3.2385	3.2768	38	.32968	.33452	102	1.0588	1.0656	166	2.1785	2.1901	230	4.6997	4.7378
39	.74001	.75210	103	3.3156	3.3557	39	.33936	.34420	103	1.0724	1.0793	167	2.2017	2.2134	241	4.7767	4.8163
40	.76355	.77576	104	3.3958	3.4387	40	.34906	.35393	104	1.0861	1.0930	168	2.2251	2.2370	232	4.8566	4.8975
41	.78714	.79909	105	3.4787	3.5235	41	.35881	.36371	105	1.0999	1.1068	169	2.2488	2.2608	233	4.9397	4.9825
42	.81110	.82318	106	3.5652	3.6108	42	.36861	.37353	106	1.1139	1.1208	170	2.2728	2.2849	234	5.0261	5.0707
43	.83537	.84756	107	3.6553	3.7019	43	.37845	.38339	107	1.1279	1.1349	171	2.2970	2.3092	235	5.1162	5.1628
44	.85995	.87221	108	3.7495	3.7982	44	.38834	.39330	108	1.1419	1.1490	172	2.3215	2.3339	236	5.2103	5.2590
45	.88485	.89714	109	3.8480	3.8990	45	.39827	.40326	109	1.1561	1.1633	173	2.3463	2.3588	237	5.3088	5.3598
46	.90975	.92240	110	3.9517	4.0050	46	.40828	.41326	110	1.1705	1.1778	174	2.3714	2.3841	238	5.4121	5.4657
47	.93514	.94795	111	4.0600	4.1164	47	.41836	.42331	111	1.1848	1.1920	175	2.3968	2.4096	239	5.5207	5.5771
48	.96094	.97381	112	4.1745	4.2333	48	.42846	.43341	112	1.1993	1.2065	176	2.4225	2.4355	240	5.6351	5.6947
49	.98686	.99999	113	4.2955	4.3567	49	.43868	.44366	113	1.2138	1.2212	177	2.4485	2.4617	241	5.7560	5.8192
50	1.0132	1.0285	114	4.4238	4.4870	50	.44885	.45386	114	1.2285	1.2359	178	2.4749	2.4882	242	5.8843	5.9514
51	1.0399	1.0533	115	4.5604	4.6262	51	.45907	.46409	115	1.2433	1.2507	179	2.5015	2.5150	243	6.0208	6.0925
52	1.0669	1.0805	116	4.7065	4.7848	52	.46934	.47438	116	1.2582	1.2657	180	2.5285	2.5422	244	6.1647	6.2436
53	1.0942	1.1081	117	4.8633	4.9543	53	.47967	.48474	117	1.2732	1.2807	181	2.5559	2.5697	245	6.3174	6.4035
54	1.1220	1.1360	118	5.0326	5.1277	54	.48994	.49504	118	1.2883	1.2958	182	2.5836	2.5976	246	6.4796	6.5725
55	1.1501	1.1642	119	5.2147	5.3151	55	.50026	.50539	119	1.3035	1.3111	183	2.6117	2.6259	247	6.6506	6.7547
56	1.1785	1.1929	120	5.4182	5.5267	56	.51063	.51579	120	1.3187	1.3265	184	2.6402	2.6545	248	6.8779	6.9861
57	1.2074	1.2221	121	5.6409	5.7617	57	.52106	.52634	121	1.3342	1.3421	185	2.6690	2.6834	249	7.1002	7.2208
58	1.2366	1.2514	122	5.8898	6.0762	58	.53153	.53714	122	1.3497	1.3577	186	2.6982	2.7130	250	7.3697	7.5049
59	1.2663	1.2817	123	6.1718	6.3743	59	.54207	.54780	123	1.3654	1.3735	187	2.7279	2.7429	251	7.6903	7.8401
60	1.2963	1.3125	124	6.4922	6.8097	60	.55267	.55853	124	1.3813	1.3895	188	2.7580	2.7732	252	7.9551	8.1342
61	1.3268	1.3437	125	6.8614	7.1936	61	.56334	.56928	125	1.3970	1.4050	189	2.7885	2.8039	253	8.3357	8.5401
62	1.3578	1.3755	126	7.3515	7.8423	62	.57408	.58010	126	1.4130	1.4211	190	2.8194	2.8351	254	8.8074	9.0873
63	1.3892	1.4081	127	7.9599	8.5547	63	.58489	.59097	127	1.4292	1.4373	191	2.8508	2.8667	255	9.4098	9.7904
64	1.4211	1.4372	128	8.8045	9.4933	64	.59563	.60191	128	1.4456	1.4536	192	2.8827	2.8988	256	10.254	10.865
			129	10.241											257	11.479	

Table A.9I Analytic Models for Some Often Used Quantizers for  
Unity Variance Probability Density Functions

Quantizer	Probability Density	Mean Square Error Model, $f(n)$ $n$ = number of bits $2^n$ = number of levels
Shannon	Arbitrary, Unity Variance	$f(n) = 2^{-2n}, n \geq 0$
Optimum Nonuniform	Gaussian $N(0,1)$ $\frac{1}{\sqrt{2\pi}} \exp(-x^2/2)$	$f(n) = \begin{cases} 2^{-1.5047n}, & 0 \leq 2^n < 5 \\ 1.5253 \cdot 2^{-1.8274n}, & 5 \leq 2^n < 36 \\ 2.2573 \cdot 2^{-1.9626n}, & 36 \leq 2^n \leq 512 \end{cases}$
Optimum Nonuniform	Laplacian Unity Variance $\frac{1}{\sqrt{2}} \exp(-\sqrt{2} x )$	$f(n) = \begin{cases} 2^{-1.1711n}, & 0 \leq 2^n < 5 \\ 2.0851 \cdot 2^{-1.7645n}, & 5 \leq 2^n < 36 \\ 3.6308 \cdot 2^{-1.9572n}, & 36 \leq 2^n \leq 512 \end{cases}$
Optimum Nonuniform	Gaussian $N(0,1)$ $\frac{1}{\sqrt{2\pi}} \exp(-x^2/2)$	$f(n) = \begin{cases} 2^{-1.5012n}, & 0 \leq 2^n < 5 \\ 1.2477 \cdot 2^{-1.6883n}, & 5 \leq 2^n < 36 \\ 1.5414 \cdot 2^{-1.7562n}, & 36 \leq 2^n \leq 512 \end{cases}$
Optimum Uniform	Laplacian Unity Variance $\frac{1}{\sqrt{2}} \exp(-\sqrt{2} x )$	$f(n) = \begin{cases} 2^{-1.1619n}, & 0 \leq 2^n < 5 \\ 1.4156 \cdot 2^{-1.4518n}, & 5 \leq 2^n < 36 \\ 2.1969 \cdot 2^{-1.5944n}, & 36 \leq 2^n \leq 512 \end{cases}$
Approximate Optimum Nonuniform (Compander)	Gaussian $N(0,1)$ $\frac{1}{\sqrt{2\pi}} \exp(-x^2/2)$	$f(n) = \begin{cases} 2^{-1.4864n}, & 0 \leq 2^n < 5 \\ 1.5597 \cdot 2^{-1.8239n}, & 5 \leq 2^n < 36 \\ 0.2677 \cdot 2^{-1.357n}, & 36 \leq 2^n \leq 512 \end{cases}$
Approximate Optimum Nonuniform (Compander)	Laplacian Unity Variance $\frac{1}{\sqrt{2}} \exp(-\sqrt{2} x )$	$f(n) = \begin{cases} 2^{-1.1491n}, & 0 \leq 2^n < 5 \\ 2.2164 \cdot 2^{-1.7710n}, & 5 \leq 2^n < 36 \\ 4.2461 \cdot 2^{-1.9928n}, & 36 \leq 2^n \leq 512 \end{cases}$

Table A.9II Formulas for  $h(x)$  for Different Quantizers

Quantizer	$h(x) = f'(x)^{-1}$
Shannon	$h(x) = -\frac{1}{2} \log_2(-x/2 \log_e 2) \quad \text{all } x < 0$
Optimum Nonuniform (Gaussian Density)	$h(x) = \begin{cases} 0.0403 - 0.6646 \log_2(-x), & -1.0430 \leq x < -0.1020 \\ 0.5199 - 0.5472 \log_2(-x), & -0.1020 \leq x < -0.0027 \\ 0.8247 - 0.5195 \log_2(-x), & -0.0027 \leq x \leq -1.48 \times 10^{-5} \end{cases}$
Optimum Nonuniform (Laplacian Density)	$h(x) = \begin{cases} -0.2569 - 0.8539 \log_2(-x), & -0.8117 \leq x < -0.1490 \\ 0.7654 - 0.5667 \log_2(-x), & -0.1490 \leq x < -0.0044 \\ 1.1753 - 0.5109 \log_2(-x), & -0.0044 \leq x \leq -2.45 \times 10^{-5} \end{cases}$
Optimum Uniform (Gaussian Density)	$h(x) = \begin{cases} 0.0382 - 0.6661 \log_2(-x), & -1.0406 \leq x < -0.0965 \\ 0.3234 - 0.5923 \log_2(-x), & -0.0965 \leq x < -0.0035 \\ 0.5170 - 0.5694 \log_2(-x), & -0.0035 \leq x \leq -3.28 \times 10^{-5} \end{cases}$
Optimum Uniform (Laplacian Density)	$h(x) = \begin{cases} -0.2688 - 0.8607 \log_2(-x), & -0.8054 \leq x < -0.1377 \\ 0.3516 - 0.6888 \log_2(-x), & -0.1377 \leq x < -0.0080 \\ 0.8026 - 0.6272 \log_2(-x), & -0.0080 \leq x \leq -1.16 \times 10^{-4} \end{cases}$
Approximate Optimum Nonuniform (Gaussian Density)	$h(x) = \begin{cases} 0.0290 - 0.6728 \log_2(-x), & -1.0303 \leq x < -0.1047 \\ 0.5371 - 0.5483 \log_2(-x), & -0.1047 \leq x < -0.0019 \\ -1.4658 - 0.7368 \log_2(-x), & -0.0019 \leq x \leq -5.29 \times 10^{-5} \end{cases}$
Approximate Optimum Nonuniform (Laplacian Density)	$h(x) = \begin{cases} -0.2857 - 0.8702 \log_2(-x), & -0.7965 \leq x < -0.1573 \\ 0.8154 - 0.5647 \log_2(-x), & -0.1573 \leq x < -0.0046 \\ 4.2461 - 0.5018 \log_2(-x), & -0.0046 \leq x \leq -2.34 \times 10^{-5} \end{cases}$



Table A.10 Optimum Nonuniform Quantizers with Quantization Levels  $N = 2, \dots, 36$   
for Signal with Gaussian Density (Mean = 0, Variance = 1)

LEVEL	2	3	4	5	6	7	8
M.S.E.	.36338	.19017	.11748	.079941	.057978	.044000	.034548
S.N.R. (dB)	6.3944	7.2985	9.3003	10.972	12.367	13.565	14.616
ENTROPY	1.0000	1.5358	1.9111	2.2029	2.4428	2.6469	2.8268

	X(1)	Y(1)	X(1)	Y(1)	X(1)	Y(1)	X(1)	Y(1)	X(1)	Y(1)	X(1)	Y(1)	X(1)	Y(1)
1	0.00000	.79788	.61201	0.00000	0.00000	.45279	.38230	0.00000	0.00000	.31773	.28030	0.00000	0.00000	.24511
2			1.2240	.98162	1.5104	1.2444	.76459	.65894	1.0001	.87440	.56060	.50059	.75605	
3							1.7242	1.4469	1.8936	1.6108	1.1882	1.0500	1.3440	
4											2.0334	1.7480	2.1520	

LEVEL	9	10	11	12	13	14	15
M.S.E.	.027853	.022937	.019220	.016340	.014063	.012232	.010737
S.N.R. (dB)	15.551	16.395	17.163	17.668	18.519	19.125	19.691
ENTROPY	2.9826	3.1245	3.2534	3.3716	3.4806	3.5819	3.6765

	X(1)	Y(1)	X(1)	Y(1)	X(1)	Y(1)	X(1)	Y(1)	X(1)	Y(1)	X(1)	Y(1)	X(1)	Y(1)
1	.22184	0.00000	0.00000	.19965	.18376	0.00000	0.00000	.16847	.15692	0.00000	0.00000	.14574	.13696	0.00000
2	.68128	.44368	.40479	.60992	.55999	.36751	.34020	.53193	.47619	.31383	.29358	.44342	.41442	.27393
3	1.1977	.91886	.83393	1.0579	.96571	.75246	.69442	.87699	.81274	.63836	.59601	.75059	.70312	.55490
4	1.8656	1.4765	1.3247	1.5914	1.4359	1.1789	1.0814	1.2859	1.1843	.98710	.91821	1.6858	1.6132	.85132
5		2.2547	1.9683	2.3452	2.0593	1.6928	1.5345	1.7832	1.6231	1.3314	1.2768	1.4677	1.3607	1.1751
6						2.4259	2.1409	2.4986	2.2147	1.8647	1.7033	1.9388	1.7765	1.5463
7										2.5647	2.2820	2.6253	2.3439	2.0067
8														2.6811

LEVEL	16	17	18	19	20	21	22
M.S.E.	.0095010	.0084669	.0075932	.0068482	.0062078	.0056533	.0051700
S.N.R. (dB)	20.222	20.723	21.196	21.644	22.071	22.477	22.865
ENTROPY	3.7652	3.8486	3.9275	4.0023	4.0773	4.1410	4.2056

	X(1)	Y(1)	X(1)	Y(1)	X(1)	Y(1)	X(1)	Y(1)	X(1)	Y(1)	X(1)	Y(1)	X(1)	Y(1)
1	0.00000	.12843	.12154	0.00000	0.00000	.11481	.10925	0.00000	0.00000	.10381	.099228	0.00000	0.00000	.94738
2	.25830	.18816	.36706	.24307	.23064	.36647	.32952	.21850	.20837	.31293	.29900	.19845	.19005	.28535
3	.52255	.65693	.62028	.49104	.46549	.58450	.55529	.44053	.41983	.52671	.50286	.39955	.38242	.47948
4	.79975	.94256	.88769	.74950	.70932	.83413	.79102	.67004	.63778	.74883	.71399	.60617	.57964	.67982
5	1.0995	1.2565	1.1785	1.0259	.96828	1.1024	1.0426	.91193	.86643	.98490	.93638	.82179	.78476	.88968
6	1.4374	1.6183	1.5080	1.3312	1.2513	1.4062	1.3187	1.1732	1.1114	1.2789	1.1756	1.0510	1.0016	1.1135
7	1.8438	2.0593	1.9060	1.6848	1.5733	1.7564	1.6360	1.4642	1.3814	1.5238	1.4399	1.3002	1.2355	1.3576
8	2.4011	2.7328	2.4542	2.1273	1.9638	2.1813	2.0177	1.8037	1.6906	1.8574	1.7437	1.5797	1.4949	1.6321
9				2.7816	2.5017	2.8261	2.5501	2.2317	2.0693	2.2791	2.1158	1.9078	1.7937	1.9533
10								2.8684	2.5937	2.9083	2.6349	2.3237	2.1606	2.3659
11												2.9460	2.6738	2.9817

Table A.10 (cont'd) Optimum Nonuniform Quantizers with Quantization Levels  $N = 2, \dots, 36$   
for Signal with Gaussian Density (Mean = 0, Variance = 1)

LEVEL	23	24	25	26	27	28	29
M.S.E.	.0047462	.0043725	.0040413	.0037464	.0034826	.0032458	.0030323
S.N.R. (DB)	23.237	23.593	23.935	24.264	24.581	24.887	25.182
ENTROPY	4.2675	4.3267	4.3837	4.4384	4.4911	4.5420	4.5911

I	X(I)	Y(I)	X(I)	Y(I)	X(I)	Y(I)	X(I)	Y(I)	X(I)	Y(I)	X(I)	Y(I)	X(I)	Y(I)
1	.090899	0.00000	0.00000	.087128	.083864	0.00000	0.00000	.080654	.077844	0.00000	0.00000	.075078	.072635	0.00000
2	.27371	.18180	.17470	.26227	.25348	.16773	.16166	.24266	.23416	.15569	.15044	.22580	.21842	.14527
3	.45963	.36561	.35120	.44013	.42333	.33704	.32474	.40681	.39242	.31264	.30202	.37824	.36576	.29156
4	.65103	.55364	.53144	.62274	.59852	.50962	.49076	.57469	.55402	.47219	.45595	.53366	.51580	.43995
5	.85077	.74841	.71764	.81254	.78007	.68740	.66142	.74813	.72060	.63584	.61358	.69348	.66981	.59163
6	1.0626	.95312	.91258	1.0126	.97067	.87273	.83877	.92940	.89414	.80535	.77646	.85942	.82931	.74797
7	1.2918	1.1721	1.1199	1.2272	1.1739	1.0686	1.0254	1.1214	1.0772	.98292	.94652	1.0336	.99619	.91063
8	1.5466	1.4116	1.3448	1.4624	1.3949	1.2792	1.2249	1.3263	1.2732	1.1715	1.1263	1.2189	1.1729	1.0817
9	1.8408	1.6816	1.5954	1.7283	1.6416	1.5105	1.4423	1.5561	1.4872	1.3750	1.3191	1.4193	1.3628	1.2640
10	2.2029	2.0001	1.8854	2.0426	1.9277	1.7725	1.6854	1.8146	1.7270	1.5995	1.5300	1.6407	1.5708	1.4615
11	2.7107	2.4058	2.2431	2.4437	2.2813	2.0829	1.9679	2.1213	2.0062	1.8546	1.7668	1.8928	1.8047	1.6501
12		3.0156	2.7458	3.0479	2.7792	2.4797	2.3177	2.5141	2.3524	2.1578	2.0428	2.1928	2.0778	1.9293
13						3.0787	2.8111	3.1081	2.8416	2.5470	2.3855	2.5744	2.4174	2.2763
14														
15										3.1363	2.8709	3.1634	2.8989	2.6085
														3.1893

LEVEL	30	31	32	33	34	35	36
M.S.E.	.0028393	.0026641	.0025047	.0023591	.0022259	.0021037	.0019913
S.N.R. (DB)	25.468	25.744	26.012	26.272	26.525	26.770	27.009
ENTROPY	4.6386	4.6856	4.7291	4.7723	4.8142	4.8550	4.8946

I	X(I)	Y(I)	X(I)	Y(I)	X(I)	Y(I)	X(I)	Y(I)	X(I)	Y(I)	X(I)	Y(I)	X(I)	Y(I)
1	0.00000	.070226	.068081	0.00000	0.00000	.065965	.064067	0.00000	0.00000	.062193	.060503	0.00000	0.00000	.058832
2	.14068	.21114	.20467	.13616	.13212	.19828	.19255	.12813	.12555	.18690	.18180	.12100	.11780	.17676
3	.28230	.35346	.34253	.27316	.26502	.33175	.32210	.25697	.24974	.31257	.30400	.24260	.23614	.29552
4	.42583	.49819	.48260	.41189	.39948	.46721	.45347	.38723	.37624	.43990	.42771	.36539	.35559	.41566
5	.57233	.64647	.62589	.55329	.53639	.60557	.58740	.51971	.50478	.56964	.55364	.49003	.47675	.53783
6	.72305	.79962	.77359	.69847	.67674	.74789	.72513	.65528	.63615	.70264	.68256	.61723	.60027	.66271
7	.87936	.95978	.92714	.84870	.82166	.89542	.86749	.79496	.77127	.83789	.81536	.74786	.72641	.79111
8	1.0434	1.1275	1.0884	1.0056	.97258	1.0497	1.0160	.93999	.91125	.98259	.95312	.88284	.85755	.92398
9	1.2173	1.3071	1.2596	1.1711	1.1313	1.2128	1.1773	1.0919	1.0574	1.1323	1.0972	1.0234	.99325	1.0625
10	1.4045	1.5019	1.4443	1.3481	1.3001	1.3874	1.3389	1.2527	1.2116	1.2909	1.2493	1.1710	1.1353	1.2041
11	1.6098	1.7177	1.6471	1.5404	1.4824	1.5773	1.5189	1.4250	1.3760	1.4611	1.4117	1.3276	1.2855	1.3628
12	1.8410	1.9642	1.8757	1.7538	1.6828	1.7881	1.7171	1.6137	1.5539	1.6367	1.5876	1.4958	1.4460	1.5292
13	2.1113	2.2584	2.1434	1.9977	1.9091	2.0298	1.9411	1.8215	1.7501	1.8334	1.7818	1.6794	1.6201	1.7110
14	2.4479	2.6375	2.4772	2.2892	2.1743	2.3188	2.2040	2.0607	1.9720	2.0905	2.0017	1.8842	1.8124	1.9138
15	2.9259	3.2143	2.9518	2.6653	2.5054	2.6921	2.5326	2.3473	2.2324	2.3748	2.2602	2.1192	2.0303	2.1469
16														
17														
18														

Table A.11 Optimum Nonuniform Quantizers with Quantization Levels  $N = 2, \dots, 36$  for Signal with Laplacian Density (Mean = 0, Variance = 1)

LEVEL	2	3	4	5	6	7	8
M.S.E.	.50000	.26424	.17619	.11981	.089868	.068088	.054476
S.N.R. (dB)	3.0103	5.7800	7.5401	9.2152	10.464	11.669	12.638
ENTROPY	1.1000	1.3169	1.7287	1.9466	2.2071	2.3745	2.5654

I	X(I)	Y(I)	X(I)	Y(I)	X(I)	Y(I)	X(I)	Y(I)	X(I)	Y(I)	X(I)	Y(I)	X(I)	Y(I)
1	0.00000	.70711	.70712	0.00000	0.00000	.41976	.41977	0.00000	0.00000	.29979	.29979	0.00000	0.00000	.23341
2			.14142	1.1269	1.8340	1.5467	.83953	.71936	1.1393	1.0194	.59958	.53321	.83299	
3							2.2538	1.8464	2.5535	2.1462		1.4391	1.2528	1.6725
4											2.8533	2.3797	3.0868	

LEVEL	9	10	11	12	13	14	15
M.S.E.	.043850	.036545	.030580	.026213	.022536	.019720	.017293
S.N.R. (dB)	13.580	14.372	15.146	15.815	16.471	17.051	17.621
ENTROPY	2.7011	2.8519	2.9661	3.0707	3.1893	3.2955	3.3822

I	X(I)	Y(I)	X(I)	Y(I)	X(I)	Y(I)	X(I)	Y(I)	X(I)	Y(I)	X(I)	Y(I)	X(I)	Y(I)
1	.23342	0.00000	0.00000	.19118	.19118	0.00000	0.00000	.16192	.16192	0.00000	0.00000	.14044	.14045	0.00000
2	.78663	.46683	.42460	.65801	.61578	.38236	.35310	.54429	.51503	.32385	.30237	.46429	.44282	.28989
3	1.4862	1.0664	.95781	1.2576	1.1490	.84920	.77771	1.0111	.93964	.70672	.65548	.84667	.79594	.60474
4	2.6131	1.9060	1.6774	2.0971	1.8686	1.4488	1.3109	1.6107	1.4729	1.1731	1.0801	1.3135	1.2206	.98712
5		3.3202	2.8043	3.5114	2.9955	2.2883	2.0305	2.4303	2.1924	1.7727	1.6133	1.9131	1.7538	1.4540
6						3.7026	3.1574	3.8645	3.3193	2.6122	2.3329	2.7527	2.4733	2.0536
7										4.0264	3.4598	4.1669	3.6002	2.8931
8														4.3073

LEVEL	16	17	18	19	20	21	22
M.S.E.	.015373	.013688	.012320	.011104	.010094	.0091873	.0084219
S.N.R. (dB)	18.133	18.636	19.094	19.545	19.959	20.368	20.746
ENTROPY	3.4747	3.5521	3.6341	3.7040	3.7776	3.8413	3.9081

I	X(I)	Y(I)	X(I)	Y(I)	X(I)	Y(I)	X(I)	Y(I)	X(I)	Y(I)	X(I)	Y(I)	X(I)	Y(I)
1	0.00000	.17400	.17401	0.00000	0.00000	.11102	.11102	0.00000	0.00000	.10049	.10050	0.00000	0.00000	.091795
2	.76445	.40490	.38347	.24801	.23503	.35903	.34605	.22204	.21151	.32253	.31207	.20099	.19229	.29279
3	.56683	.72876	.69085	.52891	.49949	.63974	.61052	.47006	.44455	.57056	.54706	.42304	.40382	.51484
4	.91995	1.1111	1.0440	.85278	.80188	.96380	.91291	.75097	.71102	.85148	.81153	.67107	.63686	.76288
5	1.3446	1.5780	1.4686	1.2352	1.1550	1.3467	1.2660	1.0748	1.0134	1.1753	1.1139	.95199	.90334	1.0438
6	1.8778	2.1776	2.0018	1.7020	1.5796	1.8130	1.6907	1.4572	1.3665	1.5577	1.4671	1.2759	1.2057	1.3677
7	2.5974	3.0171	2.7214	2.3016	2.1179	2.4126	2.2239	1.9241	1.7912	2.0246	1.8917	1.6583	1.5589	1.7501
8	3.7243	4.4314	3.8483	3.1412	2.8374	3.2522	2.9435	2.5237	2.3244	2.6242	2.4249	2.1251	1.9835	2.2149
9				4.5554	3.9573	4.6664	4.0704	3.3632	3.0449	3.4637	3.1445	2.7247	2.5167	2.8165
10								4.7775	4.1709	4.8780	4.2714	3.5643	3.2363	3.6561
11												4.9785	4.3632	5.0703



Table A.11 (cont'd) Optimum Nonuniform Quantizers with Quantization Levels  $N = 2, \dots, 36$   
for Signal with Laplacian Density (Mean = 0, Variance = 1)

LEVEL	23	24	25	26	27	28	29
M.S.E.	.0077275	.0071332	.0065898	.0061192	.0056861	.0053071	.0049563
S.N.R.(dB)	21.120	21.467	21.611	22.131	22.452	22.751	23.048
ENTROPY	3.9666	4.0277	4.0819	4.1382	4.1886	4.2403	4.2879

1	X(1)	Y(1)	X(1)	Y(1)	X(1)	Y(1)	X(1)	Y(1)	X(1)	Y(1)	X(1)	Y(1)	X(1)	Y(1)
1	.091798	0.00000	0.00000	.084484	.084487	0.00000	0.00000	.078253	.078257	0.00000	0.00000	.072880	.072883	0.00000
2	.28410	.18360	.17629	.26808	.26078	.16897	.16274	.24723	.24101	.15651	.15114	.22940	.22403	.14577
3	.49563	.38460	.36859	.46909	.45309	.35258	.33904	.43054	.41731	.32550	.31389	.39839	.38679	.30229
4	.73068	.60665	.58012	.69115	.66462	.55359	.53135	.63186	.60963	.50911	.49020	.58201	.56310	.47128
5	.99516	.85469	.81518	.93919	.89968	.77565	.74289	.85392	.82117	.71013	.68252	.78303	.75542	.65491
6	1.2976	1.1356	1.0797	1.2201	1.1642	1.0237	.97795	1.1020	1.0562	.93220	.89407	1.0051	.96628	.85593
7	1.6507	1.4595	1.3821	1.5440	1.4666	1.3046	1.2474	1.3629	1.3207	1.1803	1.1291	1.2532	1.2070	1.0780
8	2.0753	1.8419	1.7352	1.9264	1.8197	1.6285	1.5448	1.7068	1.6231	1.4612	1.3936	1.5341	1.4665	1.3261
9	2.6085	2.3087	2.1598	2.3732	2.2443	2.0109	1.8980	2.0892	1.9763	1.7851	1.6960	1.8580	1.7689	1.6070
10	3.3281	2.9083	2.6931	2.9929	2.7776	2.4778	2.3226	2.5560	2.4009	2.1675	2.0492	2.2404	2.1221	1.9309
11	4.4550	3.7479	3.4126	3.8374	3.4971	3.0774	2.8558	3.1556	2.9341	2.6343	2.4738	2.7072	2.5467	2.3133
12		5.1621	4.5395	5.2466	4.6240	3.9169	3.5754	3.9952	3.6537	3.2339	3.0070	3.3068	3.0799	2.7801
13						5.3311	4.7073	5.4094	4.7806	4.0735	3.7266	4.1464	3.7995	3.3797
14										5.4877	4.8535	5.5606	4.9264	4.2193
15														5.6335

LEVEL	30	31	32	33	34	35	36
M.S.E.	.0046466	.0043585	.0041022	.0038627	.0036481	.0034469	.0032655
S.N.R.(dB)	23.329	23.607	23.870	24.131	24.379	24.626	24.860
ENTROPY	4.3366	4.3808	4.4264	4.4660	4.5109	4.5503	4.5907

1	X(1)	Y(1)	X(1)	Y(1)	X(1)	Y(1)	X(1)	Y(1)	X(1)	Y(1)	X(1)	Y(1)	X(1)	Y(1)
1	0.00000	.058198	.068201	0.00000	0.00000	.064082	.064085	0.00000	0.00000	.060435	.060439	0.00000	0.00000	.057182
2	.14108	.21397	.20929	.13640	.13229	.20049	.19638	.12517	.12452	.18861	.18497	.12088	.11762	.17806
3	.29223	.37050	.36045	.28218	.27738	.34627	.33248	.26458	.25682	.32503	.31727	.24906	.24216	.30625
4	.45500	.53950	.52322	.43871	.42454	.50281	.48864	.41037	.39793	.47082	.45838	.38548	.37447	.44258
5	.63131	.72312	.69953	.60772	.58731	.67161	.65142	.56691	.54910	.62737	.60955	.53128	.51558	.58843
6	.82364	.92415	.89187	.79135	.76363	.85545	.82774	.73592	.71163	.79638	.77234	.68783	.66676	.74503
7	1.0352	1.1462	1.1034	.99238	.95597	1.0555	1.0201	.91956	.89820	.98002	.94867	.85684	.82954	.91405
8	1.2703	1.3943	1.3385	1.2145	1.1675	1.2786	1.2316	1.1204	1.0695	1.1811	1.1410	1.0405	1.0059	1.0977
9	1.5348	1.6752	1.6030	1.4625	1.4026	1.5766	1.4667	1.3527	1.2921	1.4031	1.3526	1.2415	1.1982	1.2987
10	1.8372	1.9991	1.9054	1.7435	1.6671	1.8076	1.7312	1.5907	1.5272	1.6512	1.5877	1.4636	1.4098	1.5208
11	2.1903	2.3815	2.2585	2.0673	1.9695	2.1314	2.0336	1.8717	1.7917	1.9321	1.8522	1.7117	1.6549	1.7689
12	2.6149	2.8484	2.6832	2.4497	2.3227	2.5138	2.3868	2.1954	2.0941	2.2560	2.1566	1.9926	1.9094	2.0498
13	3.1482	3.4480	3.2164	2.9166	2.7473	2.9897	2.8114	2.5780	2.4472	2.6384	2.5077	2.3165	2.2118	2.3737
14	3.8677	4.2875	3.9460	3.5162	3.2895	3.5893	3.3446	3.0448	2.8729	3.1053	2.9323	2.6989	2.5649	2.7361
15	4.9946	5.7017	5.0629	4.3557	4.0001	4.6199	4.0642	3.6444	3.4051	3.7049	3.4656	3.1658	2.9896	3.2230
16				5.7700	5.1270	5.8341	5.1911	4.4840	4.1247	4.5544	4.1852	3.7654	3.5228	3.8224
17								5.8982	5.2516	5.9587	5.3170	4.6049	4.2424	4.6621
18												6.0191	5.3693	6.0764

Table A.12 Optimum Uniform Quantizers with Quantization Levels  $N = 2, \dots, 36$  for Signal with Gaussian Density (Mean = 0, Variance = 1)

NO. OF OUTPUT LEVELS	STEP SIZE	M.S.E.	S.N.R. (DB)	ENTROPY
2	1.5958	.35338	4.2264	1.0500
3	1.2240	.19017	7.2085	1.5358
4	.99569	.11885	9.2502	1.9037
5	.84299	.082173	10.857	2.1831
6	.73343	.060657	12.171	2.4085
7	.65077	.046860	13.292	2.5976
8	.58602	.037550	14.267	2.7606
9	.53382	.030626	15.129	2.9039
10	.49078	.025687	15.903	3.0319
11	.45467	.021856	16.604	3.1476
12	.42379	.018853	17.246	3.2532
13	.39716	.016453	17.838	3.3503
14	.37391	.014500	18.386	3.4402
15	.35341	.012889	18.898	3.5240
16	.33520	.011543	19.377	3.6024
17	.31890	.010405	19.828	3.6761
18	.30423	.0094339	20.253	3.7456
19	.29093	.0085979	20.656	3.8115
20	.27883	.0078727	21.039	3.8740
21	.26776	.0072390	21.403	3.9334
22	.25760	.0066818	21.751	3.9902
23	.24823	.0061890	22.084	4.0445
24	.23957	.0057510	22.403	4.0965
25	.23153	.0053596	22.709	4.1464
26	.22405	.0050084	23.003	4.1944
27	.21707	.0046920	23.286	4.2407
28	.21054	.0044058	23.560	4.2853
29	.20442	.0041460	23.824	4.3283
30	.19867	.0039094	24.079	4.3699
31	.19325	.0036932	24.326	4.4102
32	.18814	.0034952	24.565	4.4493
33	.18331	.0033133	24.797	4.4871
34	.17874	.0031453	25.021	4.5239
35	.17441	.0029912	25.242	4.5596
36	.17029	.0028481	25.454	4.5943

Table A.13 Optimum Uniform Quantizers with Quantization Levels  $N = 2, \dots, 36$  for Signal with Laplacian Density (Mean = 0, Variance = 1)

NO. OF OUTPUT LEVELS	STEP SIZE	M.S.E.	S.N.R. (DB)	ENTROPY
2	1.4142	.50000	3.0103	1.0000
3	1.4142	.26424	5.7800	1.3169
4	1.0874	.19630	7.0707	1.7507
5	1.0245	.13300	8.7616	1.8649
6	.87070	.10951	9.6056	2.1234
7	.82175	.083087	10.805	2.2073
8	.73093	.071748	11.442	2.3919
9	.69397	.057992	12.366	2.6608
10	.63346	.051488	12.883	2.6029
11	.60481	.043319	13.633	2.6637
12	.56131	.039174	14.070	2.7789
13	.53847	.033881	14.700	2.8336
14	.50555	.031044	15.060	2.9303
15	.48688	.027395	15.623	2.9802
16	.46100	.025351	15.960	3.0634
17	.44544	.022716	16.437	3.1093
18	.42449	.021185	16.740	3.1823
19	.41130	.019212	17.164	3.2248
20	.39396	.018029	17.440	3.2898
21	.38261	.016509	17.823	3.3294
22	.36800	.015574	18.076	3.3879
23	.35813	.014374	18.424	3.4249
24	.34562	.013619	18.659	3.4782
25	.33694	.012654	18.978	3.5130
26	.32611	.012033	19.196	3.5618
27	.31841	.011244	19.491	3.5947
28	.30892	.010727	19.695	3.6398
29	.30204	.010072	19.969	3.6708
30	.29365	.0096354	20.161	3.7127
31	.28746	.0090851	20.417	3.7422
32	.27999	.0087132	20.598	3.7813
33	.27439	.0082459	20.838	3.8094
34	.26768	.0079258	21.010	3.8460
35	.26258	.0075251	21.235	3.8728
36	.25652	.0072473	21.398	3.9073

Table A.14 Compandors with Quantization Levels  $N = 2, \dots, 36$  for Signal with Gaussian Density (Mean = 0, Variance = 1)

LEVEL	2	3	4	5	6	7	8
M.S.E.	.36838	.19395	.12035	.082139	.059687	.045355	.03564
S.N.R.(DB)	4.3371	7.1231	9.1954	10.855	12.241	13.434	14.481
ENTROPY	1.0000	1.5675	1.9587	2.2578	2.5007	2.7056	2.8830

I	X(I)	Y(I)	X(I)	Y(I)	X(I)	Y(I)	X(I)	Y(I)	X(I)	Y(I)	X(I)	Y(I)	X(I)	Y(I)
1	0.00000	.72720	.53576	0.00000	0.00000	.42426	.35172	0.00000	0.00000	.30071	.26282	0.00000	0.00000	.23355
2	1.6215		1.9056	1.1900	.87607	1.3983	1.1217	.71874	.61084	.94207	.81451	.53188	.47144	.71862
3					2.0971		2.2425	1.5976	1.3122	1.7554	1.4672	1.1208	.98145	1.2697
4									2.3601		2.4588	1.8855	1.5972	1.9959
5													2.5438	

LEVEL	9	10	11	12	13	14	15
M.S.E.	.028747	.023678	.019442	.016868	.014516	.012623	.011077
S.N.R.(DB)	15.414	16.256	17.074	17.729	18.382	18.988	19.556
ENTROPY	3.0398	3.1803	3.3077	3.4242	3.5317	3.6314	3.7244

I	X(I)	Y(I)	X(I)	Y(I)	X(I)	Y(I)	X(I)	Y(I)	X(I)	Y(I)	X(I)	Y(I)	X(I)	Y(I)
1	.21022	0.00000	0.00000	.19119	.17536	0.00000	0.00000	.16197	.15051	0.00000	0.00000	.14058	.13188	0.00000
2	.64383	.47360	.38474	.58324	.53349	.35253	.32538	.49174	.45618	.30216	.78208	.42551	.39877	.26454
3	1.1224	.87661	.78974	1.0082	.91629	.72048	.66277	.80054	.72688	.61389	.57191	.72253	.67553	.53543
4	1.7091	1.3956	1.2440	1.5055	1.3506	1.1246	1.0277	1.2276	1.1269	.94706	.87882	1.0426	.97082	.82019
5	2.6186	2.0917	1.8069	2.1762	1.8938	1.6025	1.4455	1.6801	1.5308	1.3199	1.2164	1.4033	1.2976	1.1292
6			2.6853		2.7455	2.2517	1.9718	2.3199	2.0425	1.7674	1.6982	1.8396	1.6790	1.4793
7							2.8003		2.8506	2.3520	2.1072	2.4390	2.1664	1.9040
8											2.8972		2.9404	2.4917

LEVEL	16	17	18	19	20	21	22
M.S.E.	.0097991	.0087297	.0078261	.0070557	.0063935	.0058203	.0053207
S.N.R.(DB)	20.088	20.590	21.065	21.515	21.943	22.351	22.740
ENTROPY	3.8117	3.8938	3.9713	4.0448	4.1147	4.1812	4.2468

I	X(I)	Y(I)	X(I)	Y(I)	X(I)	Y(I)	X(I)	Y(I)	X(I)	Y(I)	X(I)	Y(I)	X(I)	Y(I)
1	0.00000	.12421	.11739	0.00000	0.00000	.11129	.10579	0.00000	0.00000	.10082	.096295	0.00000	0.00000	.092162
2	.74907	.37524	.35437	.23533	.22304	.33573	.31898	.21199	.20198	.30384	.29009	.19289	.18459	.27754
3	.50343	.63445	.59821	.47511	.44986	.56598	.53713	.42721	.40676	.51114	.48759	.38421	.37130	.46616
4	.76920	.90879	.85458	.72441	.68471	.80874	.76419	.64927	.61741	.72606	.69167	.58861	.56244	.66049
5	1.0545	1.2082	1.1313	.98977	.93293	1.0643	1.0053	.88259	.83764	.95282	.90587	.79725	.76071	.86355
6	1.3720	1.5491	1.4405	1.2808	1.2070	1.3479	1.2676	1.1337	1.0724	1.1973	1.1349	1.0182	.96952	1.0793
7	1.7441	1.9442	1.8054	1.6136	1.5040	1.6734	1.5639	1.4102	1.3287	1.4684	1.3859	1.2571	1.1935	1.3132
8	2.2217	2.5406	2.2729	2.0202	1.8605	2.0723	1.9129	1.7291	1.6182	1.7813	1.6700	1.5228	1.4395	1.5740
9	2.9808		3.0187	2.5862	2.3207	2.6290	2.3656	2.1211	1.9420	2.1669	2.0082	1.8304	1.7188	1.8766
10					3.0544		3.0881	2.6692	2.4078	2.7071	2.4477	2.2102	2.0518	2.2510
11									3.1200		3.1503	2.7430	2.4854	2.7771
12													3.1792	



Table A.14 (cont'd) Companders with Quantization Levels  $N = 2, \dots, 36$  for Signal with Gaussian Density (Mean = 0, Variance = 1)

LEVELS	23	24	25	26	27	28	29
M.S.E.	.0048827	.0044966	.0041544	.0038499	.0035775	.0033331	.0031128
S.N.R.(DB)	23.113	23.471	23.815	24.146	24.464	24.772	25.069
ENTROPY	4.3056	4.3639	4.4199	4.4738	4.5257	4.5758	4.6241

I	X(I)	Y(I)	X(I)	Y(I)	X(I)	Y(I)	X(I)	Y(I)	X(I)	Y(I)	X(I)	Y(I)	X(I)	Y(I)
1	.088371	0.00000	0.00000	.084881	.081658	0.00000	0.00000	.078672	.075898	0.00000	0.00000	.073314	.070901	0.00000
2	.26604	.17697	.16997	.25546	.24571	.16350	.15751	.23667	.22828	.15194	.14676	.22047	.21318	.14192
3	.44656	.35582	.34159	.42857	.41199	.32847	.31633	.39667	.38245	.30507	.29458	.36924	.35692	.28480
4	.63208	.53855	.51664	.60607	.58217	.49648	.47787	.56013	.53973	.46062	.44459	.52079	.50316	.42965
5	.82517	.72750	.69715	.79020	.75818	.66931	.64368	.72875	.70159	.61998	.59801	.67644	.65308	.57758
6	1.0291	.92555	.88559	.98375	.94241	.84910	.81562	.90459	.86983	.78478	.75628	.83776	.80857	.72985
7	1.2485	1.1365	1.0832	1.1905	1.1380	1.0385	.99602	1.0901	1.0467	.95701	.92115	1.0067	.96984	.88799
8	1.4901	1.3660	1.3003	1.4157	1.3493	1.2413	1.1880	1.2895	1.2353	1.1393	1.0948	1.1859	1.1405	1.0539
9	1.7648	1.6223	1.5378	1.6680	1.5830	1.4628	1.3957	1.5075	1.4398	1.3352	1.2803	1.3787	1.3231	1.2301
10	2.0931	1.9203	1.8084	1.9618	1.8497	1.7113	1.6259	1.7524	1.6667	1.5499	1.4818	1.5904	1.5218	1.4201
11	2.5213	2.2897	2.1323	2.3265	2.1696	2.0011	1.8891	2.0386	1.9266	1.7916	1.7056	1.8290	1.7428	1.6290
12	3.2068	2.8095	2.5554	2.8504	2.5879	2.3616	2.2051	2.3950	2.2791	2.0744	1.9624	2.1086	1.9967	1.8647
13			3.2732		3.2585	2.8699	2.6150	2.5981	2.6488	2.4270	2.2716	2.4576	2.3707	2.1413
14							3.2827		3.3060	2.9252	2.6773	2.9512	2.7047	2.4870
15										3.3285		3.3501		2.9762

LEVELS	30	31	32	33	34	35	36
M.S.E.	.0029136	.0027329	.0025685	.0024185	.0022812	.0021553	.0020395
S.N.R.(DB)	25.356	25.634	25.903	26.165	26.418	26.665	26.905
ENTROPY	4.6709	4.7162	4.7601	4.8027	4.8441	4.8843	4.9234

I	X(I)	Y(I)	X(I)	Y(I)	X(I)	Y(I)	X(I)	Y(I)	X(I)	Y(I)	X(I)	Y(I)	X(I)	Y(I)
1	0.00000	.068642	.065524	0.00000	0.00000	.064533	.062658	0.00000	0.00000	.060889	.059218	0.00000	0.00000	.057637
2	.13739	.20636	.19997	.13315	.12916	.19396	.18830	.12540	.12185	.18297	.17793	.11851	.11534	.17317
3	.27566	.34540	.33461	.26708	.25903	.32448	.31495	.25146	.24432	.30597	.29749	.23757	.23119	.28947
4	.41570	.48670	.47130	.40264	.39039	.45687	.44330	.37887	.36801	.43053	.41848	.35777	.34809	.40710
5	.55553	.63132	.61101	.54072	.52403	.59199	.57414	.50836	.49362	.55736	.54156	.47972	.46659	.52664
6	.70526	.78050	.75481	.68232	.66087	.73081	.70835	.64076	.62187	.68726	.66743	.60409	.58733	.64874
7	.85724	.93571	.90402	.82864	.80197	.87451	.84695	.77703	.75364	.82115	.79694	.73167	.71099	.77416
8	1.0161	1.0988	1.0603	.98115	.94861	1.0245	.99121	.91828	.88993	.96014	.93106	.86335	.83539	.90378
9	1.1841	1.2723	1.2257	1.1417	1.1024	1.1826	1.1427	1.0659	1.0320	1.1056	1.0720	1.0002	.97050	1.0387
10	1.3640	1.4597	1.4031	1.3127	1.2654	1.3512	1.3035	1.2218	1.1813	1.2593	1.2184	1.1437	1.1085	1.1802
11	1.5600	1.6659	1.5967	1.4975	1.4405	1.5338	1.4764	1.3882	1.3400	1.4237	1.3751	1.2954	1.2540	1.3301
12	1.7784	1.8990	1.8125	1.7013	1.6318	1.7352	1.6655	1.5686	1.5109	1.6020	1.5440	1.4578	1.4089	1.4907
13	2.0795	2.1727	2.0610	1.9318	1.8453	1.9634	1.8768	1.7678	1.6979	1.7992	1.7291	1.6352	1.5759	1.6652
14	2.3326	2.5152	2.3513	2.2079	2.0914	2.2319	2.1205	1.9937	1.9071	2.0229	1.9363	1.8294	1.7591	1.8585
15	2.7310	3.0002	2.7564	2.5423	2.3889	2.5685	2.4156	2.2599	2.1446	2.2868	2.1758	2.0511	1.9645	2.0783
16	3.3710		3.3911	3.0235	2.7809	3.0459	2.8045	2.5937	2.4413	2.6181	2.4661	2.3128	2.2020	2.3380
17					3.4107		3.4295	3.0675	2.8273	3.0885	2.8494	2.6416	2.4901	2.6644
18									3.4479		3.4656	3.1087	2.8707	3.1284
19												3.4829		

Table A.15 Companders with Quantization Levels  $N = 2, \dots, 36$  for Signal with Laplacian Density (Mean = 0, Variance = 1)

LEVEL	2	3	4	5	6	7	8
M.S.E.	.50008	.27703	.18346	.12608	.094180	.071622	.057136
S.N.R.(DB)	3.0096	5.5749	7.3646	8.9936	10.260	11.450	12.431
ENTROPY	1.0000	1.4719	1.8301	2.0331	2.3063	2.4880	2.6540

I	X(I)	Y(I)	X(I)	Y(I)	X(I)	Y(I)	X(I)	Y(I)	X(I)	Y(I)	X(I)	Y(I)	X(I)	Y(I)
1	0.0000	.69827	.52809	0.00000	0.00000	.42089	.34952	0.00000	0.00000	.29888	.26113	0.00000	0.00000	.27191
2	1.7462		2.2956	1.2328	.94648	1.6468	1.2904	.76821	.64688	1.0634	.90558	.55898	.49232	.78423
3					2.6993		3.0232	1.9846	1.5822	2.2704	1.8358	1.3201	1.1346	1.5473
4									3.2956		3.5314	2.5185	2.0601	2.7379
5													3.7399	

LEVEL	9	10	11	12	13	14	15
M.S.E.	.046056	.038296	.032058	.027429	.023579	.020599	.018059
S.N.R.(DB)	13.367	14.169	14.941	15.618	16.275	16.861	17.433
ENTROPY	2.7976	2.9308	3.0498	3.1614	3.2633	3.3595	3.4485

I	X(I)	Y(I)	X(I)	Y(I)	X(I)	Y(I)	X(I)	Y(I)	X(I)	Y(I)	X(I)	Y(I)	X(I)	Y(I)
1	.20862	0.00000	0.00000	.18961	.17380	0.00000	0.00000	.16045	.15901	0.00000	0.00000	.13911	.13045	0.00000
2	.69977	.44001	.39785	.62478	.57102	.36313	.33404	.52310	.48268	.30929	.28799	.44811	.41821	.26945
3	1.3400	.99584	.88795	1.1833	1.0602	.80153	.73068	.96080	.87880	.67151	.62131	.80992	.75121	.57818
4	2.2614	1.7511	1.5264	1.9360	1.6970	1.3548	1.2190	1.5179	1.3663	1.1086	1.0170	1.2464	1.1464	.93962
5	3.9271	2.9348	2.4441	3.1135	2.6113	2.1053	1.8543	2.7614	2.0003	1.6597	1.5037	1.7988	1.6325	1.3756
6			4.0971		4.2530	3.2771	2.7655	3.4781	2.9087	2.4062	2.1365	2.5414	2.2641	1.9249
7							4.3970		4.5309	3.5684	3.0423	3.6993	3.1676	2.6881
8										4.6562			4.7738	3.8222

LEVEL	16	17	18	19	20	21	22
M.S.E.	.016031	.014768	.012876	.011554	.010493	.0095446	.0087410
S.N.R.(DB)	17.950	18.456	18.919	19.373	19.791	20.202	20.584
ENTROPY	3.5332	3.6123	3.6879	3.7591	3.8274	3.8922	3.9545

I	X(I)	Y(I)	X(I)	Y(I)	X(I)	Y(I)	X(I)	Y(I)	X(I)	Y(I)	X(I)	Y(I)	X(I)	Y(I)
1	0.00000	.12281	.11602	0.00000	0.00000	.10995	.10449	0.00000	0.00000	.099541	.095045	0.00000	0.00000	.090939
2	.25318	.39204	.36904	.23876	.22591	.34859	.33079	.21439	.20398	.31384	.29895	.19455	.18595	.28542
3	.54071	.70056	.65638	.50785	.47879	.61751	.58303	.43290	.42969	.55224	.52456	.40876	.38978	.49955
4	.87343	1.0617	.98883	.81610	.76594	.92554	.87090	.72167	.68230	.82086	.77705	.64705	.61530	.73774
5	1.2682	1.4971	1.3832	1.1749	1.0981	1.2860	1.2020	1.0295	.96911	1.1285	1.0637	.91554	.86768	1.0061
6	1.7537	2.0456	1.8681	1.6119	1.4922	1.7206	1.5957	1.3897	1.3009	1.4885	1.3952	1.2230	1.1542	1.3134
7	2.3843	2.7874	2.4977	2.1594	1.9765	2.2677	2.0795	1.8738	1.6943	1.9722	1.7884	1.5827	1.4855	1.6729
8	3.2856	3.9379	3.3771	2.9001	2.6052	3.0069	2.7074	2.3703	2.1776	2.4651	2.2713	2.0181	1.8784	2.1060
9	4.8847		4.9897	4.0473	3.5027	4.1510	3.6031	3.1083	2.8047	3.2050	2.8976	2.5614	2.3609	2.6508
10					5.0893		5.1842	4.2496	3.6988	4.3437	3.7903	3.2973	2.9866	3.3857
11									5.2747		5.3612	4.4335	3.8778	4.5196
12													5.4442	

Table A.15 (cont'd) Companders with Quantization Levels  $N = 2, \dots, 36$  for Signal with Laplacian Density (Mean = 0, Variance = 1)

LEVEL	23	24	25	26	27	28	29
M.S.E.	.0080160	.0073930	.0068263	.0063338	.0058825	.0054864	.0051212
S.N.R.(dB)	20.960	21.312	21.658	21.983	22.304	22.607	22.906
ENTROPY	4.0139	4.0712	4.1261	4.1791	4.2301	4.2794	4.3270

I	X(I)	Y(I)	X(I)	Y(I)	X(I)	Y(I)	X(I)	Y(I)	X(I)	Y(I)	X(I)	Y(I)	X(I)	Y(I)
1	.087175	0.00000	0.00000	.083712	.080514	0.00000	0.00000	.077553	.074802	0.00000	0.00000	.072241	.069850	0.00000
2	.27307	.17809	.17086	.26175	.25133	.16420	.15805	.24172	.23282	.15234	.14703	.22455	.21685	.14208
3	.47683	.37251	.35670	.45611	.43712	.34219	.32883	.41966	.40356	.31647	.30501	.38865	.37480	.29436
4	.70227	.58656	.56040	.67009	.64076	.53760	.51457	.61392	.58925	.49437	.47571	.56651	.54547	.45842
5	.95454	.82466	.78576	.90810	.86604	.75041	.71813	.82776	.79277	.68857	.66136	.76066	.73108	.63625
6	1.2409	1.0929	1.0379	1.1762	1.1181	.98834	.94333	1.0656	1.0179	.90236	.86483	.97439	.93450	.83035
7	1.5721	1.4000	1.3242	1.4832	1.4042	1.2564	1.1953	1.3335	1.2698	1.1401	1.0899	1.2121	1.1595	1.0440
8	1.9647	1.7393	1.6552	1.8423	1.7351	1.5632	1.4814	1.6403	1.5557	1.4080	1.3417	1.4798	1.4115	1.2817
9	2.4468	2.1921	2.0475	2.2748	2.1272	1.9221	1.8120	1.9989	1.8862	1.7146	1.6275	1.7863	1.6970	1.5493
10	3.0718	2.7364	2.5293	2.8186	2.6076	2.3543	2.2039	2.4309	2.2779	2.0731	1.9579	2.1447	2.0272	1.8557
11	3.9617	3.4704	3.1537	3.5518	3.2324	2.8977	2.6850	2.9738	2.7587	2.5048	2.3494	2.5761	2.4185	2.2139
12	5.5239	4.6021	4.0423	4.6814	4.1198	3.6303	3.3083	3.7055	3.3814	3.0473	2.8299	3.1183	2.8987	2.6451
13			5.6005		5.6743	4.7578	4.1946	4.8313	4.2667	3.7782	3.4521	3.8485	3.5205	3.1869
14							5.7455		5.8142	4.9024	4.3364	4.9710	4.4038	3.9165
15											5.6807		5.9451	5.0374

LEVEL	30	31	32	33	34	35	36
M.S.E.	.0047980	.0044984	.0042312	.0039824	.0037591	.0035502	.0033616
S.N.R.(dB)	23.189	23.469	23.735	23.999	24.249	24.497	24.735
ENTROPY	4.3732	4.4178	4.4612	4.5032	4.5441	4.5838	4.6225

I	X(I)	Y(I)	X(I)	Y(I)	X(I)	Y(I)	X(I)	Y(I)	X(I)	Y(I)	X(I)	Y(I)	X(I)	Y(I)
1	0.00000	.067612	.065514	0.00000	0.00000	.063543	.061687	0.00000	0.00000	.059937	.058283	0.00000	0.00000	.056719
2	.11745	.20947	.20294	.13312	.12903	.19664	.19072	.17522	.12162	.18514	.17989	.11821	.11500	.17492
3	.28443	.36192	.34990	.27515	.26646	.33865	.32811	.25830	.25063	.31821	.30858	.24340	.23659	.30010
4	.44235	.52595	.50779	.42738	.41339	.49085	.47502	.40029	.38800	.46018	.44624	.37645	.36557	.43313
5	.61299	.70374	.67839	.59138	.57126	.65483	.63286	.55247	.53489	.61233	.59311	.51840	.50291	.57506
6	.79855	.89780	.86393	.76923	.74183	.83255	.80340	.71642	.69271	.77626	.75090	.67054	.64976	.72718
7	1.0019	1.1114	1.0673	.96315	.92732	1.0265	.98886	.89411	.86322	.95291	.92139	.83444	.80753	.89105
8	1.2269	1.3490	1.2922	1.1767	1.1306	1.2401	1.1921	1.0780	1.0487	1.11478	1.1068	1.0121	.97799	1.0686
9	1.4786	1.6166	1.5478	1.4142	1.3555	1.4775	1.4169	1.3015	1.2519	1.3612	1.3099	1.2059	1.1634	1.2625
10	1.7642	1.9228	1.8293	1.6817	1.6039	1.7449	1.6684	1.5389	1.4766	1.5986	1.5346	1.4193	1.3665	1.4758
11	2.0943	2.2809	2.1593	1.9879	1.8924	2.0510	1.9337	1.8062	1.7280	1.8658	1.7860	1.6566	1.5911	1.7131
12	2.4854	2.7119	2.5502	2.3458	2.2223	2.4087	2.2835	2.1122	2.0133	2.1717	2.0712	1.9238	1.8424	1.9802
13	2.9454	3.2534	3.0299	2.7766	2.6171	2.8393	2.6742	2.4498	2.3429	2.5292	2.4098	2.2296	2.1275	2.2859
14	3.5867	3.9823	3.6508	3.3177	3.0926	3.3802	3.1574	2.9003	2.7335	2.9595	2.7911	2.5870	2.4570	2.6432
15	4.4690	5.1017	4.5323	4.0461	3.7170	4.1080	3.7734	3.4608	3.2124	3.4997	3.2699	3.0170	2.8473	3.0731
16	6.0075		6.0690	5.1641	4.5937	5.2246	4.6533	4.1681	3.8321	4.2265	3.8992	3.5570	3.3258	3.6128
17					6.1268		.61840	5.2835	4.7112	5.3406	4.7676	4.2833	3.9448	4.3386
18									6.7395		6.2936	5.3962	4.8224	5.4504
19													6.3463	



# APPENDIX B

## Derivation of Approximate Rational Function Operator

The SDF of an NC1 model image is given by

$$S(z_1, z_2) = \frac{1 - r\alpha(z_1 + z_1^{-1} + z_2 + z_2^{-1})}{[1 - \alpha(z_1 + z_1^{-1} + z_2 + z_2^{-1})]^2} \quad (B-1)$$

Let  $R(z_1, z_2) \triangleq S(z_1, z_2)^{-1/2}$ , thus

$$R(z_1, z_2) = \frac{1 - \alpha(z_1 + z_1^{-1} + z_2 + z_2^{-1})}{[1 - r\alpha(z_1 + z_1^{-1} + z_2 + z_2^{-1})]^{1/2}} \quad (B-2)$$

We know from the following axiom that

$$(1-x)^{-n} = 1 + nx + \frac{n(n+1)}{2!} x^2 + \frac{n(n+1)(n+2)}{3!} x^3 + \dots \quad (B-3)$$

provided  $x^2 < 1$  exists.

Then the alternative expression of  $R(z_1, z_2)$  is, for simplicity, let  $x \triangleq \alpha(z_1 + z_1^{-1} + z_2 + z_2^{-1})$ ,

$$\begin{aligned} R(z_1, z_2) &= \frac{1-x}{(1-rx)^{1/2}} \\ &= (1-x) \left[ 1 + \frac{1}{2}rx + \frac{1 \cdot 3}{2^2} \frac{r^2 x^2}{2!} + \dots + \frac{1 \cdot 3 \cdot 5 \dots (2n-1)}{2^n} \frac{r^n x^n}{n!} + \dots \right] \\ &= 1 + \frac{1}{2}rx + \frac{1 \cdot 3}{2^2} \frac{r^2 x^2}{2!} + \dots + \frac{1 \cdot 3 \cdot 5 \dots (2n-1)}{2^n} \frac{r^n x^n}{n!} + \dots \\ &\quad - x - \frac{1}{2}rx^2 - \frac{1 \cdot 3}{2^2} \frac{r^2 x^3}{2!} - \dots - \frac{1 \cdot 3 \cdot 5 \dots (2n-3)}{2^{n-1}} \frac{r^{n-1} x^n}{(n-1)!} \\ &\quad - \frac{1 \cdot 3 \cdot 5 \dots (2n-1)}{2^n} \frac{r^n x^{n+1}}{n!} - \dots \end{aligned}$$

$$\begin{aligned}
&= 1 - \sum_{n=1}^{\infty} \frac{1 \cdot 3 \cdot 5 \cdots (2n-3)}{2^{n-1} (n-1)!} \left[ -\frac{(2n-1)r}{2n} + 1 \right] r^{n-1} x^n \\
&= 1 - \sum_{n=1}^{\infty} \frac{1 \cdot 3 \cdot 5 \cdots (2n-3)}{2^{n-1} (n-1)!} \left( 1 - r + \frac{r}{2n} \right) r^{n-1} x^n \quad (B-4)
\end{aligned}$$

Substitution of  $n = 1, 2, \dots$ , into (B-4), and after some algebraic manipulations, different order of  $R^{(n)}(z_1, z_2)$  is easily obtained as

$$R^{(1)}(z_1, z_2) = 1 - \left(1 - \frac{r}{2}\right) \alpha (z_1 + z_1^{-1} + z_2 + z_2^{-1}) \quad (B-5)$$

$$\begin{array}{ccccccc}
& & 0 & & & & \\
& & & & & & . = 1 \\
0 & & . & & 0 & & \\
& & 0 & & & & 0 = -(1 - \frac{r}{2})\alpha
\end{array}$$

Figure B.1 Construction Diagram of  $R^{(1)}(z_1, z_2)$

$$\begin{aligned}
R^{(2)}(z_1, z_2) &= 1 - \frac{1}{2} \left(1 - r + \frac{r}{4}\right) r 4\alpha^2 - \left(1 - \frac{r}{2}\right) \alpha (z_1 + z_1^{-1} + z_2 + z_2^{-1}) \\
&\quad - \frac{1}{2} \left(1 - r + \frac{r}{4}\right) r \alpha^2 [z_1^2 + z_1^{-2} + z_2^2 + z_2^{-2} + 2(z_1 z_2 + z_1^{-1} z_2^{-1} + z_1^{-1} z_2 + z_1 z_2^{-1})] \quad (B-5)
\end{aligned}$$

$$\begin{array}{ccccccc}
& & x & & & & \\
& & & & & & . = 1 - \frac{1}{2} \left(1 - r + \frac{r}{4}\right) r 4\alpha^2 \\
2x & & 0 & & 2x & & \\
x & & 0 & & . & & 0 = -(1 - \frac{r}{2})\alpha \\
& & 2x & & 0 & & 2x \\
& & & & x & & x = -\frac{1}{2} \left(1 - r + \frac{r}{4}\right) r \alpha^2
\end{array}$$

Figure B.2 Construction Diagram of  $R^{(2)}(z_1, z_2)$

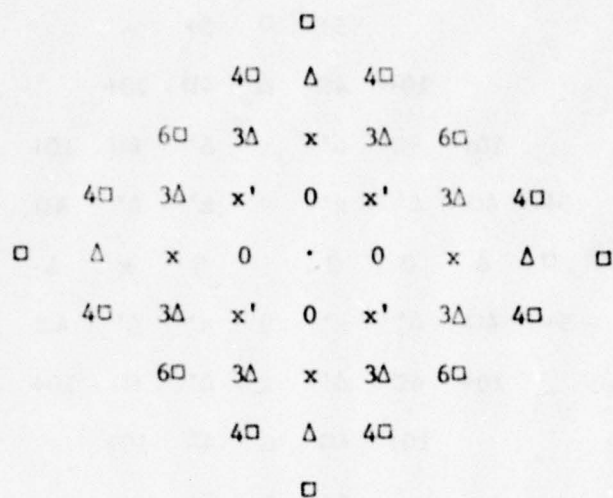
$$\begin{aligned}
R^{(3)}(z_1, z_2) = & 1 - \frac{1}{2}(1-r+\frac{r}{4})r4\alpha^2 - \left[ (1-\frac{r}{2})\alpha + \frac{1 \cdot 3}{2^2 \cdot 2!} (1-r+\frac{r}{6})r^2 9\alpha^3 \right] \\
& \cdot (z_1+z_1^{-1}+z_2+z_2^{-1}) - \frac{1}{2}(1-r+\frac{r}{4})r\alpha^2 \left[ z_1^2+z_1^{-2}+z_2^2+z_2^{-2} \right. \\
& + 2(z_1z_2+z_1z_2^{-1}+z_1^{-1}z_2+z_1^{-1}z_2^{-1}) \left. \right] - \frac{1 \cdot 3}{2^2 \cdot 2!} (1-r+\frac{r}{6})r^2\alpha^3 \\
& \cdot \left[ z_1^3+z_1^{-3}+z_2^3+z_2^{-3} + 3(z_1^2z_2+z_1^2z_2^{-1}+z_1^{-2}z_2+z_1^{-2}z_2^{-1}+z_1z_2^2+z_1z_2^{-2} \right. \\
& \left. + z_1^{-1}z_2^2+z_1^{-1}z_2^{-2}) \right]
\end{aligned}$$

$ \begin{array}{ccccccc} & & & \Delta & & & \\ & & 3\Delta & x & 3\Delta & & \\ & 3\Delta & 2x & 0 & 2x & 3\Delta & \\ \Delta & x & 0 & \cdot & 0 & x & \Delta \\ & 3\Delta & 2x & 0 & 2x & 3\Delta & \\ & & 3\Delta & x & 3\Delta & & \\ & & & \Delta & & &  \end{array} $	$ \begin{aligned} \cdot &= 1 - \frac{1}{2}(1-r+\frac{r}{4})r4\alpha^2 \\ 0 &= -(1-\frac{r}{2})\alpha - \frac{1 \cdot 3}{2^2 \cdot 2!} (1-r+\frac{r}{6})r^2 9\alpha^3 \\ x &= -\frac{1}{2}(1-r+\frac{r}{4})r\alpha^2 \\ \Delta &= -\frac{1 \cdot 3}{2^2 \cdot 2!} (1-r+\frac{r}{6})r^2\alpha^3 \end{aligned} $
---	---

Figure B.3 Construction Diagram of  $R^{(3)}(z_1, z_2)$

From the foregoing three Figures,  $R^{(4)}(z_1, z_2)$  and  $R^{(5)}(z_1, z_2)$  can be obtained in the similar manner





$$\cdot = 1 - \frac{1}{2}(1 - r + \frac{r}{4})r^4\alpha^2 - \frac{1 \cdot 3 \cdot 5}{2^3 \cdot 3!} (1 - r + \frac{r}{8})r^3 36\alpha^4$$

$$0 = -(1 - \frac{r}{2})\alpha - \frac{1 \cdot 3}{2^2 \cdot 2!} (1 - r + \frac{r}{6})r^2 9\alpha^3$$

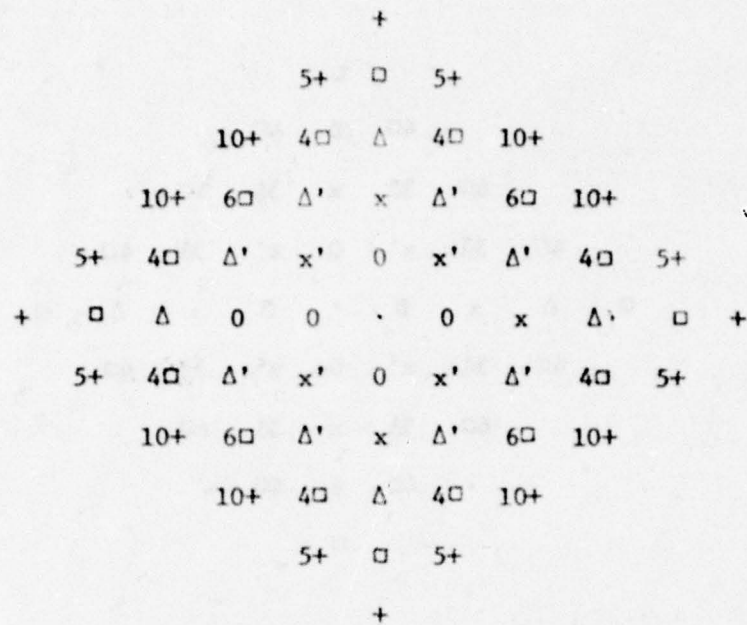
$$x = - \left[ \frac{1}{2}(1 - r + \frac{r}{4})r\alpha^2 + \frac{1 \cdot 3 \cdot 5}{2^3 \cdot 3!} (1 - r + \frac{r}{8})r^3 16\alpha^4 \right]$$

$$x' = - \left[ (1 - r + \frac{r}{4})r\alpha^2 + \frac{1 \cdot 3 \cdot 5}{2^3 \cdot 3!} (1 - r + \frac{r}{8})r^3 24\alpha^4 \right]$$

$$\Delta = - \frac{1 \cdot 3}{2^2 \cdot 2!} (1 - r + \frac{r}{6})r^2 \alpha^3$$

$$\square = - \frac{1 \cdot 3 \cdot 5}{2^3 \cdot 3!} (1 - r + \frac{r}{8})r^3 \alpha^4$$

Figure B.4 Construction Diagram of  $R^{(4)}(z_1, z_2)$



$$\begin{aligned}
 . &= 1 - \frac{1}{2}(1-r+\frac{r}{4})r4\alpha^2 - \frac{1 \cdot 3 \cdot 5}{2^3 \cdot 3!} (1-r+\frac{r}{8})r^3 36\alpha^4 \\
 0 &= - \left[ (1-\frac{r}{2})\alpha + \frac{1 \cdot 3}{2^2 \cdot 2!} (1-r+\frac{r}{6})r^2 9\alpha^3 + \frac{1 \cdot 3 \cdot 5 \cdot 7}{2^4 \cdot 4!} (1-r+\frac{r}{10})r^4 100\alpha^5 \right] \\
 x &= - \left[ \frac{1}{2}(1-r+\frac{r}{4})r\alpha^2 + \frac{1 \cdot 3 \cdot 5}{2^3 \cdot 3!} (1-r+\frac{r}{8})r^3 16\alpha^4 \right] \\
 x' &= - \left[ (1-r+\frac{r}{4})r\alpha^2 + \frac{1 \cdot 3 \cdot 5}{2^3 \cdot 3!} (1-r+\frac{r}{8})r^3 24\alpha^4 \right] \\
 \Delta &= - \left[ \frac{1 \cdot 3}{2^2 \cdot 2!} (1-r+\frac{r}{6})r^2 \alpha^3 + \frac{1 \cdot 3 \cdot 5 \cdot 7}{2^4 \cdot 4!} (1-r+\frac{r}{10})r^4 25\alpha^5 \right] \\
 \Delta' &= - \left[ 3 \frac{1 \cdot 3}{2^2 \cdot 2!} (1-r+\frac{r}{6})r^2 \alpha^3 + \frac{1 \cdot 3 \cdot 5 \cdot 7}{2^4 \cdot 4!} (1-r+\frac{r}{10})r^4 80\alpha^5 \right] \\
 \square &= - \frac{1 \cdot 3 \cdot 5}{2^3 \cdot 3!} (1-r+\frac{r}{8})r^3 \alpha^4 \\
 + &= - \frac{1 \cdot 3 \cdot 5 \cdot 7}{2^4 \cdot 4!} (1-r+\frac{r}{10})r^4 \alpha^5
 \end{aligned}$$

Figure B.5 Construction Diagram of  $R^{(5)}(z_1, z_2)$

It is noted that when the order of  $R^{(n)}(z_1, z_2)$  goes up, more sample points in the spatial domain would be involved in calculating the approximate rational function operator  $\mathcal{L}$ .

# APPENDIX C

## Unique Inverse Solution of Function $g'_1(x)$

The function  $g'_1(x)$  is given by

$$g'_1(x) = \frac{(-2\log_e 2)2^{-2x}}{(1 - \rho_1^2 2^{-2x})^2} \quad (C-1)$$

Let  $h(\cdot)$  be the inverse of  $g'(\cdot)$ . For convenience we denote  $g'_1(x)$  and  $2^{-2x}$  by  $z$  and  $y$  respectively, and rewrite (C-1) as

$$z = \frac{(-2\log_e 2) \cdot y}{1 - 2\rho_1^2 y + \rho_1^4 y^2} \quad (C-2)$$

Since  $y = 2^{-2x}$ , we have  $1 \geq y \geq 0$  for any given  $x \geq 0$ . Rearranging (C-2) and getting an explicit expression as a function of  $y$ , we have

$$(\rho_1^4 z)y^2 - 2(\rho_1^2 z - \log_e 2)y + z = 0. \quad (C-3)$$

The roots of (C-3) are

$$y_1 = \frac{-(-\rho_1^2 z + \log_e 2) + \sqrt{-2\rho_1^2 z \log_e 2 + (\log_e 2)^2}}{\rho_1^4 z} \quad (C-4a)$$

$$\text{and } y_2 = \frac{-(-\rho_1^2 z + \log_e 2) - \sqrt{-2\rho_1^2 z \log_e 2 + (\log_e 2)^2}}{\rho_1^4 z}. \quad (C-4b)$$

The admissible root should lie in the interval  $[0,1]$ . Since  $1 > \rho_1^2 > 0$ , and from (C-1), we can observe that

$$0 \geq z \geq -\frac{2\log_e 2}{(1 - \rho_1^2)^2} \text{ for } \forall n \geq 0 \quad (C-5)$$

i.e.,  $z$  is nonpositive. Therefore



$$\sqrt{-2\rho_i^2 z \log_e 2 + (\log_e 2)^2} > 0 \quad (\text{C-6a})$$

$$-\rho_i^2 z + \log_e 2 > 0 \quad (\text{C-6b})$$

and it is easy to prove that

$$-\rho_i^2 z + \log_e 2 > \sqrt{-2\rho_i^2 z \log_e 2 + (\log_e 2)^2} . \quad (\text{C-7})$$

With the above conditions (C-6) and (C-7), we conclude

$$y_2 \geq y_1 \geq 0 . \quad (\text{C-8})$$

In a similar manner, using (C-6) and (C-7), it is easy to check that

- i)  $y_2 > 1$  , hence  $y_2$  is inadmissible.
- ii)  $1 \geq y_1 \geq 0$  ,  $y_1$  is the unique solution.

# LIST OF REFERENCES

1. N. Ahmed, T. Natrarajan, and K.R. Rao, "On Image Processing and a Discrete Cosine Transform," IEEE Transactions on Computers, Vol. C-23, No. 1, pp. 90-93, January 1974.
2. V.R. Algazi, "Useful Approximations to Optimum Quantization," IEEE Transactions on Communication Technology, Vol. COM-14, No. 3, pp. 297-301, June 1966.
3. H.C. Andrews, Computer Techniques in Image Processing, Academic Press, New York, 1970.
4. H.C. Andrews, J. Kane, and W.K. Pratt, "Hadamard Transform Image Coding," Proceedings of the IEEE, Vol. 57, No. 1, January 1969.
5. H.C. Andrews and W.K. Pratt, "Fourier Transform Coding of Images," Hawaii International Conference on System Science, pp. 677-679, January 1968.
6. E. Angel and A.K. Jain, "Filtering of Multidimensional Diffusion Processes," 6th Asilomar Conference on Circuits and Systems, November 1972.
7. R. Bellman, Introduction to Matrix Analysis, McGraw Hill, New York, 1970.
8. P. Castellino, G. Madena, L. Nebbia, and C. Scngliala, "Bit Rate Reduction by Automatic Adaptation of Quantizer Step-Size in DPCM Systems," in Proc. 1974 Int. Zurich Seminar Digital Communications, pp. B6(1)-B6(6), 1974.
9. C.C. Cutler, "Differential Quantization of Communication Signals," U.S. Patent No. 2,605,301, July 29, 1952.
10. J.E. Essman, "Theory and Application of DPCM and Compression of DPCM with other Time Predictive Techniques," Ph.D. Thesis, Purdue Univ., Electrical Engineering, 1972.
11. B. Fox, "Discrete Optimization via Marginal Analysis," Management Science, Vol. 13, pp. 201-216, November 1966.
12. L.E. Franks, "A Model for the Random Video Process," Bell Systems Technical Journal, pp. 609-630, April 1966.
13. W. Frei and C.C. Chen, "Fast Boundary Detection: A Generalization and a New Algorithm," IEEE Transactions on Computers, Vol. C-26, No. 10, pp. 988-998, October 1977.
14. J.I. Gimlett, "Use of Activity Classes in Adaptive Transform Image Coding," IEEE Transactions on Communications, Correspondence, Vol. 23, pp. 785-786, July 1975.

15. D.N. Graham, "Image Transmission by Two-Dimensional Contour Coding," Proceedings of the IEEE, Vol. 55, No. 3, pp. 336-346, March 1967.
16. A.K. Griffith, "Edge Detection in Simple Scenes Using. Apriori Information," IEEE Transactions on Computers, Vol. C-22, pp. 371-381, April 1973.
17. A. Habibi, "Hybrid Coding of Pictorial Data," IEEE Transactions on Communications, Vol. COM-22, No. 5, pp. 614-624, May 1974.
18. A. Habibi, "Study of On-Board Compression of Earth Resources Data," Final Report, Contract No. NAS 2-8394, TRW No. 26566, September 1975.
19. A. Habibi, "Survey of Adaptive Image Coding Techniques," IEEE Transactions on Communications, Vol. COM-25, No. 11, pp. 1275-1284, November 1977.
20. A. Habibi, "Two Dimensional Bayesian Estimate of Images," Proceedings of the IEEE, Vol. 60, pp. 878-883, July 1972.
21. A. Habibi and P.A. Wintz, "Image Coding Linear Transformation and Block Quantization," IEEE Transactions on Communication Technology, Vol. COM-19, No. 1, pp. 50-62, February 1971.
22. A. Habibi and P.A. Wintz, "Linear Transformation for Encoding Two-Dimensional Sources," School of Electrical Engineering, Purdue Univ., Lafayette, Indiana, Technical Report EE 70-2, March 1970.
23. C.W. Harrison, "Experiments with Linear Prediction in Television," The Bell Systems Technical Journal, Vol. 31, No. 4, pp. 746-783, July 1952.
24. M.H. Hueckel, "An Operator Which Locates Edges in Digitized Pictures," J.A.C.M., Vol. 18, January 1971.
25. B.R. Hunt, "Digital Image Processing," Proceedings of the IEEE, Vol. 63, No. 4, pp. 693-708, April 1975.
26. A.K. Jain, "A Fast Karhunen-Loeve Transform for a Class of Random Processes," IEEE Transactions on Communications, Concise Paper, pp. 1023-1029, September 1976.
27. A.K. Jain, "A Fast Karhunen-Loeve Transform for Finite Discrete Images," Proceedings of the National Electronics Conference, Chicago, Illinois, pp. 323-328, October 1974.
28. A.K. Jain, "A Semicausal Model for Recursive Filtering of Two-Dimensional Images," IEEE Transactions on Computers, Vol. C-26, No. 4, pp. 343-350, April 1977.
29. A.K. Jain, "A Sinusoidal Family of Unitary Transforms," Technical Report, Dept. of Electrical Engineering, SUNY at Buffalo, New York, July 1977.



30. A.K. Jain, "Image Coding via a Nearest Neighbors Image Model," IEEE Transactions on Communications, Vol. COM-23, No. 3, pp. 318-331, March 1975.
31. A.K. Jain, "Partial Differential Equations and Finite-Difference Methods in Image Processing, Part I: Image Representation," Journal of Optimization Theory and Applications, Vol. 23, No. 1, pp. 65-91, September 1977.
32. A.K. Jain, "Some New Techniques in Image Processing," Image Science Math., Proceedings ONR Symposium on Current Problems in Image Science (1976), (C.O. Wilde & E. Barrett, Editors), West. Periodicals Co., No. Hollywood, California, 1977.
33. A.K. Jain and E. Angel, "Image Restoration, Modeling, and Reduction of Dimensionality," IEEE Transactions on Computers, Vol. C-23, No. 5, pp. 470-476, May 1974.
34. A.K. Jain and J.R. Jain, "Partial Differential Equations and Finite Difference Methods in Image Processing, Part II: Image Restoration," IEEE Transactions on Automatic Control, Vol. AC-26, No. 5, pp. 817-834, October 1978.
35. A.K. Jain and S.H. Wang, "Stochastic Image Models and Hybrid Coding," Naval Ocean Systems Center Contract N00 953-77-C-003 MJE, Final Report, Dept. of Electrical Engineering, SUNY at Buffalo, February 1978.
36. A.K. Jain, S.H. Wang and Y.Z. Liao, "Fast Karhunen Loeve Transform Data Compression Studies," 1976 National Telecommunications Conference, Dallas, Texas, December 1976.
37. H. Karhunen, "On Linear Methods in Probability Theory," (1947) (English translation by I. Selin), The Rand Corporation, Doc. T-131, August 11, 1960.
38. R.L. Kashyap and A.R. Rao, Dynamic Stochastic Models from Empirical Data. Academic Press, New York, 1976.
39. R. Kirsch, "Computer Determination of the Constituent Structure of Biological Images," Comput. Biomed. Res., Vol. 4, pp. 315-328, 1971.
40. A.J. Kurtenbach and P.A. Wintz, "Optimum Quantization," Supplement to IEEE Transactions on Aerospace and Electronic Systems, Vol. AES-3, pp. 563-580, November 1967.
41. M. Levine, "Feature Extraction: A Survey," Proceedings of the IEEE, Vol. 57, pp. 1391-1405, August 1969.
42. M. Loeve, Fonctions Aléatoires de Seconde Ordre, Hermann, Paris, 1948.
43. J.L. Mannos and D.J. Sakrison, "The Effects of a Visual Fidelity Criterion on the Encoding of Images," IEEE Transactions on Information Theory, Vol. IT-20, No. 4, pp. 525-536, July 1974.

44. J. Max, "Quantizing for Minimum Distortion," IRE Transactions on Information Theory, Vol. IT-6, pp. 7-12, March 1960.
45. R.A. McDonald, "Signal-to-Noise and Idle Channel Performance of DPCM Systems - Particular Applications to Voice Signals," B.S.T.J., Vol. 45, No. 7, pp. 1123-1151, September 1966.
46. R.W. Means, E.H. Wrench and J.J. Whitehouse, "Image Transmission via Spread Spectrum Techniques," ARPA Quarterly Technical Report, ARPA-QR6, Naval Undersea Center, San Diego, California 92132, Jan.-Dec. 1975.
47. A.Z. Meiri, "The Pinned Karhunen-Loeve Transform of a Two Dimensional Gauss-Markov Field," Proceedings 1976 SPIE Conference on Image Processing, San Diego, California, 1976.
48. N.E. Nahi and T. Assefi "Bayesian Recursive Image Enhancement," IEEE Transactions on Computers, Vol. C-12, pp. 734-738, July 1972.
49. N.E. Nahi and C.A. Franco, "Recursive Image Enhancement-Vector Processing," IEEE Transactions on Communications, Vol. COM-21, pp. 305-311, April 1973.
50. J.B. O'Neal, "Predictive Quantization Systems (Differential Pulse Code Modulation) for the Transmission of Television Signals," The Bell Systems Technical Journal, Vol. 45, No. 5, pp. 689-721, May-June 1966.
51. M.D. Paez and T.H. Glisson, "Minimum Mean-Squared-Error Quantization in Speech PCM and DPCM Systems," IEEE Transactions on Communications (Concise Papers), Vol. COM-20, pp. 225-230, April 1972.
52. W.K. Pratt, "Bibliography on Digital Image Processing and Related Topics," Electronics Sciences Laboratory, University of Southern California, USCEE Report 453, September 1973.
53. W.K. Pratt, Digital Image Processing, John Wiley & Sons Inc., 1978.
54. W.K. Pratt, H.C. Andrews, and J. Kane, "Hadamard Transform Image Coding," Proceedings of the IEEE, Vol. 57, No. 1, pp. 58-68, January 1969.
55. W.K. Pratt, W.H. Chen and L.R. Welch, "Slant Transform Image Coding," IEEE Transactions on Communications, Vol. COM-22, No. 8, pp. 1075-1093, August 1974.
56. W.D. Ray and R.M. Driver, "Further Decomposition of the Karhunen-Loeve Series Representation of a Stationary Random Process," IEEE Trans. Information Theory, Vol. IT-16, No. 6, pp. 663-668, November 1970.
57. L.G. Robert, "Machine Perception of Three Dimensional Solids," in Optical and Electro-Optical Information Processing, J.T. Tippet et al., Eds., MIT Press, Cambridge, MA, pp. 187-197, 1965.



58. J.A. Roese, W.K. Pratt, and G.S. Robinson, "Interframe Cosine Transform Image Coding," IEEE Transactions on Communications, Vol. COM-25, pp. 1329-1339, November 1977.
59. R.P. Roesser, "A Discrete State-Space Model for Linear Image Processing," IEEE Transactions on Automatic Control, Vol. AC-20, No. 1, pp. 1-10, February 1975.
60. A. Rosenfeld and M. Thurston, "Edge and Curve Detection for Visual Scene Analysis," IEEE Transactions on Computers, Vol. C-20, pp. 562-569, May 1971.
61. A.P. Sage and J.L. Melsa, Estimation Theory with Applications to Communications and Control, McGraw-Hill, 1971.
62. W.F. Schreiber, "Picture Coding," Proceedings of the IEEE, Vol. 55, No. 3, pp. 320-335, March 1967.
63. W.F. Schreiber, T.S. Huang, and O.J. Tretiak, "Contour Coding of Images," IRE Western Electron Show and Conv., pp. 8/3(1)-8/3(6), August 1968.
64. W.F. Schreiber and C.F. Knapp, "TV Bandwidth Reduction by Digital Coding," IRE National Convention Record, Vol. 6, Part 4, pp. 88-89, 1958.
65. W.F. Schreiber, C.F. Knapp, and N.D. Kay, "Synthetic Highs: An Experimental TV Bandwidth Reduction System," J. Soc. Motion Picture and Television Engineers, Vol. 68, pp. 525-537, August 1959.
66. A. Segall, "Bit Allocation and Encoding for Vector Sources," IEEE Transactions on Information Theory, Vol. IT-22, No. 2, pp. 162-169, March 1976.
67. C.E. Shannon, "Coding Theorems for a Discrete Source with a Fidelity Criterion," 1959 IRE Nat'l Conv. Rec., Pt. 4, pp. 152-163.
68. R. W. Stroh, "Optimum and Adaptive Differential Pulse Code Modulation," Ph.D. Thesis, Polytechnic Institute of Brooklyn, Electrical Engineering, 1970.
69. L.C. Wilkins and P.A. Wintz, "Bibliography on Data Compression, Picture Properties, and Picture Coding," IEEE Transactions on Information Theory, Vol. IT-17, No. 2, pp. 180-197, March 1971.
70. P.A. Wintz, "Transform Picture Coding," Proceedings of the IEEE, Vol. 60, No. 7, pp. 809-820, July 1972.
71. E. Wong, "Two Dimensional Random Fields and Representation of Images," SIAM J. Appl. Math., Vol. 16, pp. 756-770, July 1968.
72. R.C. Wood, "On Optimum Quantization," IEEE Transactions on Information Theory, Vol. IT-5, pp. 248-252, March 1969.



73. J.W. Woods, "Two Dimensional Discrete Markov Fields," IEEE Transactions on Information Theory, Vol. IT-18, pp. 232-240, March 1972.
74. J.K. Yan and D.J. Sakrison, "Encoding of Images Based on a Two-Component Source Model," IEEE Transactions on Communications, Vol. COM-25, No. 11, pp. 1315-1322, November 1977.
75. "Special Issue on Redundancy Reduction," Proceedings of the IEEE, Vol. 55, No. 3, pp. 251-480, March 1967.

## VITA

Shenq-Huey Wang was born in Shanghai, China, on April 8, 1948. He received the B.S. degree in Electrical Communication Engineering from the National Chiao Tung University, Hsinchu, Taiwan, in 1970. He served as a Radio Communication Officer in the Chinese Army from 1970 to 1971. In August, 1971, he was employed as an engineer for General Instrument Corporation of Taiwan Ltd. During 1972-74 he was a graduate assistant with the Department of Electrical Engineering, University of Connecticut, and obtained his M.S.E.E. degree in May, 1974. In September, 1974, he joined the State University of New York at Buffalo, where he was a research and teaching assistant throughout his doctoral program. During the summer of 1975, he worked at NASA, Huntsville, Alabama, where he was involved in developing computer software for satellite image processing. He spent the last half year of his graduate study in the Department of Electrical Engineering, University of California at Davis, where his thesis supervisor was on sabbatical, to complete work on his Ph.D. thesis.

Presently, he holds the position of Image Scientist at the Picker Corporation, Cleveland, Ohio, where he is working on Computed Tomography. His research interests include Digital Signal and Image Processing, Data Compression and Modeling of Images, and Computer Graphics.